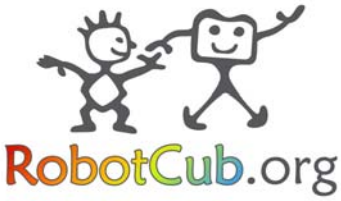

ROBotic Open-architectureTechnology for Cognition, Understanding and Behavior

Project no. 004370

RobotCub: Development of a cognitive humanoid cub

Instrument: Integrated Project
Thematic Priority: IST – Cognitive Systems

D3.1 Sensorimotor Integration

Due Date: 15/10/2008
Submission date: 17/10/2008

Start date of project: **01/09/2004** Duration: **60 months**

Organisation name of lead contractor for this deliverable: UNIFE

Responsible Person: Prof. Luciano Fadiga

Revision: **1.6**

Project co-funded by the European Commission within the Sixth Framework Programme (2002-2006)		
Dissemination Level		
PU	Public	**PU**
PP	Restricted to other programme participants (including the Commission Service)	
RE	Restricted to a group specified by the consortium (including the Commission Service)	
CO	Confidential, only for members of the consortium (including the Commission Service)	

Table of Contents

(in yellow the parts modified in this last version)

1 Introduction

This Deliverable deals with sensorimotor integration, a fundamental process linking the perceptual side of the brain with the motor one. Neuroscience of the last twenty years progressively became aware of the fact that the traditional idea of a unidirectional flow of information – from perception to action – is not true. Conversely, cortico-cortical connections are bidirectional and several evidence shows that motor planning potently modify, and sometimes filters, the incoming sensory information.

Some of the experiments here described have been carried out not only at UNIFE and UNIUP (the more neuroscience-related teams of the RobotCub community) but also at EPFL, SSSA, UGDIST, UNIHER, UNISAL, UNIZH, IST, all teams whose pedigree is essentially robotics. This is, in our view, the best demonstration in favour of the efficacy of the multidisciplinary nature of RobotCub Integrated Project.

1.1 The theoretical framework

Several lines of evidence point to a significant involvement of the motor system in supporting processes traditionally considered as `high level' or cognitive, such as action understanding, mental imagery of actions, objects perception and discrimination. The "biologically compatibility" constraint guiding the RobotCub project forces us to study these processes not only because of their scientific interest but also because our aim is to setup the artefact in a way that will allow this bi-directional information flow.

A typical example of how sensorimotor integration is used by the brain in practical tasks is provided by a population of neurons in the monkey ventral premotor cortex (mirror neurons) that discharge both when the monkey performs a grasping action and when it observes the same action performed by other individuals [Gallese et al. 1996]. Mirror neurons could provide the neurophysiological basis for the capacity of primates to recognize different actions made by other individuals: the same motor pattern which characterizes the observed action is evoked in the observer and activates its own motor repertoire. This matching mechanism, which can be framed within the motor theories of perception, offers the great advantage of using a repertoire of coded actions in two ways at the same time: at the output side to act, and at the input side, to analyse the visual percept. This matching system has also been demonstrated in humans. Transcranial Magnetic Stimulation (TMS) of the motor cortex of subjects observing hand actions made by the experimenter determined an enhancement of motor evoked potentials (MEPs) in the same muscular groups that were used by the experimenter in executing those actions [Fadiga et al. 1995]. This means that when we observe an action we utilize, as monkeys do, the same repertoire of motor representations used to produce the same action.

A further example of the involvement of the motor system in cognitive functions is given by motor imagery. Imagining a grasping action is a cognitive task that requires a conscious, detailed representation of the movement. Several brain imaging studies have shown that during motor imagery of grasping actions, premotor and inferior parietal areas are strongly activated [Decety et al. 1994, Grafton et al. 1996]. Furthermore, Parsons et al. [1995]

demonstrated by PET that implicit motor imagery (used to discriminate the orientation of visually presented hands) activates premotor and posterior parietal cortex. Moreover, Sirigu et al. [1996] showed that patients with lesions restricted to the posterior parietal cortex were selectively impaired at estimating, through mental imagery, the time necessary to perform differentiated finger movements. Taken together, all these results seem to contradict a sharp distinction between an `acting brain' and a `knowing brain'.

Among the processes traditionally considered to be `high level' or cognitive, selective attention is one of the most important. The term 'selective attention' refers to the capability of selecting a particular stimulus according to its physical properties, way of presentation, or previous contingencies and instructions. After selection, the stimulus is processed and, if convenient for the individual, acted on. A problem to solve is to understand how the sensitivity of different sectors of space can be increased in processing visual stimuli, in order to select some of them and discard others. The traditional view is that selective attention is controlled by a supramodal system `anatomically separate from the data processing systems' ([Posner and Petersen, 1990], p. 26). Like the sensory and motor systems, this `attention system' performs operations on specific inputs. It interacts with other centers of the brain but maintains its own identity [Posner and Petersen, 1990]. On the basis of data obtained from brain imaging experiments [Corbetta et al. 1990, Corbetta et al. 1991, Posner et al. 1988], it has been suggested that the attention system is not unitary but consists of at least two independent systems: a posterior one subserving spatial attention and an anterior one devoted to attention recruitment and control of brain areas involved in complex cognitive tasks [Posner and Dehaene 1994].

An alternative view of selective attention (that we favour) is that it derives from mechanisms that are intrinsic to the circuits underlying perception and action. Attention is modular, and there is no need to postulate control mechanisms anatomically separate from the sensorimotor circuits. This account for selective attention was originally formulated for visuospatial attention (premotor theory of attention; Rizzolatti and Camarda 1987, Rizzolatti et al. 1987) and it is deeply rooted in the idea that space is coded in a series of parieto-frontal circuits working in parallel and that the coordinate frame in which space is coded depends on the motor requirements of the effectors that a given circuit controls (see Rizzolatti et al. 1994). Given this strict link between space coding and action programming, the premotor theory of attention postulates that spatial attention is a consequence of the activation of those same cortical circuits and subcortical centers that are involved in the transformation of spatial information into actions. Its main assumption is that the motor programs for acting in space, once prepared, are not immediately executed. The condition in which action is ready but its execution is delayed corresponds to what is introspectively called spatial attention. In this condition, two events occur: (a) There is an increase in motor readiness to act in the direction of the space region toward which a motor program was prepared, and (b) the processing of stimuli coming from that same space sector is facilitated. There is no need, therefore, to postulate an independent control system because attention derives from the same mechanisms that generate action. Although, in principle, all the circuits responsible for spatially directed action can influence spatial attention, there is no doubt that, in humans, the central role in spatial attention is played by the circuits that code space for programming eye movements. Experiments in which the relations between attention and eye movements were either indirectly or directly tested, showed that the two mechanisms interact: Any time attention is directed to a

target, an oculomotor program toward that target is prepared. Particularly significant in this respect are experiments in which the relations between attention and eye movements were directly tested [Sheliga et al. 1995a, Sheliga et al. 1995b. Sheliga and coworkers instructed normal participants to pay attention to a given spatial location and to perform a predetermined vertical or horizontal ocular saccade at the presentation of the imperative stimulus. The results showed that the trajectory of ocular saccades in response to visual or acoustic imperative stimuli deviates according to the location of attention. Moreover, the deviation increased as the attentional task became more difficult. In a recent experiment, the role of oculomotion in orienting of attention was investigated by dissociating perceptual from motor capabilities [Craighero et al. 1994]. If a causal relationship links oculomotion and orienting of attention, any constraint limiting eye movements should abolish, or at least reduce, attentional benefits in the region of the spatial field barely reachable by the eye. On the contrary, if attention is a purely cognitive process, then no effects are expected to arise from oculomotor constraints. Subjects were submitted to a spatial attention orienting task, performing it in monocular vision and having the head rotated in such a way that the eye was kept at an extreme position in the orbit. This position limited the execution of a saccade toward the temporal hemifield, whereas it allowed saccadic execution toward the nasal hemifield. Results showed that orienting of attention was normal in the nasal but not in the temporal hemifield, indicating that eyes and attention show a common limit stop.

Whereas in primates eye movements are certainly the most important mechanism for selecting stimuli, there are also circumstances (e.g., stimuli presented very close to the face or stimuli appearing in the visual periphery) in which eye movements are not crucial for selecting stimuli in space. In these circumstances, spatial attention should depend on circuits other than those related to eye movements. In the frame of premotor theory of attention, Craighero and colleagues [2004] assumed that allocation of attention to a graspable object is a consequence of preparing a grasping movement to that same object. The authors predicted that, when a specific grasping movement was activated, there would be both: (i) increase in the motor readiness to execute that movement and, (ii) facilitation in visually process graspable objects whose intrinsic properties are congruent with the prepared grasping. In an experiment designed to investigate this hypothesis, normal subjects were required to grasp a bar after the presentation of a visual stimulus whose orientation was either congruent or incongruent with that of the bar. Results supported the hypothesis. The detection of a visual object was facilitated by the preparation of a grasping movement congruent with the object's intrinsic properties. This finding strongly suggests that the premotor theory of attention is not limited to orienting attention to a spatial location but can be generalized to the orienting of attention to any object that can be acted upon.

1.2 The organization of the document

In this Deliverable we describe experiments investigating the development and the characteristics of the capability to plan, execute and recognize actions. Three are the main experimental approaches used for this purpose: monkey electrophysiological studies based on single neurons recordings; psychophysical studies in normals and patients (both adults and children); brain imaging and transcranial magnetic stimulation studies in normals. The

presentation will follow the schema originally proposed in the Technical annex revision we presented at month 12. Thus, three main stream of research will be presented: (1) Ontogenetic cues in sensorimotor coordination; (2) Phylogenetic cues in sensorimotor coordination and (3) Schemas in artefacts for sensorimotor coordination. The experiments described here represent only one part of the work in progress. The final version of this Deliverable (D3.1b, to be presented at month 30) will give a more exhaustive description of the global picture. Some final results coming from experiments on monkey and human electrophysiology and on brain imaging of gaze sharing will be presented as well.

2 Experimental part

2.1 Ontogenetic cues in sensorimotor coordination

The results of these experiments come from a strict collaboration between UNIFE and UNIUP. Together, we have identified three main different techniques to study the development of the motor system in children (to act and to recognize actions):

1) Mu rhythm desynchronization during action observation.

2) Near infrared spectroscopy (NIRS).

3) Gaze tracking during action observation and execution

Experiments concerning point (1) are in progress and will be presented in the final version of this Deliverable at month 30. As far as (2) is concerned, art UNIFE we are actively collaborating at the setup of a new NIRS machine together with the Department of Physics at the Politecnico di Milano (Italy). The final goal of the study is to use NIRS in infants, to investigate the neural correlates of motor development (both for action execution and understanding). Moreover, the results of some experiments on crawling carried out jointly by EPFL and UNIUP, together with modelling of crawling studied at EPFL will be presented at the end of this section.

2.1.1 Mapping cerebral hemodynamics of the human motor cortex by multi-channel time-resolved near-infrared spectroscopy (UNIFE).

Introduction

Brain imaging techniques (PET and fMRI) are not usable on infants because of their invasiveness and because their require subjects' immobility. In recent years NIRS has been developed to non-invasively measure regional blood flow in infants. It allows detecting the regional modifications of blood flow by spectroscopically measuring the absorbance of low-power infrared light by regional hemoglobin concentration. In order to investigate the

applicability of the NIRS technique in the study of cognitive functions and to verify which method is the most suitable, we have conducted preliminary experiments on adults in collaboration with a group of researchers from the Politecnico di Milano (Alessandro Torricelli, Antonio Pifferi, Lorenzo Spinelli, Davide Contini), leaded by Rinaldo Cubeddu.

The problem of mapping functional activation in the human brain by optical radiation is challenging. The diffusive nature of biological tissues prevents the discrimination of absorption and scattering contributions by simple continuous wave techniques. Time domain techniques, on the contrary, are able to discriminate between them and to derive absolute values for the hemodynamic parameters in a real heterogeneous medium like the human head [1]. Moreover, relevant studies have shown that in the time domain depth sensitivity can be improved by simply exploiting the temporal information [2-4].

Here, we investigated the spatial resolution of a dual wavelength (690 and 820 nm) multi-channel time-resolved system for functional NIRS in the study of the antero-posterior extension of hand-related motor activation, and of the medio-lateral somatotopy of hand and shoulder motor representations.

Methods

Two right handed normal subjects participated to the experiment. During a preliminary mapping session, right hand and shoulder motor representations were assessed by using transcranial magnetic stimulation (TMS) [5]. The experimental session was subdivided into two tasks. The first task was aiming at investigating the antero-posterior extension of the right hand motor representation as detected by NIRS. A specially designed probe (4 source fibers and 10 collecting bundles, source-collector relative distance [rho]=2.0 cm), was placed over the right hand motor representation of the left hemisphere, perpendicularly to the central sulcus. The protocol consisted of 20 s baseline, 20 s right hand motor activity (Luria's finger tapping), and 40 s recovery. The protocol was repeated 10 times in order to increase the signal-to-noise ratio by block averaging. The acquisition rate was 1 s.The second task was designed to test the somatotopic representation of hand and shoulder motor representations by using a protocol similar to that of the previous task. The probe was placed over the shoulder/hand motor representations of the left hemisphere, along the central sulcus. The protocol consisted of 15 s baseline, 15 s right hand finger tapping or right shoulder rotation (randomized and executed according to visual instructions), and 30 s recovery. The protocol for each type of movement was repeated 5 times. The acquisition rate was 1 s. The analysis was restricted to the superior part of the probe (indicated by the yellow circle in the figure) since it was our region of interest.

Results

TASK 1: Antero-posterior extension of the right hand motor representation

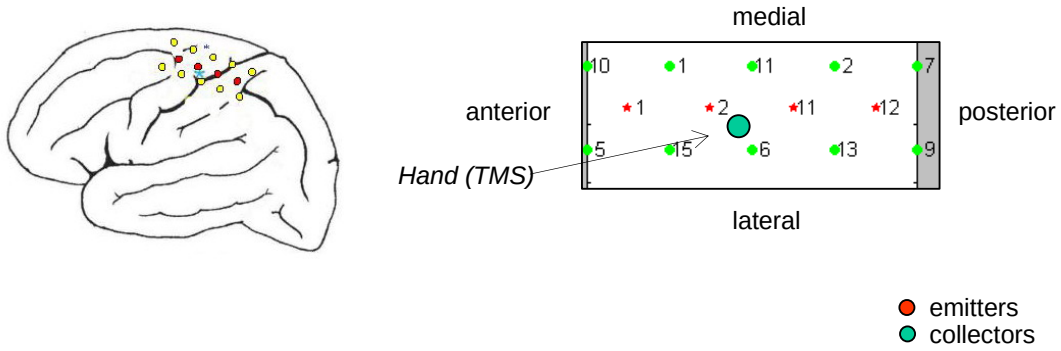

Figure 1. Blue asterisk indicates the right hand hot spot location (left hemisphere) as assessed by TMS in the subject according to the method described by Fadiga et al. (1995). On the right side, schema of the probe with the indication of the location of the hand hot spot.

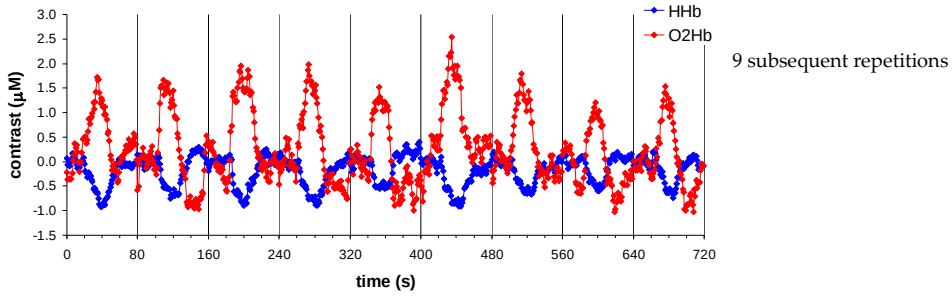

Figure 2. Deoxyhemoglobin (ΔHHb) and oxyhemoglobin (ΔO2Hb) during single trials (i.e. no block averaging) collected by a single couple of emitters-collectors during the finger tapping task.

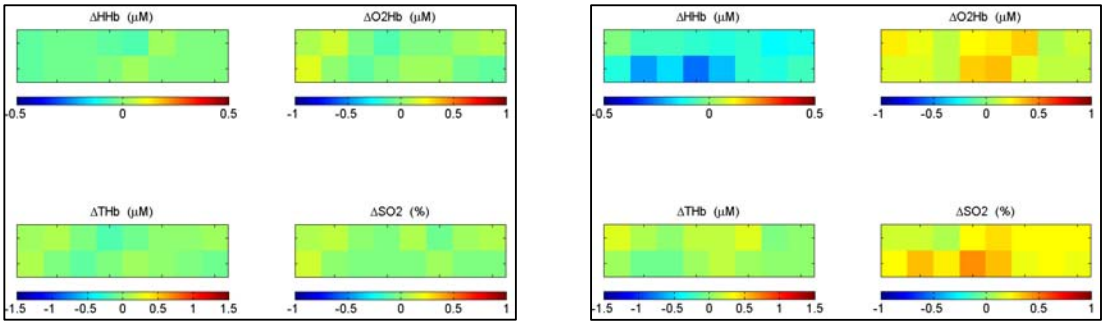

Figure 3. Spatial maps of HHb, O2Hb, THb, and SO2 concentration changes, separately presented for the baseline (left panel) and task (right panel) experimental phases (10 times block averaging).

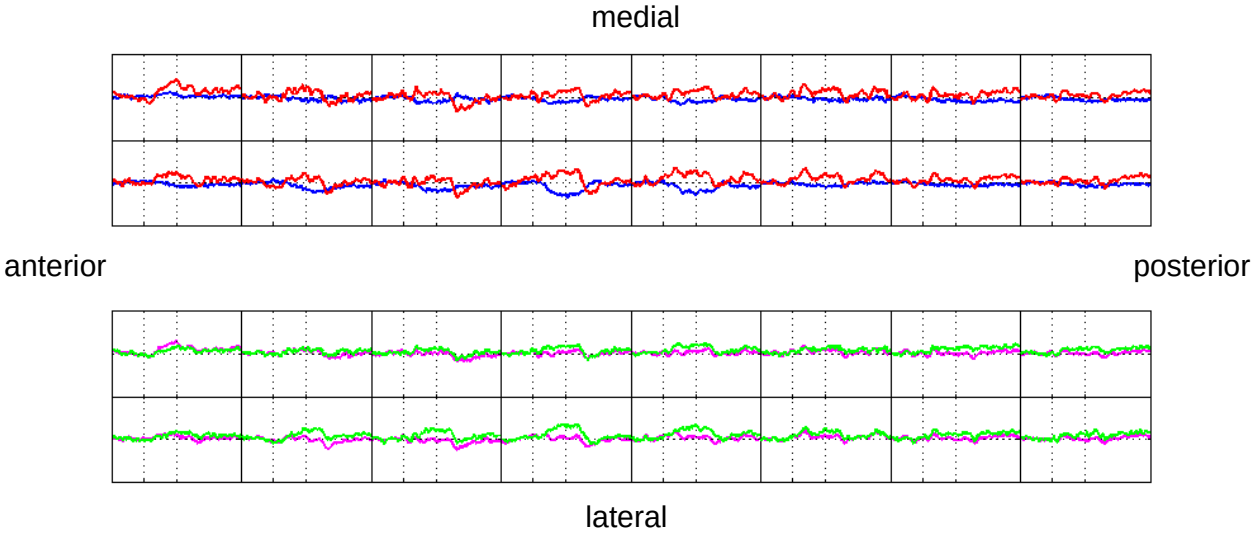

Figure 4. Average (10 trials) cerebral blood oxygenation changes in each of the 16 channels during the course of the experiment. The ordinates indicate the concentration changes of O2Hb (oxyhemoglobin, red line, ΔO2Hb -1.5 / +1.5 mM), HHb (deoxyhemoglobin, blue line, ΔHHb -1.0 / +1.0 mM), tHb (total hemoglobin, purple line, ΔtHb -2.5 / +2.5 mM), and SO2 (% of oxygen saturation, green line, ΔSO2 -1.5 / +1.5 mM). Dotted lines indicate the different phases of the experiment: 20 s baseline, 20 s task, and 40 s recovery, during time.

TASK 2: Somatotopic representation of hand and shoulder motor representations.

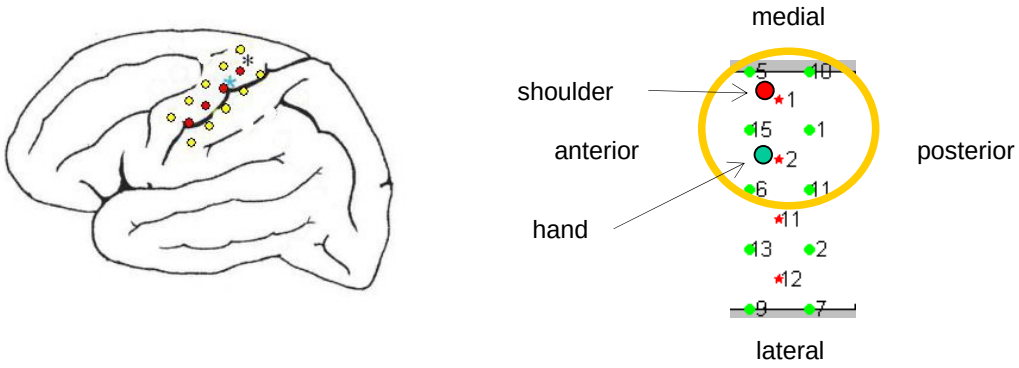

Figure 5. Blue and black asterisks indicate the right hand hot spot location (left hemisphere) and the right shoulder hot spot location, respectively, as assessed by TMS in the subject according to the method described by Fadiga et al. [5]. On the right side, schema of the probe with the indication of the location of the hand and shoulder hot spot.

TASK 3: Right shoulder rotation task

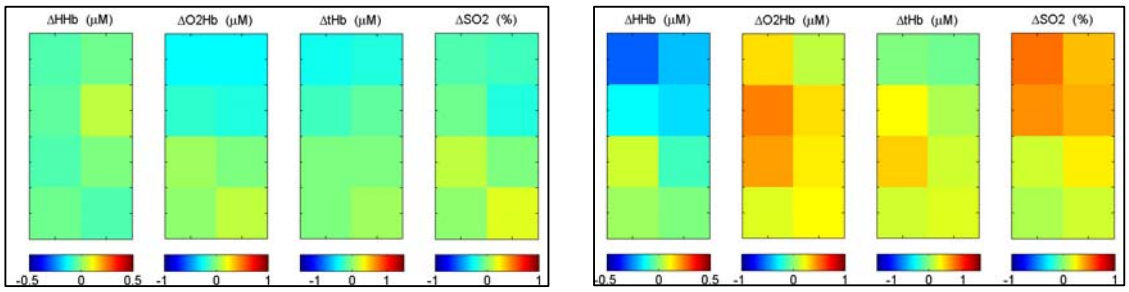

Figure 6. Spatial maps of HHb, O2Hb, THb, and SO2 concentration changes, separately presented for the baseline (left panel) and task (right panel) experimental phases (5 times block averaging).

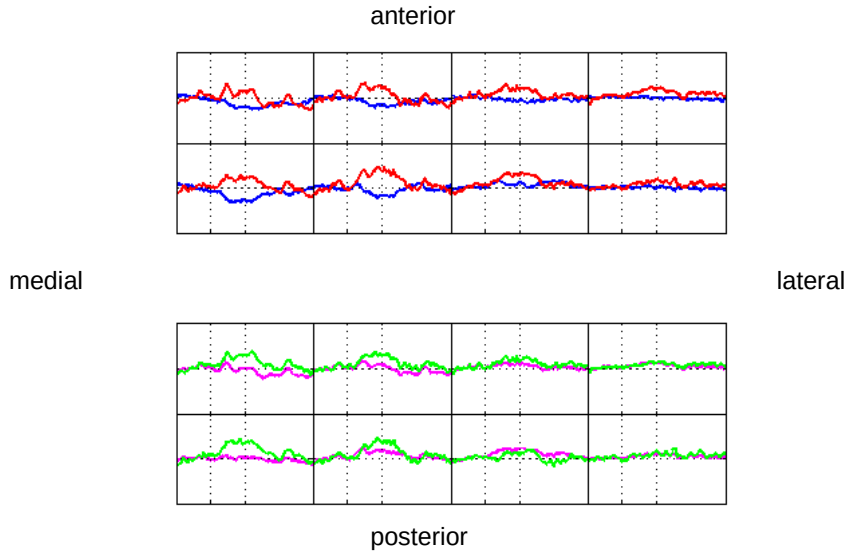

Figure 7. Average (5 trials) cerebral blood oxygenation changes in each of the 8 channels (superior part of the probe) during the course of the experiment. The ordinates indicate the concentration changes of O2Hb (oxyhemoglobin, red line, ΔO2Hb -1.5 / +1.5 mM), HHb (deoxyhemoglobin, blue line, ΔHHb -1.0 / +1.0 mM), tHb (total hemoglobin, purple line, ΔtHb -2.5 / +2.5 mM), and SO2 (% of oxygen saturation, green line, ΔSO2 -1.5 / +1.5 mM). Dotted lines indicate the different phases of the experiment: 15 s baseline, 15 s task, and 30 s recovery, during time.

Right hand finger tapping task

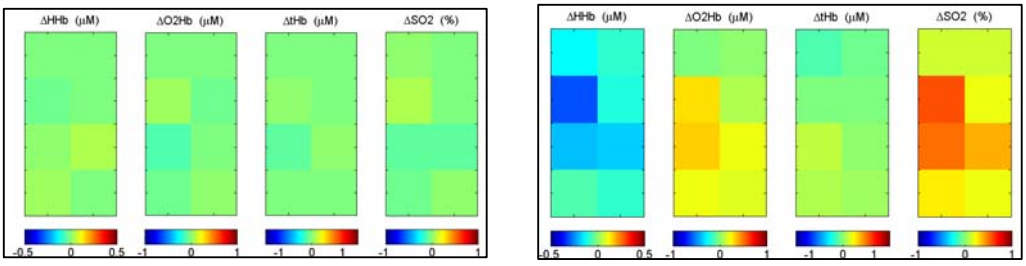

Figure 8. Spatial maps of HHb, O2Hb, THb, and SO2 concentration changes, separately presented for the baseline (left panel) and task (right panel) experimental phases (5 times block averaging).

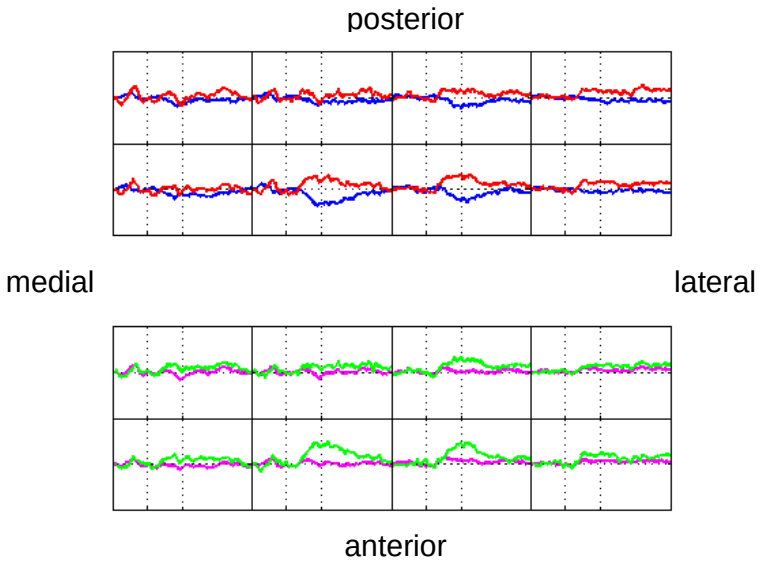

Figure 9. Average (5 trials) cerebral blood oxygenation changes in each of the 8 channels (superior part of the probe) during the course of the experiment. The ordinates indicate the concentration changes of O2Hb (oxyhemoglobin, red line, ΔO2Hb -1.5 / +1.5 mM), HHb (deoxyhemoglobin, blue line, ΔHHb -1.0 / +1.0 mM), tHb (total hemoglobin, purple line, ΔtHb -2.5 / +2.5 mM), and SO2 (% of oxygen saturation, green line, ΔSO2 -1.5 / +1.5 mM). Dotted lines indicate the different phases of the experiment: 15 s baseline, 15 s task, and 30 s recovery, during time.

Summary of Results

Results relative to the task aiming at investigating the antero-posterior extension of the right hand motor representation as detected by NIRS, demonstrated a focal increase of O2Hb and the corresponding decrease of HHb in the channels placed over the hand motor representation hot spot, determined by TMS, during the execution of a Luria's finger tapping with respect to a baseline acquisition. Results relative to the task designed to test the somatotopic representation of hand and shoulder motor representations, demonstrated a differential activation for finger and shoulder movements as detected by NIRS, when comparing right hand finger tapping and right shoulder rotation tasks.

Conclusions

In conclusion, a multi-channel time-resolved system for functional NIRS has been successfully employed to study hemodynamic response following motor activity in the adult brain. In addition, the system was able to discriminate the antero-posterior extension of hand-related motor activation and the somatotopy of hand and shoulder motor representations. Moreover, the system used in the present study is sensitive enough to significantly determine cortical motor activation in single trials. All these characteristics are strongly in favor of the possibility to use this technique in infants to study the ontogenetic development of the motor system in infants.

2.1.2 Gaze behaviour in normal and autistic children during observation of own and others' hand action (UNIFE+UNIUP).

The pattern of eye movements during action observation is the same as that recorded during action execution. In both cases, the eyes anticipate the hand and reach the target well before the arrival of the fingers. Thus, saccadic behaviour during action observation supports the direct matching hypothesis for action recognition. We decided to study the development of this predictive behaviour during action observation in developing infants (UNIUP) and in children affected by Autism Spectrum Disorders (ASD) (both UNIUP and UNIFE).

It is well known that autism spectrum disorders (ASD) are characterized by deficits in social and communicative skills. It has been proposed that the mirror-neuron system may play a critical role in higher order cognitive processes such as imitation, theory of mind, language, and empathy. Strikingly, these skills are among those mostly impaired in ASD individuals. Because of this correspondence, many have suggested that individuals with ASD may have mirror neuron system impairments, and some experimental evidence supports this interpretation. Therefore, we decided to investigate the gaze behavior of ASD children during execution of their own actions and during the observation of actions performed by others. We have tracked the gaze of 8 high-functioning autistic children while they were performing a modification of the Flanagan and Johansson paradigm, by using a version of the TOBII system that allows the recordings also during a real action (i.e. not presented by a video clip). Five normal children, matching patients for age and gender, have been tested as well as controls.

During action execution the agent's eyes never follow the acting effector, but the gaze is projected towards the end point of the action, anticipating it. More recently, it has been shown (Flanagan and Johansson, 2004) that this pro-active behaviour manifests itself not only during execution but also during the observation of action performed by others. Conversely, the presentation of moving objects, not held by hand, does not evoke the pro-active gaze behaviour. This evidence has been assumed to be a consequence of the involvement of the mirror-neuron system. Mirror neurons become however active only when observer and agent share a similar motor repertoire (see Rizzolatti and Craighero, 2004). It has been suggested that a fundamental deficit in autism could be the impairment of what has been called "the theory of mind" (i.e. the capacity to understand the intention behind the behaviour of others) (2). A full-fledged theory of mind is achieved, however, by children at about four years of age (3), while clinical signs of autism appear earlier, thus indicating that a more basic deficit should underlie the development of "theory of mind" (4). In recent years, it has been suggested that this deficit could depend on a poor development of mirror neuron system, which would be a neural precursor necessary for the development of the theory of mind. (5). Evidence coming form EEG , MEG, TMS and brain imaging data provided strong evidence that the mirror neuron system could be impaired in autistic children (6-7-8-9).

Methods

We applied four tasks to a neurologically healthy population of children, and to a group of "high-functioning" autistic children. A child with high-functioning autism fits the definition of autism but has much better cognitive and learning abilities. These children have initial difficulty in acquiring language but become then able to speak at a level appropriate for their

age. Autistic children were recruited in a centre of Paediatric Neuropsychiatry in the province of Empoli (Italy) "ASL 11". The diagnosis had been made by means of the Autism Diagnostic Observation Schedule (ADOS) (Lord et al. 1989). All subjects had an intelligence quotient (IQ) > 70, as calculated with the Wechsler Intelligence Scale for Children Revised (WISC-R). A group of 8 autistic children, 7 males and 1 female, aged 5.1 – 16.0 years (mean age: 7.1) participated to the experiment. The mean IQ of this group was of 98.7 ± 11.6 (SD). The group of neurologically healthy children that were used as a control, had IQ > 70 (WISC-R scale). A group of five children aging 5.2-11.9 years, (4 male and 1 females, mean age: 6.5) participated to the experiment. Their mean IQ was of 104.7 ± 7.7. All procedures were approved by the local ethical committee and the parents of children gave informed written consent.

Tasks: The experiment consisted in 4 conditions (see below) with 13 repetitions each (trials). Each trial started when the right hand of the participant was placed on the table in correspondence of the starting point. The four different task were:

1) To grasp with their right hand a toy placed on the table and to put it into a container, located on the table in front of them *(active condition, EXE)*

2) To observe the experimenter performing the same action with his right hand in front of them *(passive condition, Frontal Right Observation, FRO)*

3) To observe the experimenter performing the same action with his left hand in front of them ("specular" perspective-laterally reversed-) *(passive condition, Frontal Left Observation, FLO)*

4) To observe the experimenter performing the same action in lateral position: sideway to the children (the participants saw the hand of the experimenter according to their "egocentric perspective") *(passive condition, Lateral Observation, LO)*

The experimenter and the subject were sitting at a table, one in front of each other. In front of them there were a container and three objects-toys. During the "active-condition" the subject was instructed to grasp the objects, one at time, and to place them into the container. In the "passive-condition", the participants were requested to observe the same sequence of grasping-placing movements performed by the experimenter in front of them or in the lateral position. The four conditions were repeated in a pseudo-random order. All the participants performed a brief training session prior to recordings.

Experimental apparatus: During the experiment, the position of the subject's gaze was continuously recorded by using an eye-tracking device (Tobii, Sweden) and a video-camera. A transparent table with two different levels was used to run the experiment. In the lower level (behind the glass) we positioned the eye-tracking device, and in the upper plan we positioned a transparent and removable grid for the calibration. After the calibration was done, we removed the grid, so that the upper plan became the working space. Furthermore the hand/arm kinematics of the action performed by both, the subjects and the experimenter, was recorded during the whole experiment. This was done to measure the precise pattern and kinematics of goal-directed hand grasping. Indeed, autistic children might be affected in their capacity to efficiently plan goal-directed actions (see Mori et al. 2005). To this purpose, three infrared-reflecting markers were fixed to the wrist/hand of the experimenter and three on the wrist/hand

of the participants. Two markers (one on the tip of the index finger and one on the thumb) were used to measure fingers aperture during grasping. A third marker was positioned on subject's wrist to measure the transport component of the hand-reaching movements. Data were acquired by a high-speed optic tracking system (Qualysis, Sweden) which provided the contemporary 3D position of each infrared reflecting marker, at the temporal resolution up to 1 KHz.

Data pre-processing: The use of the eye-tracker to record the gaze, required a stable position of the head and a constant posture during the experimental session. We discarded part of the data, because of the difficulty to achieve this stability with young children and, particularly, with ASD children, typically presenting hyperactivity troubles, especially during the EXE condition. The object was initially positioned on a limited area of the desk and the box was not fixed on the table. Thus the trials were not performed on a standard space. In order to overcome this problem, we standardize the recordings according to a 0-1 ideal space.

Results.

In the preliminary data we present here, we restricted our analysis to the movement 'grasping the object-landing in the container' which is the most studied in the literature. After data pre-processing and cleaning, 296 valid movements were selected. The spatial distribution of wrist position in all four conditions was very similar between ASD and control subjects (movement duration and peak velocity were not significantly different between conditions). This let suppose that: 1) in FRO, FLO and LO conditions (observation) experimenter did perform similar movement in the two groups; 2) Autistics and control subjects performed similar movements (EXE condition). As a measure of pro-active gaze behaviour we determined for each trial the ratio of looking time in the goal area relative to total looking time (goal and trajectory areas) during object movement (GLT ratio). Goal area was defined as the space regions within .20 unit from the landing zone; while trajectory areas was defined as the space regions between .20 and .80 unit far from the landing zone. Therefore if subjects tracked the moving target (and hand movement is constant), the expected proportion of GLT is .20/(.60+.20)=.25. In other terms, more is the time the subject looks the target, more is her predictive behaviour.

By following this method, values of GLT exceeding significantly 25% ratio ($p<0.005$) defines a pro-active gaze behaviour. while values below it, indicate reactive gaze behaviour. Results are given in Table 2 and Figure 10.

Conditions	Normal	ASD
EXE	0.49 ± 0.08 *	0.47 ± 0.06 *
FRO	0.44 ± 0.09 *	0.34 ± 0.06
FLO	0.3 ± 0.08	0.33 ± 0.07
LO	0.33 ± 0.08	0.43 ± 0.07

Table 2. Average GLT ratio ± SEM. Asterisks indicate statistically significant pro-active gaze behaviour.

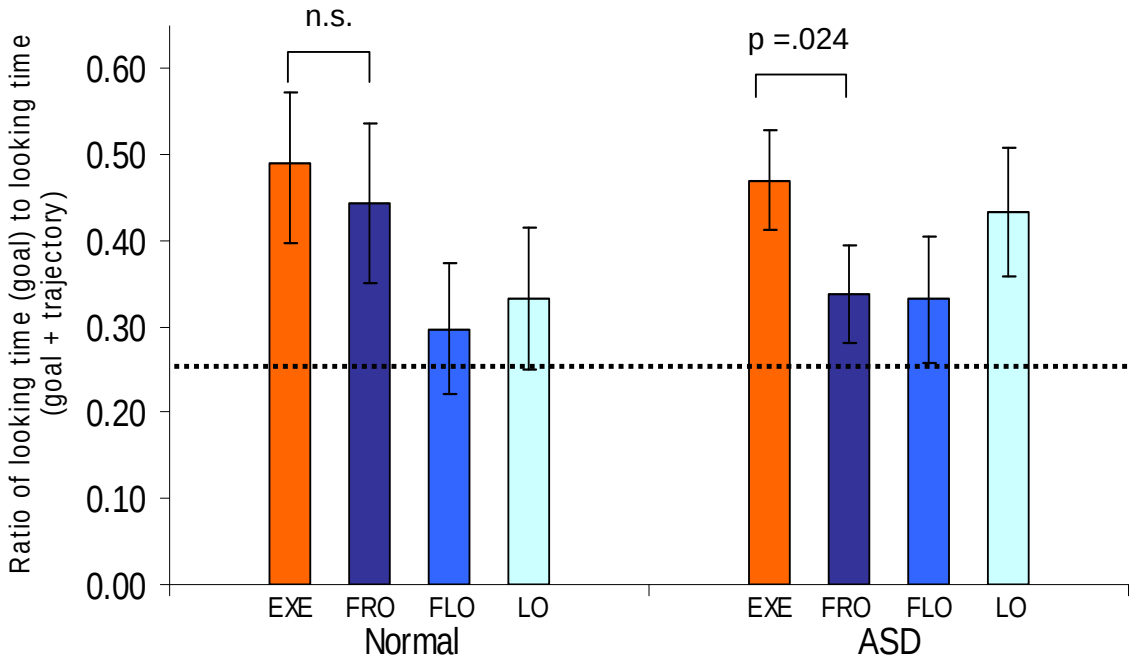

Figure 10. Gaze performance during observation of own (EXE) and other's (FRO, FLO, LO) actions. Statistics (means ± SEM) are based on all data points for controls (left) and ASD patients (right). Ratios of looking time at the goal area to total looking time in both goal are shown. The horizontal line at 0.25 shows the expected ratio if subjects were tracking the moving stimuli. Pro-active behaviour (one sample t-test for mean equal to 0.25, $p< .05$) is indicated with an asterisk the corresponding bars.

In execution (EXE condition), both normal controls and ASD patients show a pro-active gaze behaviour (*t*-test, p= 0.0238 and p=0.005 respectively). Conversely, during action observation (FRO, FLO and LO conditions), different gaze behaviours have been found. In this first phase of analysis we focus mainly on FRO condition because the higher average number of valid trials in each subject increases the stability of the single subject measurement (more trial we get for each subject, better estimate we get). In FRO condition, while data show a tendency in favour of pro-active gaze behaviour for normals (p=.052), ASD patients did not behave in a proactive way. Most importantly, while the direct comparison between EXE and FRO conditions in normals fail in reaching significance, the same comparison for ASD patients highlight a significant decrease in pro-active behaviour in FRO relative to EXE condition (paired t-test, p= 0.0241). Further interesting data comes from the comparison between EXE and LO. The statistical analysis show a tendency to the significance for normals, while ASD patient show no difference between the proactive behaviour during execution and that during observation of other's actions shown in egocentric perspective (see Figure 10).

In the present experiment, we have compared gaze and hand position during both grasping execution and grasping observation with different perspectives, in children affected or not by ASD. Preliminary analysis indicate that normal children show the same pro-active gaze behaviour both during execution (EXE) and during observation of grasping movement (FRO), while ASD patient show a pro-active gaze behaviour only during execution. This evidence is in favour of a failure of the mirror neuron system during other's action observation in ASD patients.

2.1.3 Ontogeny of locomotion: measuring and modelling crawling in infants (EPFL+UNIUP)

The neural mechanisms underlying locomotion control in humans are still not well-known. The main brain areas involved are the spinal cord, the brainstem, the cerebellum and the motor cortex. Recent studies show that like in other vertebrate animals, Central Pattern Generators (CPGs) in the spinal cord play an important role in generating and modulating the rhythmic signals underlying locomotion.

Our approach is to take inspiration from vertebrate locomotion at an abstract level and to model CPGs as systems of coupled nonlinear oscillators. This leads to the design of systems that can produce complex, coordinated, multidimensional rhythmic motor commands while being initiated and modulated by simple control signals (similarly to what has been demonstrated in decerebrated cats by Shik and colleagues in the 1960s). The CPGs produce desired trajectories (i.e. desired angles) to the PID controllers controlling the motor torques of the robot.

Our motivation is to take advantage of interesting properties of systems of coupled nonlinear oscillators and their limit cycle behaviour, namely asymptotic stability (the system returns to limit cycle after a transient perturbation), which is crucial for control the possibility to continuously modulate the periodic patterns by a few, non rhythmic, control signals, the produced trajectories remain smooth even if the control signals are abruptly changed, the system supports direct integration of feedback for modulating and synchronizing the trajectories according to sensory information (e.g. entrainment by proprioceptive signals from the body).

This CPG-based approach should make the locomotion controller easily usable by other control modules. Unless the crawling of the iCub requires specific limb placements, other modules only need to tune high-level commands determining speed and direction of crawling without having to worry about the multiple rhythmic signals that need to be sent to the actuators.

This work has 3 parts: programmable CPG, study of infant crawling kinematics, CPG-based crawling controller.

Programmable CPG

We developed a programmable CPG, i.e. a system able to automatically encode periodic signals into limit cycles. It allows control, modulation and robust integration of sensory feedback during locomotion control. We applied the system for biped locomotion control and modulation on a real robot. See our Physica D and ICRA 2006 papers, referenced below. Note that the first and main locomotion ability of the iCub will be crawling. We studied here biped walking because (1) we had biped walking trajectories available from Fujitsu for the HOAP 2 robot, and (2) because the HOAP 2 robot is not well-adapted for crawling. However, the programmable CPG offers a general method for encoding periodic trajectories into limit

cycles and can be directly applied of the control of crawling.

Study of infant crawling kinematics

There exists very few contributions on baby crawling and most of them do only qualitative analysis. We studied the kinematics of crawling babies, in collaboration with K. Rosander (Uppsala University).

Subjects: Eight infants, 9 to 11 months old have been studied. They were selected as crawlers practicing the "classic" style of locomotion using hands and knees. The parents were asked about approximate debut for crawling. Some infants were seen twice (Table 2).

Name	Birth (y/m/d)	Session 1 (y/m/d)	Body mass	Session 2(y/m/d)	Body mass 2	Start of crawling (approx.)	
Emil	050611	060324	9.5 kg	060509	10 kg	060309	
Alva	050718	060328	7kg	060510	7.5 kg	060228	
Jonathan	050613	060330	9kg			060130	
Vilmer	050614	060331	10kg			060310	
Matilda	050612	060412	11kg			060304	
Alvin	050719	060418	11kg	060516	12 kg	060328	
Elin	050623	060419	10,5kg			060216	
Oskar	050623	060508	10.5 kg			060208	
Milton	050903	060523	10 kg	060514			

Table 2. The subjects participating to the crawling experiment in Uppsala.

Procedure: When the parents came to the lab they were informed of the experiment and signed a consensus form that included permission for video recording. The parents undressed the infant and small markers were attached to the skin on places on or close to the joints (see Table 3). Three markers were put on the spine (neck, thoracic and lumbar). A hat with three markers (1 midsagittal, 2 coronal) was put on too. The complete list of the markers is the following: Head, R ear, L ear, Neck spine, Thoracic spine, Lumbar spine, R shoulder, R elbow, R

wrist, L shoulder, L elbow, L wrist, R hip, R knee, R ankle, L hip, L knee, L ankle. The markers on the wrists and knees were glued to a Velcro band. This gave stability to the critical parts that were close to the floor during locomotion. One disadvantage was that the knee markers were just above the joint. The remaining nine markers were attached with collars used for skin electrodes. When all 18 markers were properly attached the infant was encouraged to crawl on a rug (polypropylene, size 230 x 170 cm, "Arden blom" from IKEA, Sweden) on the floor. The parent and one experimenter were sitting on the floor on opposite sides of the rug using attractive toys to catch the infant´s attention. The second experimenter handled the measurements and was sitting close to the rug observing the infants behaviour.

Measurements: A motion capture system (Qualisys, Sweden) with passive markers (size 5 and 10 mm) was used in an external triggering mode. Data was collected at 240 Hz for 12 s periods. In close synchrony with the measurement sessions, a web camera monitored the infant during the trial. Before each experiment the system was calibrated. Five cameras were used, two were placed at a ceiling stand and three were placed on the floor so that the whole crawling area was covered (Figure 11). When the infant showed the intention to start crawling, the measurement was started by the second experimenter. Each trial was set to 12 seconds. Usually, 20-40 trials per infant were registered.

Data evaluation: The markers in each file (one session of 12 s) were transformed in the software and were identified. The identification was improved by comparing the web camera sessions with the movements of the markers. Short (<0.x s) intervals when one marker was hidden were interpolated using the software routines.

Results: The infants were interested and cooperative. During the trials, crawling and movements between crawling and sitting were recorded. Totally, 97 trials were selected for further analysis.

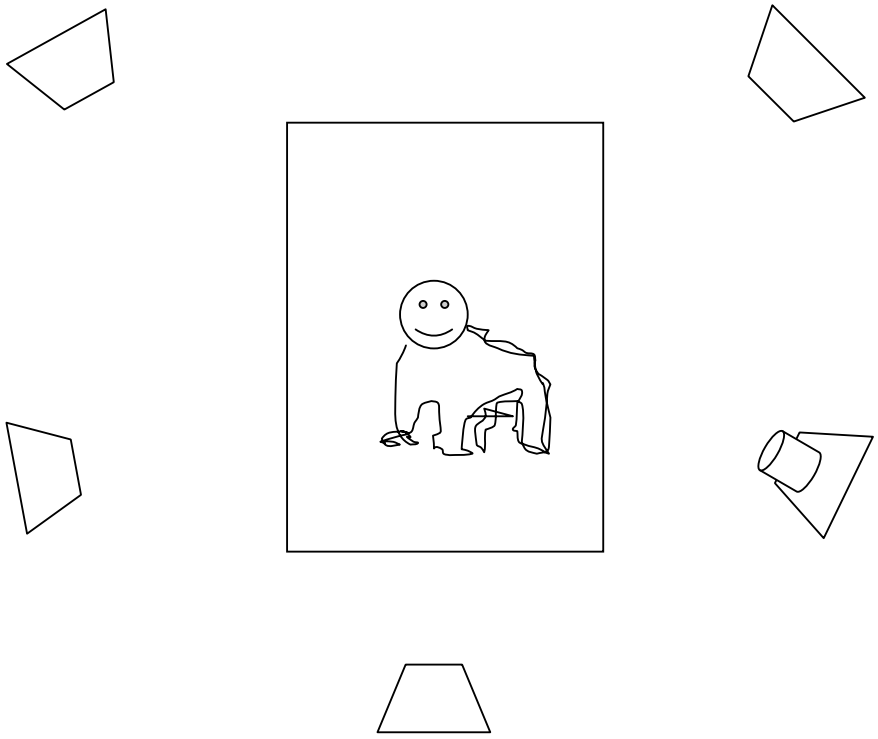

Figure 11. Schematic geometry of the experimental setup as seen from above.

The most common gait is a trot-like gait in terms of the temporal relations between the limbs. However the duration of the stance phase is much longer than the duration of the swing phase and it appears that during the swing phase of a limb, the opposite limb moves very little, which is very different from trot gait in most mammals.

CPG-based crawling controller

We developed a CPG able to reproduce the main features of crawling babies. To do so, we built an oscillator in which we can independently control the duration of the descending and ascending phases (i.e. the duration of the swing and stance phases), allowing us to shape the signal of the CPG using very simple control signals. Then we used insights from symmetric dynamical systems theory to design the CPG. We were able to reproduce the main features of real crawling and the CPG was used to control a physically realistic simulation of the iCub in Webots. Smooth modulation of the speed of the robot was also achieved. See our RSS06 paper for more details, reference below.

Note: Though we did not use the programmable CPG for crawling, the framework we developed with these two approaches is very similar and future work will show how to incorporate the properties of the programmable CPG into the crawling CPG.

Demos

We created a web page describing the crawling of the iCub and the collaboration with Uppsala (with movies), see http://birg.epfl.ch/page63115.html. See also the following page for our work and movies on biped locomotion control: http://birg.epfl.ch/page56604.html

2.2 Phylogenetic cues in sensorimotor coordination

In the framework of the phylogenetic cues in sensorimotor coordination, we are following two different lines of research:

1) Behavioural study of action observation in monkeys.

2) Single neurons recording study of grasping in monkey premotor and primary motor cortex.

3) Single neurons recording in rats.

2.2.1 Action observation behaviour in Macaque monkeys (UNIFE).

Some authors have proposed that one-year-old infants represent actions by relating relevant aspects of reality (action, goal-state and situational constraints) and assuming that actions function to realize goal-states by the most efficient means available. A series of experiments give support to this hypothesis. Indeed, the phylogeny of intentional action, namely the ability of non-human primates to interpret the other's action could be based on the attribution of a mental state, such as intention. In humans it is commonly held that the process of acquisition of mind reading unfolds during the first year of life and ends up with the ability of understanding false beliefs (i.e. to understand that other people can act by relying on beliefs that do not correspond to the state of reality). Gergely (1995) has shown that the attribution of a meaning to other people's actions can be independent from the ability to "mentalize". His experiments did show that even 12 months-old infants are able to successfully represent actions in connection with three aspects of reality (action, goal and obstacle). Such a teleological perspective (teleological stance) stems from the kernel principle of maximal efficiency, according to which actions are performed to achieve a planned final state as much effectively as possible. Uller (2003) has investigated the emergence of a teleological stance from a phylogenetic perspective by presenting chimpanzees with the experimental design that Gergley adopted with pre-verbal children. The results showed that the more evolved non-human primates are able to grasp the sense of a goal-oriented behaviour. In the present experiment we aim at verifying whether similar results can be obtained with non-human primates (macaca fascicularis and macaca nemestrina) at a lower level in the phylogeny scale. At difference with the children and chimps experiment, though, we employed as stimuli real hand actions performed by an experimenter in front of the monkey.

In order to verify the presence of action recognition in monkeys we applied a paradigm very similar to that used in infants. Gaze position in monkeys was tracked during observation of different types of actions performed by the experimenter in front of it. The experiment was subdivided into two different sessions: a “familiarization” session and a “test” session. During the familiarization session the experimenter overcame an obstacle with her arm in order to reach and grasp an object. During the test session the experimenter performed two different types of movements to grasp an object in the absence of the obstacle: “congruent” condition in which the trajectory of the experimenter’s arm is a normal one, and the “incongruent” condition

in which the trajectory of the arm simulates the presence of the obstacle.

More in detail, the experimental setting was as follows: Six macaque monkeys have been properly trained to gaze different hand actions performed by an experimenter at about 50 cm from the animal. The direction of the monkey's gaze was mapped by means of an eye-tracker (Tobii, Sweden). The experimenter's actions was simultaneously videorecorded and digitized so that it was possible to superimpose on it the monkey fixation points. Six short hand grasping actions were performed by the experimenter in front of the monkey during an experimental and a control session, respectively; the two sessions took place at 4 weeks interval. For each session, a familiarization set was presented, consisting of a short sequence (repeated 10 times) in order to refrain the animal from perceiving the sequence as a novelty event. After the familiarization set, we presented 3 blocks of 4 action sequences each (situation test), in which the familiarization scene was slightly modified. In the familiarization block of the experimental session, the experimenter's hand was overstepping an obstacle when reaching a squeeking object. During the first block of Test actions (non-congruent condition) we displayed the same action with an identical (parabolic) trajectory, but in the absence of an obstacle. During the second block of Test actions (congruent condition) we displayed the grasping action in the absence of an obstacle being performed with a straight trajectory. The control actions presented a familiarization set in which the same action of grasping was performed with a parabolic trajectory, not required by the position of the obstacle (side-placed with respect of the background). The Test conditions was identical to those selected for the experimental session.

Now a paper has been published and is attached to this Deliverable in the Appendixes Section

2.2.2 Single neuron study of visual feedback during grasping, in monkey premotor and primary motor cortex (UNIFE).

It is well known that the frontal cortex is strongly involved in action programming and motor control. In addition to the primary motor cortex (area F1) there are three pairs of areas: F3 (caudal, SMA proper) and F6 (rostral, pre-SMA) lay on the mesial wall of the frontal lobe; F2 (caudal) and F7 (rostral) form the dorsal premotor cortex and F4 (caudal) and F5 (rostral) form the ventral premotor cortex. Particularly interesting are the ventral premotor areas because of the strong visual input they receive from the inferior parietal lobule. These inputs subserve a series of visuomotor transformations for reaching (area F4, Fogassi et al., 1996) and grasping (area F5, Rizzolatti et al, 1988; Murata et al., 1997). In addition, area F5 contains neurons forming an observation/execution matching system, which maps observed actions on the observer's internal motor representations (mirror neurons). Electrical stimulation studies revealed that area F5 contains extensively overlapping representations of hand and mouth movements (Rizzolatti et al., 1988; Hepp-Reymond, et al., 1994). Single neurons studies have shown that most F5 neurons code specific actions, rather than the single movements that form them (Rizzolatti et al. 1988, Fadiga et al. 2000). It has been therefore proposed that, in area F5, a vocabulary of goals more than a set of individual movements, is stored. Several F5 neurons, in addition to their motor properties, respond also to visual stimuli. According to their visual responses, two classes of visuomotor neurons can be distinguished within area F5: canonical neurons and mirror neurons (Rizzolatti and Fadiga, 1998). Canonical neurons respond to visual presentation of three-dimensional objects (Murata et al., 1997). About one quarter of F5 neurons show object-related visual responses, which are, in the majority of cases, selective for objects of certain size, shape and orientation and congruent with the motor specificity of these neurons. They are thought to take part in a sensorimotor transformation process dedicated to select the goal-directed action, which most properly fits to the particular physical characteristics of the to-be-grasped object.

The mirror neurons form the second class of visuomotor neurons of area F5. This name was coined because of their property to "reflect" with their visual response an action executed by another individual, if the seen action is similar to that motorically coded by them (di Pellegrino, et al., 1992; Gallese et al., 1996; Rizzolatti et al., 1996). In contrast to the canonical neurons, mirror neurons do not respond to the mere presentation of objects. Thus, the vision of a real action, performed by a biological agent (the experimenter or another monkey) is essential for their activation. A mimed action, not interacting with an object, or an action executed by a tool (e.g. pliers) are ineffective in triggering most of F5 mirror neurons. Almost all mirror neurons show a certain degree of congruence between the effective observed and executed action. This congruence is very strict in about one third of F5 mirror neurons. Very recently, it has been reported that a fraction of mirror neurons, in addition to their visual response, become also active when the monkey listens to an action-related sound (e.g. breaking of a peanut) (Kohler et al., 2002). It is tempting therefore to conclude that mirror neurons may form a multimodal representation of goal directed actions, possibly involved in action recognition.

Aim.

The goal of monkey experiments was to investigate the nature of the visuomotor coupling at the basis of the "mirror" response. Our hypothesis was that mirror discharge could be initially generated by the observation of one's own acting effector, seen from different perspectives, performing repetitively the same action. We assumed that these different visual information could be associated by the brain as "common signals", having in common the same motor goal. Following this learning phase, the system could become therefore capable to extract motor invariance also during observation of actions made by others. Although the learning process described above should mainly occur during development, we postulated that also in adult animals some vestigial residuals of this visuomotor coupling could have resisted in F5 motor neurons (generally considered as devoid of any visual property). To investigate this hypothesis, we programmed a series of single neuron recordings in monkey premotor area F5 while the animal was executing a grasping movement with normal and manipulated visual information (e.g.: complete dark, brief flash of light during different phases of the movement). As a control, primary motor cortex neurons (area F1) have been recorded too.

Methods.

To standardize the grasping movement, a specially designed apparatus has been used. It consists of a box that was mounted at reaching distance (30 cm) in front of the monkey, with little pieces of food hidden inside (Figure 12).

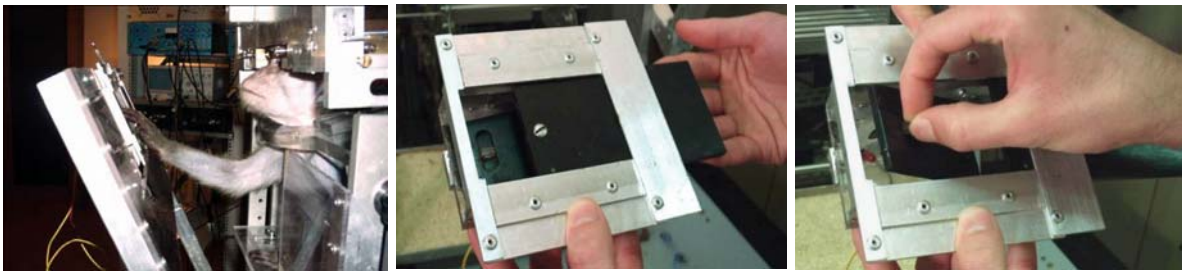

Figure 12. The experimental apparatus.

The box was covered by two doors. A more superficial one (see figure 12, center) whose opening at distance by the experimenter signaled to the monkey the beginning of the trial, and a second one (see figure 12, right), hosting a small plastic cube working as a handle. This plastic cube was translucent and back-illuminated from inside the box by a red LED in order to allow the monkey to fast reach it, also in the dark. The handle was buried inside a grove that forced the monkey to open the door by grasping the handle only by using a precision grip. When both thumb and index finger touched the handle, an electronic circuit (Schmitt's trigger) gave to the acquisition system the synchronization signal. Neuronal activity was recorded during the two seconds following handle grasping, with one second of pre-trigger acquisition.

In order to test the experimental hypothesis, recorded neurons were submitted to four conditions:
a. grasping in full vision
b. grasping in dark with no hand visual feedback
c. grasping in dark with instantaneous visual feedback before contact
d. grasping in dark with instantaneous visual feedback at object contact

In the last two conditions a very brief (20 microseconds) xenon flash illuminated the scene at two different phases of the grasping action: during hand approaching (as triggered by a pyroelectric infrared sensor) (c) and at the moment of handle touch (d).

Results.

A paper has now been written describing in details the methods and the final results of this experiment. The draft "Visual Feedback from the Own Acting Hand Modulates the Activity of Grasping Neurons in Monkey Premotor Area F5" is attached to this deliverable.

2.2.3 Single neuron study of rat premotor cortex: are there mirror neurons too? (UNIFE)

In the framework of WP3, at UNIFE we are exploring the possibility that a mirror-neuron system exist not only in primates but also in simpler animals such as rats, characterized by an intense social interaction. To this purpose, we projected and realized a multi-electrode amplifier (32 channels) and we started experiments of intracortical microstimulation and recording in rats, in collaboration with the University of Parma (Italy) and the University of Odessa (Ukraine).

Several lines of evidence demonstrate the existence in the primate's premotor cortex of a motor resonant system, the so called 'mirror-neuron system', firstly described in the rostral part of monkey ventral premotor cortex (area F5). Mirror neurons discharge both when the animal performs goal-directed hand actions and when it observes another individual performing the same or a similar action (Rizzolatti et al. 1999; Rizzolatti et al. 1996). More recently, in the same area, but more ventrally, mirror neurons responding to the observation of mouth actions have been found. Most of mouth mirror neurons become active during the execution and observation of mouth ingestive actions such as grasping, sucking or breaking food as well as of communicative mouth actions, such as lipsmacking (Ferrari et al. 2003). Mirror neurons are not limited to premotor cortex but have also been found in area PF of the inferior parietal lobule, which is bidirectionally connected with area F5 (Fogassi et al. 1998). Although at the present there are no studies in which single neurons have been recorded from the mirror-neuron areas in humans there is, however, a rich amount of data proving that a human mirror-neuron system does exist. Evidence comes from neurophysiological and brain-imaging studies (Buccino et al. 2001; Fadiga et al. 2005; Avikainen et al. 2002, see Rizzolatti and Craighero 2004 for a review). This unified representation may subserve the learning of goal-directed actions during development and the recognition of motor acts, when visually perceived.

The existence of multiple motor and premotor cortical areas that differ in some of their properties is well known in primates, but is less clear in small animals. In rats, intracorticali microstimulation reveals in the frontal cortex two separated motor representations of the anterior limb (Neafsey et al. 1986) which are located in different cytoarchitectonic areas (Rouiller et al. 1993) and receive different cortical and thalamic inputs (Wang and Kurata 1998). Some literature data (Neafsey et al. 1986; Rouiller et al. 1993) suggest that these areas (called M1 and NMC, respectively), might be the homologues of primate's primary motor and premotor cortical areas. In fact, NMC seems to participate in preparation and performance of complex coordinated movements by participating in programming and planning of movements. In addition, reciprocal cortico-cortical connections of the rostral forelimb area (RFA) share some pattern with the hodology of primate's motor areas, suggesting that rat's RFA may be considered a far precursor of primate's supplementary/premotor cortex (Wang and Kurata 1998). However, data about the functional characteristics of premotor cortex in rats are not numerous and, more importantly, nothing is known about the existence of motor-resonant systems, like primates' mirror neurons. On the other hand, rats continuously act on objects, interact with other individuals, clean their fur or scratch their skin and, in fact, actions represent the only way they have to manifest their desires and goals. It is therefore plausible that,

considering their manual dexterity and their strong social behaviour, these animals possess some mirror-like neurons in their premotor cortex.

In recent years a new paradigm of learning in small animals was developed through observational training, in which rats repeatedly observed companion rats performing different spatial tasks (Leggio et al. 2003). In some of these experiments animals were actually tested in the tasks they had previously only observed. The results obtained indicate that rats can learn complex behavioral strategies by observing some conspecifics performing the same task. Furthermore, acquisition of the single facets that form the behavioral repertoire can be separately studied as well as the role of particular brain areas (Petrosini et al. 2003). It's well known the ability of rats to manipulate food as well as their capability to retrieve food also when is attached at the end of a long string. (Molinari et al. 1990; Zhuravin and Bures 1988). Thus, a number of such behavioral tasks can be used to investigate electrical activity in the premotor cortex and to elucidate the role of mirror resonant system in rats in these conditions.

Considering that the development of the motor control during ontogenesis is one the most actual problems in the neurobiology and physiology. Despite this interest, only few data have been obtained on functional maturation of motor areas in rat pup cortex (Golikova, 1990). The discovery of mirror neurons in rat's premotor cortex could fundament to study ontogenetic peculiarities of motor resonant system formation. Although extracellular single-unit recordings in restrained, anesthetized animals have long been used in neurophysiological investigations, more recently, modified methods of single-unit recordings in freely behaving animals have converted this classic approach to a powerful new tool to study motor and cognitive behaviours. Another newly developed technique, the multi-electrode single-unit recording in freely behaving animals, is even more powerful in neural circuit studies. With this sophisticated approach, patterns of electrical activity of individual neurons from different areas forming a specific neural circuit can be measured simultaneously during specific behavioural events. This method is therefore indicated to analyse changes in the spatiotemporal patterns of neuronal activity related to goal-directed behaviours.

Methods

Behavioural paradigm and equipment: The main goal of the experiments is to record neuronal activity in rats during hand action execution and observation. To reach this goal, we composed our activity from two different options. The first one was dedicated to design and build a special cage in which rats have to perform free behaviours while the neuronal electrical activity is recorded. This cage must contain two animals, the actor and the observer and, has been conceived in order to allow the observer to easily see the performing rat through a transparent wall. The second task that we carried out was related to proper signals acquisition and analysis. The cage was built with Plexiglas. Dimensions are: length=80 cm, height=45 cm and width=40 cm. The cage is divided into three compartiments by walls made of the same material (Fig. 13, A). The first (equal to ½ size of the cage) is for the rat from which action observation-related neuronal electrical activity has to be registered. Taking into account the big mass of the wires and connectors coming from the microelectrode array connecting the array to the preamplifier and to the amplifier, we designed a special mechanical arm which holds these wires keeping and balances their weight. The remaining space inside the cage was then divided

into two further sectors (see Fig.13, B).

Figure 13. The cage for training and neuronal recording. **A**, frontal view; **B**, top view. The leftmost sector shown in B contains the observing rat; the lower-right sector contains the actor rat which retrieves food from the container visible in the separation.

The partition between these two sectors has one small window (diameter, 25 mm; distance from the floor, 70 mm) allowing the access to a small platform attached to the separation wall. During the experiments a piece of food is positioned on the platform, close to the window, and the actor rat has to grasp this food with its forearm (see Fig. 14, some coloured keys are placed on the platform to make it evident).

Figure 14. Left, the food-containing platform. Right, the cage hosting the rat #1 (left side, the 'spectator') and #2 (right side, the 'actor').

All the rats pertaining to the experimental group (Long-Evans strain) have been previously trained to grasp the pieces of food through the window. The experiments were performed daily from 10.00 to 12.30 a.m. after light food deprivation (food was removed from the cage at 6.00 p.m. the day before the experiment). On average, each rat remained inside the cage for 46±6 min and performed 94±13 grasping movements. The second rat (which also underwent the same food deprivation) was looking at the conspecific from the left compartment of the cage.

The second part of the work consisted in the setup of the recording apparatus. Utah microelectrode array (3x3 mm array containing 36 microelectrodes, Cyberkinetics Inc., USA) have been selected for the experiment (see Figure 15). The insertion of the microelectrode array was performed in deep anaesthesia induced by i.m. ketamine by using a specially designed pneumatic gun (Fig. 16, A) and the multipolar connector was screwed to the skull by using four titanium screws. The operated rats were ready for the experiment after a 7 days recovery period.

Figure 15. The Utah 6x6 microelectrodes array (**A** and **B -** bottom and side views, respectively).

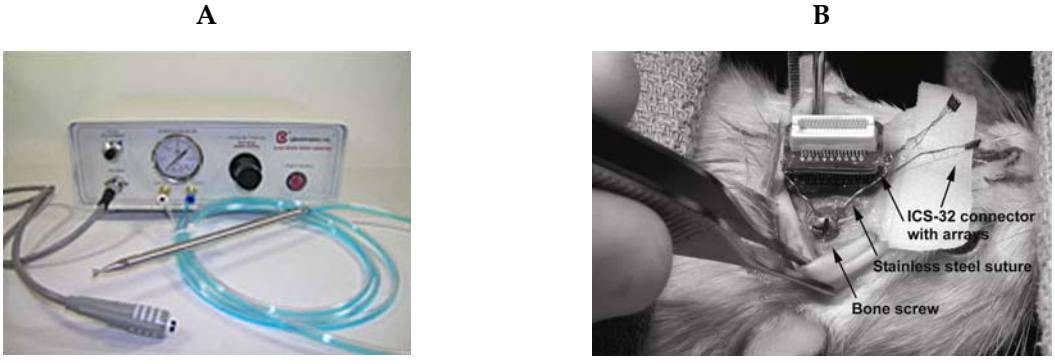

Figure 16. A, the pneumatic device used to push the microelectrode array inside the cortex minimizing tissue damages. B, the connector screwed to the skull.

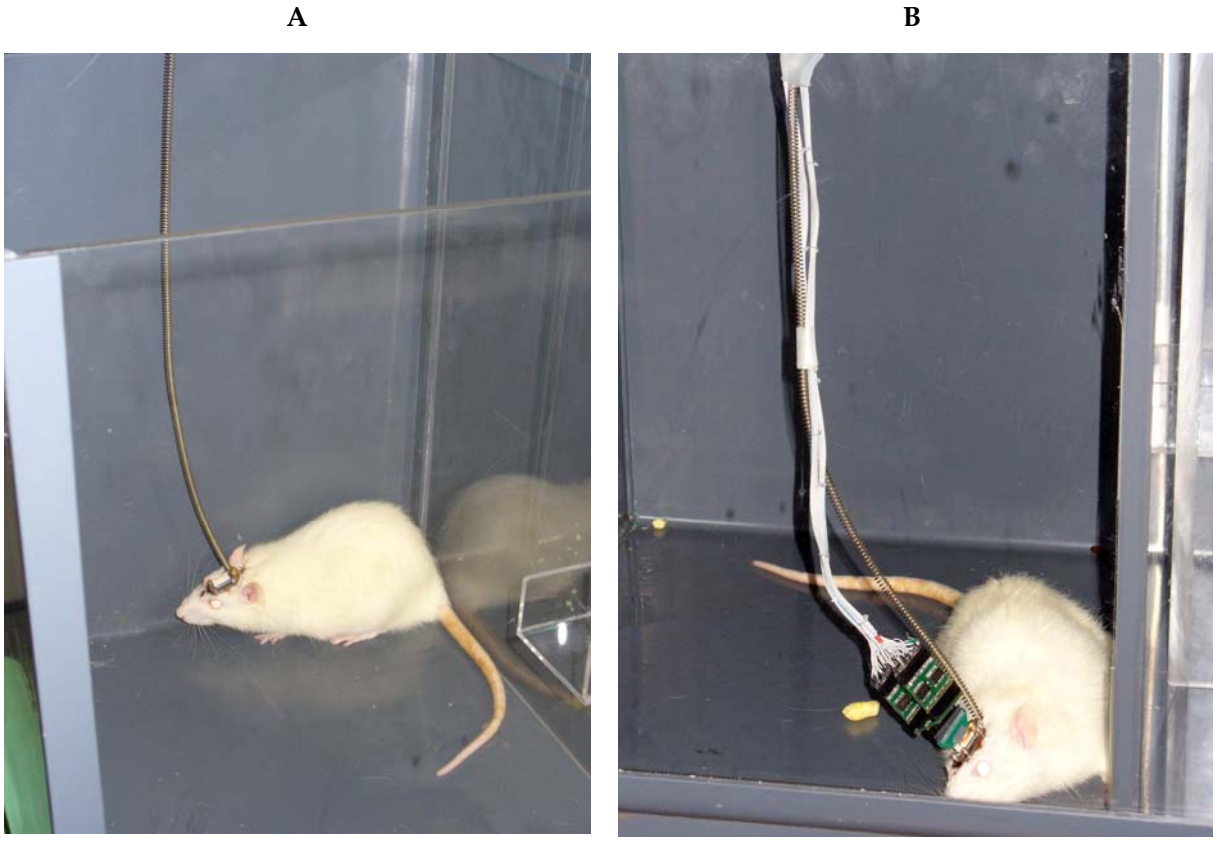

Figure 17. The preamplifiers connected to the head of the rat during recordings. Note the spiral spring providing the necessary rigidity to the system

Electronics: A 32-channels differential amplifier (with respect to a common reference) was designed and built at UNIFE. The data acquisition system for recording and processing neural signals for the 32 extracellular electrodes could be easily extended up to 128 extracellular electrodes by additional modules. Acquisition of signals is triggered by the 'actor' rat by means of a specially designed TTL-trigger (Fig. 9). The acquisition starts at the moment at which the rat touches the food. Miniature low-noise and low input bias current preamplifiers (based on TLC 2272) were fixed on the head of the animal before experiments and connected to the multielectrode microarray through a ICS-32 connector (Ciberkinetics, Inc.) (Fig. 17). After the preamplification stage, the signals reach the amplifier by a thin and flexible 36-wires flat cable. The full amplification gain has been set to x10000. The main unit containing the last-stage amplifiers (fully battery powered), is composed of four compact 8-channel processing boards (Fig. 18). The front-end modules amplify the signals and transmit them to a host PC system via a National Instruments SH100100 shielded cable. A Digital Acquisition Card (PCI-6071, National Instruments, 16-Bit, up to 1.25 MS/s, 64 analog inputs), was used to digitize the input signals. In our configuration, 32-channels were reserved for the acquisition of signals from

electrodes, 1 additional channel was used for the trigger and 2 channels were used as technical references (to control the power supply voltage and current).

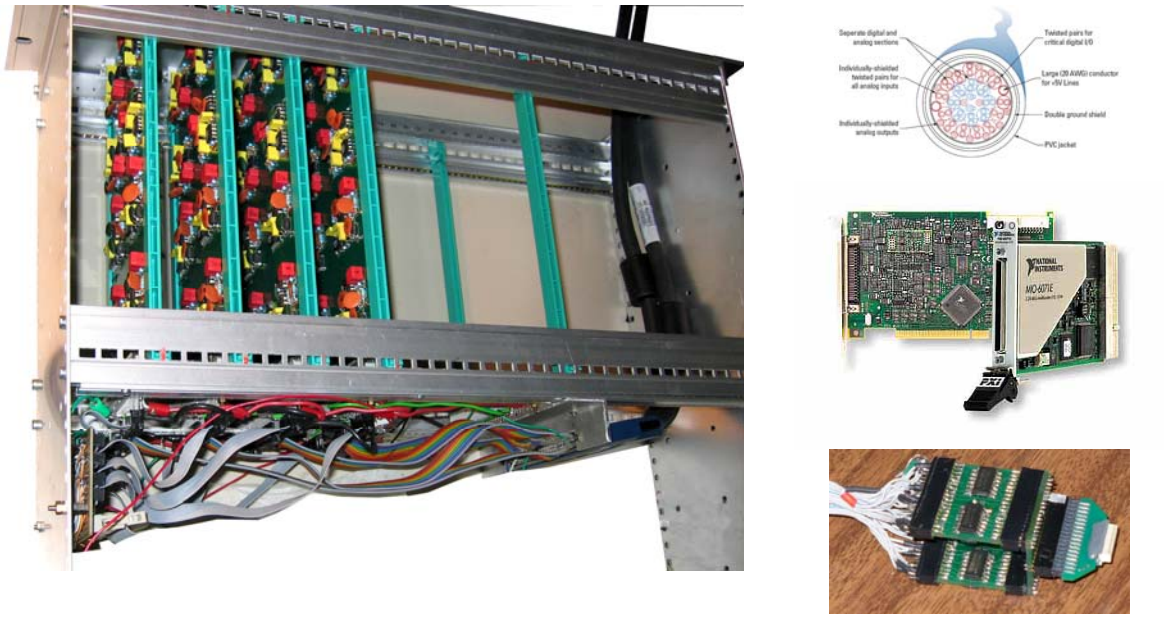

Figure 18. Overview of the multichannel acquisition system for single unit recordings in small animals. Left: the main unit, with 4 boards each hosting 8 last-stage x 10,000 amplifiers. Its rightmost compartment is reserved for the batteries. Right, upper: the shielded cable connecting amplifiers and D/A Converter (SH100100, National Instruments). Right, middle: Digital Acquisition Card (PCI-6071E, National Instruments). Right, lower: preamplifiers head stage (2 boards hosting each 16 preamplifiers connected to a miniature ICS-32 male connector).

Software: The software interface we setup at UNIFE runs on a PC (Windows XP Pro) allowing the user to configure the data processing, to visualize and to analyze the incoming data. The graphical interface is user-friendly and is entirely written in LabView 7.0 (National Instruments Inc.). In order to simplify the description the software package will be called here as 'Neuro-RAT'. The flexible digital architecture of the Neuro-RAT program allows the user to perform a variety of different on-line and off-line analyses, from simple data streaming and storage, to on-line filtering and spike sorting. The program contains three main parts: a) monitoring; b) acquisition; c) analysis.

The Monitoring part is designed for real-time observation of the activity as recorded from all the recording microelectrodes shown by colour-coding the neural activity (Fig. 19). It is therefore capable to detect spikes in all active electrodes and, moreover, to monitor one selected channel with different timescale. We found colour-coding rather helpful because it allows to quickly select and display the electrodes showing the better correlation between neuronal discharge and animal behaviour. At the same time, it helps to determine electrodes showing

noisy or corrupted activity. Another interface window (Fig.19, B) allows to visualize raw-signal from 8 different electrodes user-selectable from the 64 array.

A **B**

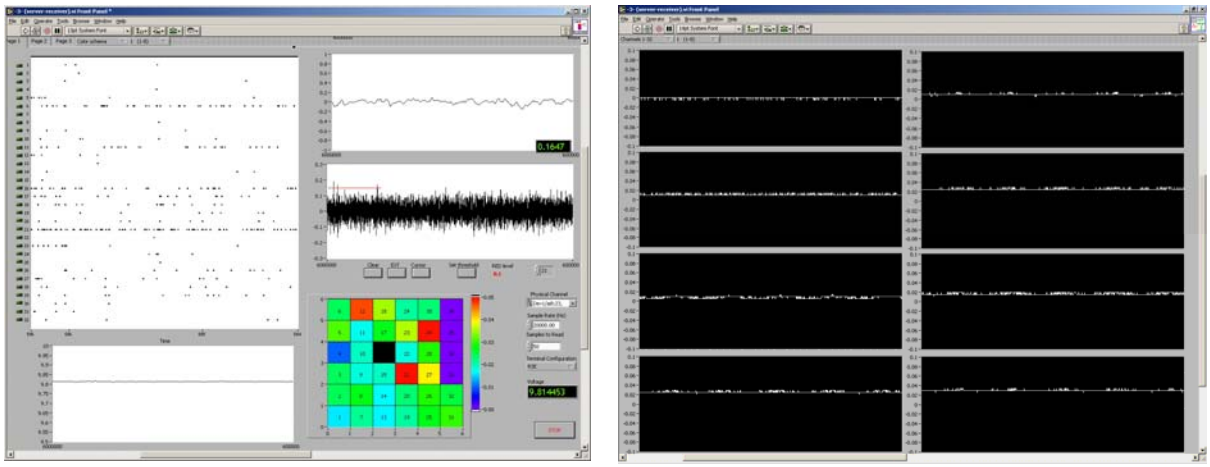

Figure 19. The main interface windows of the Monitoring component of Neuro-RAT. Note in A the color coded array where each position shows the activity of the corresponding microelectrode.

A schematic view of the Acquisition and Analysis component of Neuro-RAT is shown in Fig. 20. The Analysis part of Neuro-RAT allows to separate single units from polispike recordings and its Interface window is shown in Fig. 21.

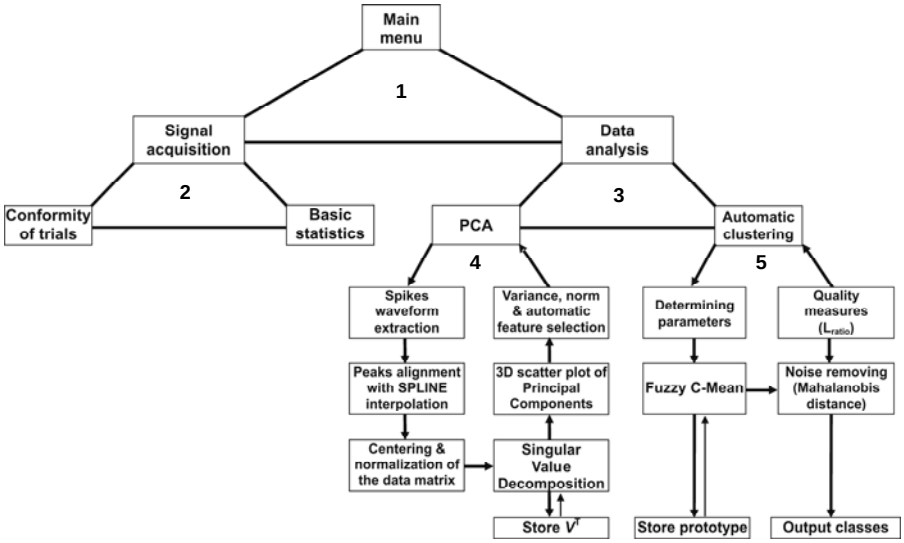

Figure 20. Block-diagram of Aquisition and Analysis part of Neuro-RAT program. The main menu (1) that is at the top level of the program, allows user to initiate new records (2) and to get fast access to any stage of the data processing (3). All other modules of the program are loop-structured and prompt the user to execute the procedure when necessary. Dynamic links between modules and storage of critical parameters of during PCA (Principal Components Analysis, 4) and FCM (Fuzzy C-Mean, 5) allows the program to solve the invariance problem during Principal Component Analysis, automatically select the features to be used in classification, to choose the best settings for clustering (new or previously calculated for a given recording site) and to remove the noise.

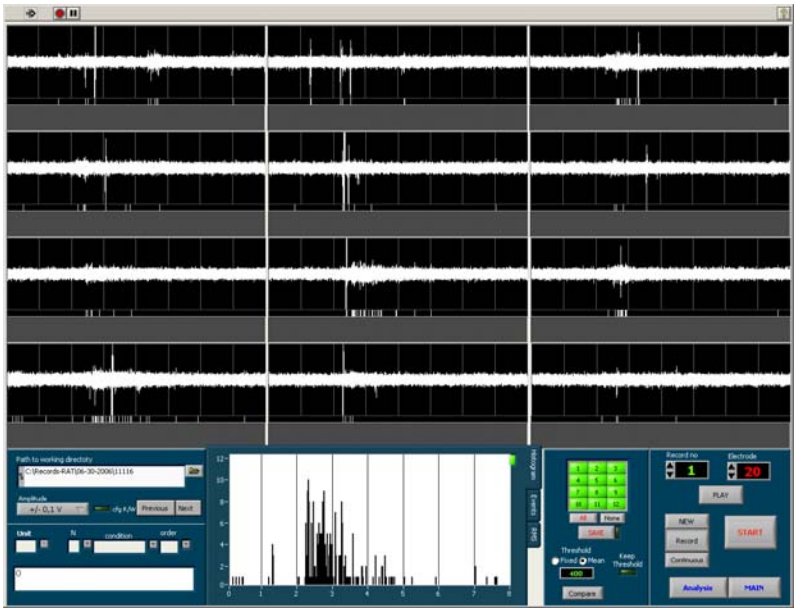

Figure 21. Interface window for the Data acquisition component of Neuro-RAT. The architecture of the user-interface window showing polyspikes acquired during twelve trials is shown. Raw data from the electrode and additional hardware information (i.e. trigger signals) are extracted and visualized. The resulting peristimulus histogram of spikes occurrence (as revealed by the spike sorting module) is shown below the rasters.

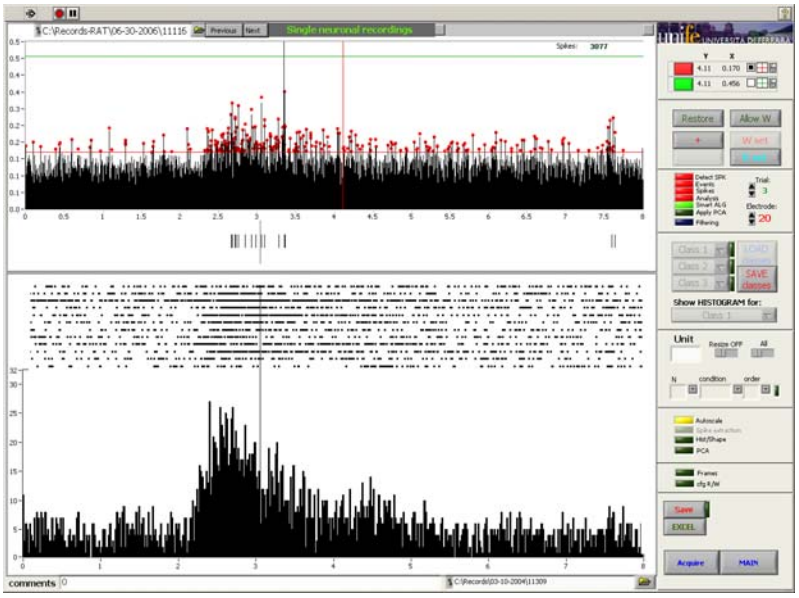

Figure 22. Interface window for the Data Analysis component. Top, the interactive thresholding used for the spike sorting algorithm. Bottom, the peristimulus histogram built from the spikes selected by the thresholding procedure. Note that this amplitude-threshold criterion is too permissive and pools together spikes coming from different neurons.
To obtain in-depth spike sorting, a dedicated part of Neuro-RAT performs Fuzzy C-Mean Classification of Principal Components in multi-dimensional space.

It should be stressed that, the possibilities and functions of the Neuro-RAT software are integrated by filters, smoothing algorithms signal and other useful math tools, implemented available when needed.

Current state of the art and perspectives:

1) Preliminary exploration and functional characterization of rat premotor cortex by intracortical microstimulation: done.

2) Setup of the training procedure of Long-Evans rats: done.

3) Setup of surgical implant: done.

4) Readiness of preamplifiers: 100%

5) Readiness of last-stage amplifiers: 100%

6) Readiness of acquisition hard & software: 100%.

7) Readiness of analysis software: 100%.

The intracortical microstimulation mapping study, done in collaboration with University of Parma confirms availability in the frontal cortex of two separated motor representations of the anterior limb (M1 and RFA), which are located in different cytoarchitectonic areas and receive different cortical and thalamic inputs. In some recent studies it was shown that reciprocal cortico-cortical connections of the Rostral Forelimb Area (RFA) (figure A) share some pattern with the hodology of primate's motor areas (Nudo and Frost, 2006), suggesting that rat's RFA may be considered a far precursor of primate's supplementary/premotor cortex (Wang and Kurata 1998).

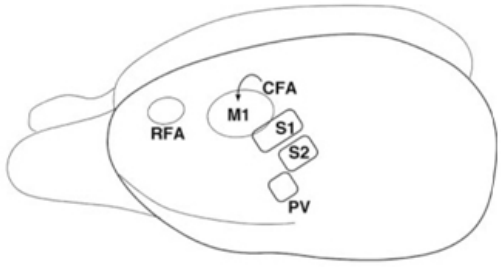

Figure A. Schematic view of somatosensory and motor areas in rodents.

On the other hand, rats continuously act on objects, interact with other individuals, clean their fur or scratch their skin and, in fact, actions represent the only way they have to manifest their desires and goals.

During the fourth year of the project, we optimized the setup and, as programmed, we started neuronal recordings with good success.

The main achieved objectives are:

a) hosting cages for 'spectator' (figure B, right side) and 'actor' (figure B, left side) animals;
b) miniature high-impedance preamplifiers for single-unit acquisitions (32 channels) (figure C);
c) specialized acquisition and analysis software, including on-line spike sorting module.

Figure B. The cage for training and neuronal recording

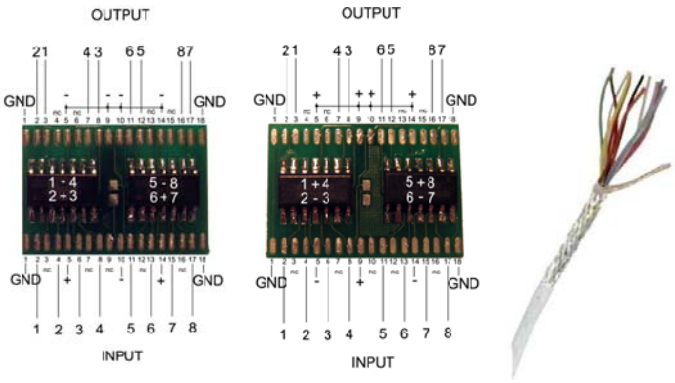

Figure C. New miniature low noise and low input bias current preamplifiers (based on the TLC2272 series of OPA, shown at the left side); main unit containing last-stage amplifiers (at the right) connected by thin flexible sub-miniature cable 12xUAN3807 TNU (INDUSTRIFIL, France) ∅ 1.52 mm (in the center of the figure).

Our special attention was focused on the reliability of the system. For this purpose we have developed and successfully tested our own supraosteal adapter (figure D), which was implanted by using commercial dental implant system (MIDPLANT, HDC srl.).

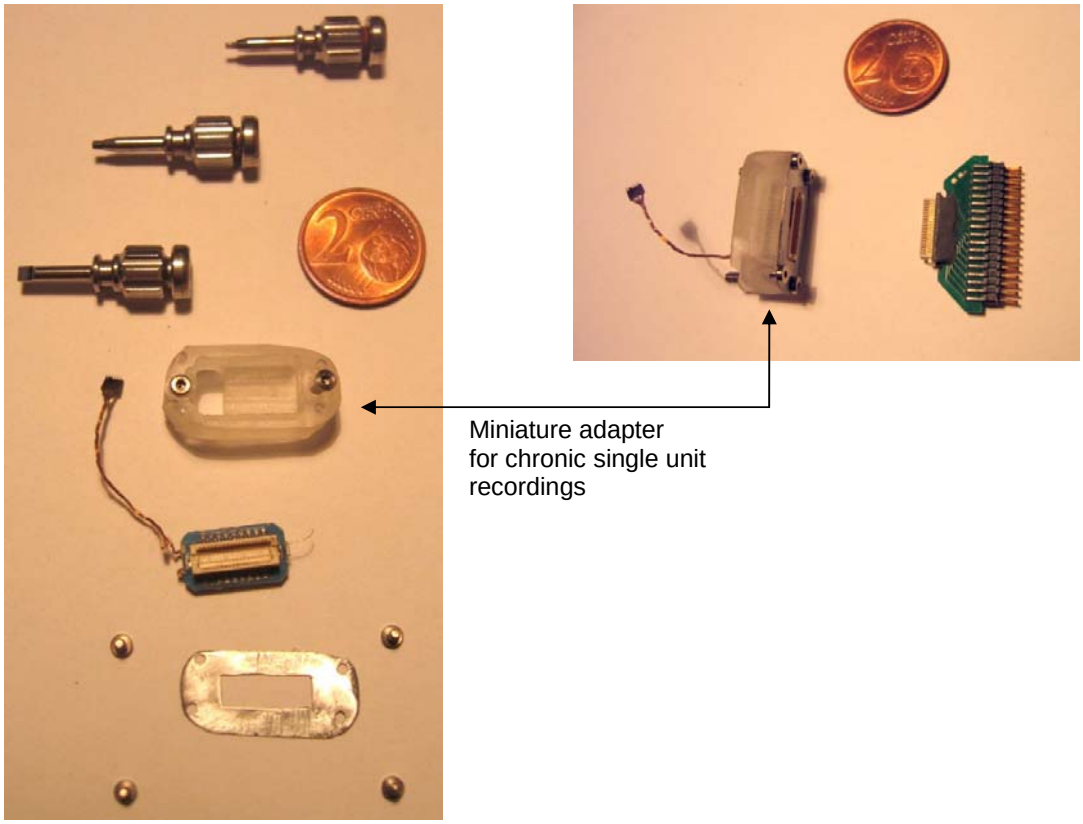

Figure D. Supraosteal construction for ICS-32 connector for chronic recording free behaving rats

The surgery protocol has been modified and markedly improved (see below: figure E).

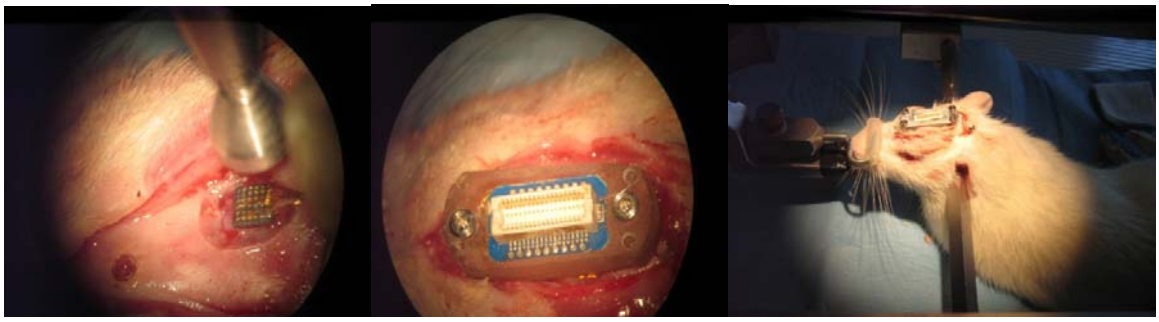

Figure E. Surgical procedures. A – transdural insertion of the microarray; B - mounting of the of assembled superosteal construction.; C – closing of ICS-32 connector and plastic adapter attached to the skull.

Preliminary result shows excellent stability of mentioned superosteal implant over 3 month after surgery. Test acquisitions indicate good quality and noise-tolerant electrical activity enabling an isolation of single neurons (figure F).

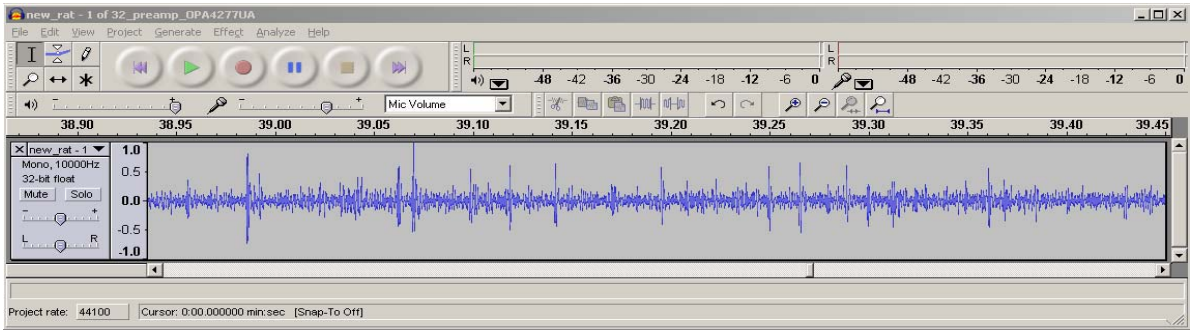

Figure F. An example of recording signal (0,5s interval of channel no. 8 is visualized by using Audacity software).

Important modifications in the custom acquisition and analysis Neuro-RAT software were introduced. Namely, in addition to the previously described spike sorting procedure, the cluster's validation module based on ISI distribution was added (figure G).

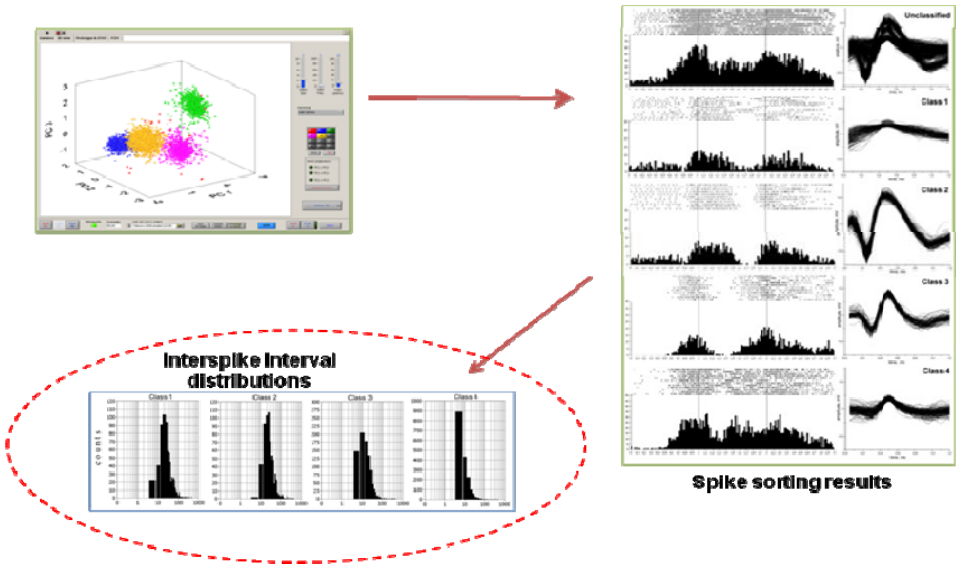

Figure G. The validation of the quality of the isolation of single units based on ISI interval distribution.

New on-line Fuzzy C-Mean spikes classification procedure in the Principal Components feature space was implemented in the Neuro-RAT software and successfully tested with simulated datasets (figure H).

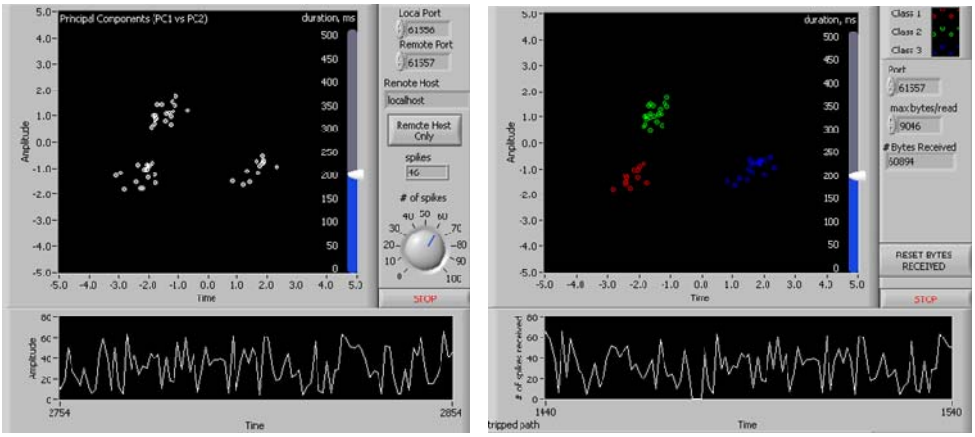

Figure H. DEMO version of 'Server' (VI 1) and 'Client' (VI 2) modules of the on-line FCM-classifier (downloadable from http://neurolab.unife.it/andrey/programs.htm)

The project is proceeding as expected. The extensive recordings of at least four animals in paradigm condition will be completed by the end of the last year.

2.3 Schemas for artefacts

2.3.1 Cortico-spinal (CS) excitability during interception with precision grip (UNIFE)

Interception in humans is a complex visuo-motor task that requires in few hundreds of milliseconds to detect and process visual motion information, to estimate future position of objects in space and time, to transform visual information into an appropriate motor action and to trigger this action in advance, to compensate for physiological and biomechanical delays.

Despite this complexity, humans demonstrate rather good performance in interceptive actions, especially in high-speed ball games (Bootsma & van Wieringen, 1990; McLeod, 1987) but also in laboratory environment (Day & Lyon, 2000; Soechting & Lacquaniti, 1983). One of the critical point is to be able to estimate the time remaining before contact (or time to contact, TTC) in order to trigger the action at the right time. Thirty years of research in this field has led to the proposal that humans use anticipatory mechanisms based on on-line visual information (Lee, 1976) that can be combined with *a priori* implicit knowledge of the rules of physics for the target motion (Lacquaniti, Carrozzo & Borghese, 1993; McIntyre, Zago, Berthoz & Lacquaniti, 2001). By this mean, an estimate of TTC can be updated and improved on line from object appearance until the time at which the action must be triggered.

If the psychophysics of this mechanism is well documented, our knowledges in the physiology of interception are rather poor. However, recent experiment in monkeys ((Merchant, Battaglia-Mayer & Georgopoulos, 2004; Port, Kruse, Lee & Georgopoulos, 2001)) have shown that the activity of neurons in the primary motor cortex (M1) during interception is modulated by the stimulus parameters and especially by an estimate of TTC. At UNIFE we began a series of experiments in order to investigate the excitability of the cortico-spinal (CS) system in humans during the interception of a falling object and its relationship to the target parameters. The hypothesis is that CS excitability should increase as the estimate of TTC is updated until it reach the threshold value at which the muscular activity is triggered.

It is known that action, observation of action and internal simulation of action share some common neural mechanisms and substrate in humans (Decety, 1996; Fadiga, Fogassi, Pavesi & Rizzolatti, 1995; Rizzolatti & Craighero, 2004). Moreover, it has been shown that the timing of simulated actions is similar to the timing of real actions (Decety, Jeannerod & Prablanc, 1989) and that the temporal parameter of actions are coded in motor cortex during action observation (Gangitano, Mottaghy & Pascual-Leone, 2001). Thus, a second aspect of the project was then to determine if similar modulations of the CS excitability could be seen during execution, observation and simulation of an interceptive action.

Methods

We used transcranial magnetic stimulation (TMS), as this technique has already shown to be relevant for testing CS excitability modulation in all these tasks (Fadiga et al., 1995; Fadiga et al., 1999).

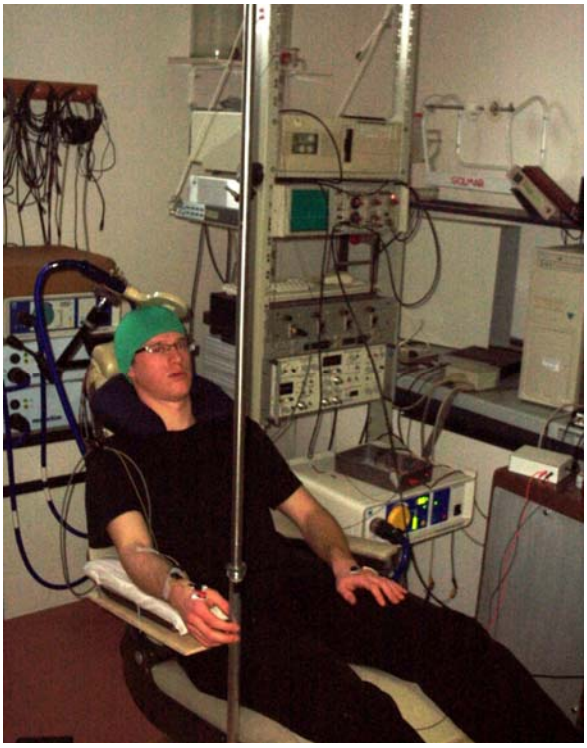

Figure 23. The experimental setup

To this purpose, single pulse TMS applied at different timings during the fall of the target was used to assess the time-course of CS excitability through the amplitude of moto evoked potentials (MEP). MEPs were recorded from the right first dorsal interosseus (FDI) muscle while the subject try to intercept with a precision grip a bar sliding down along a vertical bar (see Figure 23). In a first experiment, single pulse were delivered at -200 ms, 0 ms, +100 ms and +200 ms relative to the release of the target bar. CS excitability was computed as MEP area and compared to a baseline level recorded while subject was at rest. Four experimental conditions have been studied: Execution, No-Go (subjects were instructed to refrain from grasping), Simulation (motor imagery of the grasping movement triggered at the instant of object's fall), and Observation of others (while performing the same grasping movement).

Results

The results (see Fig. 24) showed clear modulation of CS excitability during *Execution* and *No-go* but no significant modulation were found in other conditions. CS excitability started to

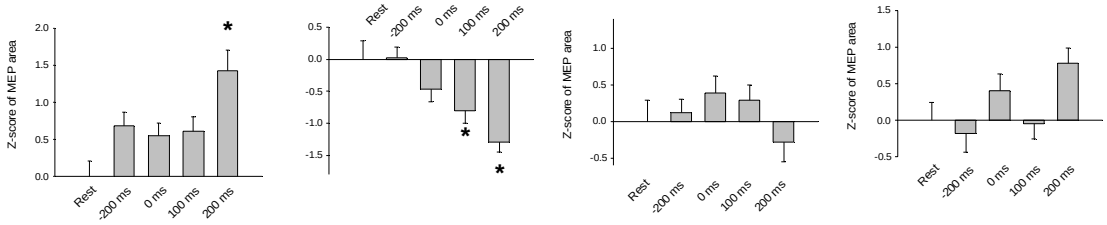

Figure 24. From left to right, Z-score of MEP area in the Execution, No-go, Observation and Simulation conditions. Asterisks signal significant ($p<0.05$) difference relative to baseline.

increase before target release and then slightly decrease at release to increase again until 200 ms. However, despite we found a significant effect of ST (one way ANOVA, $F(4,52)=4.57$; $p<.05$) on MEP area, a Newman-Keuls post-hoc analysis demonstrated that only MEP evoked when TMS pulse was delivered at 200 ms were significantly larger than those evoked at rest and at all other latencies except than at time of release. In summary, CS excitability increases above baseline between 100 and 200 ms after ball release.

During the No-go condition, we observed a general decrease of the CS excitability relative to the *Rest* condition. The one way ANOVA revealed a significant effect of ST ($F(4,52) = 5.8$, $p < 0.05$) and Newman-Keuls post-hoc analysis demonstrated that MEPs evoked when stimulation occurred at 100 and 200 ms after release were significantly smaller than the ones evoked at other latencies and during *Rest* ($p < 0.05$) but not significantly different from each other.

In summary of the first experiment, we found a facilitation of cortico-spinal excitability 200 ms after target release in the *Execution* condition whereas a global inhibition was seen during the *No-go* condition, being significant from 100 ms after release. During *Observation*, despite no significant modulation of MEP area relative to the *Rest* condition, we observe a specific inhibition of CS system at 200 ms, that is when CS excitability increase significantly in the *Execution* condition. During action simulation, no significant difference was found relative to Rest but slight increases of CS excitability were observed at ST 0 and 200 ms relative to target release.

The increase of CS excitability in time during the *Execution* condition reflects the characteristics of interceptive task in which, in contrary to reaction time tasks, the action must be triggered in response to an internal signal (TTC threshold) and not an external one (stimulus). This internal signal should reach its threshold value at about 250 ms as EMG activity began at 280 ms in average. It can be assumed that the CS excitability is rising whereas the TTC

estimate is updated in order to be closer from motor threshold at the triggering time. On the other hand, the decreasing CS excitability during the *No-go* condition is likely reflecting a mechanism dedicated to lower the sensitivity of motor cortex to neural command triggered by the stimulus.

Previous (submitted) data in MEG shown remarkably similar activations during catching and a No-go condition along the dorsal visuo-motor pathways suggesting a stimulus- rather than a task-driven processing. The absence of significant modulation in the *Observation* condition could be expected as TMS pulses were applied before the action begins to be in line with the stimulation time in the Execution condition. A second experiment with different time of stimulation has been performed and results are under process. Finally, the absence of modulation in the simulation condition is difficult to explain. Contribution of M1 to motor imagery is demonstrated by some studies and not by others (see (Lotze et al., 2006)). The observation of M1 activation during motor imagery seems to depend on methodological considerations and our lack of results could be attributed to the difficulty to simulate the task.

2.3.2 Robotic implementation of models of sensory-motor coordination for reaching, grasping and tracking tasks. (SSSA, UNIZH, UNISAL)

The availability of robotic platforms with adequate levels of anthropomorphism, in the sensory systems and in the kinematic structure, allows an experimental investigation of the models of sensory-motor coordination in reaching and grasping.

2.3.2.1 The SSSA humanoid robot.

The SSSA humanoid robot mimics human mechanisms of perception and action, and can implement neurophysiological models of sensory-motor coordination, for experimental validation. The system is composed of sensors and actuators replicating some level of anthropomorphism, in the physical structure and/or in the functionality. It is worth noting that their specifications were defined together by roboticists and neuroscientists (Dario et al., 2005). The platform is constituted by a 1-link trunk which supports one arm/hand system and a neck/head system (see Fig.1). The 2-dof trunk is part of the arm (Dexter arm, by S.M. Scienzia Machinale srl, Pisa, Italy) which has in total 8 dofs, and integrates the 4 motors of the three-fingered hand on the forearm. The arm structure is anthropomorphic in reproducing a 2-dof shoulder, a 1-dof elbow and a 3-dof wrist (Zollo et al., 2003). The mechanical transmission system is realized through steel cables, which allow the 6 distal motors to be located on the first link, which represents the trunk, by achieving low weight and low inertia for the distal joints. The proprioceptive information for the arm 8 joints are given by a measure of the power consumption of each joint as well as joint positions provided by incremental encoders located on each motor. The hand is has anthropomorphic dimensions and weight (Roccella et al., 2004). Each finger consists of 3 underactuated dofs driven by a single cable allowing flexion/extension. A 2-dofs trapezo-metacarpal joint at the base of the palm allows thumb opposition movement (adduction/abduction). In total the hand has 10 dofs, 6 of which are underactuated. The perception system of the hand includes proprioceptive and exteroceptive sensory systems, and in particular: 9 position Hall-effect sensors, 3 for each finger, one per phalanx; 4 motor encoders; 3 3D force sensor, one for each finger, embedded in the fingertips providing the three force components of the contact; 9 ON/OFF contact sensors, 3 for each finger, one per phalanx. The anthropomorphic robotic head has been designed on the basis of the physical structure and performance of the human head in terms of dofs, ranges of motion, speeds and accelerations (Dario et al., 2005). The head has a total of 7 dofs equipped with incremental encoders for measuring the positions of all the joints as proprioceptive information: 4 dofs on the neck (1 yaw, 2 pitches at different heights, 1 roll), 1 dof for a common eye tilt movement and 2 dofs for independent eye pan movements. The 4 dofs on the neck allow the head to perform dorsal/ventral and right/left neck flexion movements as well as neck rotation. The 2 dofs performing pan movement of the eye permit vergence of the two eyes, thus allowing foveation of targets. The performance of the head allows performing human eye movements such as smooth pursuit and saccades. The head is equipped with 2 cameras providing retina-like images, i.e. space variant image whose resolution is higher in the centre (fovea) and degrades towards periphery, as an imitation of images generated onto the human retina (Sandini & Metta, 2003).

Functional biologically-plausible models of sensory-motor mapping and of learning of sensory-motor coordination have been implemented on different parts of the ARTS humanoid platform. Such models have been adapted from the DIRECT (Direction to Rotation Effector Control Transform), proposed in (Bullock et al., 1993). The implementation of these sensory-motor coordination models on the ARTS humanoid is based on self-organizing neural networks that learn how to coordinate motor actions with sensory feedbacks.

Figure 25. The ARTS humanoid robotic platform.

The model builds a mapping between the positions of the robot in the external space (Cartesian space), as given by the sensory systems, and in the internal space (joint space), as given by the proprioceptive systems. The neural networks start with few information about the robot kinematics, like the number of DOFs and the maximum ranges of motion. During an initial learning phase, associations are created between spatial directions of movements and joint rotations, through random endogenous movements whose effects are detected by vision or touch (similarly to human infants). After learning, the built associations are used to set the proper joint rotation in order to reach a target position. This model has been implemented with Grossberg's outstar cells and Growing Neural Gas (GNG) Networks, as proposed by Bernd Fritzke (Fritzke, 1994). Differently from other techniques, these networks do not have predefined dimension nor topology and can grow, reduce, and re-configure in order to better solve the problem they are designed and trained for. Based on this model, we developed and experimentally validated a neurocontroller for positioning and orienting the robot hand in the 3-dimensional Cartesian space (Asuni et al., 2006; Asuni et al., 2005(b)) and a neurocontroller for

gazing a point in the three-dimensional space, with the robot head, by controlling the neck and eye movements (Asuni et al., 2005(a)). An adaptation of the model includes predictive control of grasping and has been implemented on the ARTS humanoid to obtain 'adaptable grasping', that is the robot was capable of looking at an object, determining the position of the hand for grasping, and accomplish the grasping action by using the tactile perception with an expected perception control loop (Laschi et al., 2006). An alternative biological model (Goossens & Van Opstal, 1997) has been implemented for the coordination of the ARTS humanoid neck and eye movements (Maini et al., 2006).

During the fourth year of the project, SSSA developed two main interacting modules: A vision module (that provides objects visual information), and a reaching module (that learns how to move, based on the information provided by vision).

The vision Module

The vision module receives the images from the two cameras mounted on the iCub head. It is responsible of processing these images in order to obtain the relevant information about the object to be grasped. These are: shape, dimension, orientation, and position within the 3D surrounding environment (this is accomplished by triangulating the information received from the binocular vision and the head and neck encoders). In our particular case we made our experiments by using a ball of different colors as the object of interest.

In order to detect the ball, and all its features, we implemented a simple but efficient image processing algorithm. We detect the ball by means of a color filter. The pixels of the ball are detected by setting color thresholds for the pixels belonging to the ball. We implemented a technique that creates a database for all the possible colors. Each color (detected with an image of interest) is represented with the HSV representation by its histogram evaluated within the image it owns to. Then, our application for the iCub loads the correspondent color representation from this database at runtime. Once the ball pixels are identified, the image is converted into a binary image with ball pixels set to '1'. The binary image contains not only the blob relative to the ball, but also other smaller blobs caused by color variation in the image. For the identification of the blob corresponding to the ball, we use a connected components algorithm. We assume the largest blob is the ball, so we look for the blob with the largest area. Subsequently we proceeded by applying the algorithm by Maini [8], to the found blob, in order to detect all the parameters of the curve that describes the boundary of the blob. This is a new interesting LS technique, the Enhanced Least-Square Fitting of Ellipses (EDFE), that has been developed recently, and it was proposed in [8]. It is a LS procedure that improves the work described in [9]. In this work, Fitzgibbon et al. developed a direct computational method (i.e. B2AC) based on the algebraic distance with a quadratic constrain. This new approach overcomes the state of the art by solving the problems of numerical instability that can produce completely wrong results, such as infinite or complex solutions, not reported in the original work [9].

We tested our algorithms by using the icub simulator. We used the iCub ODE simulator present in the iCub repository. Moreover, we slightly modified the simulator in order to create different scenarios for our experiments (such as by changing the color of the ball, by removing the table, etc.). In Fig. 6a and 6b an example of the ball detection algorithm output is shown. In Fig. 6a the input to the left camera is presented, i.e. the experimental scenario, while in Fig. 6b

output of the algorithm is presented, These images are the input image as seen by the robot with the egocentric view (6a) and the same image with the superimposition of an ellipse, drawn by using the characteristic parameters obtained by computing the EDFE.

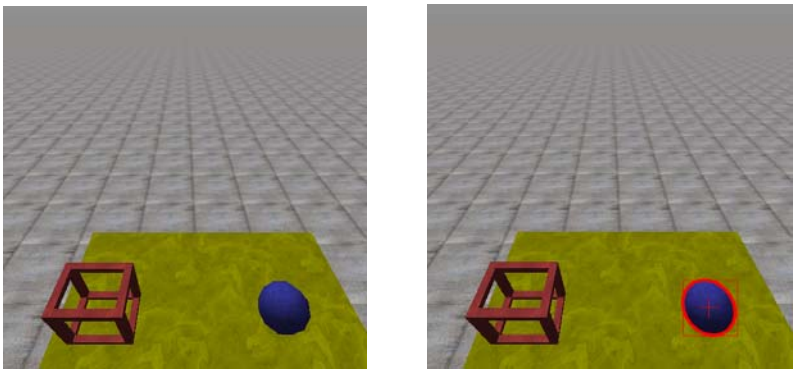

a **b**

Figure 26. The input image, as seen by the robot with the egocentric view (2a) and the same image with the superimposition of an ellipse, drawn by using the characteristic parameters obtained by computing the EDFE.

In addition, we implemented a tracking algorithm that directly commands the head of the robot, in order to be able to reconstruct the target object position (in terms of its centroid) by triangulating the information of the neck and head encoders (see Fig. 27).

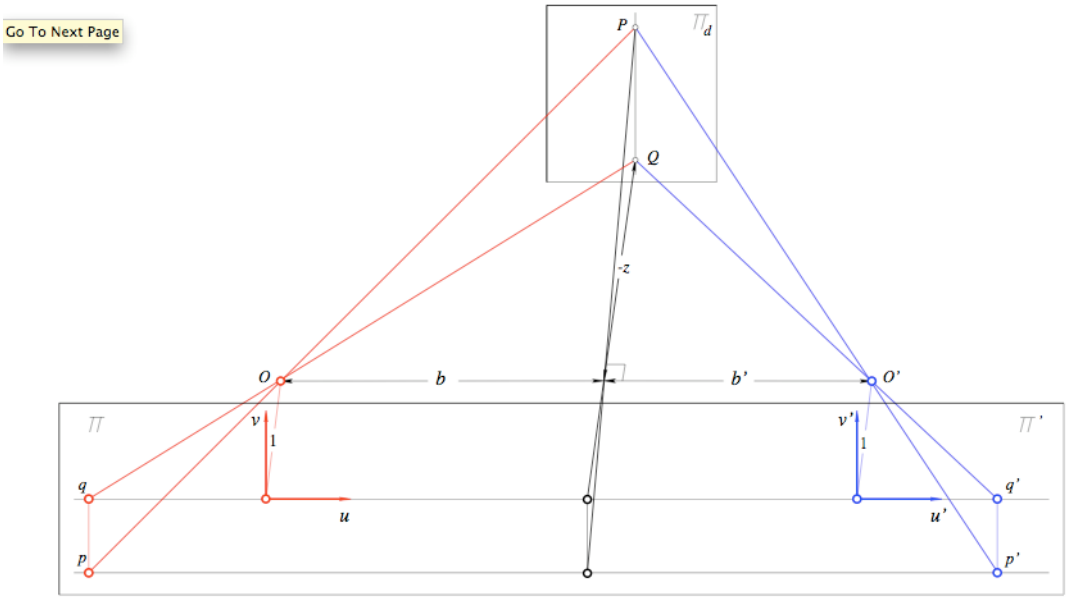

Figure 27. An example of triangulation of an object. Once the object has been detected by the cameras and tracked, it is possible to evaluate its 3D position in the surrounding space geometrically, by knowing the encoders position of the head and the neck of the robotic platform (in this case we refer to a humanoid robot).

This will be fundamental for computing the Sensory-Motor maps, as will be explained in the next section In Fig. 8 a print screen is depicted, that shows an operative situation in which the simulator tracked the ball. The iCub program we implemented the position of the ball (which is the target to be grasped in this case), in terms of Cartesian position. We adopted the same system reference as the simulator, in order to be fully compatible with the measures and the signs adopted in the virtual environment[1]. This allowed us not only an easier implementation of the software, but also to test easily our tracking algorithm by simulating different scenarios, i.e. by putting the ball in different positions (under the table, as in Fig. 26 or on the floor, as in Fig. 28).

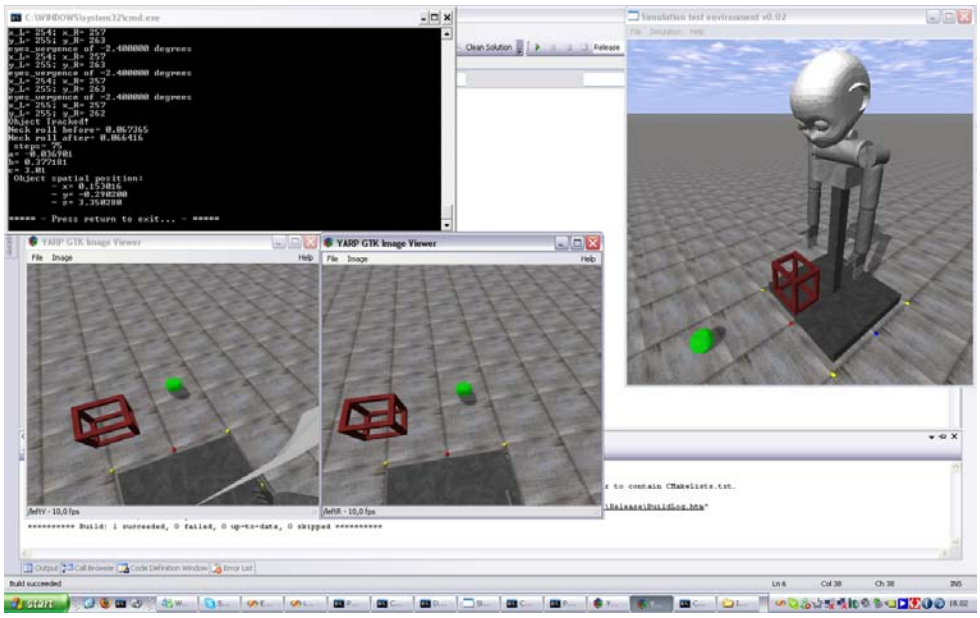

Fig. 28. A screenshot depicting the moment in which the simulated robot tracked the position of the ball in the 3D surrounding environment. Therefore, our program uses the encoders information to triangulate the position of the centroid of the object within the simulated space.

Again, this is a test for using this software for testing our algorithms for the sensory-motor maps generation. In fact, with the simulator it is possible to test our neural networks that generate the internal models for the sensory-motor maps without having the hardware iCub platform in the laboratory. Clearly, the simulator information is not exhaustive, but it is a good approximation for the software debug before using it on the rear robot, which can be extremely dangerous in case of wrong movements, due to the elevate torque of its motors.

[1] The reference system is centered on the floor plane, at the center of the pole that sustains the robot. The x axis evolves along the front of the robot, the y axis runs along the left of the robot, and the z axis evolves along its height.

The reaching module

The development of sensory motor coordination maps have been explored through the creation of forward models. The forward model created relates the relations that could exist between the vision system and the robot joints. We are concerned in solving the reaching problem for the iCub, so the forward model uses the information of the two robot cameras and the joint positions of one of the manipulator arms. The construction of the forward model starts with a babbling motor phase, in this phase the robot as a new born start exploring its environment through a series of goal directed movements within its workspace. The data obtained in this exploratory phase come from the vision system and the encoder readings of the joints. The vision system uses a color based algorithm to detect the position of the end-effector in the image. Once the data has been obtained and stored is used to generate a forward model using an ANFIS (Adaptive Neuro Fuzzy Inference System) neural network. The neural network trained with the storage data encodes the relation that exists between the joint angular positions and the end effector position in the vision System. Figures 29 and 30 show the babbling motor phase of a robotic manipulator simulated in Matlab.

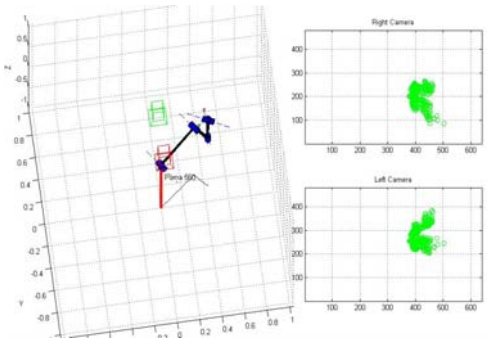

Fig. 29. The left subplot shows the position of the robot after the second babbling stage (joint 0 is initialized to 20 degrees). The top and bottom subplots show the imaged end-effector points at each babbling step.

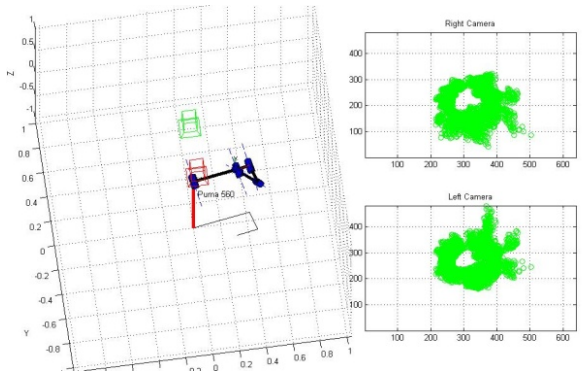

Fig. 30. The left subplot shows the position of the robot at the end of the babbling. The right top and right bottom subplots are the end effector accumulated positions of the end effector in the right and left camera.

The forward model is used for the reaching controller. The reaching controller identifies an end position where the robot should arrive. Once the final position has been identified by the vision system; the image based visual servoing controller uses for initializing the image Jacobian the forward model of the robot. The visual servoing algorithm drives the robot from and initial position to its final position. Figure 31 shows the general reaching architecture.

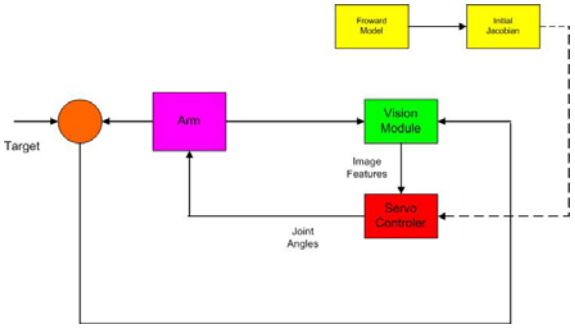

Fig. 31. General Architecture for a reaching task using a forward model

The reaching architecture has been tried first in matlab, and after it has been used the iCub simulator constructed in ODE to implement the described architecture. Final tests and experiments with the robot are on going. Figures 32 and 33 are snapshots of some of the experiments developed in the iCub ODE simulator for the reaching.

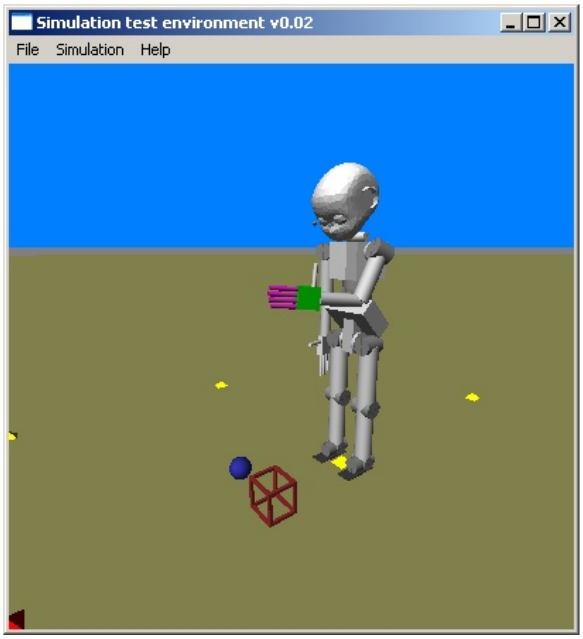

Fig. 32. ICub ODE simulator

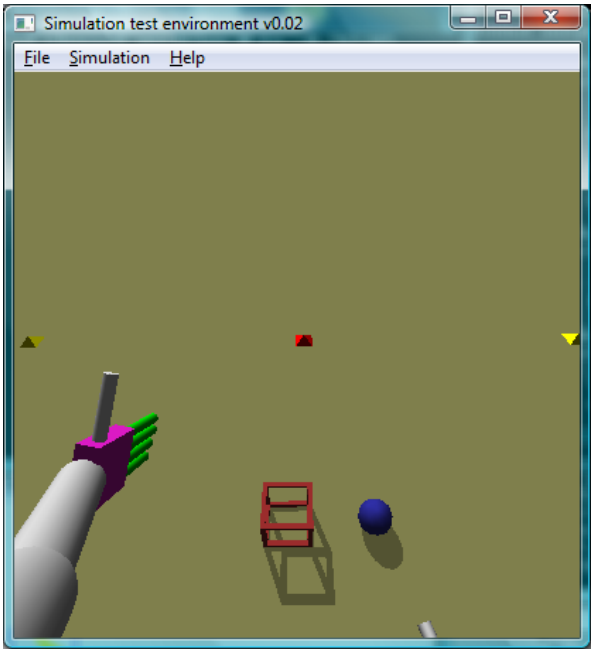

Fig. 33. Left hand of the iCub taken from the left camera.

2.3.2.2 The UNIZH approach to grasping.

At UNIZH, we investigated how the shape adaptation can be taken over by morphological computation performed by the morphology of the hand, the elasticity of the tendons, and the deformability of the material covering the finger tips, as the hand interacts with the shape of an object. When the hand is closed, the fingers will, because of its anthropomorphic morphology, automatically come together. For grasping an object, a simple control scheme, a "close" is applied. Because of the morphology of the hand, the elastic tendons, and the deformable finger tips, the hand will automatically self-adapt to the object it is grasping. Thus, there is no need for the agent to "know" beforehand what the shape of the to-be-grasped object will be. The shape adaptation is taken over by morphological computation performed by the morphology of the hand, the elasticity of the tendons, and the deformability of the finger tips, as the hand interacts with the shape of the object. Because of this morphological computation, control of grasping is very simple, or in other words, very little brain power is required for grasping. (Pfeifer et al., 2006; Pfeifer et al., in press). We also implemented a learning mechanism in order that the robotic hand can learn to grasp objects by itself as described in WP2 Cognitive development (Gomez et al, 2005 and Gomez et al, 2006).

If the robotic hand actively manipulates an object, there are likely to be correlations in the sensorimotor space. This "good" sensory-motor data can be exploited for perceptual categorization, adaptation, and learning. In a previous series of studies, we have investigated how the usage of correlation, entropy, and mutual information can be employed (a) to segment an observed behaviour into distinct behavioural units, (b) to analyze the informational relationship between the different components of the sensory-motor apparatus, and (c) to identify patterns (or fingerprints) in the sensorimotor interaction between the agent and its local environment. These methods were applied to real robots (Lungarella and Pfeifer, 2001; teBoekhorst et al., 2003) and simulated robotic agents (Lungarella et al., 2005; Gomez et al., 2005; Tarapore et al., 2006) and we are using them now in experiments where the robotic hand is involved in grasping tasks (Lungarella and Gomez, in preparation).

2.3.2.3 The UNIZH approach to Tracking.

In order to detect objects moving in the environment we have implemented 2 different systems:

The first one is based on elementary motion detectors (EMDs) based on the well-known elementary motion detector of the spatio-temporal correlation type (Marr, 1982), a description of the model implemented, can be found in (Iida, 2003), that successfully implemented a biologically inspired model of the bee's visual "odeometer" based on EMDs. The model was used to estimate the distance traveled based on the accumulated amount of optical flow measured by EMDs. Fig. 1c and 1d show the EMDs responding to motion.

The second one is based on the optic flow extraction. We used the generalized gradient method based on Spatio-Temporal Filtering (Sobey and Srinivasan, 1991; Nagai et al., 1999). A

detailed explanation can be found in Fig. 35 and for an example of the performance see Fig 34b.

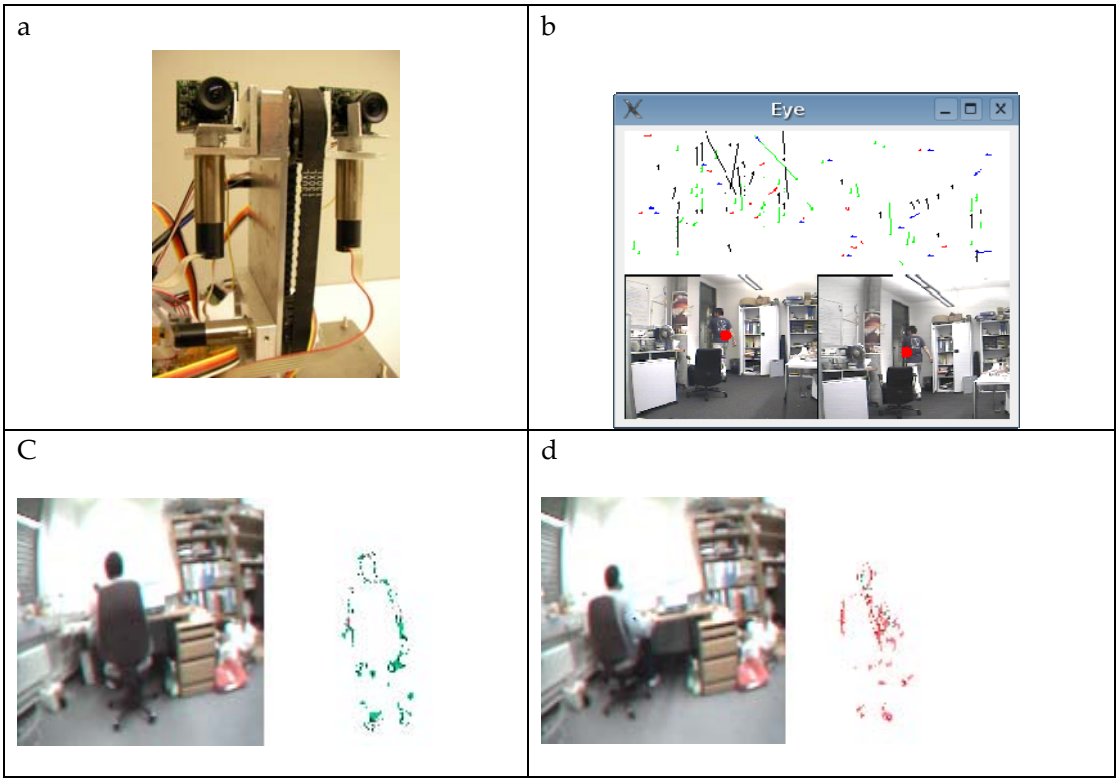

Figure 34. Active vision system. (a) Hardware implementation (b) the lower part consists on the left and right images captured by the cameras, the upper part are the corresponding optical flow. The red dots are the centroid of the motion (i.e., where the robot should gaze). (c-d) EMDs reacting to motion towards the right side of the image (green dots) and to motion to the left direction (red dots).

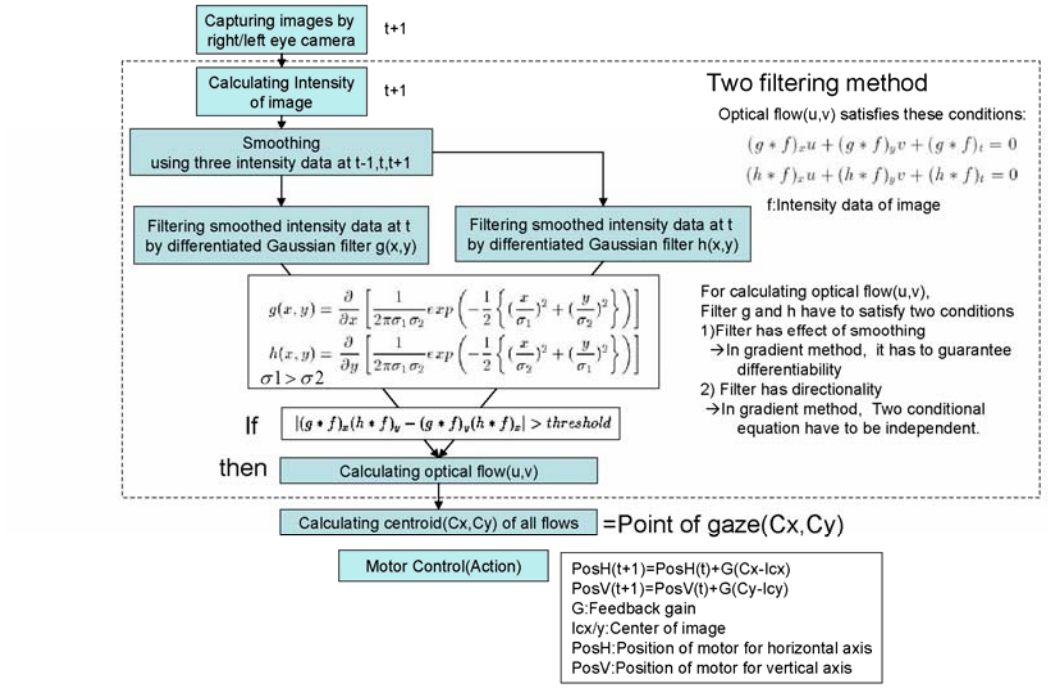

Figure 35. Optical flow extraction.

2.3.2.4 The contribution of UNISAL to track the acting hand (UNISAL, UNIUP, UNIFE).

At UNISAL, the efforts concerning WP3 have been directed towards:

i) Development of a input tracker glove in conjunction with UNIUP looking at the development of technology to accurately track hand actions in infants up to 24 months. This work has produced a new miniaturised wireless sensory glove able to track the motions of the all finger and the thumb. The current work is developing the software interface and refining the glove design for ease of use and acceptance by the child. These refinements have been based on initial trials with children. It is expected that a new version with testing will be completed within the next recording period permitting the collection of real data.

ii) To permit a greater more accurate analysis than is currently available from glove systems a new high resolution finger tracking systems has been designed and is undergoing testing. This system has been developed based on input from UNIFE. At this time the system has been design and tested with operational software showing accurate 6 dof tracking (accuracy better than 0.1 mm at finger tip). With further development this will be integrated with the work at UNIFE and UNIUP.

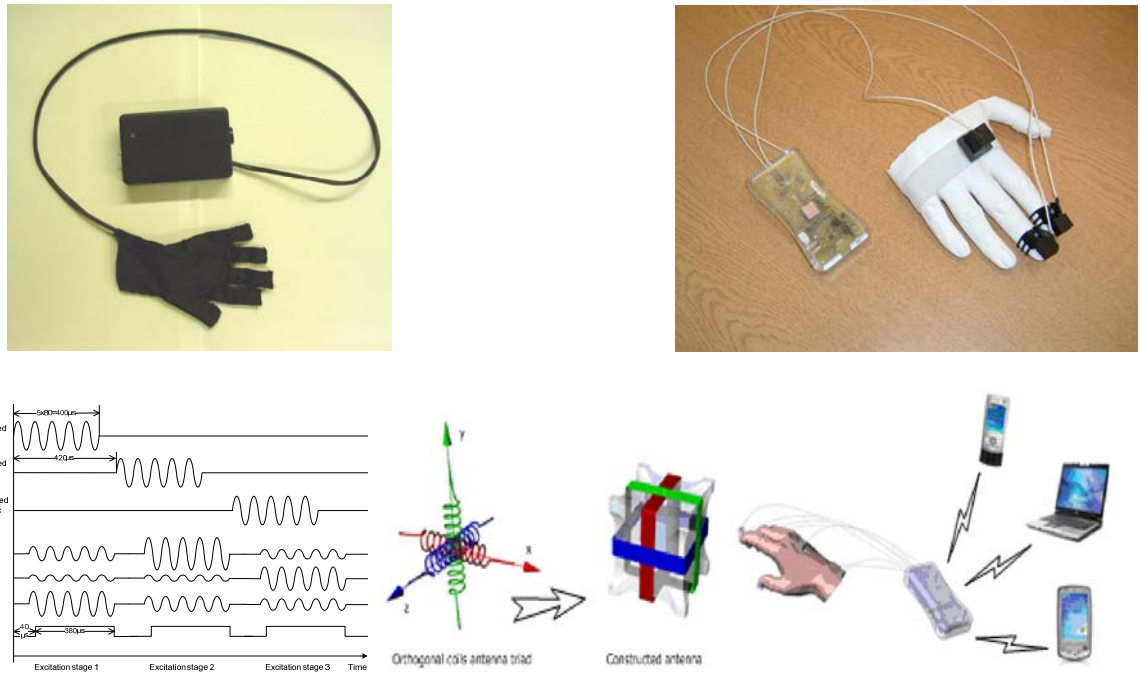

Figure 36. The two hand tracking systems developed at UNISAL with UNIUP (left) and UNIFE (right).

This second tracker, in particular, associates high precision to small dimensions. The signal relative to fingertips positions can be remotely transmitted via WiFi of Bluetooth protocols.

iii) At the same time, UNISAL is continuing its work on the development of an understanding of the sensory systems for legs, hips, feet and the sensory requirements of the iCUB. The data relative to this approach will be presented in the final version of this Deliverable 3.1 (month 30).

2.3.2.5 The contribution of EPFL-A and UNIFE to a computational model for reaching.

Although point-to-point reaching motions have received a lot of attention, the way these movements are controlled remains incompletely resolved. Different controllers seem to be recruited depending on the task. Unconstrained reaching movements in space are strongly curved, in opposition to the widely accepted view of quasi-straightness. We argue that the curvature of the movement is due to environmental constraints that affect directly the planning of the movement. We propose a mathematical model whereby movements are planned through the combination of two concurrent controllers for the wrist and elbow in space. Coherence constraints are enforced between the two systems to simulate biomechanical constraints at the wrist, elbow and shoulder levels. External constraints, such as the presence of obstacles, are encapsulated in a virtual force which affects the planning of the movement.

The predictions of the model are validated against kinematic data from human reaching motions. Four types were contrasted: intransitive versus transitive reaching motions and natural versus un-natural motions. In the un-natural case, subjects were requested to exaggeratedly elevate the elbow during the movement. In all four movements types, the movements are highly curved. The model renders with high accuracy the kinematics of the movements and accounts for the curvature as an effect of the virtual force.

A joint paper is now under submission and the draft "Point-to-Point Unconstrained Gestures: Modeling Wrist and Elbow Trajectories" is attached to this deliverable

2.3.3 Sensorimotor Integration of gravity models. (UGDIST)

The work for WP3 at UGDIST has proceeded along two main lines of research. We investigated the acquisition and construction of internal models both in humans and in robots. In particular, as a starting point, we concentrated on the acquisition of models of the gravity load during point-to-point movements: i.e. reaching. In the following we illustrate these two aspects.

2.3.3.1 Gravity models in humans

Introduction

Many are the circumstances in which action–perception dissociations have been observed (e.g. [1], [2]). Among the best known cases there are the pictorial illusions which induce errors in perception but cannot deceive a motor act. It is not yet clear however in which other conditions this separation could be noticed [3]. Following the work of Dubrowski [4] and Zago [5] we wanted to investigate whether action-perception dissociations affect also prediction. We performed an experiment to evaluate whether prediction is differently realized when it's aimed at driving a motor act and when instead its purpose is "perceptual-only". In particular we focused on how dynamical information of target motion is used depending on prediction goal. In a previous experiment (an interception task) we observed that predictive performances where significantly better when the target maintained unvaried its dynamic features (i.e. the force field that drove its motion). Furthermore, when the target was driven by a force field similar to gravity interception resulted easier. We wanted to check if the same results could be found in a predictive task in which no motion was involved.

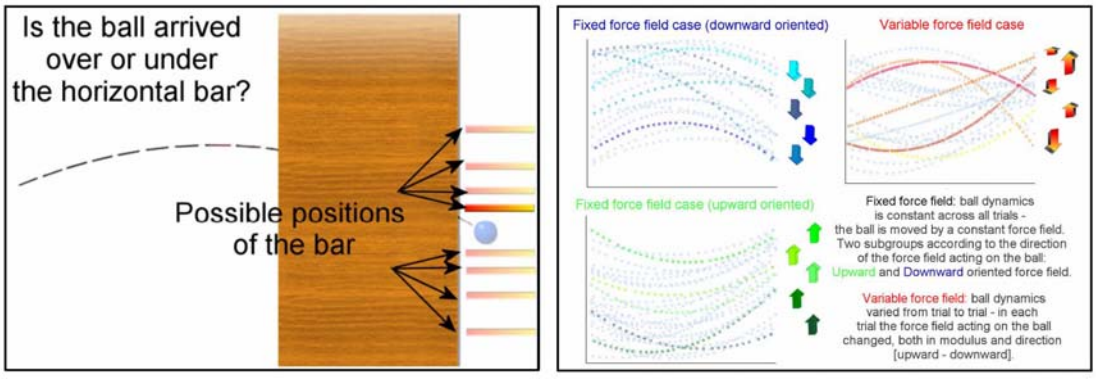

Figure 2-1: The experimental setup and stimuli used for the two experiments described below.

Methods

37 subjects participated in the experiment. They sat in front of a monitor (BARCO Calibrator system) at a distance of 57 cm and kept in their hand a small push-button panel (CB6 Response Box, Cambridge Research Systems). The stimulus, realized with a ViSaGe stimulus

generator (C.R.S.), was a ball, which crossed the screen following a parabolic path and disappeared behind an occlusion. Subjects were instructed to press a button, as soon as the ball disappeared, to select whether the ball would have arrived over or under an horizontal line. The line was placed at the right extremity of the scene, at a fixed distance from the real ball arrival point (see Fig.2-1). After subjects had made their choice the ball arrival point was shown and a further key press was awaited, to start another trial. In each experiment subjects were presented with 14 possible distances between the ball arrival point and the horizontal line and each distance was presented in 10 different trials. Moreover before the real experiment all subjects were trained with 70 straight trajectories (10 trials x 7 distances), to let them familiarize with the setup and to assess subjects baseline ability in the task. To analyze the results the psychometric curve for each subject was obtained by fitting with a cumulative Gaussian the probability of answering "ball under line" as a function of the real ball-line distance. From each curve two parameters were extracted: the PSE (point of subjective equality), a measure of the minimum distance perceivable by the subject, and the slope of the curve, an indicator of the perceived task difficulty. Subjects were divided into different groups: some of them had to predict the ending positions of balls driven by a constant force field, while others had to deal with balls that changed their dynamical features from trial to trial (red panel in Fig.2-2). Furthermore we considered two different kinds of fixed force fields: both were vertical, one was downward oriented, similar to gravity (blue panel in Fig.2-2) and one was instead characterized by upward orientation (green panel in Fig.2-2). In all cases trajectories were always parabolic and each trial differed from the previous one, since ball initial position and speed changed. The main difference among conditions was therefore given by the constancy or variability of the force field acting on the ball and by force field orientation.

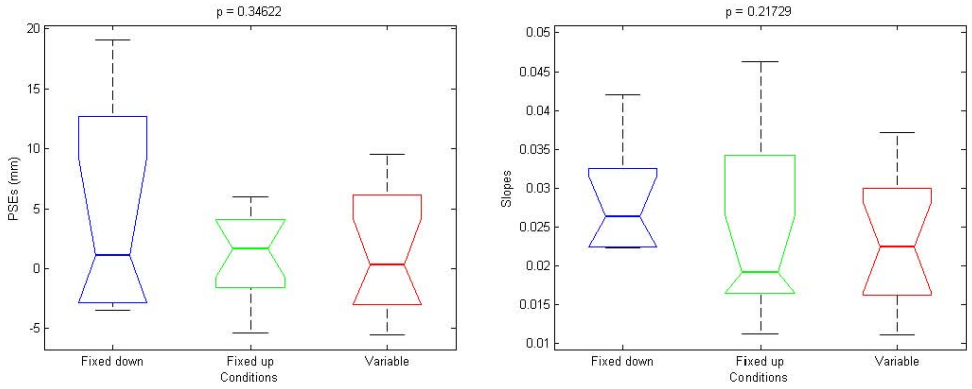

Figure 2-2: Results showing no significant difference between conditions when the task is purely perceptual.

Results and discussion

We ran a single factor ANOVA and a Tukey – Kramer multiple comparison test to evaluate if the different conditions (fixed or variable force fields, and gravitational or anti-gravitational oriented force fields) were characterized by different perceived difficulty. If prediction was based on a unifying model of ball dynamics features, as we have previously observed in an interception task, the condition in which ball dynamics changed each time would have been perceived as significantly more difficult. Furthermore we could estimate whether a gravitational like environment allowed for better prediction even when no motor act

was involved. The analyzed indicators (PSEs and slopes) result to be not significantly different between the condition in which the force field is kept constant and those in which the force field changes from trial to trial. Also "gravitational" and "anti-gravitational" conditions are perceived as equally easy in prediction. Results show therefore that, in contrast to what we observed in an interceptive task, ball dynamics stability doesn't affect perceptual prediction. The dynamic visual information seems to be processed differently when its purpose is a motor act versus a perceptual one.

References (for this section only)

[1] Aglioti, S. et al., Current Biology, 1995, 5: 679-685

[2] Brenner, E. et al., Experimental Brain Research, 1996, 111: 473-476

[3] Kerzel, D. & Gegenfurtner, K. R. Experimental Brain Research, 2005, 162: 191-201

[4] Dubrowski, A. et al. Vision Research, 2002, 42: 1465-1473

[5] Zago, M. et al., Journal of Neurophysiology, 2004, 91: 1620-1634

2.3.3.2 Gravity models in robots

During the execution of (even simple) arm movements, the effects of gravity need to be taken into account in order to avoid undesired. Therefore, the issue of gravity compensation has always been crucial in the field of robotics [Murray et a. 1994]. Different gravity compensation techniques have been proposed in literature. Among these various techniques, we here focus on model based gravity compensation, limiting our attention on arm point-to-point movements. The main section is divided into three subsections. First, we describe a dynamical model of the arm dynamics. Then, we show how the model can be written in a parametric way. Finally, in the last subsection, we show some experimental results on the how to compensate gravity on a real robot.

Model of the arm. We model the dynamics of the arm as a fully actuated kinematic chain with n degrees of freedom corresponding to n revolute joints. It is well known in literature that such model can be expressed as follows:

$$M(q)\ddot{q} + C(q,\dot{q})\dot{q} + g(q) = u$$

where q are the generalized coordinates which describe the pose of the kinematic chain, u are the control variables (nominally the torques applied at the joints) and the quantities M, C and g are the inertia, Coriolis and gravitational components.

Parametric model of the arm. In this section, we describe the above dynamic equation in a parametric way. The considered parameters are the masses, the inertias and the center of mass positions for each of the n links which compose the controlled arm. The vector with components represented by these parameters will be denoted p and is composed by the link masses (m_0, m_1, …), the link center of mass positions (c_{0x}, c_{0y}, c_{0z}, c_{1x}, c_{1y}, c_{1z}, …), the link lengths (l_0, l_1, …), and the

link inertia tensors (I_{0xx}, I_{0xy}, I_{0xz}, I_{0yy}, I_{0yz}, I_{0zz}, I_{1xx}, I_{1xy}, I_{1xz}, I_{1yy}, I_{1yz}, I_{1zz},…). Obviously, the matrices M, C and g depend on the given vector of parameters, i.e.:

$$M(q,p)\ddot{q} + C(q,\dot{q},p)\dot{q} + g_p(q,p) = u$$

Interestingly, it can be proven that the above parametric dynamics can be rewritten as (see [1] for details):

$$M(q,p)\ddot{q} + C(q,\dot{q},p)\dot{q} + g_p(q,p) = \sum_{j=1}^{J} \Psi_j(p) Y^j(\ddot{q},\dot{q},q)$$

for suitably chosen functions Y^j and Ψ^j. As a special case we have that the gravity term g can be written as:

$$g(q,p) = \sum_{j=1}^{J} \Psi_j(p) Y^j(0,0,q) = \sum_{j=1}^{J} \alpha_j g^j(q)$$

where $\alpha_j=\Psi^j(q)$.Therefore, the effects of gravity on a robotic arm can always be expressed as the linear superposition of terms $g^j(q)$ which do not depend on the dynamical properties of the system. Interestingly enough, this observation has strong connections with the "spinal filed" theory (see [Mussa-Ivaldi et al. 2000] and [Nori et al. 2006] for details) but these connections will not be discussed here being out of our main focus. What is worth saying is that the gravitational properties of the controlled system are represented by mixing coefficients α_j.

Experiments. We designed a set of experiments in order to test if the model:

$$g(q,p) = \sum_{j=1}^{J} \alpha_j g^j(q)$$

agrees with the experimental data taken from the arm of our robot, James (see Figure 30). This test is necessary since the above model is based on a set of assumptions which cannot be completely fulfilled by a real manipulator. In this specific example the arm is four degrees of freedom (three degrees of freedom in the shoulder and one degrees of freedom in the arm) and given the kinematics of the arm we have J=7 and :

J	$g^j(q)$
1	-cos(q1)
2	sin(q1)cos(q2)
3	-sin(q1)sin(q2)
4	sin(q1)cos(q2)cos(q3)-cos(q1)sin(q3)

5	-sin(q1)cos(q2)sin(q3)-cos(q1)cos(q3)
6	[sin(q1)cos(q2)cos(q3)-cos(q1)sin(q3)]cos(q4)-sin(q1)sin(q2)sin(q4)
7	[-sin(q1)cos(q2)cos(q3)+cos(q1)sin(q3)]sin(q4)-sin(q1)sin(q2)cos(q4)

Practically, we can measure the value of g(q,p) at different configurations of the arm by measuring the torques u which has to be applied at the joints in order to keep the system in the specific configuration with zero velocity. We have:

$$g(q^i, p) = u^i$$

where q^1, q^2, …, q^N is a set of configurations and u^i are the torques necessary to counterbalance gravity in order to maintain the configuration q^i. To verify the validity of our model we have to check whether there exists a set of mixing coefficients α_1, α_2,…,α_7 that satisfy the following equations:

$$u^i = \sum_{j=1}^{7} \alpha_j g^j(q^i)$$

Obviously, given a sufficient number of measurements (u^i, q^i) the above equations cannot be exactly fulfilled by real data, which are always affected by noise. Therefore, the adopted solution was to estimate the parameters with a least squares procedure:

$$\alpha = \arg\min_{\alpha} \sum_{k=1}^{K} \left\| \sum_{j=1}^{23} \alpha_j g^j(q_i) - u^i \right\|^2$$

and to verify the validity of the estimated parameters on new data samples. Results are shown in Figure 39. Training the model with two hundred measurements (u^1, q^1) … (u^{200}, q^{200}) was sufficient to obtain good predictive capabilities thus showing that the model is in good agreement with the real system.

Non-parametric approximation. The same data were also processed by a non-parametric method which is based on Gaussian processes for regression, a kernel method based on Bayesian inference. The specific algorithm is incremental and sparsifies the solution; it also estimates the hyper-parameters of the algorithm by optimizing a specific quantity (called marginal likelihood). We leave any further detail of the method to the reference in [Csato' et al. 2002] and only show here the result of the approximation of the gravity data from James. The results in the following figures Figure 40 and Figure 41 show that non-parametric estimation is efficient and it can be a good alternative to internal model acquisition. We will explore both possibilities in the future with extensions to the full dynamical model of the robot and its links to other sensing modalities: i.e. vision, vestibular, etc.

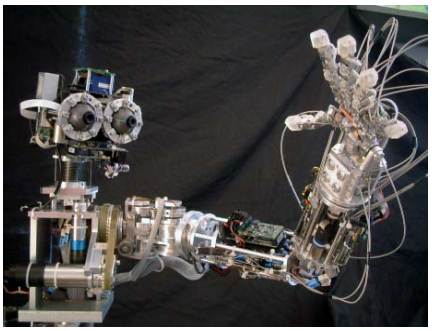

Figure 38. The picture shows our robotic platform, James.

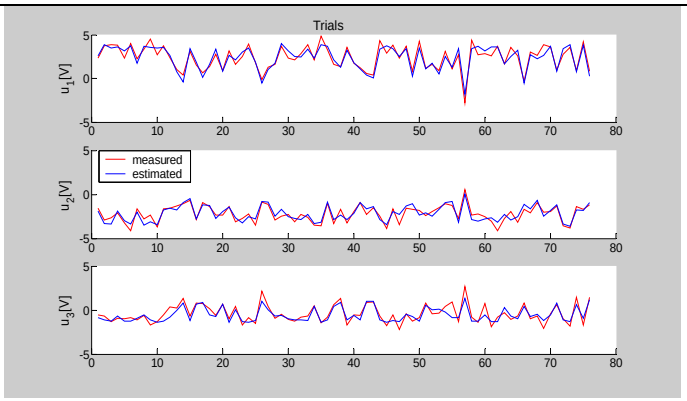

Figure 39. Test of the predictive capabilities of the parametric model. On the horizontal axis, a total of 75 different postures q^1, q^2, …, q^{75} have been considered for testing. For each of these postures we considered the torques necessary to keep the arm at rest (vertical axis). The blue line corresponds to the estimated compensation; the red line instead is the measured compensation.

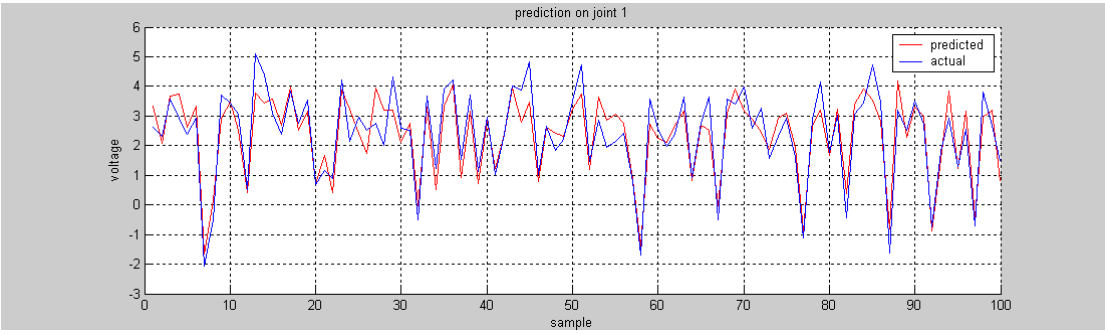

Figure 40. Prediction for joint 1, on a random subset of the available data.

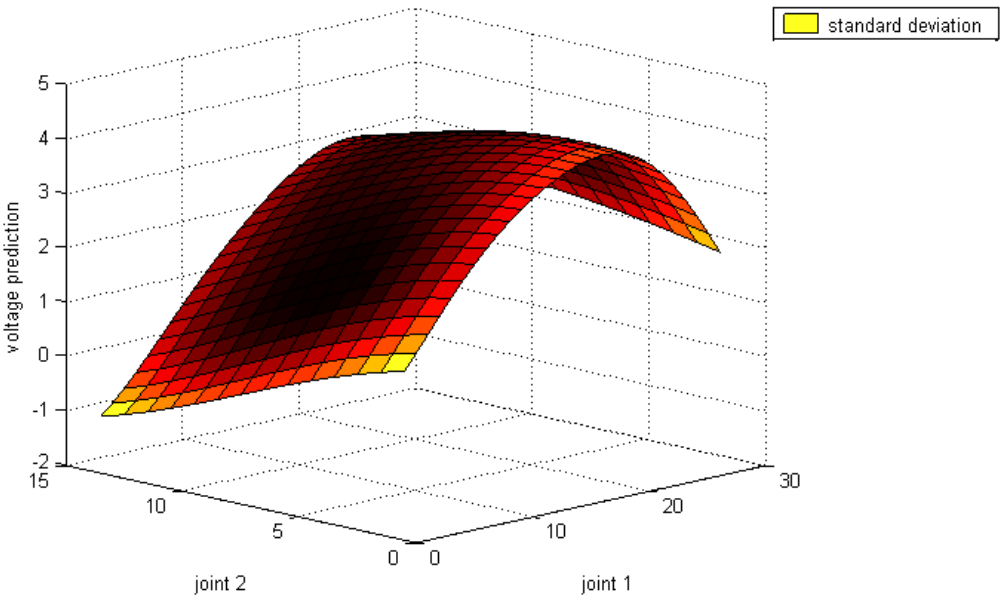

Figure 41. Plot of the predicted function; the shading represents the standard deviation of the prediction. Note how uncertainty grows toward the borders of the region where training points are not available.

2.3.3.3 Acquisition of a kinematic internal model

We discuss the implementation of a precise reaching controller on a humanoid robot upper torso. The proposed solution is based on a learning strategy which does not rely on a priori models of the arm and head kinematics. The only major simplification is represented by the assumption that a visual model of the hand is available (i.e. the robot can visually localize the hand). In fact, from a practical point of view, the problem of creating a visual model of the hand is a stand alone problem which falls outside the scope of this project. Future experiments will be based on a self-acquired model of the hand.

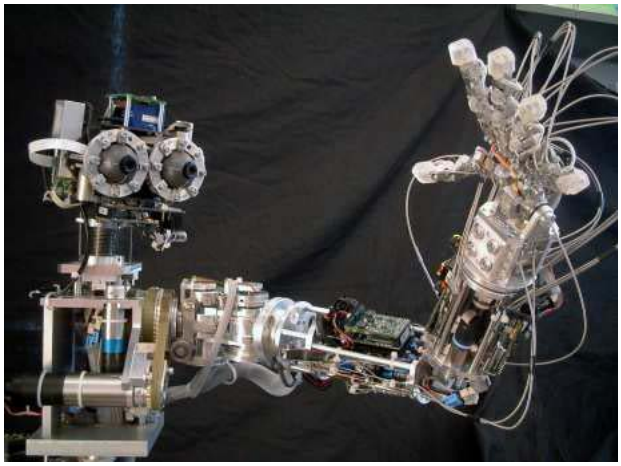

Figure 2-3: the upper torso humanoid robot used in these experiments.

System description

The reaching controller has been implemented on our humanoid robot James (see Figure). James consists of 22 DOFs, actuated by a total of 23 motors, whose torque is transmitted to the joints by belts and stainless-steel tendons. The head is equipped with two eyes, which can pan and tilt independently (4 DOFs), and is mounted on a 3-DOF neck, which allows the movement of the head as needed in the 3D rotational space. The arm has 7 DOFs: three of them are located in the shoulder, one in the elbow and three in the wrist. The hand has five fingers and is under-actuated with a total of 20 degrees of freedom controlled by 8 motors.

The next section (inserted) is about the learning of the arm kinematics. The next step, described later, is then to learn also the robot arm dynamics.

0.1 Head and eyes actuation structure

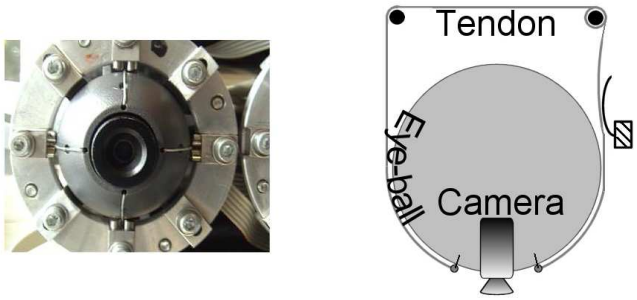

Figure 1: The left picture shows the tendon driven eye. The two tendons are actuated by two motors. The first motor moves the vertical tendon (tilt motion). The second motor moves the horizontal tendon (pan motion). The right figure sketches the actuation scheme.

The head structure has a total of 7 degrees of freedom, actuated by 8 motors. Four of these motors are used to independently actuate the pan and tilt movements of the left and right eyes (see Figure 1 for a scheme of the tendon actuation). The following notation will be used from now on:

$$\alpha_t^r : \text{right eye tilt} \qquad \alpha_p^r : \text{right eye pan}$$
$$\alpha_t^l : \text{left eye tilt} \qquad \alpha_p^l : \text{left eye pan}$$

Even though the eyes can be moved independently, our strategy was to couple their movements so as to achieve a more human-like motion. In particular, instead of controlling α_t^r, α_p^r, α_t^l, α_p^l (see Figure 2) we decided to use common tilt α_t^c, differential tilt α_t^d, vergence α_v^d and version α_v^c (see Figure 3) defined as follows:

$$\alpha_v^d = \frac{\alpha_p^r - \alpha_p^l}{2}, \qquad \alpha_v^c = \frac{\alpha_p^r + \alpha_p^l}{2},$$
$$\alpha_t^d = \frac{\alpha_p^r - \alpha_p^l}{2}, \qquad \alpha_t^c = \frac{\alpha_p^r + \alpha_p^l}{2}.$$

In practice, the differential tilt angle is not used. The underlying assumption is the perfect orthogonality between the camera axis and the pan

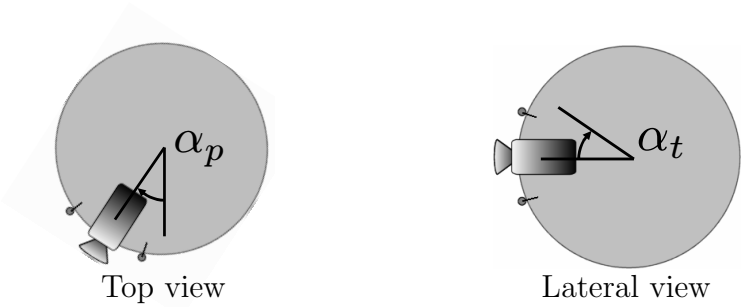

Figure 2: The left picture shows a top view of the eyeball and indicates the pan angle. The right picture instead shows the lateral view with the tilt angle.

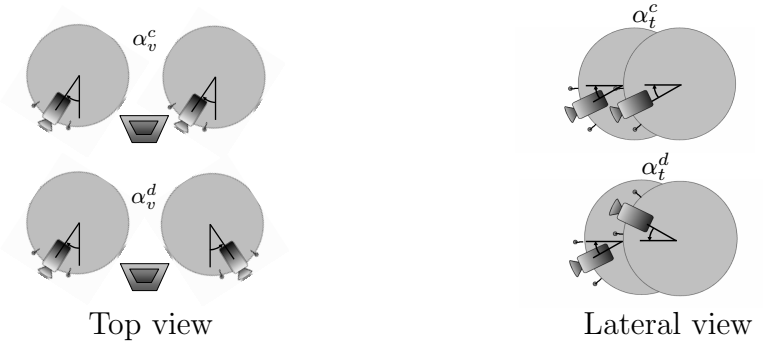

Figure 3: The left picture shows a top view of the eyeball and indicates the version (top) and the vergence (down) angles. The right picture instead shows the lateral view with the common (top) and differential tilt (down) angles.

axis of rotation[1]. Practically, the eyes configuration will be denoted $\mathbf{q}_{eyes} = \begin{bmatrix} \alpha_v^d & \alpha_v^c & \alpha_t^c \end{bmatrix}^\top \in \mathbb{R}^3$.

The neck actuation is also non conventional. One motor directly actuates the head yaw, denoted θ_y. The remaining three motors actuate the two additional rotations of the head: head pitch θ_p and head roll θ_r. These two rotations are achieved with an unconventional actuation structure (see Figure 5). Each motor pulls a tendon; the tension of the three tendons determines the equilibrium configuration of the spring on which the head is mounted. The structure has an implicit compliance but it can become fairly stiff when needed by pulling the three tendons simultaneously. The overall neck configuration will be denoted $\mathbf{q}_{neck} = \begin{bmatrix} \theta_y & \theta_p & \theta_r \end{bmatrix}^\top \in \mathbb{R}^3$.

[1]Suppose that our task consists in fixating a given target, i.e. putting the target projections in the center of the left and right image planes. Since the target moves in a three dimensional space, in principle we only need three control variables to actually fixate the target in every possible configuration. It can be shown that these three variables can be α_v^d, α_v^c and α_t^c (while keeping $\alpha_t^d = 0$) if the system mechanics and optics are perfectly aligned. In particular, the assumptions are the following:

1. the cameras behave as a perfect pin-hole camera model,
2. the cameras optical axes are orthogonal to the corresponding pan axes of rotation,
3. the pan axes of rotation are orthogonal when $\alpha_t^d = 0$.

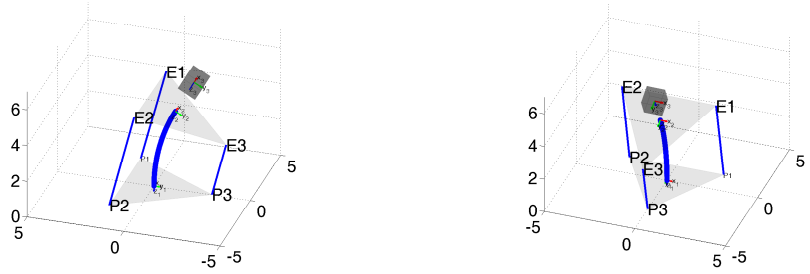

Lateral view Frontal view

Figure 4: The pictures show two views of the neck actuation structure. The two equilateral triangles represent the basis and the top of the neck (on which the head is mounted). The thick line represents the spring (a sort of neck bone). The three thin lines (segments $\overline{E_1P_1}$, $\overline{E_2P_2}$ and $\overline{E_3P_3}$) are the tendons used to move the neck in different configurations. Finally, the dark cube is a sensor, the use of which will be descibed in Section 1.

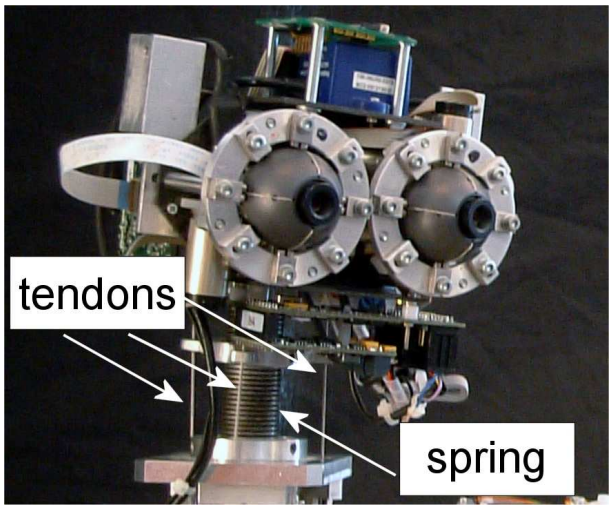

Figure 5: The pictures describes the neck actuation. The head is mounted on a spring. The spring is moved by shortening and lengthening the three tendons by the use of conventional DC motors.

1 Control of the neck

The neck is characterized by a peculiar structure and has required the design of an original control technique. The final design is based on the use of a set of gyroscopes, which have been positioned on top of the robot head. The sensors measure the (absolute) pitch and roll rotations[2] of the head with respect to an inertial reference frame. Using the information from this sensor we developed a closed loop controller to orient the head in any desired configuration.

1.1 Neck control in details

As already pointed out, the neck structure is characterized by three degrees of freedom: pitch θ_p, roll θ_r and yaw θ_y. The yaw movement, is directly actuated by a single dc motor; its control is based on a standard PID controller. The control strategy for the remaining two movements will be instead described in details in this section.

The design of the pitch and roll control loops has required the development of a MATLAB model of the neck structure. The model is based on the assumption that the spring has a constant length[3]. When the spring is bent, the assumption is that its curvature is constant along the entire spring length. Using this model we were able to compute the ideal tendons lengths given the pose of the neck, or equivalently the ideal tendons lengths (l_1, l_2, l_3) given the inertia sensor measurement (θ_r, θ_p). Practically, the model of the system is a function $f : \mathbb{R}^2 \longrightarrow \mathbb{R}^3$ such that:

$$\begin{bmatrix} l_1 \\ l_2 \\ l_3 \end{bmatrix} = f(\theta_r, \theta_p). \tag{1}$$

The final control loop for positioning the neck in the desired configuration

[2]The rotation is expressed by three angles which will be denoted roll (θ_r), pitch (θ_p) and yaw (θ_y). The three motors of the neck influence the first two angles (θ_r), pitch (θ_p). The remaining degree of rotation (θ_y) is directly influenced by the head pan which is moved by a specific motor.

[3]Practically, when the spring bends on a side, it maintains its length on that side while stretching on the opposite side. This kinematic can be easily modeled with MATLAB.

$(\theta_r^d,\, \theta_p^d)$ is the following:

$$\begin{bmatrix} \frac{dl_1}{dt} \\ \frac{dl_2}{dt} \\ \frac{dl_3}{dt} \end{bmatrix} = - \begin{bmatrix} \frac{\partial f}{\partial \theta_r} & \frac{\partial f}{\partial \theta_p} \end{bmatrix} \begin{bmatrix} \theta_r - \theta_r^d \\ \theta_p - \theta_p^d \end{bmatrix}, \tag{2}$$

where $\begin{bmatrix} \frac{\partial f}{\partial \theta_r} & \frac{\partial f}{\partial \theta_p} \end{bmatrix}$ is the Jacobian of the function f with respect to θ_r, θ_p computed at the current configuration θ_r, θ_p.

The above model (1) is ideal and assumes that the three tendons are always subject to a minimum tension. Due to the imperfections in the model, the tendons may loose tension if the control strategy (2) is applied. Given a long enough time window th controller might drift. A corrective term is therefore required. The solution is:

$$\begin{bmatrix} \frac{dl_1}{dt} \\ \frac{dl_2}{dt} \\ \frac{dl_3}{dt} \end{bmatrix} = -(1-\gamma) \begin{bmatrix} \frac{\partial f}{\partial \theta_r} & \frac{\partial f}{\partial \theta_p} \end{bmatrix} \begin{bmatrix} \theta_r - \theta_r^d \\ \theta_p - \theta_p^d \end{bmatrix} - \gamma \left(\begin{bmatrix} l_1 \\ l_2 \\ l_3 \end{bmatrix} - f(\theta_r, \theta_p) \right), \tag{3}$$

where γ is an arbitrary constant in the range $[0, 1]$. The second term of the controller (the one multiplied by γ) guarantees that the the length of the cables remains similar to the length of the model. This strategy is sufficient to guarantee that the tendons maintain a tension which is more or less constant across different configurations of the structure. In this final configuration the jacobian $\begin{bmatrix} \frac{\partial f}{\partial \theta_r} & \frac{\partial f}{\partial \theta_p} \end{bmatrix}$ can be substituted with a constant jacobian computed at the reference configuration θ_r=θ_p=0.

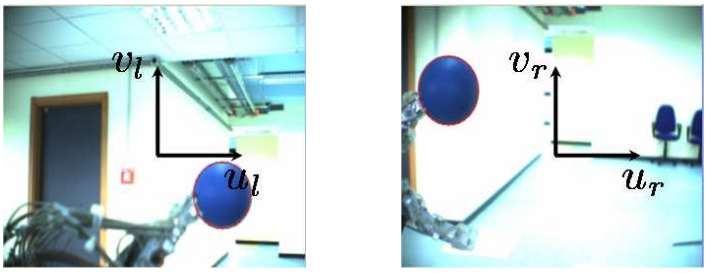

Figure 6: Two typical images taken from the two cameras mounted on the eyes of the robot. The attention system gives us the target position on the two image planes (in this case the center of the blue ball). The coordinates of the target on the right image plane will be denoted u_r, v_r, while on the left image will be denoted u_l, v_l. The `tracker controller` task consists in moving the eyes and the neck in order to keep the target point at the center of the two image planes, i.e. $u_r = v_r = u_l = v_l = 0$.

2 Tracker controller

One of the main modules in the reaching controller is represented by the `tracker controller`. The control objective of this specific module consists in directing gaze toward a given target. The input of this module is represented by the target location in the image planes of the right and left eyes; this information is received by the `target locator` module whose task is to find the target in the right and left image planes. The output instead consists in the head motor commands necessary to direct gaze toward the target.

2.1 Implementation

In this section we describe how the tracker has been implemented on James. The crucial aspect concerns the redundancy of the control problem as it has been stated above. In order to state this more clearly, we need to be more rigorous in defining the control task previously described as "directing gaze toward a given target". Specifically, let u_r and v_r be the coordinates of the target on the right image plane. Similarly, let u_l and v_l be the coordinates of the target on the left image plane (see Figure 6). The values of u_r, v_r, u_l, v_l are the output of another module, the `target locator`. Therefore, directing gaze toward the target consists in moving the neck and the eyes so as to obtain $u_r = 0$, $v_r = 0$, $u_l = 0$, $v_l = 0$. Let us define the vector

$\tilde{\mathbf{u}}_{target} = \begin{bmatrix} u_r & v_r & u_l & v_l \end{bmatrix}^\top \in \mathbb{R}^4$ corresponding to the target location in the image planes. Assuming that the target is stationary with respect to the robot, we have that $\tilde{\mathbf{u}}_{target}$ can be expressed as a function of the head configuration $\mathbf{q}_{head} = \begin{bmatrix} \mathbf{q}_{eyes}^\top & \mathbf{q}_{neck}^\top \end{bmatrix}^\top \in \mathbb{R}^6$:

$$\tilde{\mathbf{u}}_{target} = \tilde{f}_{head}(\mathbf{q}_{head}),$$

where the function $\tilde{f}_{head} : \mathbb{R}^6 \longrightarrow \mathbb{R}^4$ depends on the head kinematics. Under suitable assumptions[4], we do not need to impose simultaneously the four conditions $u_r = 0$, $v_r = 0$, $u_l = 0$, $v_l = 0$ since one of them will be automatically satisfied given that the other three conditions are satisfied[5]. Under this simplification we have that our control task can be redefined as the problem of controlling $\mathbf{u}_{target} = \begin{bmatrix} u_r & u_l & v_l \end{bmatrix}^\top \in \mathbb{R}^3$ to zero. The kinematic function will be in this case:

$$\mathbf{u}_{target} = f_{head}(\mathbf{q}_{head}), \qquad f_{head} : \mathbb{R}^6 \longrightarrow \mathbb{R}^3.$$

Clearly, the task specification does not constrain all the head degrees of freedom. Roughly speaking[6], we are imposing $m = 3$ constraints but we have $n = 6$ free variables available so that we remain with $n - m = 3$ additional degrees of freedom. Practically, we can have different configuration of the head ($\mathbf{q}_{head,1} \neq \mathbf{q}_{head,2}$) both keeping the same target in fixation ($\mathbf{u}_{target,1} = \mathbf{u}_{target,2} = 0$). This redundancy issue has to be addressed carefully given the kinematic and dynamic properties of the head. Specifically, a trivial solution (such as constraining/blocking three degrees of freedom out of six) is not to be recommended since a good tracking behavior should involve all the head

[4]The hypothesis is that we do not move the differential tilt, i.e. $\alpha_t^d = 0$ and that the camera optical axes are somehow aligned with the pan rotation axes. See also Section 0.1 for further details.

[5]In practice we have that if $u_l = 0$, $v_l = 0$ and $u_r = 0$ then $v_r = 0$. Alternatively, if $u_l = 0$, $u_r = 0$ and $v_r = 0$ then $v_l = 0$. This fact follows trivially considering that the target moves in a three dimensional space.

[6]More formally, let $\bar{\mathbf{q}}_{head} = \begin{bmatrix} \bar{\mathbf{q}}_{eyes} & \bar{\mathbf{q}}_{neck} \end{bmatrix}$ be a fixating position, i.e. $f_{head}(\bar{\mathbf{q}}_{head}) = 0$. Moreover, let's assume that the given head configuration is non-singular, i.e. the Jacobian matrix:

$$\frac{\partial f_{head}}{\partial \mathbf{q}_{head}}(\bar{\mathbf{q}}_{head}),$$

has full row rank. Then, by the implicit function theorem there exists a function $\mathbf{q}_{neck}(\cdot) : \mathbb{R}^3 \longrightarrow \mathbb{R}^3$ (locally defined around $\bar{\mathbf{q}}_{eyes}$) such that $f_{head}(\mathbf{q}_{eyes}, \mathbf{q}_{neck}(\mathbf{q}_{eyes})) = 0$ for all the configuration $\mathbf{q}_{eyes}$ belonging to the neighborhood of $\bar{\mathbf{q}}_{eyes}$.

degrees of freedom. Therefore, a good tracker should take advantage of the eyes reduced inertia to perform fast movements; at the same time the eyes limited range of movements should be overcome by moving the neck which is instead capable of wider movements.

With these ideas in mind the strategy we have chosen consists in using the eyes version and common tilt to perform a sort of saccadic movement on the desired target and then to follow the movement of the eyes with the neck yaw and pitch, respectively. This choice is a consequence of the fact that the eyes can make fast movements because of their low inertia. However, their range of movement is small if compared to the neck which has a wider range even if with a larger inertia. This strategy allows us to keep the target at the center of the image while allowing fast and large movements of the target itself. Mathematically the above strategy can be implemented as follows:

$$\begin{cases} \frac{d\alpha_v^c}{dt} &= K_p(u_l + u_r) \\ \frac{d\theta_y}{dt} &= K_y \alpha_v^c \\ \frac{d\alpha_t^c}{dt} &= K_t(v_l + v_r) \\ \frac{d\theta_p}{dt} &= K_r \alpha_t^c \end{cases}, \tag{4}$$

where α_t^c and α_v^c are the eyes version and common tilt and where θ_y and θ_p are the yaw and pitch movement of the neck. In the proposed control scheme, the vergence degree of freedom α_v^d, which somehow corresponds to the distance of the target does not influence the neck position and is therefore controlled separately from the neck:

$$\frac{d\alpha_v^d}{dt} = K_p(u_l - u_r). \tag{5}$$

Finally, the neck roll degree of freedom θ_r is maintained fixed, i.e. $\theta_r^d = 0$.

The proposed control strategy allows us to asymptotically fixate the target ($u_l \to 0$, $v_l \to 0$, $u_r \to 0$ which implies $v_r \to 0$) while also also guaranteeing an asymptotically straight gaze ($\alpha_v^c \to 0$, $\alpha_t^c \to 0$). Moreover, by choosing a suitable value for the gains K_p, K_y, K_t and K_r it is possible to achieve an asymptotic behavior with the eyes moving rapidly on the target and the neck

following the eye movement with a slower movement[7] (see Figure 7).

[7]Choosing suitable values for the gains K_p, K_y, K_t and K_r is not an easy task. Practically, this is due to the fact that the controlled system is nonlinear. Therefore, the system time response (settling time, overshoot, step time) may vary considerably depending on the system initial configuration. The large overshoot observed in Figure 7 is a consequence of this non-linearity.

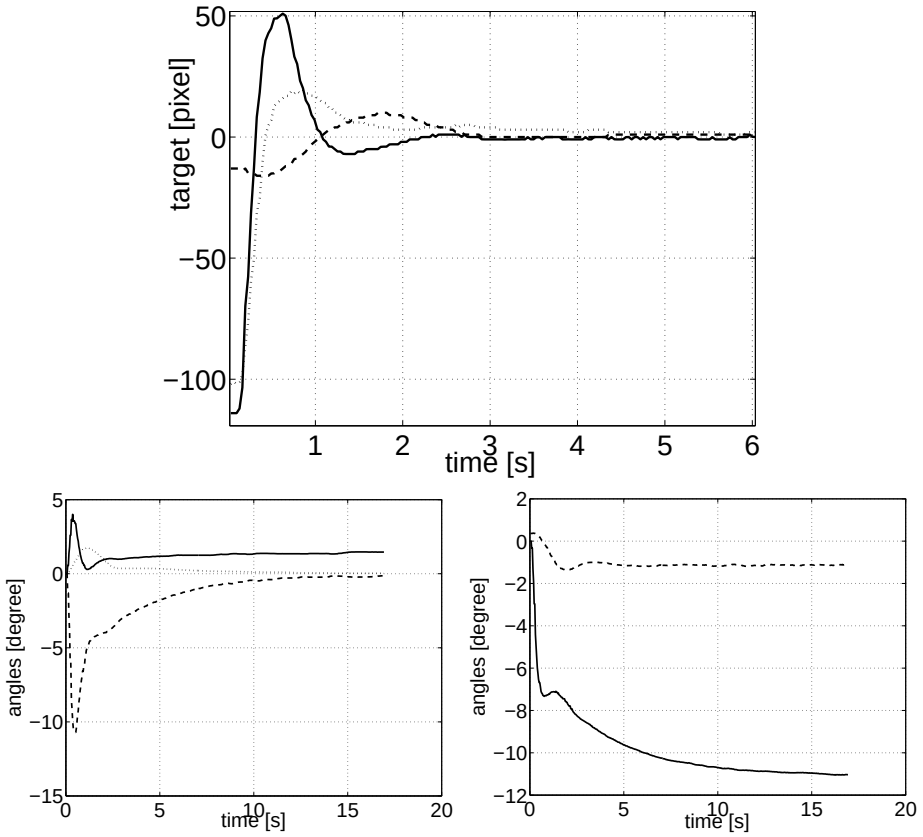

Figure 7: The top picture shows the time response of target position (u_l: solid, v_l: dashed, u_r: dotted) during a fixation movement. It can be seen that the target is effectively driven to the image center (to an accuracy up to one pixel). The bottom left picture shows the time response of the eyes position (α_v^d: solid, α_v^c: dashed, α_t^c: dotted); notice that the eyes effectively reach a straight gaze configuration ($\alpha_v^c \to 0$, $\alpha_t^c \to 0$) and the target distance is encoded in the vergence α_v^d whose steady state value is different from zero. Finally, the right bottom picture shows the neck movement (θ_p: solid, θ_y: dashed). The pan and tilt steady state values converge to the target direction.

3 Reaching

In this section, we describe the two approaches we followed to solve the reaching task on our robot.The first method uses the forward mapping between the arm joint space and the three dimensional position of the hand represented in the head reference frame. The second method uses a visual servoing technique to control the speed of the arm to minimize the position of the hand in the image plane with respect to a desired target (usually the fixated object).

3.1 Open Loop Reaching

Suppose the robot is tracking a target using the control strategy described in Section 2. In the assumption of perfect tracking (the visual error is zero), the three dimensional spatial position of the target with respect to the robot, denoted $\tilde{\mathbf{x}}_{target} \in \mathbb{R}^3$, is a function of the head configuration $\mathbf{q}_{head} = \begin{bmatrix}\theta_y & \theta_p & \theta_r & \alpha_v^d & \alpha_v^c & \alpha_t^c\end{bmatrix}^\top \in \mathbb{R}^6$. However, the representation of the target position, $\tilde{\mathbf{x}}_{target}$, in terms of the full head configuration, $\mathbf{q}_{head}$, is clearly redundant. Specifically, the same target position can be represented by different head configurations. To obtain a one to one mapping between the target position and the head configuration we have to analyze the `tracker controller`. The latter maintains θ_r stationary ($\theta_r^d = 0$) and poses additional constraints on the head joints. In particular we know from section 2 that the controller minimizes α_t^c and α_v^c (see equation (4)) so that they asymptotically converge to zero ($\alpha_t^c \to 0$ and $\alpha_v^c \to 0$). Ideally, after fixation is achieved, we have:

$$\mathbf{q}_{head} = \begin{bmatrix}\theta_y & \theta_p & 0 & \alpha_v^d & 0 & 0\end{bmatrix}^\top \in \mathbb{R}^6. \tag{6}$$

Since there exists a one to one mapping between the three dimensional position of the target $\tilde{\mathbf{x}}_{target}$ and the three non-zero variables θ_y, θ_p and α_v^d, we can define:

$$\mathbf{x}_{target} = \begin{bmatrix}\theta_y & \theta_p & \alpha_v^d\end{bmatrix}^\top \in \mathbb{R}^3. \tag{7}$$

This new variable $\mathbf{x}_{target} \in \mathbb{R}^3$ uniquely codes the spatial position of the target in a way that resembles a three dimensional polar representation. In particular θ_y and θ_p code respectively *azimuth* and *elevation*, while *distance* is substituted with α_v (the *vergence* angle).

If the robot tracks the hand, the same subset of the head joint space can be used to code the spatial location of the hand:

$$\mathbf{x}_{hand} = \begin{bmatrix} \theta_y & \theta_p & \alpha_v^d \end{bmatrix}^\top \in \mathbb{R}^3.$$

Under these assumptions, the *forward mapping* $f_{arm} : \mathbb{R}^4 \longrightarrow \mathbb{R}^3$ relates the arm configuration $\mathbf{q}_{arm}$ with the position of the hand $\mathbf{x}_{hand}$:

$$\mathbf{x}_{hand} = f_{arm}(\mathbf{q}_{arm}), \qquad f_{arm} : \mathbb{R}^4 \longrightarrow \mathbb{R}^3. \tag{8}$$

In the next section we show how we trained a neural network to approximate the arm forward mapping (Eq. 8):

$$\mathbf{x}_{hand} = \hat{f}_{arm}(\mathbf{q}_{arm}), \qquad \hat{f}_{arm} : \mathbb{R}^3 \longrightarrow \mathbb{R}^4. \tag{9}$$

Suppose now that the robot is fixating a target and that we want to control the robot to reach for it. Formally the problem can be formulated as determining the value of $\mathbf{q}_{arm}$ which solves the following optimization problem:

$$\min_{\mathbf{q}_{arm}} (J) = \min_{\mathbf{q}_{arm}} \left\| \mathbf{x}_{hand} - \mathbf{x}_{target} \right\|^2, \tag{10}$$

where $\mathbf{x}_{target}$ is measured from the encoders of the head, while $\mathbf{x}_{hand}$ is computed from $\mathbf{q}_{arm}$ through Eq. (9). Given the redundancy of the arm kinematics the minimization (10) has infinite solutions. We constrained the problem by forcing one of the joints, for example joint number 2, to remain as close as possible to a predefined value q_{20}:

$$\min_{\mathbf{q}_{arm}} (J_c) = \min_{\mathbf{q}_{arm}} \left[\left\| \mathbf{x}_{hand} - \mathbf{x}_{target} \right\|^2 + (q_{arm,2} - q_{20})^2 \right]. \tag{11}$$

The optimization of (11) can be performed numerically using various algorithms. Discussing the different properties of these numerical solutions falls outside the scope of this paper. In our implementation, we used the downhill simplex method [1] as implemented in [2].

3.2 Learning the open loop reaching

To learn the forward map of Eq. (8) we programmed the robot to perform random movements with the arm (chosen to uniformly sample a predefined region in the robot workspace). During this "exploratory" phase the robot tracked the hand, and collected samples of the form:

$$\left(\mathbf{q}^i_{arm}, \mathbf{x}^i_{hand} \right)_{i=0,1\ldots}$$

A neural network was then trained to learn the relation:

$$\mathbf{x}_{hand} = \hat{f}_{arm}\left(\mathbf{q}_{arm}\right), \tag{12}$$

which approximates Eq. (8).

In the experiment reported in this paper we collected a data set of about 2890 samples that we divided in a training set ($N_{train} = 2168$ samples) and a test set ($N_{test} = 725$ samples). The neural network we employed was the Receptive Field Weighted Regression model proposed by [3]. This network implements an online learning method, meaning that a learning step is performed every time a new sample is presented to the network. All samples in the training set were shown to the network in a random order. After each training step the performance of the network was validated on the whole test set, by computing the Mean Squared Error (MSE) between each sample in the test set, $\mathbf{x}^i_{hand}$, and the corresponding network output, $\hat{\mathbf{x}}^i_{hand}$:

$$MSE = \frac{1}{N_{test}} \sum_{i=0}^{N_{test}-1} \|\mathbf{x}^i_{hand} - \hat{\mathbf{x}}^i_{hand}\|^2 \tag{13}$$

The plot in figure 8 shows the trend of the error on the test set during learning. At the end of the training the network reached the performance of $MSE = 5.7$ (with $STD = 10.4$).

In the experiment reported in this paper the network was trained offline. This was to simplify the analysis of the results and perform cross-validation on a predefined test set. However, the learning algorithm we used was purely incremental (each sample was shown to the network only once and immediately discarded), so in this regard it would be straightforward to have an online implementation of the same mechanism.

3.3 Closed Loop Reaching

If the robot can visually measure the distance between the hand and the target, reaching can also be solved visually, by implementing a closed loop control. The underlying idea consists in performing a preliminary (open loop) reaching movement and then refining the action by visually correcting any residual error.

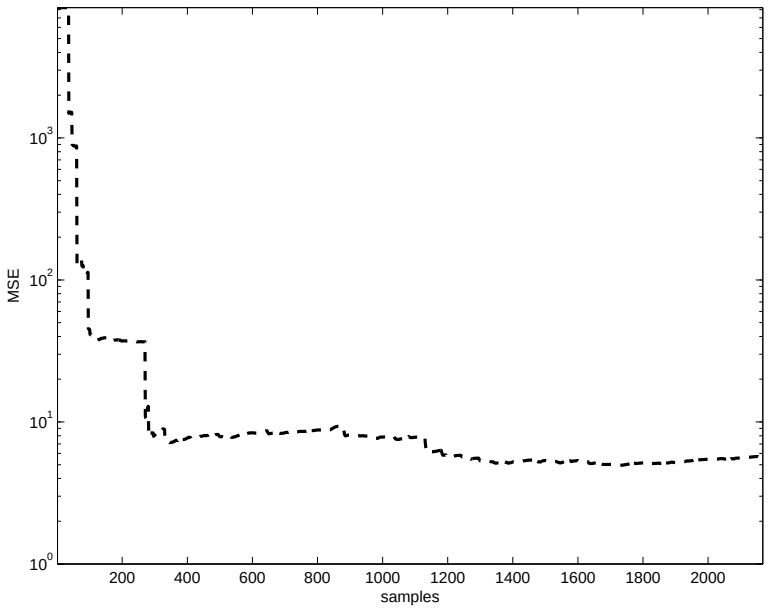

Figure 8: Learning of the arm forward function. The plot reports the *MSE* on the test set during learning (see the text for details).

We know that the Jacobian matrix relates arm velocities $\dot{\mathbf{q}}_{arm}$ with hand velocities in the image plane $\dot{\mathbf{u}}_{hand} = \begin{bmatrix} \dot{u}_r & \dot{u}_l & \dot{v}_l \end{bmatrix}^\top$:

$$\dot{\mathbf{u}}_{hand} = \tilde{\mathbf{J}}\left(\mathbf{q}_{arm}, \mathbf{q}_{head}\right) \dot{\mathbf{q}}_{arm}, \tag{14}$$

where $\tilde{\mathbf{J}} \in \mathbb{R}^{3\times 4}$ depends on both the configuration of the arm and the head. Practically, assuming sufficiently small arm movements $\Delta\mathbf{q}_{arm}$, we can use the following approximation:

$$\Delta\mathbf{u}_{hand} = \tilde{\mathbf{J}}\left(\mathbf{q}_{arm}, \mathbf{q}_{head}\right) \Delta\mathbf{q}_{arm}, \tag{15}$$

where $\Delta\mathbf{u}_{hand} = [\Delta u_r, \Delta u_l, \Delta v_l]^\top$ is the image plane displacement resulting from the arm movement $\Delta\mathbf{q}_{arm}$. Due to the additional constraints posed by the head tracker, we showed that only a subset of $\mathbf{q}_{head}$, $\mathbf{x}_{target}$, is sufficient to uniquely identify the position of the head, so we can rewrite equation (15) as:

$$\Delta\mathbf{u}_{hand} = \tilde{\mathbf{J}}\left(\mathbf{q}_{arm}, \mathbf{x}_{target}\right) \Delta\mathbf{q}_{arm}, \qquad \tilde{\mathbf{J}} \in \mathbb{R}^{3\times 4}. \tag{16}$$

Moreover, after the preliminary open loop reaching movement, we know

that $\mathbf{x}_{target} = \hat{f}(\mathbf{q}_{arm})$ so that Eq. (16) can be further simplified to:

$$\Delta\mathbf{u}_{hand} = \mathbf{J}\left(\mathbf{q}_{arm}\right)\Delta\mathbf{q}_{arm}, \qquad \mathbf{J} \in \mathbb{R}^{3\times 4} \tag{17}$$

in which $\mathbf{J}$ depend only on the arm joint configuration $\mathbf{q}_{arm}$.

Suppose now the robot has to reach for an object, whose visual position is represented by $\mathbf{u}_{target}$. To solve this problem the controller of the arm needs to compute the arm command which minimizes the error:

$$e = \left\|\mathbf{u}_{hand} - \mathbf{u}_{target}\right\|^2. \tag{18}$$

When the head tracker has achieved convergence on the object, $\mathbf{u}_{target} \approx 0$ and $e \approx \|\mathbf{u}_{hand}\|^2$. Due to the redundancy of the arm, the minimization of e can have infinite solutions. Among them, the minimum norm solution corresponds to the one which produces the minimum joint speeds, that is:

$$\dot{\mathbf{q}}_{arm} = -k \cdot \mathbf{J}^{\#}\mathbf{u}_{hand}, \qquad \mathbf{J}^{\#} \in \mathbb{R}^{4\times 3}, \tag{19}$$

where $\mathbf{J}^{\#}$ is the pseudo-inverse of $\mathbf{J}$.

3.4 Learning the Arm Jacobian

In the previous section we used the Jacobian of the manipulator $\mathbf{J}$ (actually its pseudo-inverse $\mathbf{J}^{\#}$) to control the arm to reach for a visually identified object. In this section we describe a procedure by which the robot can autonomously acquire $\mathbf{J}$ and $\mathbf{J}^{\#}$.

As described in Section 3.2, the robot moves the arm randomly, while maintaining gaze on the hand. At the end of each movement j the arm is in a configuration $\mathbf{q}^j_{arm}$, while the eyes are fixating the hand ($\mathbf{u}_{hand} \approx 0$) with a straight gaze (the head tracker has reached convergence). Each arm configuration corresponds to a different value of $\mathbf{J}_j = \mathbf{J}\left(\mathbf{q}^j_{arm}\right)$. Now the robot inhibits the head tracker and performs a sequence m of small arm movements $\Delta\mathbf{q}^k_{arm}$ which perturb $\mathbf{u}_{hand}$ of small amounts $\Delta\mathbf{u}^k_{hand}$:

$$\left(\ \Delta\mathbf{u}^k_{hand}, \Delta\mathbf{q}^k_{arm}\ \right)_{k=0,1\ldots,m}$$

All m perturbations $\Delta\mathbf{u}^k_{hand}$ and $\Delta\mathbf{q}^k_{arm}$ are linearly related through $\mathbf{J}_i$ as described in Eq. (16). From these m observations we can derive a least squares estimation of $\mathbf{J}_j$ from which, in turn, we can compute the Moore-Penrose pseudo-inverse $\mathbf{J}^{\#}_j$.

Re-iterating this procedure leads to the collection of a series of examples:

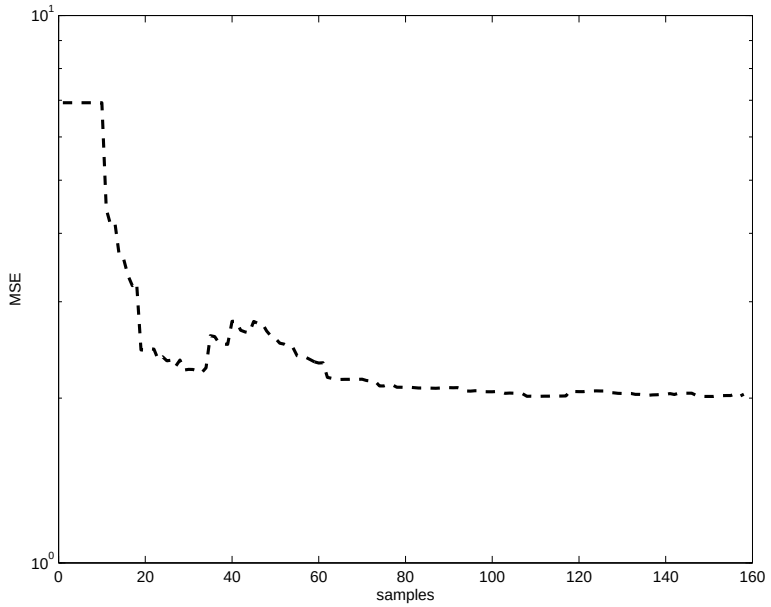

Figure 9: Learning the arm jacobian. The plot represents the *MSE* on the test set during learning. See text.

$$\left(\ \mathbf{q}_{arm}^{j}, \mathbf{J}_{j}^{\#} \ \right)_{j=0,1...}$$

An approximation $\hat{\mathbf{J}}^{\#}$ of $\mathbf{J}^{\#}$ is finally obtained by training a neural network:

$$\mathbf{g}\left(\mathbf{q}_{arm}\right), \qquad g : \mathbb{R}^4 \longrightarrow \mathbb{R}^{12}, \tag{20}$$

whose output components are the coefficients of $\hat{\mathbf{J}}^{\#} \in \mathbb{R}^{4\times 3}$.

We report here the result of a learning session. The robot explored 210 different arm positions $\mathbf{q}_{arm}^{j}$ randomly distributed within a region of the workspace. In each of these positions the robot executed $m = 10$ perturbations $\Delta\mathbf{q}_{arm}^{k}$ and estimated an example $\mathbf{J}_{j}^{\#}$ for the neural network. Overall we collected 210 samples for $\mathbf{J}^{\#}$. We trained the neural network on a subset of $N_{train} = 158$ elements (training set); each sample was shown to the network only once and then discarded. Following each training step, we evaluated the performance of the network by computing *MSE* on the remaining $N_{test} = 52$ elements (test set). At the end of the training the error on the test set was $MSE = 2$ ($STD = 7.1$). Figure 9 reports the plot of the error during learning.

4 Results

In this section we describe the reaching performance obtained with the reaching controller described in the previous section. Within this context, it is important to note that a formal definition of the performance index is a nontrivial task.

If we were to consider a robot which operates in an highly structured environment, the definition of the performance index would have been much easier. Specifically, for an industrial robot, the reaching task can be identified with the problem of positioning the hand accurately with respect to a world reference frame[8]. In this case, the reaching precision can be measured in terms of the distance between the desired and actual position of the hand in the world reference frame.

In our case, a similar performance index definition cannot be applied. James has not been designed to operate in an industrial scenario. Moreover, in our context, the definition of a reference frame fixed with respect to the external world does not play the same crucial role played in the industrial framework. In our mind, it is more important to precisely locate the hand with respect to the object than to precisely locate the hand in the external world frame. Therefore, our reaching performance index should measure the Cartesian distance between the object to be grasped and the final position of the hand. However, measuring this distance is not an easy task. In this section we approximate the real distance with the (stereo) *image plane distance*. Practically speaking, suppose the robot sees a target $\mathbf{u}_{target}$ to be grasped. Following our strategy, in order to reach the target we need to fixate it, i.e. $\mathbf{u}_{target} = 0$. Using the available sensor (i.e. vision) the best we can do to precisely reach the target is moving the hand to the fixation point, i.e. $\mathbf{u}_{hand} \longrightarrow 0$. Clearly, the image plane distance $\|\mathbf{u}_{hand} - \mathbf{u}_{target}\|$ can be used as a rough estimate of the reaching precision, i.e. of the Cartesian distance between the target to be reached and the position of the hand. Specifically, assuming infinite resolution of the camera sensor, if $\|\mathbf{u}_{hand} - \mathbf{u}_{target}\| = 0$ then the hand has exactly reached the target. In a more realistic case, when the image plane distance is null, we can only guarantee that the Cartesian target-hand distance is upper bounded by a quantity which depends only on

[8]Typical industrial robots do not use vision. Their grasping movement is the result of 3-D positioning the gripper exactly in the position where they know the object to be grasped will be positioned. The problem of positioning the object is then left to the user.

the camera intrinsic parameters[9].

4.1 Open Loop

The first attempt to reach the target consists in using (11) to choose the arm configuration $\mathbf{q}_{arm}$ which brings the hand to the center of the image planes. Clearly, if the forward kinematic function (8) were perfectly represented and if the target were reachable, we would have $\mathbf{x}_{hand} = \mathbf{x}_{target}$, which implies that the target-hand Cartesian distance is null (see Section 3 for details). Therefore, in this ideal case, the open loop strategy already results in $\|\mathbf{u}_{hand} - \mathbf{u}_{target}\| = 0$. In practice, the model (8) cannot exactly represent the system kinematic[10]. Therefore, even tough we can find $\mathbf{q}_{arm}$ such that $\mathbf{x}_{hand} = \hat{f}_{arm}(\mathbf{q}_{arm})$ it is not guaranteed that after the movement execution $\|\mathbf{u}_{hand} - \mathbf{u}_{target}\| = 0$. Figure 10 shows the image plane errors after the execution of the open loop movement. The plot has been obtained by fixating a target and performing a series of open loop movements. Each open loop movement was different because (11) was solved by choosing a different value q_{20}. Let us denote the open loop movements $\mathbf{q}^1_{arm}, \ldots, \mathbf{q}^K_{arm}$ such that:

$$\mathbf{q}^k_{arm} = \arg\min_{\mathbf{q}_{arm}} \left[\left\| \hat{f}_{arm}(\mathbf{q}_{arm}) - \mathbf{x}_{target} \right\|^2 + \left(q_{arm,2} - q^k_{20} \right)^2 \right]. \qquad (21)$$

The above minimization is such that $\hat{f}_{arm}(\mathbf{q}^k_{arm}) = \mathbf{x}_{target}$. Ideally, in absence of modeling errors we would have $\mathbf{x}_{hand} = \mathbf{x}_{target}$ since $\mathbf{x}_{hand} = f_{arm}(\mathbf{q}^k_{arm})$. In practice we have $\mathbf{x}_{hand} \simeq \hat{f}_{arm}(\mathbf{q}_{arm})$ so that we can only achieve an approximate reaching $\mathbf{x}_{hand} \simeq \mathbf{x}_{target}$ which reflects into small image plane errors $\|\mathbf{u}_{hand} - \mathbf{u}_{target}\| \simeq 0$. Different choices of the free variables $q^1_{20}, \ldots, q^K_{20}$ lead to different image plane errors as shown in Figure 10.

4.2 Closed Loop

As we described in Section 3.3 the residual image plane errors due to imperfections in the forward kinematic model can be reduced by a visual closed

[9] Computing this upper bound is out of the scope of this paper.

[10] Part of the representational errors are related to the way we have chosen the represent the kinematic function, in this case the so called Receptive Field Weighted Regression model. Part are due to the mechanical plays of the kinematic structure.

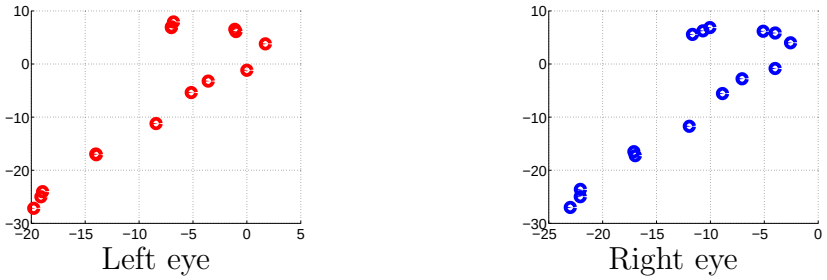

Figure 10: The figure shows the open loop image plane errors $\mathbf{u}_{hand}$ for different choices of the redundant variable q_{20}. For both pictures, on the horizontal axis we have u_r and u_l while on the vertical axis we have v_r and v_l (always in pixels). In this specific case the target is in the middle of the two image planes $[u_{r,target}, v_{r,target}] = [0, 0]$ and $[u_{l,target}, v_{l,target}] = [0, 0]$. The hand position in the image plane is instead represented by the small circles. Each circle corresponds to the hand position after a different open loop movement, i.e. a different value of q_{20}.

loop control strategy. This control strategy moves the arm so as to progressively drive the hand position in the image planes ($\mathbf{u}_{hand}$) to zero. Of course this is guaranteed only if the Jacobian matrix has been learned in a sufficient accuracy. Figures 11, 12, 14 and 13 show how the hand is actually driven to the exact image center in both the image planes. Moreover, it is important to notice the approximative linearity of the path followed by the hand. This linearity denotes a good accuracy of the learned Jacobian.

4.3 Superimposed Open and Closed Loop

Finally, we tested an alternative control strategy based on activating the closed loop phase immediately after the hand becomes visible on both image planes. This second strategy is such that the open a closed loop strategies will be active at the same time for a certain period. The structure is based on a classical control scheme, which can be represented as follows:

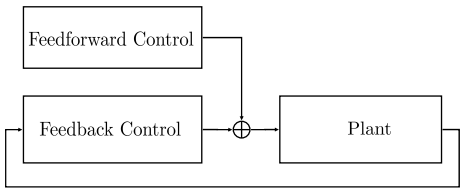

Practically, the feedforward control corresponds to the open loop part of the reaching movement. It is activated exactly as described in Section 3.1 and therefore it does not require the hand to be visible in the image plane. The feedback control instead corresponds to the closed loop part of the movement and can be activated when the hand has been localized in both the image planes. Practically, the final solution can be described by the following scheme:

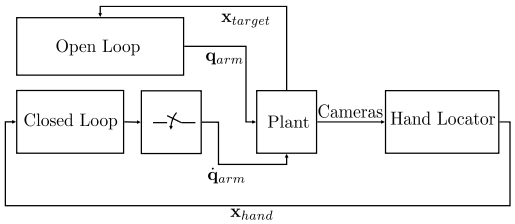

Clearly, when both the open and closed loop controllers are active, the system receives position and velocity control simultaneously[11].

[11] A position command $\mathbf{q}_{arm,d}$ is always translated into a trajectory following command by moving the hand along a trajectory $\mathbf{q}_{arm}(t)$, $t \in [0, T]$ such that: T is the execution time, $\mathbf{q}_{arm}(0)$ is the arm position when the command is received, $\mathbf{q}_{arm}(T) = \mathbf{q}_{arm,d}$ is the desired final position. If a velocity command $\dot{\mathbf{q}}_{arm,d}$ is received while executing a position command $\mathbf{q}_{arm}(t)$, the original velocity command is transformed into a different one which takes into account the position command. In particular, the resulting commanded velocity is $\dot{\mathbf{q}}_{arm} = \dot{\mathbf{q}}_{arm}(t) + \dot{\mathbf{q}}_{arm,d}$.

A comparison between this control strategy and the one proposed in Section 4.2 is given in Figure 15 and 16. Performances are clearly improved. First the image plane movement (Figure 15) is much more regular resulting in a unique linear movement instead of begin divided into two segments. Secondly, the execution time is clearly reduced as it can be noted in Figure 16.

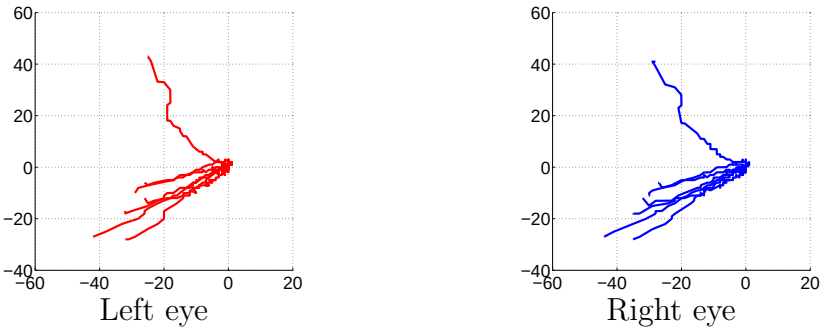

Figure 11: The picture shows different closed loop control actions. Each trace correspond to a different Cartesian position of the target to be reached (which is always at the center of the image planes). The traces start exactly after the execution of the open loop movement, so that the initial position corresponds to the initial open loop error. Notice that all the traces end up in the image center (both left and right image planes) thus indicating that the visual errors are completely eliminated by the closed loop controller.

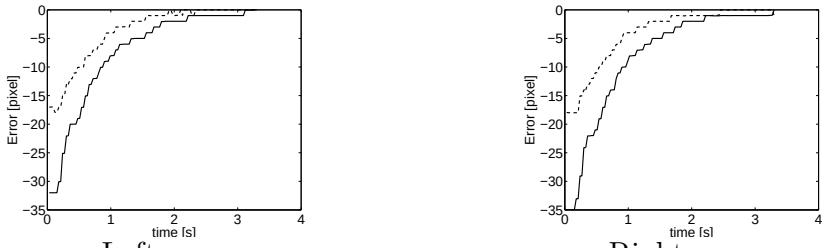

Figure 12: The picture shows the time response of the closed loop controller. The solid lines corresponds to the hand horizontal position in the left (u_l) and right (u_r) image planes. The dashed lines correspond to the vertical position, v_l and v_r. Clearly, the hand is driven to the image center with a null steady state error. Even if velocity was not our primarily concern, the time response is reasonably fast (an error of thirty pixels is eliminated in about three seconds).

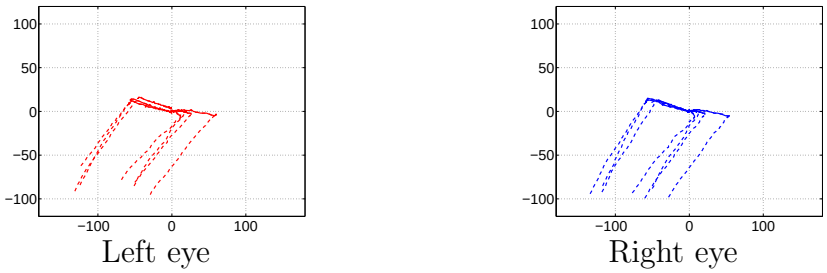

Figure 13: The figure shows the movement of the hand on the image planes during the execution of different reaching actions. For both pictures, on the horizontal axis we have u_r and u_l while on the vertical axis we have v_r and v_l (always in pixels). The traces correspond to the hand position during the movement. The solid line is the hand movement during the closed loop phase. The dashed trace is instead the hand movement during the open loop phase. Clearly the open loop movement drives the hand to the target (the image centers) with a relatively small error. The closed loop phase reduces this error to zero.

Figure 14: The picture shows the time response of the closed loop and open loop strategy. The solid lines correspond to the hand horizontal position in the left (u_l) and right (u_r) image planes. The dashed lines correspond to the vertical position, v_l and v_r. Remarkably, the open loop phase is faster but does not drive the hand exactly on the target. The closed loop is slower but more accurate.

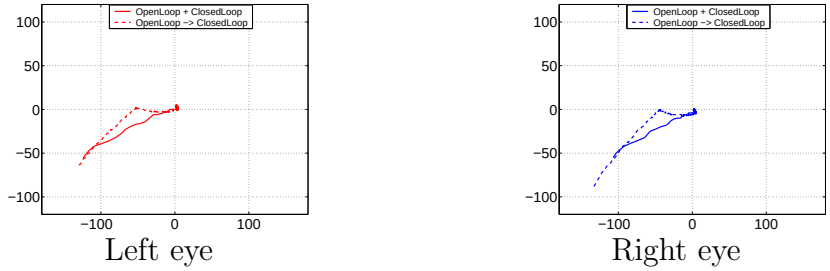

Figure 15: The figure shows the movement of the hand on the image planes during the execution of a single reaching movement. For both pictures, on the horizontal axis we have u_r and u_l while on the vertical axis we have v_r and v_l (always in pixels). The traces correspond to the hand position during the movement. The dashed line is the hand movement during an open loop movement followed by a closed loop phase. The solid trace is instead the hand movement during the superposition of open and closed loop strategies. Clearly this second control architecture is more effective in terms of driving the hand directly to the target in spite of waiting the end of open loop movement.

Figure 16: The pictures show the time response of u_l (left picture) and v_l (right picture). The dashed line is the hand movement during an open loop movement followed by a closed loop phase. The solid trace is instead the hand movement during the superposition of open and closed loop strategies. Remarkably, this second control architecture results in a faster response because when the hand becomes visible it is directly driven to the target without waiting for the open loop phase end.

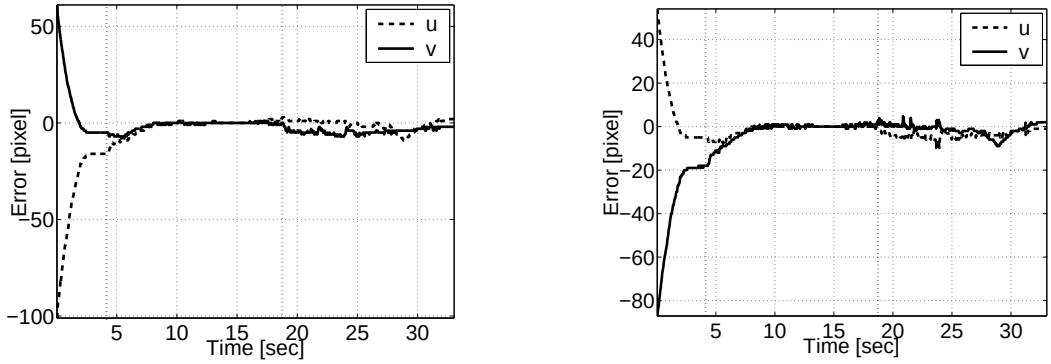

Left eye Right eye

Figure 17: The figure shows image plane movements during a three phase movement. First the open loop movement, then the closed loop movement and finally a movement in the null space of the given task (keeping the hand in fixations). Remarkably, there's a minor image plane movement (less then ten pixels) during the null space movement, thus indicating a very good jacobian estimation.

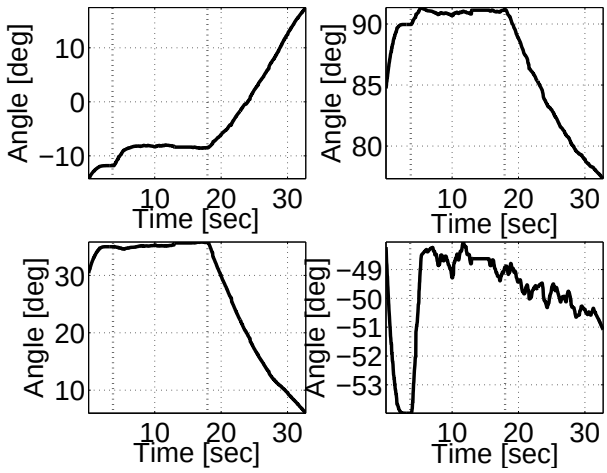

Figure 18: The picture shows the arm movement corresponding to the image plane movements shown in Figure 17. Remarkably, the null space movement is characterized by large joint movements which are however not visible in the image plane due to the jacobian based compensation.

References

[1] J. A. Nelder and R. Mead. A simplex method for function minimization. *Computer journal*, 7:308–313, 1965.

[2] W. H. Press. *Numerical Recipes in C*. Cambridge University Press, Cambridge, 1990.

[3] S. Schaal and C.G. Atkenson. Constructive incremental learning from only local information. *Neural Computation*, 8(10):2047–2084, 1998.

2.3.3.4 Acquisition of dynamic internal model

In the present section we describe a procedure for estimating the internal dynamic model of a robotic arm. This model will also be used to estimate torques at the joint, information which is usually very helpful when performing highly dynamical tasks (e.g. trowing a ball). All the described procedures will be based on a force/torque sensor positioned at the the root of the kinematic chain describing the arm structure (see the following Figures).

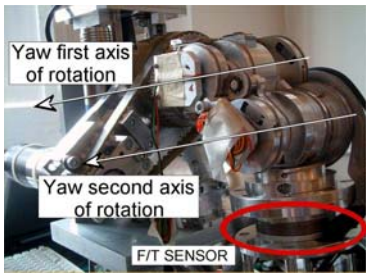

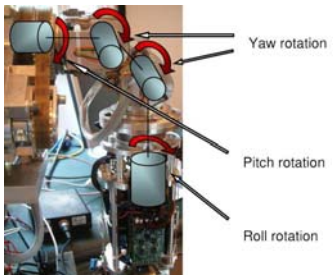

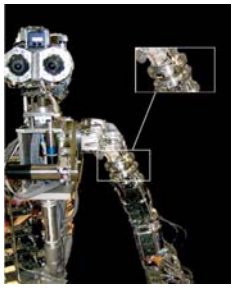

2.3.3.4.1 Force-torque sensing and dynamical models

The essential dynamic equations for describing the force/torque sensor measurement are essentially two: one describing the dynamic equation of motion and one describing the force/torque dynamic equation at the F/T sensor reference frame. Since our setup presents a force/torque sensor at the beginning of the kinematic chain, its measurements will not be the only external forces acting on the end effector of the robot, as in usual manipulators. This means that, depending on the configuration and on the trajectory followed by the manipulator, inertial, centrifugal and Coriolis, and gravitational forces and moment are measured.

This measurement can be modelled with the following dynamic equations:

$$M_{FT}(q)\ddot{q} + C_{FT}(q,\dot{q})\dot{q} + G_{FT}(q) = \begin{Bmatrix} F \\ T \end{Bmatrix}$$

where the variable q represents the generalized coordinates describing the arm configuration. Since we have a dynamical model of the sensor's measurements, which contains dynamical terms, our first goal is the calibration of the model. We want to find out which are the dynamical parameters involved. To do this, an identification algorithm has to be used. It is based on the following equation:

$$D_{FT}(q,\dot{q},\ddot{q})\,X_{FT} = \begin{Bmatrix} F \\ T \end{Bmatrix}$$

where $D_{FT}(q,\dot{q},\ddot{q})$ is a nonlinear matrix which depends only on trigonometric functions and X_{FT} is a constant vector of possible, which depend linearly with respect to $D_{FT}(q,\dot{q},\ddot{q})$ in the equation above. The estimation procedure is done using for example an LQ method, using F/T measurements as input.

In order to estimate joint torques, a different formulation has to be used. Considering an augmented system, composed of both joint d.o.f. and six sensor's d.o.f., the motion equations are:

$$\begin{bmatrix} M_{11} & M_{12} \\ M_{12}^T & M_{22} \end{bmatrix} \begin{Bmatrix} \ddot{q}_{jnt} \\ \ddot{q}_{sens} \end{Bmatrix} + \begin{bmatrix} C_{11} & C_{12} \\ C_{12}^T & C_{22} \end{bmatrix} \begin{Bmatrix} \dot{q}_{jnt} \\ \dot{q}_{sens} \end{Bmatrix} + \begin{Bmatrix} G_1 \\ G_2 \end{Bmatrix} = \begin{Bmatrix} \tau \\ FT \end{Bmatrix}$$

With this equation, a relationship between the F/T sensor measurements and the joint torques can be found as follows:

$$M_{12}^T \ddot{q}_{jnt} + M_{22}\ddot{q}_{sens} + C_{21}\dot{q}_{jnt} + C_{22}\dot{q}_{sens} + G_2 = FT \rightarrow M_{22}\ddot{q}_{sens} = FT - M_{12}^T \ddot{q}_{jnt} - C_{21}\dot{q}_{jnt} - C_{22}\dot{q}_{sens} - G_2 = 0$$

The equation is equal to zero because the sensor is linked to the arm, so there cannot be relative acceleration with the frame of reference behind. Setting also the velocities and the position equal to zero, and substituting the Joint torque equation into the F/T one, one obtains:

$$FT = M_{12}^T \left(M_{11}^{-1} \left(\tau - C_{11}\dot{q}_{jnt} - G_1 \right) \right) + C_{12}\dot{q}_{jnt} + G_2$$

And inverting with respect to τ, the torques at each joint can be found:

$$\tau = M_{11}^{-1} \left(\left(M_{12}^T \right)^{\dagger} \left(FT - C_{12}\dot{q}_{jnt} G_2 \right) \right) + C_{11}\dot{q}_{jnt} + G_1$$

Matrices M_{12}, C_{21}, G_2 are still not known. Considering the equation of motion in the form:

$$M(q)\ddot{q} + C(q,\dot{q})\dot{q} + G(q) = \tau$$

And proceeding as for the F/T identification algorithm, a linear dependency of the dynamical parameters involved with respect to trigonometric functions can be found, so that this system of equations can be written as:

$$D_\tau (q, \dot{q}, \ddot{q}) X_\tau = \tau$$

Notice that the vector of parameters of the F/T equations X_{FT} is not the same X_τ.

Vector X_τ can be identified through a relationship with X_{FT}. In our case, this relation is linear, if some kinematic parameters are set to be known (for example the length of the links from the base frame to the F/T sensor frame), but a more accurate analysis of that has to be done. This relation is:

$$X_{FT} = \Lambda \cdot X_\tau$$

where Λ is a mxn linear matrix, identified offline with an LQ method. Once the parameters are estimated, it is possible to determine the torques acting on each joint, using the equations above. This equation is invertible if matrix M_{12}^T is invertible. The invertibility of this matrix is still an open issue of this project, but we have seen that it loses rank when the Jacobian matrix is singular.

It is then important to notice that in the best case, in which one can identify the complete vector X_τ, these correspond to the real torques. In fact, depending on where the sensor is positioned, there would be some parameters of the motion equation that cannot be identified in this way.

Experimental results:

The experimental results, at the moment, only concern with the validation of the dynamical model of the arm of the robot, and with the identification algorithm for forces and moments sensor equations parameters. The picture below shows that the algorithm is able to find best parameters then the one given by the CAD. Here are shown the forces and moment acquired by the sensor (red line), the one, due to the same movement, using the CAD parameters (green line), and the estimation of forces and moments using the parameter estimation algorithm to find the parameters.

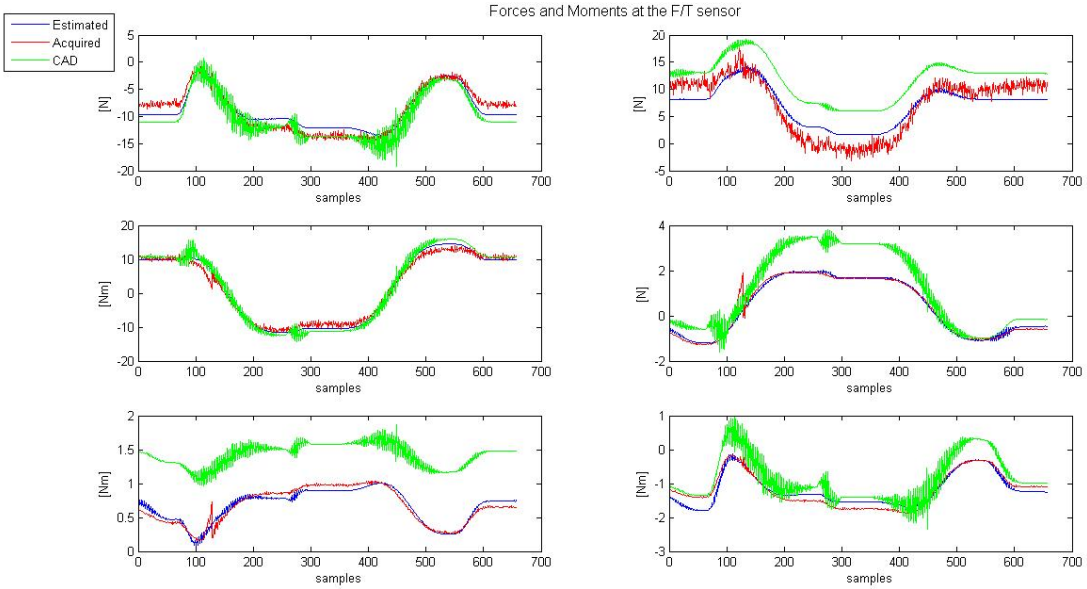

In any case, these parameters are not reliable. The reason of this unreliability is due to the high condition number of the matrix:

$$D(q,\dot{q},\ddot{q})^{\dagger} = \left(D'(q,\dot{q},\ddot{q}) * D(q,\dot{q},\ddot{q})\right) * D(q,\dot{q},\ddot{q})$$

$$A = D'(q,\dot{q},\ddot{q}) * D(q,\dot{q},\ddot{q})$$

and the condition number of A needs to be minimized. That has to be used in the pseudo-inverse algorithm, in order to estimate the parameters of the robot arm. Since the matrix D only depend on the kinematic variables $q, \dot{q}, \ddot{q}$, an optimal joint trajectory has to be found. We have decided to find a minimum jerk trajectory in the joint space, since it is already implemented on the control boards. This trajectory will minimize the condition number of matrix A and finding reliable parameters to describe the robot dynamical model.

2.3.4 Sensorimotor Integration and cortical sensorimotor maps. (UNIHER)

The work at Hertfordshire has addressed the fundamental question: How can raw, uninterpreted information from unknown sensors come to be used by a developing embodied agent with no prior knowledge of its motor capabilities? The approach to answer this in RobotCub is to pursue the development of artificial cortex using information theory as a means for self-organizing sensorimotor structures grounded in experience.

In nature, cognitive structures appear to be organized in the course of evolution and also in the course of development so as to reflect information-theoretic relations arising in the interaction of sensors, actuators, and the environment (including the social environment). Information distance (rather than mutual information or other measures such as Hamming distance) appears to lead to the best structured cortex-like maps of sensorimotor variables [see the paper below]. (For two jointly distributed random variables (e.g. two sensors), information distance is defined as the sum of their conditional entropies $d(X,Y)=H(X|Y)+H(Y|X)$. This satisfies the mathematical axioms for a metric, inducing a geometric structure on the agent's set of sensorimotor variables.) Sensory fields may be constructed on the basis of information methods [Olsson et al. 2004] and then used to autonomously discover sensorimotor laws, e.g. optical or tactile flow and visually guided movement [Olsson et al. 2006]. The particular environment experienced and changes in it can shape the sensorimotor maps and their unfolding in ontogeny [Olsson et al. 2006]. Details were reported in D3.2 "Initial results of experiments on the functional organization of the somatotopic maps and on the cortical representation of movements (report)", and also published as [Olsson et al. 2006a].

More recent work on the informational relationships between the agent, its actions, and the environment [see the paper below] considers a number of statistical measures to compute the informational distance between sensors including the information metric, correlation coefficient, Hellinger distance, Kullback-Leibler, and Jensen-Shannon divergence. The methods are compared using the sensory reconstruction method to fund spatial positions of visual sensors of different modalities in a sensor integration task. The results show how the information metric together with adaptive entropy maximization captures relations not found by the other measures for the construction of somatosensoritopic maps and the development of cross-modal sensory integration. Moreover, these methods are extended to temporally extended experience in WP6, where they are applied to interaction (see the attached paper "Measuring informational distances between sensors and sensor integration")

2.3.5 Work done by IST on sensorimotor maps. (IST)

The IST group has been addressing the problem of learning sensory-motor maps of high dimension robotic systems. Sensory-motor maps are the mathematical relationships between the information coming from the sensors and the actuators of the robotic system. For instance, one map may determine how visual perception of the robots' hand (image coordinates and velocities) relates to robots' arm motor actions (angular positions and velocities of arm joints).

One of the biggest challenges in the analysis of high dimension systems arises from the existence of redundancies in the motor space, e.g. several arm configurations result in the same hand position. This is advantageous in many situations because we can use the redundant (free) degrees of freedom to avoid obstacles, minimize energy consumption, achieve more comfortable postures, and many others. However, conventional learning mechanisms associating sensory to motor information may not work under these circumstances because the sensory motor maps are no longer unambiguous. In the context of redundant systems we have worked in the above mentioned problems. In particular we are interested in learning the sensory-motor maps, but, at the same time, to use the redundancy to achieve secondary tasks, such as obstacle avoidance and energy minimization. We present three approaches to deal with this problem.

Another problem addressed in this report is related to the learning the sensory motor maps in a way the fully the constraints existing in the joint sensory-motor data. Most existing works to date try to learn either forward (motor-to-sensory) or inverse (sensory-to-motor) maps, which mask some of the underlying structure in the data, mainly when there are redundant degrees of freedom or perceptual aliasing. We propose a manifold learning method, and associated data query and retrieve algorithms, that have the potential ability to address these problems. We present some encouraging results on its application to simulated kinematics and, in future work, will perform tests on real robotics platforms.

2.3.5.1 Minimum Order Sensory Motor Maps

A “Minimum Order Sensory Motor Map (SMM)” is a map that takes the desired image configuration and the Degrees Of Redundancy (DOR) as input variables, while the non-redundant Degrees of Freedom are viewed as outputs. Since the DORs are not frozen in this process, they can be used to solve additional tasks or criteria. This method provides a global solution for positioning a robot in the workspace, without the need to move in an incremental way. We provide examples where these tasks correspond to optimization criteria that can be solved online. We show how to learn the “Minimum Order SMM” using a local statistical learning method. Extensive experimental results with a humanoid robot are discussed to validate the approach, showing how to learn the Minimum Order SMM of a redundant system and using the redundancy to accomplish auxiliary tasks.

Mathematical Formulation

In this section we show how to define a Sensory-Motor Map that explicitly takes the DOR into consideration, thus allowing the completion of several simultaneous tasks.

Let us define a *SMM* that maps a vector of control variables *(n,r)* to a vector of image point features *I*, where *n* is a minimum set of degrees of freedom that spans the full output space and r is a set of redundant degrees of freedom. Note that there are several partitions of the input space, into redundant versus non-redundant degrees of freedom that can give this same property. This forward model can thus be written as:

$$I = f(n, r)$$

and allows predicting the image configuration of the robot given a set of motor commands. In many cases, we are more interested in the inverse map, i.e. computing the motor commands that drive the robot to a desired image configuration, *I*. If there were an inverse mapping $(n, r) = f^{-1}(I)$, this problem could be solved in a straight forward manner. However, as the dimension of the input space is larger than that of the output space, there are many input combinations that generate the same image point features. In other words, because of the DOR, *f(n, r)* is not bijective and, therefore, not invertible.

We built a cost function, *K*, with two terms: one weighting the error in the position of the end effector (data fitness) and another one corresponding to the weights on the control (regularization term).

$$K(I^*, n, r) = \lambda \left\| I - I^* \right\|^2 + c(n, r)$$

This cost function expresses that we are willing to accept some error in the position if another task can be solved at the same time, in this case control costs. Examples of control cost criteria *c* can be ``Comfort'' (e.g. distance to joint limits), Energy minimization (e.g. the position with lower momentum) or Minimum motion (i.e. minimize total motion from current to desired position), posture control, amongst others.

Finding the Solution

The regularized solution can be found by minimizing the defined cost as follows:

$$(\hat{n}, \hat{r}) = \arg\min_{n,r} (\lambda \left\| I - I^* \right\|^2 + c(n, r))$$

where *I* can be computed with the forward model. This formula integrates two terms: one describing the task part and another related to posture control.

There are two important observations to this formulation. Firstly, the optimization is

done with respect to all control variables, which translates into a significant computational cost. Secondly, the DORs are not treated as such, since they undergo exactly the same process as the non-redundant DOFs.

The consequence of this approach is that the extra degrees of freedom are frozen from the beginning and can no longer be used for a different purpose during execution. In a way, redundancy is lost. Instead, in our approach, we would like to keep the redundant degrees of freedom free for solving additional tasks online. In essence, we split the problem in two steps. Firstly, we define a ``Minimal Order Sensory Motor Map'', $n = g(I, r)$. By taking the DORs as input (independent variables) instead of output signals, the problem of computing the non-redundant DOFs becomes well posed. The DORs, *r*, are left unconstrained and can be fixed during runtime, when a secondary task or optimization criterion is specified.

The definition of the ``Minimum Order SMM'' allows us to use the redundancy to meet additional criteria or task-constraints, that can be changed online. The DORs can be determined as the solution of a new optimization problem, with cost function *L*:

$$\hat{r} = \arg\min_{r}(L(I^*, r))$$

Note that, in contrast with the previous case, this optimization is done with respect to the redundant degrees of freedom, only. The optimization complexity is thus substantially lower and lends itself to be used as an online process. In general, the solutions in the two cases are not the same, because different local minima could be reached and the criteria are slightly different.

Our approach guarantees zero prediction error, because the *Minimum Order SMM* allows us to determine the values of *n* corresponding to the exact image position, for the selected redundant degrees of freedom. This solution is similar to the first (regularized) problem when λ becomes large. If the *Minimum Order SMM* is not exact, then it will introduce some error in the final image configuration.

Results

The following figure shows the minimization in energy obtained when holding the robot hand in a pre-defined position.

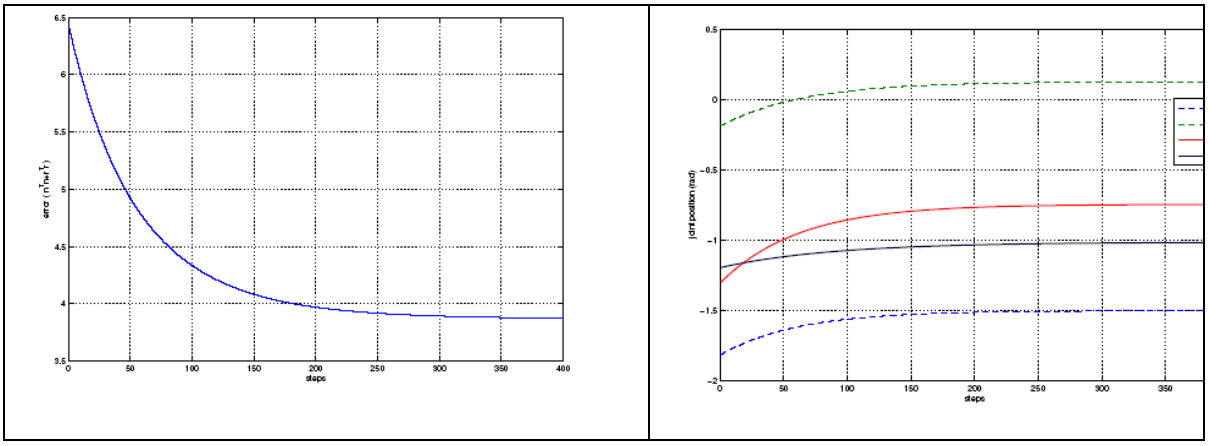

Figure 2-4 Minimization in energy obtained when holding the robot hand in a pre-defined position (left). Motion of the joints to achieve the result.

2.3.5.2 Visual Controlled Uncalibrated Redundancy Control

Visual servoing methods provide very efficient and robust solutions to control robot motions. They provide high accuracy for the final pose and good robustness to camera calibration and other settings. The redundancy formulation presented in the previous section can be extended to the Visual Servoing framework, to compute a control law that realizes a main task, while simultaneously taking supplementary constraints into account. It can be used when the main task does not constrain all the robot degrees of freedom (DOF). A secondary task can then be added to meet a second objective without disturbing higher priority tasks.

The control law for the second task is computed in the within the set of motions that do not change the primary task. This is achieved by projecting motion hypotheses into the set of motions constituting the null space of the first task, thus leaving the first tasks unmodified. The computation of the projection operator is based on the jacobian of the first task. This approach involves the computation of the task jacobian, linking the evolution of the visual features to the robot articular motion. It thus requires knowledge about the camera world and world-actuator transformations that influence the interaction matrix (relating image and camera velocities) and the robot jacobian (relating end-effector and joint velocities). Such transformations are usually obtained during an offline calibration phase.

However, full system calibration (and even a coarse one) is not always possible and/or desirable. Some robots may lack proprioceptive sensors to provide the necessary information and some parameters may vary over time, due to malfunction, changes in mechanical parts or modification in the camera lenses. Even when calibration information is available, the analytic computation of the interaction matrix often requires an estimate of the depth of the tracked features. For all these reasons, a perfect computation of the task jacobian can be very difficult or even impossible in practice.

Redundancy formulation for two tasks.

Let q be the articular vector of the robot. Let e_1 and e_2 be two tasks,

$$\mathbf{J_i} = \frac{\partial \mathbf{e_i}}{\partial \mathbf{q}} \ (i = 1, 2)$$

Their jacobian is defined by:

$$\dot{\mathbf{e}}_\mathbf{i} = \frac{\partial \mathbf{e_i}}{\partial \mathbf{q}} \dot{\mathbf{q}} = \mathbf{J_i} \dot{\mathbf{q}}$$

Since the robot is controlled using its articulation velocity $\dot{q}$, the jacobian has to be (pseudo-) inverted. The general solution (with i = 1) is:

$$\dot{q} = J_1^+ \dot{e}_1 + P_1 z$$

where P_1 is the orthogonal projection operator on the null space of J_1 and J_1^+ is the pseudo-inverse of J_1. Vector *z* can be used to apply a secondary command, that will not disturb e_1. Here, z is used to carry out at best a task e_2. With further algebraic manipulations we have:

$$\dot{e}_2 = J_2 J_1^+ \dot{e}_1 + J_2 P_1 z$$

By inverting this last equation, and introducing the computed *z*, we finally get:

$$\dot{q} = J_1^+ \dot{e}_1 + P_1 (J_2 P_1)^+ (\dot{e}_2 - J_2 J_1^+ \dot{e}_1)$$

Results

We have tested several estimation methods for J and the results are the following

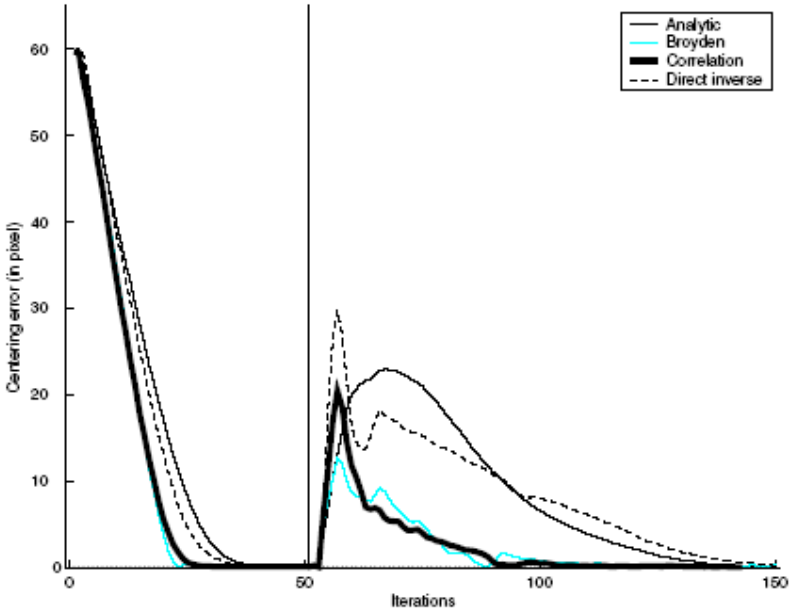

Figure 2-5. Results of task sequencing. The vertical line shows the time instant when the second task was activated.

From the results show in Figure 2 we can see that when a second task is activated there is a small perturbation on the first task that is rapidly reduced to zero.

2.3.5.3 Joint representation of sensory-motor relations

Learning a structure jointly representing both sensory and motor information can provide significant advantages, if such knowledge can later be used to recover any (partial) map between perception and action. In this section we present a new approach to work with unknown redundant systems. For this we have developed:

- An online algorithm that learns the input-output constraints of a generic smooth map (manifold);

- A method that, given a partial set of input-output variables, provides an estimate of the

remaining ones, using the learned constraints.

Referring to our problem, the manifold estimate can be used to obtain the direct and inverse robot kinematics, i.e., to provide an estimate of the observed variables given an actuation value, or, inversely, obtain the actuators position that leads to a desired observation. This constitutes a new approach to learn forward-backward models, allowing to easily recovering the relationship among any set of variables. The key point of our approach is to consider the problem from an unsupervised learning point of view, where data points consist of vectors containing both input and output variables. These vectors define a surface that can be seen as the graphic of a function.

Consider D_c to be the number of controlled — or independent — variables and D_o the number of observed variables. A point x belonging to the manifold in a $D = D_c + D_o$ dimensional space will lie in a sub-space of dimension D_c. This manifold can be represented by the implicit function

$H(x) = 0$

where $H(x)$ imposes the $D - D_c$ restrictions arising from kinematics considerations. Note that the dimension of the manifold is D_c because this corresponds to the number of independent variables. The observed variables are generic smooth, frequently non-injective functions of the independent variables. In almost all cases these manifolds are highly nonlinear, hard to parameterize without any a priori knowledge.

However, they are smooth and so can be approximated by local linear parameterizations estimated from sample data. Unsupervised learning of a D_c-dimensional manifold in a D-dimensional space can be interpreted as a probability density estimation problem: given a set of (possibly corrupted with noise) sample points x_i belonging to the manifold, i = 1 . . .N, estimate the probability of a point x belonging

to the manifold, i.e.,

$p(H(x) = 0 \mid x_1, x_2, \ldots, x_N)$

After estimating the manifold, and given a partial set of input-output variables, we can query for an estimate of the remaining ones. Suppose data points x are divided into a query component and an answer component, $x = [x^T_q \; x^T_a]^T$, such that $D_q + D_a = D$, where D_q is the query dimension and D_a is the answer dimension, not necessarily equal to D_c and D_o. The answer component is the set x_a of elements of x to be estimated given a specific value of the remaining elements x_q. For instance, for a forward kinematics problem x_q corresponds to the actuation variables, while for an inverse kinematics problem x_q matches the observed variables. Note that if the dimension of the query exceeds D_c, the manifold dimension, the estimation problem is over-determined and a solution may not exist. Conversely, if the dimension of the query is lower than D_c, the estimation problem is under-determined and a continuum of solutions exist — in this case, as will be explained later, our algorithm will provide multiple answers that can be interpreted as a sampling of that continuous solution. The M local models that describe the learned manifold can be used to provide an estimate x_a for a specific query x_q. For a single

model m, we can choose the estimate of x_a to be the value that maximizes the likelihood of the data point x given model m, i.e., that maximizes $p(x|m)$. Maximization of this likelihood can be achieved by minimizing the corresponding Mahalanobis distance to the center of the model m_1:

$$J_1 = (x - \mu)^T C^{-1} (x - \mu)$$

The data is characterized by its first (mean ◎) and second order (covariance matrix C) moments. Consider the following decomposition for the covariance matrix:

$$C^{-1} = \begin{bmatrix} C_{qq} & C_{qa} \\ C_{aq} & C_{aa} \end{bmatrix}$$

where C_{qq}, C_{qa}, C_{aq} and C_{aa} are, respectively, of dimensions $D_q \times D_q$,

$D_q \times D_a$, $D_a \times D_q$ and $D_a \times D_a$. Then after some simple calculations we get the estimate

$$\hat{x}_a(x_q) = -C_{aa}^{-1} C_{aq} (x_q - \mu_q) + \mu_a$$

The following experiment shows a simple example of a sensory-motor relation. We can see that the correct relation (in blue) is accurately estimated (red lines) and that a one-to-many relation can be recovered.

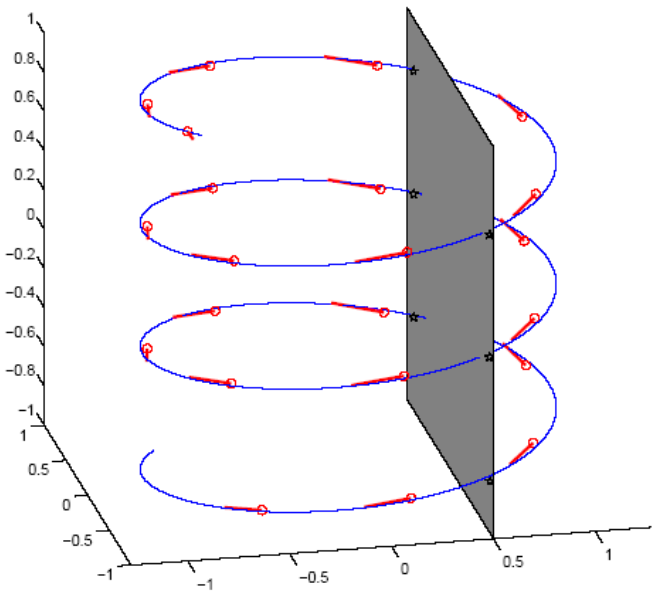

Fig. 4. Recovering the forward model embedded in the manifold. With $x_q = 0.5$ the six possible outcomes are successfully estimated (represented in the figure by black asterisks).

In future work we will apply and evaluate the performance of the proposed model to data

obtained from redundant robots with multiple degrees of freedom.

2.3.6 Work done by UNIFE on sensorimotor maps (UNIFE)

The brain network for the recognition of biological motion includes visual areas and structures of the mirror-neuron system. The latter respond during action execution as well as during action recognition. As motor and somatosensory areas predominantly represent the contralateral side of the body and visual areas predominantly process stimuli from the contralateral hemifield, we were interested in interactions between visual hemifield and action recognition. In the present study, human participants detected the facing direction of profile views of biological motion stimuli presented in the visual periphery. They recognized a right-facing body view of human motion better in the right visual hemifield than in the left; and a left-facing body view better in the left visual hemifield than in the right. In a subsequent fMRI experiment, performed with a similar task, two cortical areas in the left and right hemispheres were significantly correlated with the behavioural facing effect: primary somatosensory cortex (BA 2) and inferior frontal gyrus (BA 44). These areas were activated specifically when point-light stimuli presented in the contralateral visual hemifield displayed the side view of their contralateral body side. Our results indicate that the hemispheric specialization of one's own body map extends to the visual representation of the bodies of others.

In 2008, a paper on the interaction of visual hemifield and body view in biological motion perception has ben published on the European Journal of Neuroscience. The work is co-authored by Ferrara, Muenster, Zurich and Duesseldorf Universities. We think that the results and the teorethical conclusions are quite relevant as far as WP3 is concerned. The topic of the study is outlined below and the paper is attached to this deliverable in the appendixes section.

2.3.7 A sensorimotor approach to orienting of attention (UNIFE).

Traditionally, attention is conceived as a supramodal mechanism subserved by anatomical circuits separated from those involved in data processing. The premotor theory of attention proposes that attention results from an activation of the same "pragmatic" circuits that program oculomotion, in the case of spatial attention, and that program hand grasping movements, in the case of attention directed towards graspable object. This theory have found a large amount of experimental evidence.

2.3.7.1 Early behavioral evidence in favor of premotor theory of attention

The ability to detect visual stimuli in space could be enhanced by the knowledge of the incoming stimulus location. The term commonly used to indicate this phenomenon is visuospatial attention. Although shifts of attention are normally accompanied by overt eye and body movements there is ample evidence that perceptual enhancement can be obtained even in the absence of movement execution.

From early Eighties a theory was formulated on how attention works (see Posner & Dehaene, 1994). This "classic theory of attention" claimed that attention is a unitary, supramodal system, anatomically separated from the circuits underlying sensorimotor transformations, that acts as a control system, increasing the efficiency of the basic sensorimotor system. The idea of a global attentional system was abandoned with the introduction of modern brain imaging techniques that showed that different brain circuits become active according to the task the subjects were required to execute. Recent versions of the classic theory suggest the existence of at least two different control systems: a posterior, parietal system subserving spatial attention and an anterior one involved in the attentional recruitment and control of brain areas to perform complex cognitive tasks (see Posner & Dehaene, 1994). In this new formulation, however, is still present the basic tenet of the theory: that attention is a supramodal control system. The idea of a unidirectional influence from attention to perceptual and motor systems finds severe difficulties particularly in explaining two experimental results, one coming from electrophysiology and the other from psychophysics, that indicate that orienting of attention is strictly influenced by anatomical and physiological constrains of sensorimotor systems.

The former experimental result concerns the impossibility to anatomically localize a global system for attention in space. The initial demonstration of a dissociation between space sectors was provided by a lesion experiment in monkeys. According to the site of the lesion, monkeys showed either (lesion of area 8, frontal eye fields) a contralateral neglect, stronger for stimuli presented far from the monkey, in the absence of a "personal neglect", or (lesion of ventral area 6) the ignorance of stimuli presented near the monkey, even when they touched its skin, in the presence of accurate detection of stimuli presented in the extrapersonal space (Rizzolatti *et al.*, 1983). Subsequently, similar dissociations between different space sectors were reported in patients with lesion of parietal and frontal lobe. It appears therefore that the neglect

as full-fledged syndrome, which includes attentional deficits for personal, peripersonal and extrapersonal space, is not a consequence of the destruction of an attention control system, but results from lesions of anatomically distinct circuits. This result is obviously a strong blow to the classic theory of visuospatial attention.

The psychophysical result concerns a very robust phenomenon, called "meridian effect", which is commonly found when a typical experimental paradigm on orienting of visuospatial attention is used. The basic visual display used in these experiments consists of a central box and a peripheral row of boxes on each side of the central box, either vertically or horizontally oriented. Subjects are instructed to maintain fixation on the central box, to direct attention to the cued box, and to press a switch as fast as possible at the occurrence of the imperative stimulus. The cue indicates that the incoming stimulus will appear at the cued location with a probability higher than in the other locations. The imperative stimulus usually consists of a small geometrical shape that appears at the center of one of the peripheral boxes. In experiments on voluntary orienting of spatial attention the cue consists of a symbol, such as a digit, placed close to the central box, that require a conscious interpretation in order to individuate the cued box. Results commonly show that reaction times to stimuli at the cued location (valid trials) are faster than those to stimuli at an uncued location (invalid trials). According to the classical theory of spatial attention, when the target is shown at an uncued box, attention has to move from the cued box to the target, determining a lengthening of reaction times. The lengthening is greater when the invalid stimulus is far from the cued box than when it is close to it because the time depends on the distance attention has to cover. The classic theory has, however, serious difficulties in explaining why attention takes more time to cross the visual fields meridians rather then to move along the same visual hemifield in which it is already focussed (meridian effect). This is a robust phenomenon of the order of 20-25 ms, which has been described by many authors in different experimental conditions (see Rizzolatti & Craighero, 1998). If attention is a control system independent of basic anatomical and physiological circuits, why should its action be delayed by anatomical landmarks such as the principal meridians of the visual field?

In the late Eighties an alternative view to the classic theory of attention was formulated, to give a theoretical framework able to explain why orienting of attention is strictly linked to anatomical and physiological constrains of sensorimotor systems. The fundamental claim of this new theory, called "premotor theory", was that attention does not result from nor requires a control system separated from sensorimotor circuits. On the contrary, attention derives from the activation of the same circuits that, in other conditions, determine perception and motor activity (Rizzolatti *et al.*, 1994), giving, in this way, an easy explanation of the strict link between attention and sensorimotor limits.

At the beginning the premotor theory of attention addressed specifically spatial attention. According to it, spatial attention derives from an endogenous or exogenous activation of cortical maps that transform spatial information into movements. The activation of these pragmatic maps determine both an increase in the motor readiness to respond to some space sectors, and a facilitation in processing stimuli coming from that space sector toward which the motor program controlled by the pragmatic map was prepared. The fundamental assumption is that in humans there is a stage in which motor programs are set, but not executed (evidence

supported by electrophysiological data). This stage, which occurs either in response to a stimulus or endogenously, is what introspectively is felt as spatial attention. Even if premotor theory of attention maintains that spatial attention can be produced by any map that codes space, the strong development of the foveal vision and neural mechanisms related to foveation present in humans, indicates that a central role in the attentional selection of a location in the visual space is played by those maps that code space for oculomotion. In other words, orienting attention to a determined spatial location in the visual field is a consequence of the programming of an ocular movement toward that location, even if the saccade is not subsequently executed.

In the light of this consideration, let us examine how the premotor theory explains the results of the classical experimental paradigm on orienting of attention previously described, commonly called the "Posner paradigm". As soon as the location of the imperative stimulus can be predicted, a motor program for saccade toward the expected location is prepared. This program specifies the direction and the amplitude of the saccade. At this point, two events occur: the location of the expected stimulus becomes salient with respect to all other locations, and the stimuli appearing in that location are responded to faster. This is true both when the required response is a saccade, towards or not the target, or another arbitrary response. If the target does not appear in the cued location, in agreement with the classic theory, the response can be emitted only when attention is allocated to the new point. Thus, the invalid response is delayed both because the expected location is not facilitated and because a time-consuming change in the saccade program should take place before the emission of the response. This way to consider attention one of the consequences of programming and reprogramming ocular movements gives to the premotor theory an easy explanation of the meridian effect. Given the fact that goal-directed saccades are prepared firstly deciding the saccade direction and then deciding the saccade amplitude, changes in the direction require a radical modification in the oculomotor program while changes in the amplitude imply only a readjustment of a pre-existing program. The premotor theory refers to this anatomical constrain of the oculomotor system to explain the meridian effect. When the amplitude of the attention movement has to be modified without changing the basic direction parameters, only an adjustment of the motor program is needed. In contrast, when the target appears in the hemifield opposite the one containing the cued location, then it is the direction of the attention that has to be modified. In this case, the process is more time-consuming because a new program, involving (if executed) a radically different set of muscles, has to be constructed. This complete program change would be the origin of the meridian effect.

2.3.7.2 Direct evidence in favor of the premotor theory of attention come from two different series of experiments both using slight modifications of the Posner paradigm.

The first series of experiments regards the use of a vertical saccade as measured variable and visual or acoustic stimuli as target. The logic of the experiment started on evidence coming from studies on oculomotor system in man that demonstrated that when the oculomotor system is activated by two simultaneous or closely consecutive stimuli, there is an effect of one stimulus on the other, resulting in an interference between the responses to them. According to the premotor theory, if spatial attention involves an activation of oculomotor circuits, then this

activation should influence an overt oculomotor response. The results showed that when subjects paid active attention to a given spatial location, the saccade trajectory deviated contralateral to the attention site, even when the imperative stimulus, triggering the saccade, was auditory and not lateralized. The deviation was therefore due to purely attentional factors (Sheliga *et al.*, 1995). These data indicate that any time attention is oriented to a certain spatial location, attention orientation is accompanied by an oculomotor programming. Although obviously this does not prove a causal relation between oculomotion and attention, it fully confirms the prediction of premotor theory, while, in contrast, the account of this phenomenon is not clear if one accepts the tenets of the classic theory.

The second series of experiments try to prove the existence of a causal relation between oculomotion and attention. To this purpose, conditions in which, either for the presence of a peripheral palsy or for the maintenance of an extreme eye posture, the execution of a saccade towards the cued position is prevented were studied. If this conditions determine an influence on orienting of attention it is difficult to find an alternative hypothesis to an oculomotor involvement causal for orienting of attention.

A first experiment investigated if a peripheral oculomotor lesion, that determines the impossibility to normally execute an eye movement, affects also the possibility to voluntarily orient attention in a task in which no eye movements are required. To this purpose, patients with rectus lateralis (abducens) oculomotor muscle palsy and with normal visual acuity were submitted to a Posner paradigm. Due to lesion lateralization, participants were asked to perform the experiment in monocular vision, both with the paretic and the non-paretic eye. The driving hypothesis was that, if a peripheral oculomotor lesion affects eye movement execution, the altered efferent copy/or the altered re-afferent signals from the plegic eye should influence the oculomotor function. If the involvement of the oculomotor system during visuospatial attentional tasks is not a mere epiphenomenon and reflects the existence of a true causal relationship, one should expect that any pathological modification in oculomotor ability should be paralleled by a modification in the ability to orient visuospatial attention. Results indicated that patients show dissociation in their performance according to the performing eye. Patients were able to correctly orient attention (valid trials reaction times faster than invalid ones) when the performing eye was the normal one, while they were not able to orient attention (no difference between valid and invalid trials) when they were using the paretic eye. This data demonstrate that also a pathological state involving the more peripheral levels of the oculomotor system can determine specific effect on visuospatial attention allocation (Craighero *et al.*, 2001).

A second experiment wanted to reproduce in normals the impossibility to normally execute an eye movement and to verify if this condition influences the ability to orient spatial attention. To this purpose normal subjects were submitted to the same spatial attention orienting task used in the previously reported study. Subjects were submitted to two different monocular sessions, having the precise instruction to maintain continuously their gaze on the fixation square. In the "frontal" session, subjects performed the experiment being in front of the computer screen, while in the "rotated" session they were rotated of 40° clockwise or counterclockwise. The performing eye was always the eye closer to the screen. While in the frontal session, both the right and the left eye were able to execute a movement toward the

temporal and the nasal visual hemifield, in the rotated one, the performing eye had a posture that renders impossible a movement toward the temporal visual hemifield. It is important to note that the distance between the fixation point and the stimulus location was such to allow a perfect detection of the appearance of the stimulus. Considering the influence that an oculomotor palsy has on the ability to orient attention, the hypothesis at the basis of the present experiment was that also an artificial "palsy" induced in normals by an extreme eye posture should influence the orienting of attention. Results confirmed the hypothesis indicating that while in the frontal session participants were able to correctly orient attention when the stimulus was presented both in the nasal and in the temporal visual hemifield, in the rotated session, attention was correctly allocated only when the target was presented in the nasal visual hemifield. No difference in reaction times between valid and invalid trials was found when the stimulus appeared in the temporal visual hemifield (Craighero et al. 2004).

Therefore these last two experiments indicate that the oculomotor activation coincident with attention allocation, being far from be a mere epiphenomenon, could reflect a volitional attempt to enhance perception by backward activating the circuits normally involved in sensorimotor transformation for eye movements towards visual stimuli.

2.3.7.3 Electrophysiological evidence of an oculomotor involvement during orienting of spatial attention

Recent neuroimaging studies have supported a neuroanatomical link between visuospatial attention and eye movements, either by noting that patterns of activations obtained in attentional tasks resemble those in oculomotor tasks (Nobre *et al.*, 1997) or by comparing attentional tasks of visuospatial orienting in the presence or absence of eye movements (Corbetta *et al.*, 1998; Nobre *et al.* 2000). Corbetta and collegues (1998) found overlapping regional networks in parietal, frontal, and temporal lobes both during a task involving covert shifts of attention to peripheral visual stimuli and during a task involving both attentional and saccadic shifts to the same stimuli. Nobre *et al.* (2000) compared brain areas activated in tasks of covert visuospatial orienting and in tasks requiring large and repetitive saccades toward peripheral stimuli. Results showed that the two tasks activated highly overlapping neural systems. No system of distinct brain areas was activated exclusively by the covert attention or by the saccades task. Beauchamp *et al.* (2001) wanted to better understand how the network subserves attentional shifts by examining overt shifts of spatial attention (shifts of attention with saccadic eye movements) and covert shifts of spatial attention (shifts of attention without eye movements) using identical tasks and stimuli located at similar distance from fixation. Results showed that both overt and covert shifts of visuospatial attention induced activations in frontal cortex (especially the precentral sulcus) parietal cortex (especially the intraparietal sulcus) and lateral occipital cortex. Overt shifts of attention elicited more neural activity than did covert shifts, reflecting additional activity associated with saccade execution. These results confirmed that overt and covert attentional shifts are subserved by the same network of areas.

A series of electrophysiological experiments performed on monkeys' brain have given a well-proven anatomical and physiological basis to the premotor theory of attention. In particular, Kustov and Robinson (1996) gave a physiological explanation to the saccade deviation found during an orienting of attention task when an ocular movement is required as

response (Sheliga *et al.*, 1995), by recording neurons activity from the monkey superior colliculus. These authors showed that when a monkey pays attention to a given location in space there is a change in the excitability of the superior colliculus. This change was demonstrated by the presence of a saccade shift with respect to their normal trajectory (elicited by the electrical stimulation of the superior colliculus) during allocation of spatial attention. The change was present when attention was allocated as a consequence of both an endogenous and an exogenous cue presentation. Particularly striking was the observation that the collicular excitation also changed when the monkey was instructed to make a manual response and keep the eyes still after imperative stimulus presentation. This last finding clearly shows that a mere shift of attention without any eye movement requirement determines a change in the oculomotor system.

In a very brilliant electrophysiological experiment Moore and Fallah (2001) have reported evidence that it is possible to enhance spatial attention by altering oculomotor signals within the brain. The authors trained two monkeys to make manual responses to signal the transient dimming of a peripheral visual target in the presence of flashing distractors and tested the effects of FEF microstimulation on monkeys' performance. They firstly determined the location in space to which suprathreshold microstimulation shifted the direction of gaze, defining the motor field, and then they tested the effects of subthreshold microstimulation of the on monkeys' performance when the target was placed inside and outside the motor field. The idea at the basis of the experiment was that if oculomotor planning gives rise to attentional filtering of visual signals, stimulation of an oculomotor area at levels below the movement threshold should allocate attention to targets positioned in the part of space represented by neurons at the stimulation site. Results have showed that subthreshold stimulation of the FEF facilitates attention to the target stimulus (lower psychophysical threshold level) when but only when the target stimulus was positioned in the motor field, providing evidence of a direct effect of oculomotor signaling on the allocation of spatial attention.

2.3.7.4 Non-oculomotor attention

In everyday life most of our actions in space are preceded by foveation and this gives to the oculomotor system a special central position in spatial attention. There are, however, some conditions in which we do not use, or do not use primarily, eye movements to select stimuli in space. In these cases spatial attention should depend basically on circuits other than those related to eye movements. Probably the best documented evidence in favor of spatial attention not related to eye movements is that deriving from experiments conducted by Tipper et al. (1992). They studied, in normal participants, the effect of an irrelevant stimulus located in or out of the arm trajectory necessary to execute a pointing response. The result showed that an interference effect was present only when the distractor was located in the trajectory necessary to execute a pointing response. Control experiments suggested that the effect was not due to a purely visual representation of the stimuli or to spatial attention related to eye movements. Rather, the organization of the arm-hand movement determined a change in the attentional relevance of stimuli close to the hand or far from it.

A series of experiments tried to verify if the premotor theory of attention could be extended from orienting of attention to spatial locations, to orienting of attention to graspable

objects. Objects are represented in both the ventral and the dorsal stream. Whereas processing in the ventral stream is responsible for perceptual and cognitive representations of the visual characteristics of objects and their significance, processing in the dorsal stream underlies the organization of the appropriate object-related hand movements. There is increasing neurophysiological evidence that this "pragmatic" function is performed by a circuit in the dorsal stream that codes the intrinsic visual characteristics of the objects and transforms them into the appropriate distal movements. Evidence in favor of the presence in humans as well of a strict link between the representation of an object's visual properties and specific motor programs to act on it has been provided by a recent study (Tucker and Ellis, 1998). Normal human subjects were presented with photographs of common graspable objects. The subjects had to decide by a key-pressing made either with the left or the right hand whether the presented object was upright or inverted. The results showed that the reaction times were faster when the key-press response was executed by the hand most suited to grasp the presented object, suggesting that visual objects potentiate actions that may be performed on them, even in the absence of explicit intentions to act. On the base of this strict link between objects and congruent actions, it is possible to modify the claim of the premotor theory of attention by saying that allocation of attention to a graspable object is a consequence of preparing a grasping movement to that same objects. An experiment was performed to test this hypothesis (Craighero *et al.*, 1999). Normal human participants were required to prepare to grasp a bar and then to grasp it as fast as possible on presentation of a visual stimulus. On the basis of the degree of sharing of their intrinsic properties with those of the to-be-grasped bar, visual stimuli were categorized as "congruent" or "incongruent". Results showed that grasping reaction times to congruent visual stimuli were faster than reaction times to incongruent ones. These data indicate that preparation to act on an object produces faster processing of stimuli congruent with that object. The same facilitation was present also when, after the preparation of hand grasping, participants were suddenly instructed to inhibit the prepared grasping movement and to respond with a different motor effector. There is a clear parallelism between the facilitation resulting from the preparation of a grasping movement and that resulting from oculomotor programming. In the former case detection of a given object's graspability properties is facilitated, whereas in the latter case facilitation favors a specific spatial location.

2.3.8 Do we share gaze with robots? A pilot experiment on the interaction between humans and the i-cub (UNIFE+IST)

In order to study and model oculomotor involvement in orienting of visuospatial attention, UNIFE and IST collaborated to perform an experiment based on recent behavioral data indicating that gaze direction triggers reflexive shifts of attention toward the gazed-at location. Two are the main goals of the experiment. The first one concerns the comparison of effectiveness in orienting of attention between the drawing of a schematic face apparently moving its eyes, and the real face of an experimenter seated in front of the subject and directing his gaze. In literature, only schematic drawings, or static face pictures have been used. The second goal addresses the way in which individuals consider the i-Cub: is it considered more similar to the drawing of a schematic face or to a real human face? In other words, is the effectiveness in orienting of attention determined by the direction of the i-Cub gaze, more similar to that obtained by observing gaze direction in a schematic face or in a human face?

In order to answer these questions we performed an experiment in which participants were required to press a button as soon as an LED placed on their right or on their left was switched on (see the figure below).

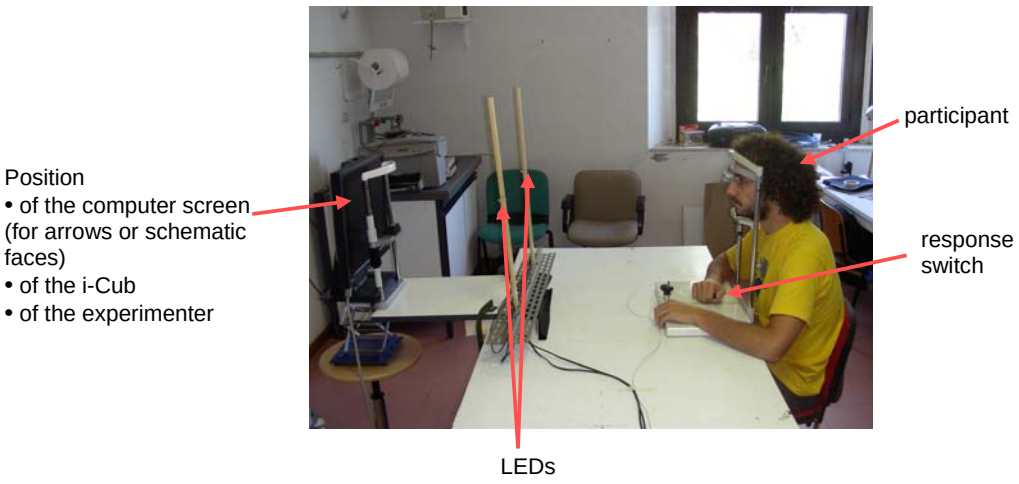

Before the appearance of the imperative stimulus, four different experimental situations, each of them presented separately in different experimental sessions, could be presented: (1) a central horizontal arrow pointing either towards the left or towards the right; (2) a schematic face with its eyes deviated either towards the left or towards the right; (3) the i-Cub directing its gaze towards the left or towards the right; (4) the experimenter directing his gaze towards the left or towards the right.

Preliminary results of the experiment indicate, firstly, that the orienting of attention determined by the schematic face is more similar to that determined by an arrow than to that determined by a real human face. Thus, a schematic face can't be considered a "biological stimulus" as it is often defined in literature. Secondly, the performance of the participants in the i-Cub session is statistically more similar to the performance in the experimenter session than to the one in the other two sessions. Consequently, from this preliminary experiment, we can suggest that the i-Cub is perceived to be "more biological" than the drawings of schematic faces.

4 Conclusions

This deliverable presents the current state of the art of experiments and models on sensorimotor integration together with some demos on infants crawling modelling. This is the final version of the Deliverable that has been provided at month 48 and includes all the contributions to Workpackage 3 provided by RobotCub partners during the first four years of the project.

5 References

Adolphs R, Tranel D and Damasio AR. Dissociable neural systems for recognizing emotions. Brain Cogn 52: 61-9, 2003.

Altschuler, E.L., A. Vankov, V. Wang, V.S. Ramachandran, J.A. Pineda, Person See, Person, poster session presented at the 27th Annual Meeting of the Society for Neuroscience, New Orleans, LA, November 1997.

Asuni G, G. Teti, C. Laschi, E. Guglielmelli, P. Dario, 2005(a). "A Robotic Head Neuro-controller Based on Biologically-Inspired Neural Models", IEEE International Conference on Robotics and Automation – ICRA 2005, Barcelona, Spain, April 18-22, 2005, pp.2373-2378.

Asuni G, G. Teti, C. Laschi, E. Guglielmelli, P. Dario, 2005(b). "A Bio-Inspired Sensory-Motor Neural Model for a Neuro-Robotic Manipulation Platform", IEEE International Conference on Advanced Robotics – ICAR 2005, Seattle, WA, USA, July 18-20, 2005.

Asuni G, G. Teti, C. Laschi, E. Guglielmelli, P. Dario, 2006. "Extension to End-effector Position and Orientation Control of a Learning-based Neurocontroller for a Humanoid Arm", IEEE/RSJ International Conference on Intelligent Robots and Systems (IROS 2006), Beijing, China, October 9-15, 2006.

Avikainen S, Forss N and Hari R. Modulated activation of the human SI and SII cortices during observation of hand actions. Neuroimage 15: 640-6, 2002.

Baron-Choen, S, A.M. Leslie, U. Frith, Cognition, 21, 37, 1985.

Beauchamp, M.S., Petit, L., Ellmore, T.M., Ingeholm, J. and Haxby J.V. (2001). A parametric

Bootsma, R. & van Wieringen, P. (1990). Visual control of an attacking forehand drive in table tennis. , 16, 21-29.

Brighina, F., La Bua, V., Oliveri, M., Piazza, A. & Fierro, B. (2000). Magnetic stimulation study during observation of motor tasks. J Neurol Sci, 174, 122-6.

Buccino G, Binkofski F, Fink GR, Fadiga L, Fogassi L, Gallese V, Seitz RJ, Zilles K, Rizzolatti G and Freund HJ. Action observation activates premotor and parietal areas in a somatotopic manner: an fMRI study. Eur J Neurosci 13: 400-4, 2001.

Bullock D, S. Grossberg, and F. H. Guenther, 1993. "A self-organizing neural model of motor equivalent reaching and tool use by a multijoint arm", Journal of Cognitive Neuroscience, 5(4):408–435, 1993.

Carr L, Iacoboni M, Dubeau MC, Mazziotta JC and Lenzi GL. Neural mechanisms of empathy in humans: a relay from neural systems for imitation to limbic areas. Proc Natl Acad Sci U S A 100: 5497-502, 2003.

Corbetta M., F. M. Miezin, S. Dobmeyer, G. L. Shulman, and S. E. Petersen. Selective and divided attention during visual discriminations of shape, color, and speed: functional anatomy by positron emission tomography. J Neurosci., 11:2383.2402, 1991

Corbetta M., F. M. Miezin, S. Dobmeyer, G. L. Shulman, and S. E. Petersen. Attentional modulation of neural processing of shape, color, and velocity in humans. Science, 248:1556.9, 1990

Corbetta, M., Akbudak, E., Conturo, T.E., Snyder, A.Z., Ollinger, J.M., Drury, H.A., Linenweber, M.R., Petersen, S.E., Raichle, M.E., Van Essen, D.C. and Shulman, G.L. (1998). A common network of functional areas for attention and eye movements. Neuron 21, 761-73.

Craighero L, Nascimben M, Fadiga L. (2004) Eye position affects orienting of visuospatial attention. Curr Biol.;14(4):331-3.

Craighero L.. Nascimben, and L. Fadiga. Eye position affects orienting of visuospatial attention. Current Biology, 14:331.333, 2004.

Craighero, L., Carta, A., and Fadiga, L. (2001). Peripheral oculomotor palsy affects orienting of visuospatial attention. NeuroReport 12, 3283-3286.

Craighero, L., Fadiga, L., Rizzolatti, G. and Umiltà, C. (1999). Action for perception: a motor-visual attentional effect. J. Exp. Psychol. Hum. Percept. Perform. 25, 1673-1692.

Csato', L., and M. Opper. Sparse On-Line Gaussian Processes. Neural Computation, 14, 641–668, 2002.

Dapretto, M. et al., Nature Neuroscience, 9, 28 (2006).

Dario P, M.C. Carrozza, E. Guglielmelli, C. Laschi, A. Menciassi, S. Micera, F. Vecchi, 2005. "Robotics as a "Future and Emerging Technology: biomimetics, cybernetics and neuro-robotics in European projects", IEEE Robotics and Automation Magazine, Vol.12, No.2, June 2005, pp.29-43.

Day, B. & Lyon, I. (2000). Voluntary modification of automatic arm movements evoked by motion of a visual target. Exp Brain Res, 130, 159-168.

Decety J., D. Perani, M. Jeannerod, V. Bettinardi, B. Tadary, B. Woods, and J. C. Mazziotta. Mapping motor representations with PET. Nature, 371:600.602, 1994.

Decety, J. (1996). Do imagined and executed actions share the same neural substrate?. Brain Res Cogn Brain Res, 3, 87-93.

Decety, J., Jeannerod, M. & Prablanc, C. (1989). The timing of mentally represented actions. Behav Brain Res, 34, 35-42.

Del Bianco S, F. Martelli and G. Zaccanti "Penetration depth of light re-emitted by a diffusive medium: theoretical and experimental investigation", Phys. Med. Biol. 47, 4131-44 (2002).

Di Pellegrino, G., Fadiga, L., Fogassi, L., Gallese, V. & Rizzolatti, G. (1992). Understanding

motor events: a neurophysiological study. Exp Brain Res, 91, 176-80.

Esslen M, Pascual-Marqui RD, Hell D, Kochi K and Lehmann D. Brain areas and time course of emotional processing. Neuroimage 21: 1189-203, 2004.

Fadiga L, Craighero L and Olivier E. Human motor cortex excitability during the perception of others' action. Curr Opin Neurobiol 15: 213-8, 2005.

Fadiga L, Fogassi L, Gallese V, Rizzolatti G. Visuomotor neurons: ambiguity of the discharge or 'motor' perception? Int J Psychophysiol, 35:165-77, 2000.

Fadiga, L., Buccino, G., Craighero, L., Fogassi, L., Gallese, V. & Pavesi, G. (1999). Corticospinal excitability is specifically modulated by motor imagery: a magnetic stimulation study. Neuropsychologia, 37, 147-58.

Fadiga, L., Fogassi, L., Pavesi, G. & Rizzolatti, G. (1995). Motor facilitation during action observation: a magnetic stimulation study. J Neurophysiol, 73, 2608-11.

Ferrari PF, Gallese V, Rizzolatti G and Fogassi L. Mirror neurons responding to the observation of ingestive and communicative mouth actions in the monkey ventral premotor cortex. Eur J Neurosci 17: 1703-14, 2003.

Flanagan, J. R., R.S. Johansson, Nature, 424, 769 (2003)

fMRI study of overt and covert shifts of visuospatial attention. Neuroimage 14, 310-21.

Fogassi L, Gallese V, Fadiga L and Rizzolatti G. Neurons responding to the sight of goal directed hand/arm actions in the parietal area PF (7b) of the macaque monkey. Society of Neuroscience Abstracts 24: 255, 1998.

Fogassi L, Gallese V, Fadiga L, Luppino G, Matelli M, Rizzolatti G. Coding of peripersonal space in inferior premotor cortex (area F4). J Neurophysiol, 76:141-57, 1996.

Frith, U., Autism: Explaining the Enigma (Blackwell Publishing, 2003).

Fritzke B, 1994. "Growing cell structures a self-organizing network for unsupervised and supervised learning", Neural Networks, 7(9):1441–1460, 1994. ICSI TR-93-026.C.

Gallese, V. & Goldman, A. (1998). Mirror neurons and the simulation theory of mind-reading. Trends in cognitive science, 2, 493-501.

Gallese, V., Fadiga, L., Fogassi, L. & Rizzolatti, G. (1996). Action recognition in the premotor cortex. Brain, 119 (Pt 2), 593-609.

Gangitano, M., Mottaghy, F. M. & Pascual-Leone, A. (2001). Phase-specific modulation of cortical motor output during movement observation. Neuroreport, 12, 1489-92.

Gangitano, M., Mottaghy, F. M. & Pascual-Leone, A. (2004). Modulation of premotor mirror neuron activity during observation of unpredictable grasping movements. Eur J Neurosci, 20,

2193-2202.

Gergely G. et al. (1995) Taking the intentional stance at 12 months of age. Cognition 56, 165-193

Golikova T.V. Vibrissa inputs into motor cortex in adult and developing rats. Zh. Evol. Biohim. Fisiol. 26: 193-199, 1990.

Gomez, G., Hernandez, A., Eggenberger Hotz, P. (2006). An adaptive neural controller for a tendon driven robotic hand. In Proceedings of the 9th International Conference on Intelligent Autonomous Systems (IAS-9). T. Arai et al. (Eds.), IOS Press, Tokyo, Japan, pp. 298-307.

Gomez, G., Hernandez, A., Eggenberger Hotz, P., and Pfeifer, R. (2005). An adaptive learning mechanism for teaching a robot to grasp. International Symposium on Adaptive Motion of Animals and Machines (AMAM 2005).

Gomez, G., Lungarella, M. and Tarapore, D. (2005). Information-theoretic approach to embodied category learning. Proc. of 10th Int. Conf. on Artificial Life and Robotics. (AROB 10): Proceedings of the 10th Int. Symp. on Artificial Life and Robotics, Beppu, Oita, Japan. pp. 332-337.

Goossens H.H. and Van Opstal A.J., 1997. "Human eye-head coordination in two dimensions under different sensorimotor conditions", Exp. Brain Res.1997, Vol. 114, pp. 542–560.

Grafton S. T., M. A. Arbib, L. Fadiga, and G. Rizzolatti. Localization of grasp representations in humans by PET: 2. observation compared with imagination. Experimental Brain Research, 112:103.111, 1996.

Hayhoe MM., Mennie, N., Sullivan, B. & Gorgos, K. The role of Internal Models and Prediction in Catching balls. American Association for Artificial Intelligence (AAAI), 2005 Fall Symposium, From Reactive to Anticipatory Cognitive Embodied Systems. Conference paper.

Hepp-Reymond MC, Husler EJ, Maier MA, Ql HX. Force-related neuronal activity in two regions of the primate ventral premotor cortex. Can J Physiol Pharmacol, 1994; 72: 571-9.

Iida, F. (2003) Biologically inspired visual odometer for navigation of a flying robot, Robotics and Autonomous Systems, Vol 44/3-4, pp. 201-208

Koelsch S, Fritz T, V Cramon DY, Muller K and Friederici AD. Investigating emotion with music: an fMRI study. Hum Brain Mapp 27: 239-50, 2006.

Kohler E, Keysers Cm, Umiltà A, Fogassi L, Gallese V, Rizzolatti G. Hearing sounds, understanding actions: Action representation in mirror neurons. Science, 297, 846-848, 2002

Kozlowski, K. Modelling and Identification in Robotics. Springer-Verlag, 1998. Murray, R.M., Z. Li, and S.S. Sastry. A Mathematical Introduction to Robotic Manipulation. CRC Press, 1994.

Kustov, A.A. and Robinson, D.L. (1996). Shared neural control of attentional shifts and eye movements. Nature 384, 74-7.

Lacquaniti, F., Carrozzo, M. & Borghese, N. (1993). The role of vision in tuning anticipatory motor responses of the limbs. In A. Berthoz (Ed.), Multisensory control of movement (Volume , pp. 379-393). Oxford University Press, Oxford.

Laschi, G. Asuni, G. Teti, M.C. Carrozza, P. Dario, E. Guglielmelli, R. Johansson, 2006. "A Bio-inspired Neural Sensory-Motor Coordination Scheme for Robot Reaching and Preshaping", IEEE/RAS-EMBS International Conference on Biomedical Robotics and Biomechatronics, Pisa, Italy, February 20-22, 2006.

Lee, D. (1976). A theory of visual control of bracking based on information about time-to-collision. Perception, 5, 437-459.

Leggio MG, Graziano A, Mandolesi L, Molinari M, Neri P and Petrosini L. A new paradigm to analyze observational learning in rats. Brain Res Brain Res Protoc 12: 83-90, 2003.

Lopes M and Damas B, The manifold structure of sensory-motor coordination. IEEE – Intelligent Robotic Systems (IROS'07), 2007.
Lopes M, Santos-Victor J, Learning sensory-motor maps for redundant robots. Proc. IEEE/RSJ International Conference on Intelligent Robots and Systems, IROS, Beijing, China, Oct. 9-15, 2006.
Lotze, M., Heymans, U., Birbaumer, N., Veit, R., Erb, M., Flor, H. & Halsband, U. (2006). Differential cerebral activation during observation of expressive gestures and motor acts. Neuropsychologia, , .

Lungarella, M. and Gomez, G. (In preparation). Information transfer at multiple scales. To be submitted to Physical Review E.

Lungarella, M. and Pfeifer, R. (2001). Robots as cognitive tools: Information-theoretic analysis of sensory-motor data. In Proceedings of the 2nd International Conference on Humanoid Robotics, Waseda, Japan.

Lungarella, M., Pegors, T., Bulwinkle, D. and Sporns, O. (2005). Methods for quantifying the information structure of sensory and motor data. Neuroinformatics, 3(3):243-262.

Maeda, F., Kleiner-Fisman, G. & Pascual-Leone, A. (2002). Motor facilitation while observing hand actions: specificity of the effect and role of observer's orientation. J Neurophysiol, 87, 1329-35.

Maini E.S., G. Teti, C. Laschi, M. Rubino, P. Dario, 2006. "Bio-inspired control of eye-head coordination in a robotic anthropomorphic head", IEEE/RAS-EMBS International Conference on Biomedical Robotics and Biomechatronics, Pisa, Italy, February 20-22, 2006.

Mansard N, Lopes M, Santos-Victor J, Chaumette F, Jacobian Learning Methods for Tasks Sequencing in Visual Servoing, Proc. IEEE/RSJ International Conference on Intelligent Robots and Systems, IROS, Beijing, China, Oct. 9-15, 2006.

Marr, D. (1982). Vision. A computational investigation into the human representation and processing of visual information. W. H. Freeman and Company.

Martelli F, S. Del Bianco and G. Zaccanti, "Perturbation model for light propagation through diffusive layered media", Phys. Med. Biol. 50, 2159-2166 (2005).

McIntyre, J., Zago, M., Berthoz, A., & Lacquaniti, F. (2001). Does the brain model Newton's laws? Nature Neuroscience, 4, 693-694.

McLeod, P. (1987). Visual reaction time and high-speed ball games. Perception, 16, 49-59.

Merchant, H., Battaglia-Mayer, A. & Georgopoulos, A. (2004). Neural responses during interception of real and apparent circularly moving stimuli in motor cortex and area 7a. Cereb Cortex, 14, 314-331.

Molinari M, Petrosini L and Gremoli T. Hemicerebellectomy and motor behaviour in rats. II. Effects of cerebellar lesion performed at different developmental stages. Exp Brain Res 82: 483-92, 1990.

Moore, T. and Fallah, M. (2001). Control of eye movements and spatial attention. Proc. Natl. Acad. Sci. USA. 98, 1273-6.

Murata A, Fadiga L, Fogassi L, Gallese V, Raos V, Rizzolatti G. Object representation in the ventral premotor cortex (area F5) of the monkey. J Neurophysiol. 1997;78:2226-30.

Mussa-Ivaldi F.A., E. Bizzi. Motor learning through the combination of primitives. Philosophical transactions of the Royal Society: biological sciences. Vol 335: Issue 1404 Dec 2000. Pag 1755-1769.

Nagai, A., Kuno, Y. and Shirai¡, Y. (1999) Detection of Moving Objects against a Changing Background.Systems and Computers in Japan, Vol. 30, No. 11, pp. 107-116.

Neafsey EJ, Bold EL, Haas G, Hurley-Gius KM, Quirk G, Sievert CF and Terreberry RR. The organization of the rat motor cortex: a microstimulation mapping study. Brain Res 396: 77-96, 1986.

Nishitani, N., S. Avikainen, R. Hari, Ann. Neurol., 55, 558 (2004).

Nobre, A.C., Gitelman, D.R., Dias, E.C. and Mesulam, M.M. (2000) Covert visual spatial orienting and saccades: overlapping neural systems. Neuroimage 11, 210-6.

Nobre, A.C., Sebestyen, G.N., Gitelman, D.R., Mesulam, M.M., Frackowiak, R.S. and Frith, C.D. (1997) Functional localization of the system for visuospatial attention using positron emission tomography. Brain 120, 515-33.

Nori, F., G. Metta, L. Jamone, and G. Sandini. Adaptive combination of motor primitives. Proceedings of AISB'06, Adaptation in Artificial and Biological Systems.

Nudo RJ, Frost SB. The evolution of motor cortex and motor systems. In: Krubitzer LA, Kaas JH, eds. Evolution of Nervous Systems in Mammals. Oxford, UK: Elsevier; 2006.

Oberman, L..M. et al., Cognitive Brain Research, 24, 190(2005).

Olsson L., C. L. Nehaniv, & D. Polani, "Sensory Channel Group and Structure from Uninterpreted Sensor Data", IEEE NASA/DoD Conference on Evolvable Hardware 2004, IEEE Computer Society, pp. 153-160, 2004.

Olsson L., C. L. Nehaniv, & D. Polani, From Unknown Sensors and Actuators to Actions Grounded in Sensorimotor Perceptions, Connection Science, special issue on Developmental Robotics (D. Bank & L. Meeden, guest eds.), volume 18(2), 2006.

Parsons L. M., P. T. Fox, J. H. Downs, T. Glass, T. B. Hirsch, C. C. Martin, P. A. Jerabek, and J. L. Lancaster. Use of implicit motor imagery for visual shape discrimination as revealed by PET. Nature, 375:54.58, 1995.

Petrosini L, Graziano A, Mandolesi L, Neri P, Molinari M and Leggio MG. Watch how to do it! New advances in learning by observation. Brain Res Brain Res Rev 42: 252-64, 2003.

Pfeifer, R., Iida, F., and Gomez, G. (2006). Morphological computation for adaptive behavior and cognition. International Congress Series 1291: 22-29.

Pfeifer, R., Iida, F., and Gomez, G. (In press). Designing intelligent robots – on the implications of embodiment. To appear in the International Journal of the Robotics Society of Japan.

Port, N., Kruse, W., Lee, D. & Georgopoulos, A. (2001). Motor cortical activity during interception of moving targets. J Cogn Neurosci, 13, 306-318.

Posner M. I. and S. Dehaene. Attentional networks. Trends Neurosci., 17:75.9, 1994.

Posner M. I. and S. E. Petersen. The attention system of the human brain. Annu Rev Neurosci., 13:25.42, 1990.

Posner M. I., S. E. Petersen, P. T. Fox, and M. E. Raichle. Localization of cognitive operations in the human brain. Science, 240(1627-31), 1988

Posner, M.I., and Dehaene, S. (1994). Attentional networks. Trends neurosci. 17, 75-79.

Premack, D. Woodruff, G. (1978). Does the chimpanzee have a theory of mind?. Behav Brain Sci, 1, 515.

Rizzolatti G, Camarda R, Fogassi L, Gentilucci M, Luppino G, Matelli M. Functional organization of inferior area 6 in the macaque monkey: II. Area F5 and the control of distal movements. Experimental Brain Research, 71:491–507, 1988.

Rizzolatti G, Fadiga L, Fogassi L and Gallese V. Resonance behaviors and mirror neurons. Arch Ital Biol 137: 85-100, 1999.

Rizzolatti G, Fadiga L. Grasping objects and grasping action meanings: the dual role of monkey rostroventral premotor cortex (area F5). In: G. R. Bock & J. A. Goode (Eds.), Sensory Guidance of Movement, Novartis Foundation Symposium (pp. 81-103). Chichester: John Wiley and Sons, 1998.

Rizzolatti G, Luppino G and Matelli M. The organization of the cortical motor system: new concepts. Electroencephalogr Clin Neurophysiol 106: 283-96, 1998.

Rizzolatti G. and R. Camarda. Neural circuits for spatial attention and unilateral neglect. In M. Jeannerod, editor, Neurophysiological and neuropsychological aspects of spatial neglect, pages 289.313, Amsterdam, 1987. North-Holland.

Rizzolatti G., L. Riggio, and B. M. Sheliga. Space and selective attention. In C. Umiltà and M. Moscovitch, editors, Attention and performance XV, pages 231.265, Cambridge, MA, 1994. MIT Press.

Rizzolatti G., L. Riggio, I. Dascola, and Umilta C. Reorienting attention across the horizontal and vertical meridians: evidence in favor of a premotor theory of attention. Neuropsychologia, 25:31.40, 1987.

Rizzolatti, G. & Craighero, L. (2004). The mirror-neuron system. , 27, 169-192.

Rizzolatti, G., and Craighero, L. (1998). Spatial attention: Mechanisms and theories. In M. Sabourin, F. Craik, & M. Robert (Eds.), Advances in psychological science: Vol.2. Biological and cognitive aspects (pp. 171-198). East Sussex, England: Psychology Press.

Rizzolatti, G., Fadiga, L., Gallese, V. & Fogassi, L. (1996). Premotor cortex and the recognition of motor actions. Brain Res Cogn Brain Res, 3, 131-41.

Rizzolatti, G., Matelli, M., and Pavesi, G. (1983). Deficit in attention and movement following the removal of postarcuate (area 6) and prearcuate (area 8) cortex in monkey. Brain 106, 655-673.

Rizzolatti, G., Riggio, L., and Sheliga, B.M. (1994). Space and selective attention. In C. Umiltà & M. Moscovitch (Eds.), Attention and Performance XV (pp. 231-265). Cambridge, MA: MIT Press.

Roccella S, M.C. Carrozza, G. Cappiello, P. Dario, J.J. Cabibihan, M. Zecca, H. Miwa, K. Itoh, M. Matsumoto, A. Takanishi, 2004. “Design, fabrication and preliminary results of a novel anthropomorphic hand for humanoid robotics: RCH-1”, 2004 IEEE/RSJ International Conference on Intelligent Robots and Systems, Sendai, Japan, September 28 - October 2, 2004, Page(s):266 - 271 vol.1.

Rouiller EM, Moret V and Liang F. Comparison of the connectional properties of the two forelimb areas of the rat sensorimotor cortex: support for the presence of a premotor or supplementary motor cortical area. Somatosens Mot Res 10: 269-89, 1993.

Sandini G, G. Metta, 2003. "Retina-like sensors: motivations, technology and applications", in Sensors and Sensing in Biology and Engineering, by Friedrich G. Barth, Timothy W. Secomb, and Joseph A. C. Humphrey, (Ed.s), Springer Verlag, 1st edition, March 28, 2003, pp.109-125.

Selb J, J. J. Stott, M. A. Franceschini, A. G. Sorensen, and D. A. Boas, "Improved sensitivity to cerebral hemodynamics during brain activation with a time-gated optical system: analytical model and experimental validation", J. Biomed Opt. 10, 11013 (2005).

Sheliga B. M., L. Riggio, L. Craighero, and G. Rizzolatti. Spatial attention and eye movements. Exp Brain Res, 105:261.75, 1995b.

Sheliga B.M., L. Riggio, L. Craighero, and G. Rizzolatti. Spatial attention-determined modifications in saccade trajectories. Neuroreport, 6:585.8, 1995a.

Sheliga, B.M., Riggio, L., and Rizzolatti, G. (1995). Spatial attention and eye movements. Exp. Brain Res. 98, 507-522.

Sirigu A., J. R. Duhamel, L. Cohen, B. Pillon, B. Dubois, and Y. Agid. The mental representation of hand movements after parietal cortex damage. Science, 273:1564.1568, 1996

Sobey, P. and Srinivasan, M. V. (1991). Measurement of optical flow by a generalized gradient scheme. J. Opt. Soc. Am. A 8, 1488.

Soechting, J. & Lacquaniti, F. (1983). Modification of trajectory of a pointing movement in response to a change in target location. , 49, 548-564.

Steinbrink H, H. Wabnitz, A. Obrig, Villringer and H. Rinneberg, "Determining changes in NIR absorption using a layered model of the human head", Phys. Med. Biol. 46, 879-896 (2001).

Strafella, A. P. & Paus, T. (2000). Modulation of cortical excitability during action observation: a transcranial magnetic stimulation study. Neuroreport, 11, 2289-92.

Tarapore, D., Lungarella, M. and Gomez, G. (2006). Quantifying patterns of agent-environment interaction. Robotics and Autonomous Systems, 54(2):150-158.

Te Boekhorst, R., Lungarella,M., and Pfeifer, R. (2003). Dimensionality reduction through sensory-motor coordination. In Kaynak,O., Alpaydin, E., Oja, E., and Xu, L. (Eds). Proc. of the Joint Int. Conf. ICANN/ICONIP, pp 496-503.

Theoret, H. et al., Current Biology, 15, 84 (2005).

Tipper, S.P., Lortie, C., and Baylis, G.C. (1992). Selective reaching: Evidence for action-centered attention. J. Exp. Psychol. Hum. Percept. Perform. 23, 823-844.

Tucker, M. & Ellis, R. (1998). On the relations between seen objects and components of potential actions. J. Exp. Psychol. Hum. Percept. Perform. 24, 830-846.

Uller C. (2003) Disposition to recognize goals in infant chimpanzees. Animal Cognition

Umilta, M., Kohler, E., Gallese, V., Fogassi, L., Fadiga, L., Keysers, C. & Rizzolatti, G. (2001). I know what you are doing. a neurophysiological study. Neuron, 31, 155-165.

Wang Y and Kurata K. Quantitative analyses of thalamic and cortical origins of neurons

projecting to the rostral and caudal forelimb motor areas in the cerebral cortex of rats. Brain Res 781: 135-47, 1998.

Wang Y and Kurata K. Quantitative analyses of thalamic and cortical origins of neurons projecting to the rostral and caudal forelimb motor areas in the cerebral cortex of rats. *Brain Res* 781: 135-47, 1998.
Wimmer, H., J. Perner, Cognition, 13, 103 (1983).

Xiao D and Barbas H. Circuits through prefrontal cortex, basal ganglia, and ventral anterior nucleus map pathways beyond motor control. Thalamus & Related Systems. 2: 325–343, 2004.

Zago, M., Bosco, G., Maffei, V., Iosa, M., Ivanenko, Y. P., & Lacquaniti, F. (2004). Internal models of target motion: Expected dynamics overrides measured kinematics in timing manual interceptions. Journal of Neurophysiology, 91, 1620-1634.

Zhuravin IA and Bures J. Changes of cortical and caudatal unit activity accompanying operant slowing of the extension phase of reaching in rats. Int J Neurosci 39: 147-52, 1988.

Zollo L, B. Siciliano, C. Laschi, G. Teti, P. Dario, 2003. "An Experimental Study on Compliance Control for a Redundant Personal Robot Arm," Robotics and Autonomous Systems, vol. 44, pp. 101–129, 2003.

6 Appendices

Measuring Informational Distances Between Sensors and Sensor Integration

Lars Olsson*, Chrystopher L. Nehaniv*† and Daniel Polani*†
Adaptive Systems* and Algorithms† Research Groups
School of Computer Science, University of Hertfordshire
United Kingdom
{L.A.Olsson, C.L.Nehaniv, D.Polani}@herts.ac.uk

Abstract

In embodied artificial intelligence is it of interest to study the informational relationships between the agent, its actions, and the environment. This paper presents a number of statistical measures to compute the informational distance between sensors including the information metric, correlation coefficient, Hellinger distance, Kullback-Leibler, and Jensen-Shannon divergence. The methods are compared using the sensory reconstruction method to find spatial positions of visual sensors of different modalities in a sensor integration task. The results show how the information metric can find relations not found by the other measures.

Introduction

In the early 1960s H. B. Barlow suggested (Barlow, 1961) that the visual system of animals "knows" about the structure of natural signals and uses this knowledge to represent visual signals. Ever since then neuroscientists have analysed the informational relationships between organisms and their environment. In recent years, with the advent of embodied artifical intelligence, there has also been an increased interest in robotics and artificial intelligence to study the informational relations between the agent, its environment, and how the actions of the agent affect its sensory input. It is believed that this research can give us new principles and quantitative measures which can be used to build robots that can exploit bootstrapping (Prince et al., 2005) and continously learn, develop, and adapt depending on their particular environment, environment, and task to perform. This paper presents some work in this area and presents a number of methods for computing the distance between sensors and how these methods can be useful for sensor integration of different sensor modalities.

The informational relationships between sensors are dependent on the particular embodiment of an agent. Thus, these relationships can be useful for the agent to learn about its own body, the potential actions it can perform, and how the sensors relate to its particular environment. In (Olsson et al., 2004b) the sensory reconstruction method, first described by Pierce and Kuipers (1997), was applied to robots and extended by considering the informational relations between sensors. The results showed how the visual field could be reconstructed from raw and uninterpreted sensor data and how some symmetry of the physical body of the robot could be found in the created sensoritopic maps. This method was also used in (Olsson et al., 2005b) to show how a robot can develop from no knowledge of its sensors and actuators to perform visually guided movement.

One other aspect of the information available in an agent's sensors is that the particular actions of the agent can have an impact on the nature and statistical structure of its sensoric input. This has been studied in a number of papers since (Lungarella and Pfeifer, 2001); see for example (Sporns and Pegors, 2003, 2004; Lungarella et al., 2005). The results show how saliency guided movement decreases the entropy of the input while increasing the statistical dependencies between the sensors. The specific environment of an agent also limits in principle what an agent can know about the world and the physical and informational relationships of its sensors (Olsson et al., 2004a).

Information-theoretic measures have also been used to classify behaviour and interactions with the environment using raw and uninterpreted sensor data from the agent. In (Tarapore et al., 2004) the statistical structure of the sensoric input was used to fingerprint interactions and environments. Mirza et al. (2005b) considered how the informational relationships between its sensors, as well as actuators, can be used to build histories of interaction by classifying trajectories in the sensorimotor phase space. In (Kaplan and Hafner, 2005) the authors also considered clustering behaviours by the informational distances between sensors by considering configurations of matrices of information distances between all pairs of sensors.

One important issue in this research is what measures to use to quantify the informational relationships. In (Lungarella et al., 2005) the authors present a number of methods for quantifying informational structure in sensor and motor data. The focus is on integration, i.e., how much information two or more sources have in common. In this paper we focus on the opposite, i.e., how to compute how different two

or more sources are. Following (Olsson et al., 2004b), several papers including (Olsson et al., 2004a, 2005b,c,a, 2006; Mirza et al., 2005a,b; Kaplan and Hafner, 2005; Hafner and Kaplan, 2005) have used the information distance metric disucssed by Crutchfield (1990) to compute the informational distance between sensors. An important question the authors have received several times in reviews of papers and in discussions is "why the information metric?". This is a good question and in this paper we present a number of alternative distance measures suggested by colleagues and reviewers as well as the information metric. To compare the potential utility of the methods we apply them as the distance measure used in the sensory reconstruction method (Pierce and Kuipers, 1997; Olsson et al., 2004b). In the experiment the sensors of the visual field of a robot is split into three different modalities: red, blue, and green, and the problem is to find the relationships between sensors, including which sensors come from the same pixel in the camera. This is an example of sensor integration. The results show how the information metric performs better in this problem as it measures both linear as well as non-linear relationships between sensors.

The rest of this paper is structured as follows. The next section presents a number of methods to compute the distance between two sensors. Then a short introduction to the sensory reconstruction method is given before the results of the experiments are presented. The final section concludes the paper.

Measuring the Distance Between Sensors

In this section we present a number of methods for computing the distance between two sensors S_x and S_y. Each sensor can assume one of a discrete number of values (continuous values are discretized) $S_x^t \in \mathcal{X}$ at each time step t where $\mathcal{X}$ is the alphabet of possible values. Thus, each sensor can be viewed as a time series of data $\{S_x^1, S_x^2, \ldots, S_x^T\}$ with T elements. Each sensor can also be viewed as a random variable X drawn from a particular probability distribution $p_x(x)$, where $p_x(x)$ is estimated from the time series of data. Similarly the joint probability distribution $p_{x,y}(x,y)$ is estimated from the sensors S_x and S_y.

A distance measure $d(X,Y)$ is a distance function on a set of points, mapping pairs of points (X,Y) to non-negative real numbers. A *distance metric* in the mathematical sense also needs to satisfy the three following properties:

- $d(X,Y) = d(Y,X)$ (Symmetry).
- $d(X,Y) = 0 \quad \text{iff} \quad Y = X$ (Equivalence).
- $d(X,Z) \leq d(X,Y) + d(Y,Z)$. (Triangle Inequality).

If (2) fails but (1) and (3) hold, then we have a pseudometric, from which one canonically obtains a metric by identifying points at distance zero from each other. This is done here and in (Crutchfield, 1990).

Why can it be useful to use distance measures which are metrics in the mathematical sense? If a space of information sources has a metric, is it possible to use some of the tools and terminology of geometry. It might also be useful to be able to talk about sensors in terms of spatial relationships. This might be of special importance if the computations are used to actually discover some physical structure or spatial relationships of the sensors, for example as in (Olsson et al., 2004b), where the spatial layout of visual sensors as well as some physical symmetry of a robot was found by information theoretic means.

Distance Measures

The *1-norm distance* used in (Pierce and Kuipers, 1997) is different from the distance measures that follows in that it does not take in to account the probabilites of the different values that a sensor can take. It is normalized between 0.0 and 1.0 and is defined as

$$d_1(S_x,S_y) = \frac{1}{T}\sum_{t=1}^{T} |S_x^t - S_y^t|. \tag{1}$$

The *correlation coefficient* is defined as

$$r = \frac{\sum_{t=1}^{T}(S_x^t - \bar{S}_x)(S_y^t - \bar{S}_y)}{\sqrt{\sum_{t=1}^{T}(S_x^t - \bar{S}_x)^2}\sqrt{\sum_{t=1}^{T}(S_y^t - \bar{S}_y)^2}} \tag{2}$$

where $\bar{S}_x$ and $\bar{S}_y$ are the mean of S_x and S_y respectively. The range of r is $-1.0 \leq r \leq 1.0$, where 1.0 means that they are perfectly correlated in a linear way, 0 that they are not linearly correlated, and -1.0 perfectly negatively correlated. This can be made symmetric by computing the squared correlation coefficient, which is in the range $0 \leq r^2 \leq 1.0$, and then

$$d_{CC}(S_x,S_y) = 1 - r^2_{S_x,S_y}. \tag{3}$$

This is still not a metric since it does not satisfy the triangle inequality (Ernst et al., 2005).

The *information metric* is proved to be a metric in (Crutchfield, 1990) and is defined as the sum of two conditional entropies, or formally

$$d_{IM}(S_x,S_y) = H(X|Y) + H(Y|X), \tag{4}$$

where

$$H(Y|X) = -\sum_{x\in\mathcal{X}}\sum_{y\in\mathcal{Y}} p(x,y)\log_2 p(y|x). \tag{5}$$

The *Kullback-Leibler divergence* (Cover and Thomas, 1991) is defined as

$$D(p_x||p_y) = \sum_{x\in\mathcal{X}} p_x(x)\log_2\frac{p_x(x)}{p_y(x)}, \tag{6}$$

where $0 \log_2 \frac{0}{p_y} = 0$ and $p_x \log_2 \frac{p_x}{0} = \infty$. The Kullback-Leibler measure is not a metric because it is not symmetric. It can be made symmetric by adding two Kullback-Leibler measures,

$$d_{KL}(S_x, S_y) = D(p_x||p_y) + D(p_y||p_x), \quad (7)$$

where p_x is the probability distribution associated with sensor S_x and p_y with S_y. This is still not a metric since it does not satisfy the triangle inequality.

The square root of the *Hellinger distance*, also known as *Bhattacharya distance* (Basu et al., 1997) , is a metric and is defined as

$$d_H(S_x, S_y) = \sqrt{\frac{1}{2} \sum_{x \in X} \left(\sqrt{p_x(x)} - \sqrt{p_y(x)} \right)^2}. \quad (8)$$

Finally, the *Jensen-Shannon divergence*, presented in (Lin, 1991), is defined as

$$d_{JS}(S_x, S_y) = H(\pi_X X + \pi_Y Y) - \pi_X H(X) - \pi_Y H(Y), \quad (9)$$

where $\pi_X, \pi_Y \leq 0, \pi_X + \pi_Y = 1$, are the weights associated with the sensors S_x and S_y. In this paper the weights were always $\pi_X = \pi_Y = 0.5$. In (Endres and Schindelin, 2003) it was proved that the Jensen-Shannon is the square of a metric, i.e., $\sqrt{d_{JS}}$ is a metric, which was used in the experiments presented in this paper.

Sensory Reconstruction Method

In the sensory reconstruction method (Pierce and Kuipers, 1997; Olsson et al., 2004b) sensoritopic maps are created that show the informational relationships between sensors, where sensors that are informationally related are close to each other in the maps. The sensoritopic maps might also reflect the real physical relations and positions of sensors. For example, if each pixel of a camera is considered a sensor, is it possible to reconstruct the organization of these sensors even though nothing about their positions is known. It is important to note that using only the sensory reconstruction method, only the positional relations between sensors can be found, and not the real physical orientation of the visual layout. To do this requires higher level feature processing and world knowledge or knowledge about the movement of the agent (Olsson et al., 2004b). Figure 1 shows an example of a sensoritopic map for a SONY AIBO robot.

To create a sensoritopic map the value for each sensor at each time step is saved, where in this paper each sensor is a specific pixel in an image captured by the robot. The first step of the method is to compute the distances between each pair of sensors. In the paper by Pierce and Kuipers (1997) the 1-norm distance was used but after (Olsson et al., 2004b) the information metric has been used in a number of papers. In this paper the different distance measures presented

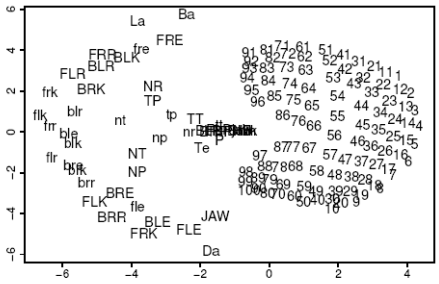

Figure 1: A sensoritopic map created by the sensory reconstruction method taken from (Olsson et al., 2004b) using the information metric. In this example there are 150 sensors, including 100 image sensors that are labeled 1-100 to the right in the map.

in the previous section are used. From the matrix of pairwise distance measurements between the sensors the dimensionality of sensory data (two in this case of a visual field) is computed and a sensoritopic map of that dimensionality can be created, using a number of different methods such as metric-scaling, which positions the sensors in the two dimensions of the metric projection. In our experiments we have used the relaxation algorithm described by Pierce and Kuipers (1997).

Experiment

This section describes the performed experiment and the results.

Method

In our experiments a SONY AIBO robotic dog was placed in a sitting position on a desk in the lab. The robot only moved its head with uniform speed using the pan and tilt motors in eight directions: up, down, left, right, and four diagonal directions. Five sequences of 6000 frames each of visual data was collected from the camera at a resolution of 88 by 72 pixels with 8 bits for each channel (red, green, blue) at an average rate of 20 frames per second. The collected images were downsampled to 8 by 8 pixels using averaging. Each pixel of the image had one red, one green, and one blue sensor. Thus, there is a total of 192 sensors (64 of each modality) where the red sensors are labeled $R1 - R64$, the green $G1 - G64$, and the blue sensors $B1 - B64$. The sensors labeled 1 are located at the upper left corner of the image and 64 at lower right corner. In the collected data the range of

Measure \ Exp.	64R	192RGB	192ARGB
1-norm	0.06 (0.01)	0.32 (0.01)	–
Correlation coefficient	0.19 (0.02)	0.23 (0.03)	0.21 (0.05)
Information metric	0.07 (0.02)	0.12 (0.03)	0.09 (0.03)
Kullback-Leibler	0.37 (0.03)	0.35 (0.01)	0.41 (0.05)
Hellinger	(0.45 (0.05)	0.40 (0.02)	0.46 (0.04)
Jensen-Shannon	0.45 (0.04)	0.39 (0.01)	0.45 (0.04)

Table 1: Average distances between all pairs of correct and reconstructed sensors using equation 10 with standard deviation in parentheses. The column 64R shows the average distances for the 64 red sensors of figure 2 and 192RGB the red, green, and blue sensors of figure 3, both using normal binning. 192ARGB shows the results for the adaptive binning of figure 4.

the blue sensors was slightly lower than the red and green sensors with a slightly smaller variation.

Sensoritopic maps were created from each of the five sequences of data by the sensory reconstruction method using the different distance measures previously described. The presented maps are examples but all maps created using one particular distance measure had the same characteristics as the ones presented here.

Results

Figure 2 shows sensoritopic maps computed with the different distance measures of only the red sensors $R1 - R64$. First, if we look at the maps for the Kullback-Leibler, Hellinger, and Jensen-Shannon distance, we find no real structure. For the correlation coefficient distance, figure 2(b), we find that sensors that are close in the visual field tend to be closer in the sensoritopic map, but it is not very clear. Now, compare this to the sensoritopic maps for both the 1-norm distance, figure 2(a), and the information metric, 2(c). Here the spatial relationships of the red sensors have been found, with sensor $R1$ in the upper left corner and $R64$ in the lower left corner for the 1-norm distance and the $R1$ sensor in lower left corner for the information metric. Since the sensory reconstruction method cannot find the true physical location of sensors but only the spatial relationships both of these maps represent the visual field.

Up until now the term "reconstructed" has been used in an informal way, where a visual field is reconstructed if the sensoritopic map and the real layout of the sensors look similar. One way this similarity can be formally quantified is by

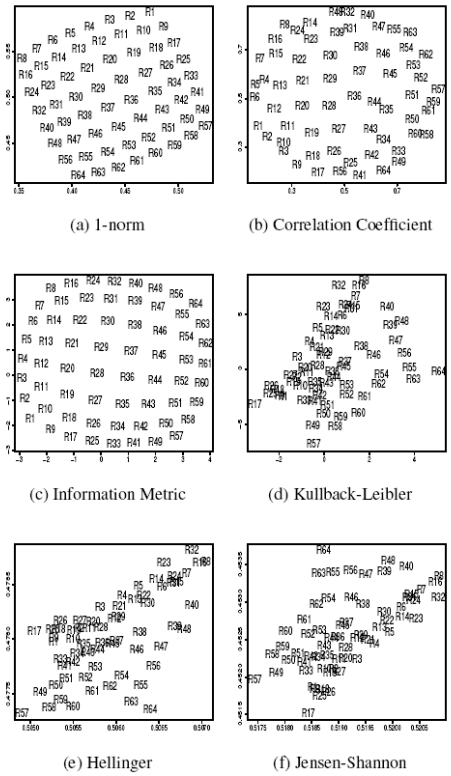

(a) 1-norm (b) Correlation Coefficient

(c) Information Metric (d) Kullback-Leibler

(e) Hellinger (f) Jensen-Shannon

Figure 2: Sensoritopic maps of the red sensors.

computing the relative distances between pairs of sensors in the reconstructed visual field and the real layout of the sensors. Let $r_{i,j}$ be the Euclidean distance between two sensors i and j in the reconstructed map, and $\ell_{i,j}$ the distance between the same two sensors in the real layout, where the x and y coordinates in both cases have been normalised into the range $[0.0, 1.0]$. Now the average distance between all pairs of sensors can be compared,

$$d(r,\ell) = \frac{1}{N^2}\sum_{i,j} |r_{i,j} - \ell_{i,j}|, \qquad (10)$$

where N is the number of sensors. This compares the relative positions of the sensors and not the physical positions, and $d(r,\ell)$ will have a value in the range $[0.0, 1.0]$. A distance of zero means that the relative positions are exactly the same,

and sensors placed at completely random positions will have an average distance of approximately 0.52.

Table 1 shows the average distances for 10 created maps for each of the five sets of data using equation 10. The 64R column shows that the 1-norm and information metric have a significantly lower average distance then the other measures, indicating that using these two measures more accurately reconstructs the real visual field.

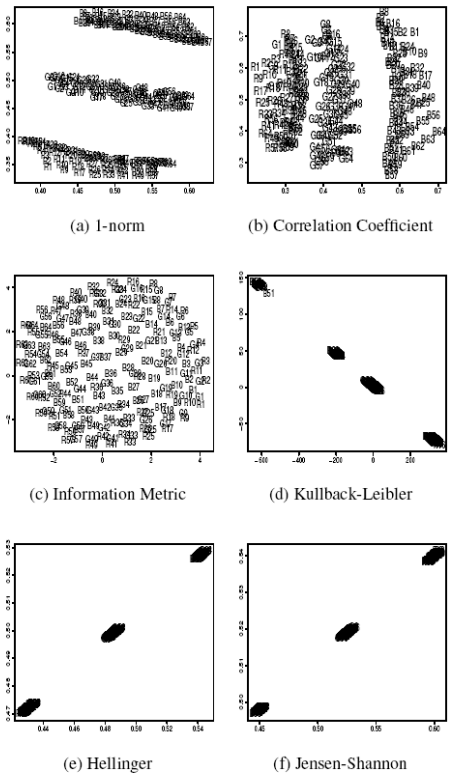

(a) 1-norm (b) Correlation Coefficient

(c) Information Metric (d) Kullback-Leibler

(e) Hellinger (f) Jensen-Shannon

Figure 3: Sensoriopic maps of 192 sensors using uniform binning.

Figure 3 shows sensoritopic maps for all the red, green, and blue sensors, and column 192RGB of table 1 show the corresponding average distances. This is an example of sensor integration where the problem is to find what sensors that are from the same location of the visual field, when the only input data to the system is the raw and unstructured data from the 192 sensors without any classification. The

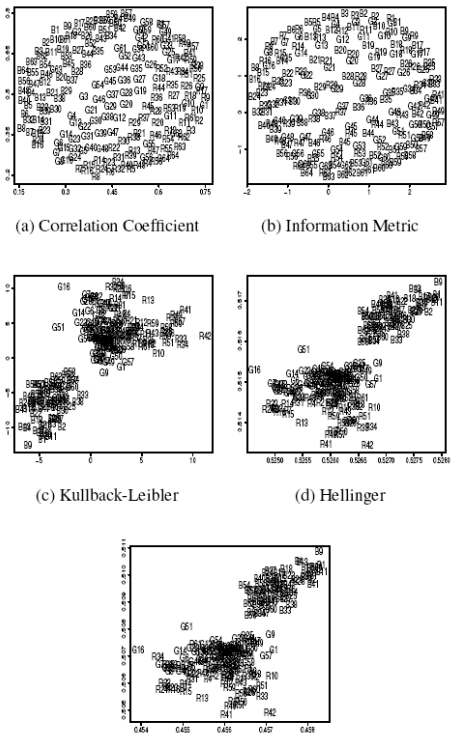

(a) Correlation Coefficient (b) Information Metric

(c) Kullback-Leibler (d) Hellinger

(e) Jensen-Shannon

Figure 4: Sensoriopic maps of 192 sensors using entropy maximization of the sensor data.

Hellinger map and Jensen-Shannon map both contain three clusters, one for each modality. The Kullback-Leibler map is divided in to four clusters. The 1-norm distance shows how structure within the modalities is present but there is no fusion of the sensors from different modalities. The correlation coefficient measure shows a similar structure but there is some overlap between the red and the green sensors. For the information metric, figure 3(c), the situation is different. Here the sensors of different modalities from the same location in the visual field are clustered together. This is an example of autonomous sensory fusion where sensors of different modalities are combined. A well-studied example of this in neuroscience is the optic tectum of the rattlesnake, where nerves from heat-sensitive organs are combined with nerves from the eyes (Newman and Hartline, 1981).

In (Olsson et al., 2005c) it was shown how entropy maximization of the data in individual sensors might be useful to find correlations between sensors of different modalities. Figure 4 shows sensoritopic maps and column 192ARGB of table 1 the average distance computed using the same data as before where it has been preprocessed by maximizing the entropy in each sensor using a window of 100 time steps (see (Olsson et al., 2005c) for details of this method). The 1-norm distance is not included since it is operating on raw sensor values and not on probabilities. The Kullback-Leibler, Hellinger, and Jensen-Shannon measures now cluster the red and green together and the blue in another cluster. The map of the correlation coefficient is similar, albeit with with more structure showing the layout of the individual sensors of the different modalities, as also can be seen in the average distance in table 1. The information metric in figure 4(b) again shows clustering of the different modalities according to their spatial location in the visual field. For example is sensor $R28$ clustered together with $B28$ and $G28$.

Discussion

Why is it the case that the information metric enables the sensory reconstruction method to find these relations between sensors of different modalities when the other measures do not? By considering the individual as well as joint entropies of the sensors the information metric provides a general method for quantifying all functional relationships between sensors, while many other methods only find some relationships. For example, a correlation coefficient approaching 0 does not imply that two variables actually are independent (Steuer et al., 2002).

Conclusions

For purposes of autonomous construction of the relations among sensors in an embodied agent, in this paper we compared the information metric to five other distance measures: the 1-norm distance, the correlation coefficient, Kullback-Leibler divergence, Hellinger distance, and the Jensen-Shannon divergence. Among these the information metric, 1-norm distance, Hellinger distance, and the squared Jensen-Shannon divergence are metrics in the mathematical sense. The comparision was performed by applying the distance measures as the distance measure used in the sensory reconstruction method. The created sensoritopic maps were evaluated by comparing the average spatial distances of the sensors of the reconstructed maps with the spatial distances between the sensors of the real square layout of the sensors.

The results showed that for autonomous construction of the relationships between sensors of different modalties, sensoritopic reconstruction using the information metric was the only successful method, outperforming all the other distance measures. When using sensors from only one modality the average reconstruction distance of the information metric was similar to the 1-norm distance. Among the other proposed measures the correlation coefficient had a shorter average distance than the others, but still significantly greater than the information metric. This is due to the fact that the information metric captures general relationships between sensors and not just linear relationships, as is the case with many other measures.

In recent years there has been an increased interest in studying the informational relationships between robots, their environment, and how their actions affect the information available in their sensors. Here the information metric is useful since it captures general relationships between sensors. This has, for instance, been exploited to discover optical and information flow in sensors of different modalities (Olsson et al., 2005a, 2006), and to build "interpersonal maps" that represent the informational relationships between two agents (Hafner and Kaplan, 2005). It has also been used to study the informational content available to robots in environments with oriented contours (Olsson et al., 2004a), inspired by the developmental studies of kittens reared in restricted visual environments (Wiesel, 1982; Callaway, 1998).

One possible avenue for future research is to study how robots, just like animals, can optimize their sensory system based on the statistics of their specific environments, as well as the actions and embodiment of the particular robot. Here the construction of sensoritopic maps using the information metric can be used as a general method to find the informational relationships between the sensors and the actions of the robot. It would also be of interest to study how a robot actively can shape the informational relationships among its sensors by deliberate actions.

Acknowledgements

The work described in this paper was partially conducted within the EU Integrated Project RobotCub ("Robotic Open-architecture Technology for Cognition, Understanding, and Behaviours") and was funded by the European Commission through the E5 Unit (Cognition) of FP6-IST under Contract FP6-004370.

References

Barlow, H. B. (1961). Possible principles underlying the transformation of sensory messages. *Journal of Sensory Communication*, pages 217–234.

Basu, A., Harris, I. R., and Basu, S. (1997). Minimum distance estimation: The approach using density-based distances. In Maddala, G. S. and Rao, C. R., editors, *Handbook of Statistics*, volume 15, pages 21–48.

Callaway, E. M. (1998). Visual scenes and cortical neurons: What you see is what you get. *Proceedings of the National Academy of Sciences*, 95(7):3344–3345.

Cover, T. M. and Thomas, J. A. (1991). *Elements of Information Theory.* John Wiley & Sons, Inc.

Crutchfield, J. P. (1990). Information and its Metric. In Lam, L. and Morris, H. C., editors, *Nonlinear Structures in Physical Systems – Pattern Formation, Chaos and Waves*, pages 119–130. Springer Verlag.

Endres, D. M. and Schindelin, J. E. (2003). A new metric for probability distributions. *IEEE Transactions on Information theory*, 49(7):1858–1860.

Ernst, J., Nau, G. J., and Bar-Joseph, Z. (2005). Clustering short time series gene expression data. In *Proceedings of ISMB*. to appear.

Hafner, V. and Kaplan, F. (2005). Interpersonal maps and the body correspondance problem. In Demiris, Y., Dautenhahn, K., and Nehaniv, C. L., editors, *Proceedings of the AISB 2005 Third International Symposium on Imitation in Animals and Artifacts*, pages 48–53.

Kaplan, F. and Hafner, V. (2005). Mapping the space of skills: An approach for comparing embodied sensorimotor organizations. In *Proceedings of the 4th IEEE International Conference on Development and Learning (ICDL-05)*, pages 129–134.

Lin, J. (1991). Divergence measures based on the Shannon entropy. *IEEE Transactions on Information Theory*, 37(1):145–151.

Lungarella, M., Pegors, T., Bulwinkle, D., and Sporns, O. (2005). Methods for quantifying the informational structure of sensory and motor data. *Neuroinformatics*, 3(3):243–262.

Lungarella, M. and Pfeifer, R. (2001). Robots as cognitive tools: Information-theoretic analysis of sensory-motor sata. In *Proceedings of the 2nd International Conference on Humanoid Robotics*, pages 245–252.

Mirza, N. A., Nehaniv, C. L., te Boekhorst, R., and Dautenhahn, K. (2005a). Robot self-characterisation of experience using trajectories in sensory-motor phase space. In *Proceedings of the fifth international workshop Epigenetic Robotics*, pages 143–144.

Mirza, N. A., Nehaniv, C. L., te Boekhorst, R., and Dautenhahn, K. (2005b). Using sensory-motor phase-plots to characterise robot-environment interactions. In *Proceedings of the 6th IEEE International Symposium on Computational Intelligence in Robotics and Automation (CIRA-2005)*, pages 581–586.

Newman, E. A. and Hartline, P. H. (1981). Integration of visual and infrared information in bimodal neurons of the rattlesnake optic tectum. *Science*, 213:789–791.

Olsson, L., Nehaniv, C. L., and Polani, D. (2004a). The effects on visual information in a robot in environments with oriented contours. In *Proceedings of the Fourth International Workshop on Epigenetic Robotics*, pages 83–88. Lund University Cognitive Studies.

Olsson, L., Nehaniv, C. L., and Polani, D. (2004b). Sensory channel grouping and structure from uninterpreted sensor data. In *Proceedings of the 2004 NASA/DoD Conference on Evolvable Hardware*, pages 153–160. IEEE Computer Society Press.

Olsson, L., Nehaniv, C. L., and Polani, D. (2005a). Discovering motion flow by temporal-informational correlations in sensors. In *Proceedings of the Fifth International Workshop on Epigenetic Robotics*, pages 117–120. Lund University Cognitive Studies.

Olsson, L., Nehaniv, C. L., and Polani, D. (2005b). From unknown sensors and actuators to visually guided movement. In *Proceedings of the Fourth International Conference on Development and Learning (ICDL 2005)*, pages 1–6. IEEE Computer Society Press.

Olsson, L., Nehaniv, C. L., and Polani, D. (2005c). Sensor adaptation and development in robots by entropy maximization of sensory data. In *Proceedings of the Sixth IEEE International Symposium on Computational Intelligence in Robotics and Automation (CIRA-2005)*, pages 587–592. IEEE Computer Society Press.

Olsson, L., Nehaniv, C. L., and Polani, D. (2006). From unknown sensors and actuators to actions grounded in sensorimotor perceptions. *Connection Science*, 18(2).

Pierce, D. and Kuipers, B. (1997). Map learning with uninterpreted sensors and effectors. *Artificial Intelligence*, 92:169–229.

Prince, C., Helder, N. A., and Hollich, G. J. (2005). Ongoing emergence: A core concept in epigenetic robotics. In *Proceedings of the fifth international workshop Epigenetic Robotics*, pages 63–70.

Sporns, O. and Pegors, T. K. (2003). Generating structure in sensory data through coordinated motor activity. *Proceedings of the International conference Neural Networks*, page 2796.

Sporns, O. and Pegors, T. K. (2004). Information-theoretic aspects of embodied artificial intelligence. *Embodied Artificial Intelligence, LNCS 3139*, pages 74–85.

Steuer, R., Kurths, J., Daub, C. O., J., W., and Selbig, J. (2002). The mutual information: Detecting and evaluating dependencies between variables. *Bioinformatics*, 18:231–240.

Tarapore, G., Lungarella, M., and Gómez, G. (2004). Fingerprinting agent-environment interaction via information theory. In Groen, F., Amato, N., Bonarini, A., Yoshida, E., and Kröse, B., editors, *Proceedings of the 8th International Conference on Intelligent Autonomous Systems, Amsterdam, The Netherlands*, pages 512–520.

Wiesel, T. (1982). Postnatal development of the visual cortex and the influence of environment. *Nature*, 299:583–591.

Current Biology 18, 227–232, February 12, 2008 ©2008 Elsevier Ltd All rights reserved DOI 10.1016/j.cub.2007.12.021

Report

The Evolution of Social Cognition: Goal Familiarity Shapes Monkeys' Action Understanding

Magali J. Rochat,[1] Elisabetta Serra,[1] Luciano Fadiga,[2,3] and Vittorio Gallese[1,*]
[1]Section of Physiology
Department of Neuroscience
University of Parma
I-43100 Parma
Italy
[2]Section of Human Physiology
Department of Biomedical Sciences
University of Ferrara
I-44100 Ferrara
Italy
[3]The Italian Institute of Technology
1-16163 Genova
Italy

Summary

What is the evolutionary origin of the human ability to understand and predict the behavior of others? Recent studies suggest that human infants' early capacity for understanding others' goal-directed actions relies on nonmentalistic strategies [1–8]. However, there is no consensus about the nature of the mechanisms underpinning these strategies and their evolutionary history. Comparative studies can shed light on these controversial issues. We carried out three preferential looking-time experiments on macaques, modeled on previous work on human infants [1–5], to test whether macaques are sensitive to the functional efficacy of familiar goal-related hand motor acts performed by an experimenter in a given context and to examine to which extent this sensitivity also is present when observing non-goal-related or unusual goal-related motor acts. We demonstrate that macaque monkeys, similar to human infants, do indeed detect action efficacy by gazing longer at less efficient actions. However, they do so only when the observed behavior is directed to a perceptible and familiar goal. Our results show that the direct detection of the functional fitness of action, in relation to goals that have become familiar through previous experience, is the phylogenetic precursor of intentional understanding.

Results and Discussion

The evolutionary origin of the human ability to understand and predict the behavior of others has become a matter of controversy since the apparent inability of nonhuman primates to understand others as intentional agents [9] was recently challenged. In fact, there is evidence that chimps, when engaged in a competitive setting, are able to infer what others know on the basis of where they are looking [10]. Even more impressively, it has been shown that rhesus monkeys can establish a cognitive link between seeing and knowing [11] and hearing and knowing [12]. These results show that nonhuman primates possess the ability to understand what others know about the world on the basis of observable behavioral cues.

We decided to address the issue of the evolution of human ability to understand the intentional behavior of others by studying how macaque monkeys evaluate the efficacy of the observed motor behavior of a human agent in terms of the adequacy between means and ends in a given context. To that purpose, we carried out three preferential looking-time experiments modeled on Gergely et al.'s previous work with infants [1] and substituted their computer-generated stimuli with real actions performed in front of the monkeys by a human agent. In experiment 1, macaque monkeys were tested to assess their sensitivity to the adequacy between the means (the type of reaching-to-grasp trajectory) and the goal (grasping an object) of observed goal-directed motor acts according to the contextual constraints (presence or absence of an obstacle). In experiment 2, macaque monkeys were tested to evaluate to which extent this sensitivity correlates with the goal relatedness of the monkeys' observed motor acts by showing them non-goal-related movements. Finally, experiment 3 was designed to assess whether the observation of any goal-directed motor act, regardless of whether it is part of the monkeys' behavioral repertoire, would trigger the sensitivity to its means-end adequacy.

In contrast to previous studies [1–7, 13], we introduced quantitative methods to assess the monkeys' gaze by means of an infrared eye-tracking device. We also measured the kinematics components of the actions observed by the monkeys via a high-resolution video motion analysis (see the Supplemental Data).

Experiment 1

Experiment 1 included two testing sessions (Figure 1). In the experimental session, monkeys (n = 6) were familiarized with a human experimenter who moved her hand above an obstacle to grasp an object (see Movie S1). In the following two test events, the obstacle was removed. In one test event (motor acts were congruent to the physical context), the experimenter canonically reached and grasped the object by following a novel, straight-line trajectory (see Movie S2). In the other test event (motor acts were incongruent to the physical context), the experimenter reached up and grasped the object by following a curvilinear path identical to the one executed during the familiarization trial to bypass the obstacle (see Movie S3).

If during the familiarization trial monkeys interpreted the observed motor act as the shortest path to the goal with respect to the context, a motor act displaying the same curvilinear path to the goal in a context free from any obstacle should have triggered monkeys' attention (expressed by a greater amount of looking time) more often than when observing a motor act that follows a shorter, straight-line path. Alternatively, if monkeys attended to the surface structure of the observed motor act without relating it to the target object or the context, we expected a reverse pattern of gaze behavior during test trials, indicating sensitivity to novel actions.

In the control session, the same monkeys (n = 6) were familiarized with a motor act identical to that used in the

*Correspondence: vittorio.gallese@unipr.it

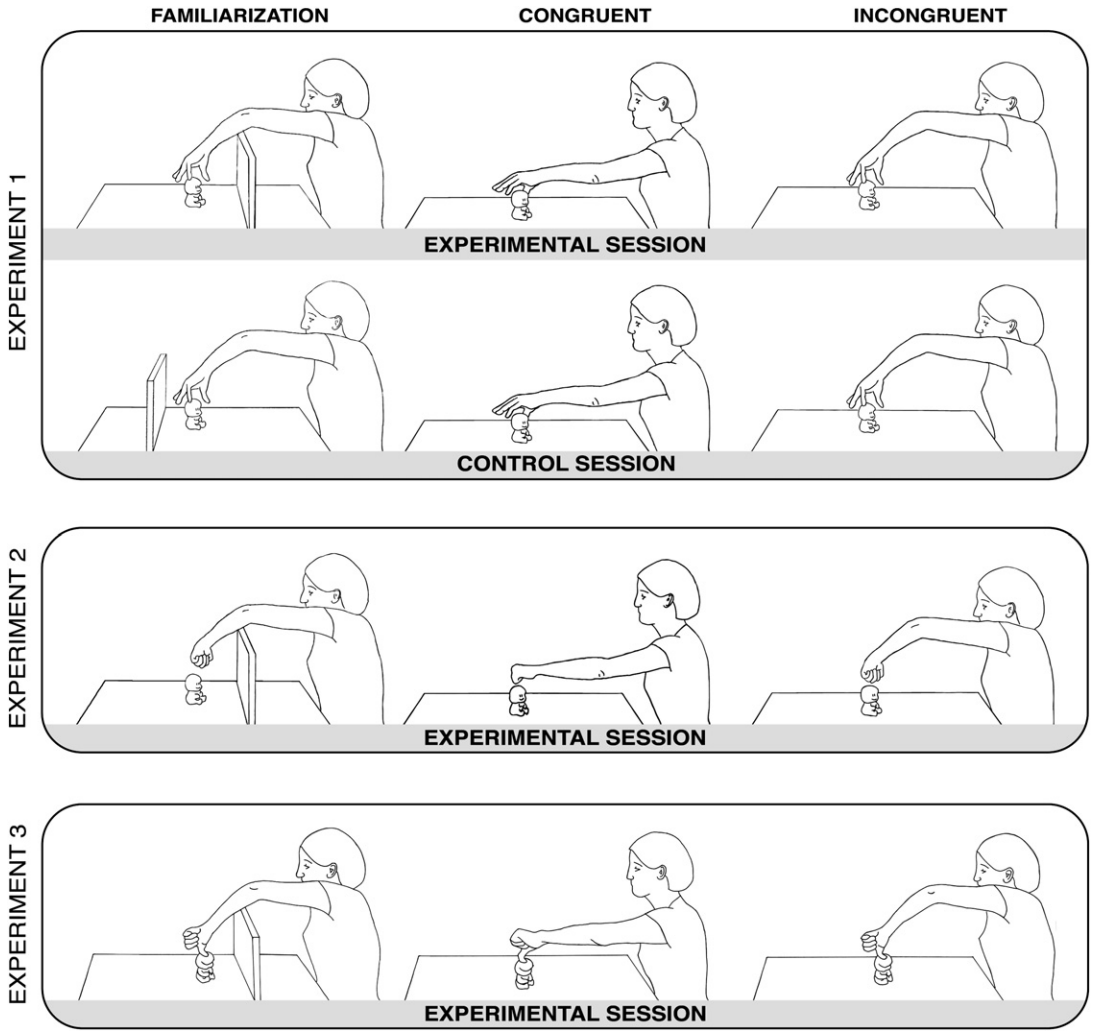

Figure 1. Testing Conditions in Experiments 1, 2, and 3

The top two panels illustrate the familiarization condition followed by the congruent and incongruent test events in both experimental and control sessions in experiment 1. The middle panel shows the familiarization condition followed by the congruent and incongruent test events presented in experiment 2. The bottom panel illustrates the familiarization condition followed by the congruent and incongruent test events presented in experiment 3.

experimental session (curvilinear trajectory, see Figure 1) but executed in a situation where the location of a physical obstacle didn't block the direct access to the target object (see Movie 4). The familiarization trial was then followed by the same two test events presented during the experimental session (see Movies S2 and S3). The rationale was to assess the importance of contextual features during motor-act observation and prediction. First, an analysis of variance (ANOVA) with repeated measures, with session (experimental or control) as the within-subjects variable, was conducted on the normalized (Arcsine transformation) mean looking time for the familiarization events (for further details on the statistical analyses, see the Supplemental Data). Results revealed no session effect on looking time ($F_{(1,5)} = 0.138$, $p = 0.726$). Thus subjects' familiarization with the events was comparable between both sessions.

Second, in order to assess looking-time differences between test events for both sessions and to control for the presentation order of test events, a 2 × 2 × 2 repeated-measures ANOVA was carried out on the normalized mean looking time, with session (experimental or control) and condition (congruent or incongruent) as within-subjects factors and order (congruent first or incongruent first) as the between-subjects factor. Results revealed no significant main effect or interaction for order (all p values are >0.05). Thus this variable was collapsed in the subsequent analyses. The interaction between the factors session × condition was significant, $F_{(1,4)} = 28.576$, $p = 0.006$. A separate two-way ANOVA (session × condition) was therefore performed, followed by Tukey's post-hoc test. The results (Figure 2A) showed that in the experimental session, monkeys looked significantly longer at the incongruent events (mean = 43.26 ± SD = 10.12) than at the congruent events (24.76 ± 7.42), $p = 0.001$. A sign test confirmed that all monkeys (100%) behaved the same way ($p = 0.031$). This difference, however, didn't reach significance during the control session, $p = 0.692$; sign test, n.s. (Figure 2B).

Because it is known that monkeys use gaze information as an indicative behavioral cue (see [14] for a review), we compared the amount of time monkeys spent looking at the experimenter's face (see the Supplemental Data) when congruent and incongruent events were observed. Results from the two-way ANOVA (session × condition) showed that only the

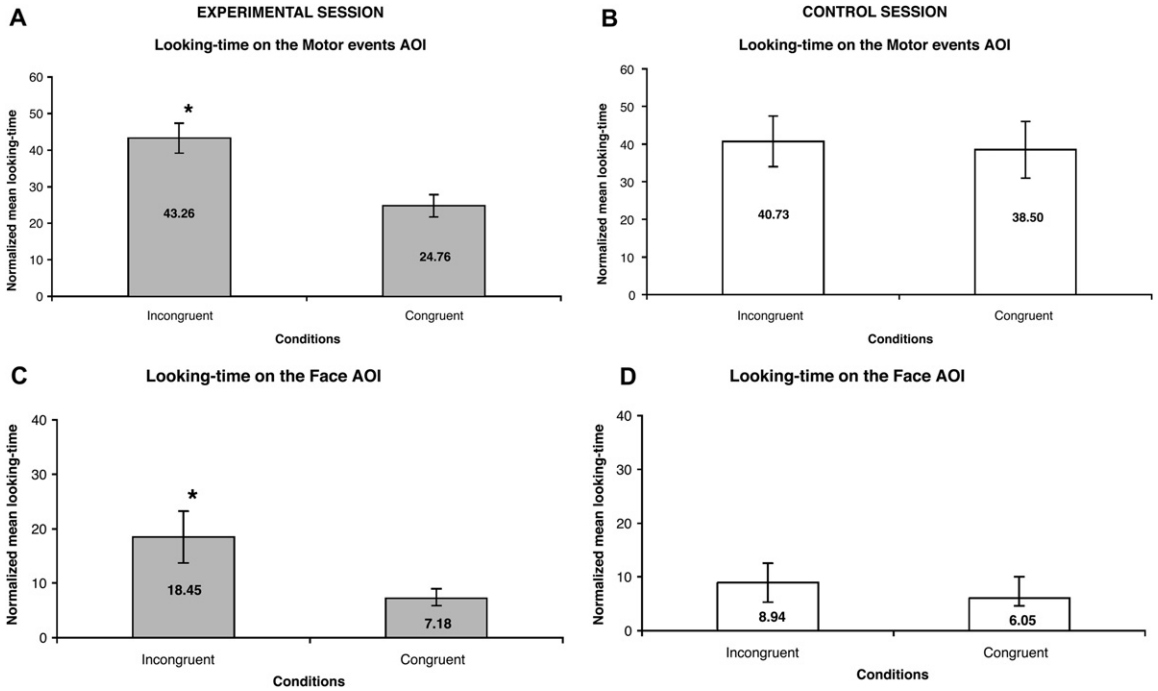

Figure 2. Looking-Time Analysis in Experiment 1

(A and B) Shown are the normalized mean looking-time ± SEM directed to the motor events area of interest (AOI) in the experimental session (A) and in the control session (B).

(C and D) Shown are the normalized mean looking-time ± SEM directed to the face AOI in the experimental session (C) and in the control session (D). *p < 0.05.

main condition factor was significant, $F_{(1,5)} = 15.222$, p = 0.011. Results from Tukey's post-hoc test demonstrated that monkeys looked longer at the experimenter's face during incongruent events than during congruent ones, p = 0.011. We further explored the looking time with a sample-paired t-test for both the experimental and control sessions. The results showed that during the experimental session, monkeys explored the experimenter's face significantly more when she performed incongruent actions (18.45 ± 11.65) compared to when she performed congruent actions (7.18 ± 4.47), t(5) = 3.496, p = 0.017 (Figure 2C). No significant differences emerged during the control session, t(5) = 1.41576, p = 0.216 (Figure 2D).

Experiment 2

In experiment 2 (Figure 1), we investigated the influence of the goal directedness of the experimenter's movements on the modulation of the monkeys' looking time. To this purpose, we familiarized the monkeys (n = 6) to the observation of a non-goal-related curvilinear trajectory of the experimenter's arm in which she brought her hand above the obstacle and stopped it in a fist posture above the target object without touching it (see Movie S5). In the following two test events, the obstacle was removed. In one test event (trajectory congruent with the physical context), the experimenter moved her hand toward the target object by following a novel straight-line trajectory and stopped it in a fist posture without touching it (see Movie S6). In the other test event (trajectory incongruent with the physical context), this movement was executed by following a curvilinear path identical to the one performed during the familiarization trial to bypass the obstacle (see Movie S7). If the monkeys' appreciation of means-ends adequacy depended on their sensitivity to the goal relatedness of observed movements, the absence of a concrete goal shouldn't evoke any attentional enhancement during the observation of incongruent hand trajectories. A one-way ANOVA showed no difference between the amount of looking-time during the familiarization condition of both experiment 2 and experiment 1 (experimental session) ($F_{(1,10)} = 1.182$, p = 0.302). Two separated repeated-measures ANOVAs showed no main effect of condition on the amount of looking time during both test events, $F_{(1,5)} = 3.514$, p = 0.119 (Figure 3A) and on the amount of looking time directed to the experimenter's face during test events observation, $F_{(1,5)} = 0.341$, p = 0.585 (Figure 3B).

Experiment 3

In experiment 3 (Figure 1), we explored whether the evaluation of the action' s efficiency in a certain context is extended to goal-related motor acts the monkeys most likely never observed before and certainly never executed, such as lifting an object with the thumb. To this purpose, monkeys (n = 5) observed the actions of a human experimenter who had a piece of Velcro wrapped around the tip of her thumb. They were first familiarized to the observation of the experimenter moving her hand above an obstacle to contact and lift the target object (the same one used in experiment 1) with the thumb (see Movie S8). In the following test events, the obstacle was removed. In one test event, the experimenter contacted and lifted the object by following a novel, straight-line trajectory (see Movie S9), whereas in the other test event the experimenter executed this action by following a curvilinear path identical to the one monkeys had been familiarized with (see Movie S10).

If the observation of any goal-directed motor act automatically triggered a particular sensitivity to its efficiency within

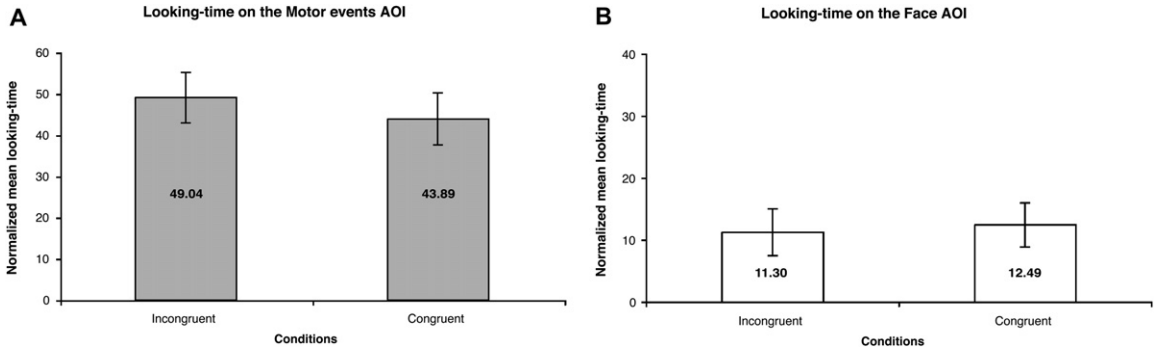

Figure 3. Looking-Time Analysis in Experiment 2

Normalized mean looking time ± SEM directed to the motor events AOI (A) and to the face AOI (B).

a given context, then watching a human agent achieve her/his goal through an inefficient trajectory should provoke a reliably greater attentional enhancement than would watching her/him following a path congruent to the context (see results of experiment 1). On the other hand, if the appreciation of the means-ends adequacy was restricted to the goal-directed motor acts previously practiced by the monkey, the observation of unfamiliar goal-related motor acts shouldn't evoke any attentional enhancement even when following incongruent trajectories. A one-way ANOVA showed no difference between the amount of looking time during the familiarization condition of experiments 3 and 1 (experimental session), ($F_{(1,9)}$ = 0.010, p = 0.920). Two separated repeated-measures ANOVAs showed no main effect of condition on the amount of looking time during both test events, $F_{(1,4)}$ = 6.796, p = 0.596 (Figure 4A) and on the amount of looking time directed to the experimenter's face during test-event observation, $F_{(1,4)}$ = 0.402, p = 0.560 (Figure 4B).

Finally, in order to compare the results of experiments 1 and 3, a crossexperiment mixed-design ANOVA with experiment (experiment 1, experimental session; experiment 3) as a between-factor and condition (congruent or incongruent) as a within-factor was conducted. Results yielded a significant interaction between experiment and condition, $F_{(1,9)}$ = 11,565, p = 0.008. Results from Tukey's post-hoc test showed that in experiment 1 (experimental session), monkeys looked significantly longer at the incongruent events than at the congruent ones (p = 0.0003), whereas no significant differences occurred between those two conditions in experiment 3, p = 0.132.

Conclusions

Results from experiment 1 show that macaque monkeys, similar to 9- to 12-month-old human infants, detect the goal of an observed motor act and, according to the physical characteristics of the context (position of the obstacle), construe expectancies about the most likely action the agent will execute in a given context and therefore react differently to the same goal (object grasping) when accomplished by different means (type of hand trajectory). Monkeys' sensitivity to means-ends adequacy was further corroborated by their longer exploration of the experimenter's face in the experimental incongruent condition. It could be hypothesized that when the experimenter started to execute motor acts that violated the expected means-ends adequacy that monkeys tried to disambiguate the situation by searching for additional cues such as exploring experimenter's gaze direction and/or facial expression.

How do the present data relate to the evidence of Gergely et al. [1] on human infants given that our paradigm was modeled on theirs? Csibra and Gergely [2] proposed that the development in ontogeny of a full-blown, mentalistic intentional stance [15] is preceded by a nonmentalistic teleological stance based on a similar rationality principle applied to factual reality and not on mental states. Teleological reasoning is described as a "normative evaluation of actions based on the principle of rational action, which allows for the assessment of the relative efficiency of the action performed to achieve the goal within the situational constraints given" [16]. According to the teleological hypothesis, revolving around an emerging theory of

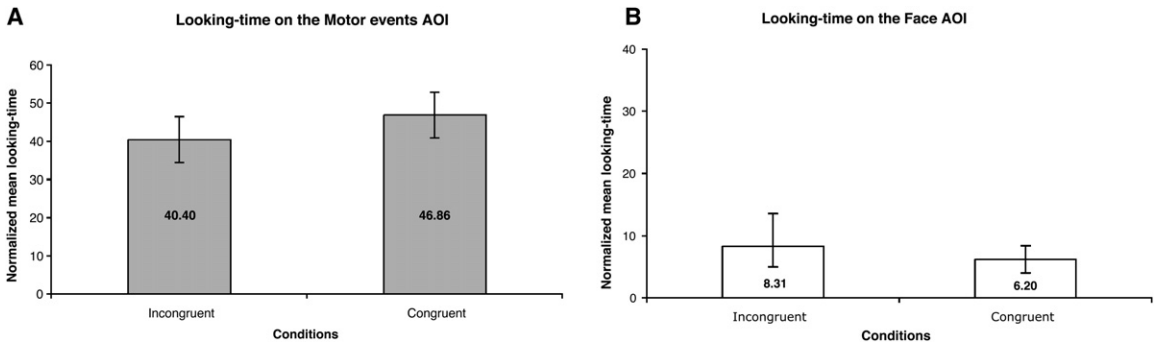

Figure 4. Looking-Time Analysis in Experiment 3

Normalized mean looking time ± SEM directed to the motor events AOI (A) and to the face AOI (B).

rational action, infants assume that agents pursue their goal in the most efficient manner available given the constraints of reality. Thus, 9- and 12-month-old infants refer to this interpretational system to attribute goals to humans [4] as well as to nonhuman [1–3] agents.

The results of our experiment 1, in spite of the different types of stimuli employed, show an apparent similarity with those obtained by Gergely et al. [1]. Experiment 2 demonstrates that macaque monkeys' evaluation of the action mean employed in a certain context strictly depends upon the achievement of a goal state (e.g., a motor act producing an observable change in the state of reality). Just like 12-month-old human babies observing actions directed to an absent target object [4], our results show that when no interaction exists between effector and target object with the resulting lack of causal effect in reality, the evaluation of the observed motor act's fitness to the physical constraints of its context becomes impossible.

The results of our first two experiments demonstrate that macaque monkeys pay attention to the relation between the observed motor acts and their observable outcome within the constraints of a certain context (see also [17]). The results from experiment 3, though, reveal that the specific sensitivity to means-ends adequacy disappears when the goal-related behavior and its end state are unfamiliar to the observing monkeys. However, given that the action in experiment 3 was both visually unfamiliar and absent from monkeys' action repertoire, our data do not enable us to firmly establish whether the monkeys' failure to see the observed action as goal directed was due to either a lack of motor or perceptual familiarity. Both hypotheses are, in principle, equally possible. The issue of whether motor training or extensive perceptual exposure would allow monkeys to extract the action's goal remains to be assessed through future experiments. Nevertheless, we think that evidence both from monkeys and humans makes it reasonable to propose the "lack of motor expertise" hypothesis as a viable option. Let us see why.

Single neurons recording studies in macaque monkeys revealed the existence of a class of motor neurons (mirror neurons) that discharge during both the execution and the observation of goal-directed motor acts [18, 19]. It has been proposed that the mirror neuron system (MNS), by matching observed, implied, or heard goal-directed motor acts on their motor representation in the observer's motor system, allows a direct form of action understanding through a mechanism of embodied simulation [20].

Recent neurophysiological studies have reported that a particular class of ventral premotor mirror neurons starts to respond to the observation of unfamiliar actions after extensive visual exposure to them [21] or after motor training [22]. The results of both experiments seem to suggest that when an action performed by others becomes familiar, independently from the perceptual or motor source of its familiarization, it is nevertheless always mapped onto the motor representation of a similar goal (to take possession of an object) belonging to the observing individual (on the impact of visual familiarity on motor representations, see also [23, 24]).

A similar MNS involving homolog cortical areas has been discovered in the human brain [18]. Even more strikingly, several brain-imaging studies have shown that the intensity of the MNS activation during action observation depends on the similarity between the observed actions and the participants' action repertoire [25–30]. In particular, one fMRI study [27] focused on the distinction between the relative contribution of visual and motor experience in processing an observed action. The results revealed greater activation of the MNS when the observed actions were frequently performed with respect to those that were only perceptually familiar but never practiced. Finally, it has been shown that motor familiarity, but not perceptual familiarity, influences the capacity of 3-month-old infants to extract goals from observed actions [5].

Our study does not provide direct evidence about the neural mechanisms underpinning the present results. However, we believe that a plausible explanation could be that macaques evaluate the observed human acts by mapping them on their own motor representation through the activation of the MNS. Furthermore, we propose that the monkeys' experience in programming and executing goal-directed hand motor acts within certain contextual constraints would result in an automatic activation of the very same neural clusters when observing a motor act that reflects a similar adequacy to the context [19]. It is possible that when the monkeys are familiarized with an observed motor act consonant with their motor repertoire (like passing over an obstacle to grasp an object), its resulting embodied simulation automatically drives the perception of the other experimenter as a "like-me" entity [31], thus enabling the observer to predict the trajectories of future actions in different contexts (see congruent and incongruent test events). This, however, appears to be true only to the extent that observed motor acts are familiar to the observer, whereas familiarization with inadequate motor acts (experiment 1, control session), non-goal-related movements (experiment 2), or unfamiliar goal-related motor acts (experiment 3) does not allow any simulation and prediction.

One final point worth discussing is related to the possible different level of complexity of the actions displayed in experiments 1 and 3 as a potential source of the difference in results obtained in these experiments. Yet, if the displayed actions are parsed as a sequence of goal-related motor acts, both of them appear to be composed of two sequentially chained motor acts ("reach-to-grasp" in experiment 1 and "reach-to-lift" in experiment 3), thus showing a similar level of complexity.

Let us finally turn to the relevance of our results to the ontogeny of action understanding. An increasing body of experimental evidence shows that human infants develop early action understanding abilities within the first year of life [32, 33] and that the capacity to detect the goal of another's action is closely related to the infants' prior motor experience [5–8]. Furthermore, a recent study demonstrates that 3-day-old human neonates [34], similar to other species of animals such as chicks [35], show an inborn predisposition to attend to biological motion. Such a mechanism has high evolutionary relevance because it allows the act of recognizing the movement of others in order to make an appropriate response [36]. Although no strong evidence directly links human infants and nonhuman primates' ability to understand others as goal-oriented agents to the natural tendency to attend to biological motion, it seems reasonable to hypothesize that these two abilities are grounded on a common implicit embodied mechanism. Such a mechanism might account for the phylogenetic evolution of goal attribution [37, 38].

Taken together, our results suggest that nonhuman primates and human infants possess a similar ability to recognize and evaluate the adequacy of goal-related behavior, which, however, seems to operate at a broader level in infants. The present evidence shows that perceptual and/or motor expertise are important elements for the evolution of humans' capacity of understanding the intentional behavior of others.

We propose that the direct detection of the functional fitness of action, in relation to goals that have become familiar, is the phylogenetic precursor of intentional understanding.

Supplemental Data

Experimental Procedures, three figures, and ten movies are available online at http://www.current-biology.com/cgi/content/full/18/3/227/DC1/.

Acknowledgments

We thank G. Csibra, P.F. Ferrari, L. Riggio, C. Sinigaglia, and M.A. Umiltà for their helpful comments on the paper and F. Rodà and A. Jezzini for their help collecting data in experiment 3. This work was supported by Ministero Italiano dell'Università e della Ricerca and by the EU grants NESTCOM and DISCOS.

Received: September 24, 2007
Revised: December 6, 2007
Accepted: December 7, 2007
Published online: January 24, 2008

References

1. Gergely, G., Nàdasdy, Z., Csibra, G., and Bìrò, S. (1995). Taking the intentional stance at 12 months of age. Cognition *56*, 165–193.
2. Csibra, G., Gergely, G., Birò, S., Koòs, O., and Brockbank, M. (1999). Goal attribution without agency cues: the percetion of "pure reason" in infancy. Cognition *72*, 237–267.
3. Csibra, G., Birò, S., Koòs, O., and Gergely, G. (2003). One-year-old infants use teleological representations of actions productively. Cognitive Science *27*, 111–133.
4. Phillips, A.T., and Wellman, H.M. (2005). Infants' understanding of object-directed action. Cognition *98*, 137–155.
5. Sommerville, J.A., Woodward, A., and Needham, A. (2005). Action experience alters 3-month-old perception of other's actions. Cognition *96*, 1–11.
6. Woodward, A.L. (1998). Infants selectively encode the goal object of an actor's reach. Cognition *69*, 1–34.
7. Sommerville, J.A., and Woodward, A. (2005). Pulling out the intentional structure of action: the relation between action processing and action production in infancy. Cognition *95*, 1–30.
8. Falck-Ytter, T., Gredebäck, G., and von Hofsten, C. (2006). Infant predict other people's action goals. Nat. Neurosci. *9*, 878–879.
9. Povinelli, D.J., and Eddy, T.J. (1996). What young chimpanzees know about seeing. Monogr. Soc. Res. Child Dev. *61*, 1–152.
10. Hare, B., Call, J., Agnetta, B., and Tomasello, M. (2000). Chimpanzees know what conspecifics do and do not see. Anim. Behav. *59*, 771–785.
11. Flombaum, J.I., and Santos, L.R. (2005). Rhesus monkeys attribute perceptions to others. Curr. Biol. *15*, 447–452.
12. Santos, L.R., Nissen, A.G., and Ferrugia, J. (2006). Rhesus monkeys (Macaca mulatta) know what others can and cannot hear. Anim. Behav. *71*, 1175–1181.
13. Uller, C. (2004). Disposition to recognize goals in infant chimpanzees. Anim. Cogn. *7*, 154–161.
14. Emery, N.J. (2000). The eyes have it: the neuroethology, function and evolution of social gaze. Neurosci. Biobehav. Rev. *24*, 581–604.
15. Dennett, D.C. (1987). The Intentional Stance (Cambridge, MA: Bradford Books/MIT Press).
16. Csibra, G., and Gergely, G. (2007). 'Obsessed with goals': functions and mechanisms of teleological interpretation of actions in humans. Acta Psychol. (Amst.) *124*, 60–78.
17. Wood, J.N., Glynn, D.D., Phillips, B.C., and Hauser, M.D. (2007). The perception of rational, goal-directed action in nonhuman primates. Science *317*, 1402–1405.
18. Rizzolatti, G., and Craighero, L. (2004). The mirror-neuron system. Annu. Rev. Neurosci. *27*, 169–192.
19. Fogassi, L., Ferrari, P.F., Gesierich, B., Rozzi, S., Chersi, F., and Rizzolatti, G. (2005). Parietal lobe: from action organization to intention understanding. Science *308*, 662–667.
20. Gallese, V. (2005). Embodied simulation: from neurons to phenomenal experience. Phenom. Cogn. Sci. *4*, 23–48.
21. Ferrari, P.F., Rozzi, S., and Fogassi, L. (2005). Mirror neurons responding to observation of actions made with tools in monkey ventral premotor cortex. J. Cogn. Neurosci. *17*, 212–226.
22. Umiltà, M.A., Escola, L., Intskirveli, I., Grammont, F., Rochat, M., Caruana, F., Jezzini, A., Gallese, V., and Rizzolatti, G. (2008). How pliers become fingers in the monkey motor system. Proc. Natl. Acad. Sci. USA, in press.
23. Porro, C.A., Facchin, P., Fusi, S., Dri, G., and Fadiga, L. (2007). Enhancement of force after action observation. Behavioural and neurophysiological studies. Neuropsychologia *45*, 3114–3121.
24. Ertelt, D., Small, S., Solodkin, A., Dettmers, C., McNamara, A., Binkofski, F., and Buccino, G. (2007). Action observation has a positive impact on rehabilitation of motor deficits after stroke. Neuroimage *36* (*Suppl 2*), 164–173.
25. Buccino, G., Lui, F., Canessa, N., Patteri, I., Lagravinese, G., Benuzzi, F., Porro, C.A., and Rizzolatti, G. (2004). Neural circuits involved in the recognition of actions performed by nonconspecifics: an FMRI study. J. Cogn. Neurosci. *16*, 114–126.
26. Calvo-Merino, B., Glaser, D.E., Grèzes, J., Passingham, R.E., and Haggard, P. (2005). Action observation and acquired motor skills: an FMRI study with expert dancers. Cereb. Cortex *15*, 1243–1249.
27. Calvo-Merino, B., Grèzes, J., Glaser, D.E., Passingham, R.E., and Haggard, P. (2006). Seeing or Doing? Influence of visual and motor familiarity in action observation. Curr. Biol. *16*, 1905–1910.
28. Cross, E.S., Hamilton, A.F., and Grafton, S.T. (2006). Building a motor simulation de novo: Observation of dance by dancers. Neuroimage *31*, 1257–1267.
29. Casile, A., and Giese, M.A. (2006). Nonvisual motor training influences biological motion perception. Curr. Biol. *16*, 69–74.
30. Reithler, J., van Mier, H.I., Peters, J.C., and Goebel, R. (2007). Nonvisual motor training influences abstract action observation. Curr. Biol. *17*, 1201–1207.
31. Meltzoff, A.N. (2007). "Like me": A foundation for social cognition. Dev. Sci. *10*, 126–134.
32. Tomasello, M. (1999). The Cultural Origins of Human Cognition (Cambridge, MA: Harvard University Press).
33. Camaioni, L. (1992). Mind knowledge in infancy: the emergence of intentional communication. Early Development and Parenting *1*, 15–22.
34. Simion, F., Regolin, L., and Bulf, H. (2008). A predisposition for biological displays in the newborn baby. Proc. Natl. Acad. Sci. USA *105*, 809–813.
35. Vallortigara, G., Regolin, L., and Marconato, F. (2005). Visually inexperienced chicks exhibit spontaneous preference for biological motion patterns. PLoS Biol. *3*, e208. 10.1371/journal.pbio.0000051.
36. Blackmore, S.J., and Decety, J. (2001). From the perception of action to the understanding of intention. Nat. Rev. Neurosci. *2*, 561–567.
37. Lyons, D.E., Santos, L.R., and Keil, F.C. (2006). Reflections of other minds: how primate social cognition can inform the function of mirror neurons. Curr. Opin. Neurobiol. *16*, 230–234.
38. Barrett, L., Henzi, P., and Rendall, D. (2007). Social brains, simple minds: does social complexity really require cognitive complexity? Philos. Trans. R. Soc. Lond. B Biol. Sci. *362*, 561–575.

Biological Cybernetics manuscript No.
(will be inserted by the editor)

A. Just · B. Petreska · A. Billard · L. Craighero · A. D'Ausilio · A. Oliynyk · L. Fadiga

Point-to-Point Unconstrained Gestures: Modeling Wrist and Elbow Trajectories

the date of receipt and acceptance should be inserted later

Abstract Although point-to-point reaching motions have received a lot of attention, the way these movements are controlled remains incompletely resolved. Different controllers seem to be recruited depending on the task. Unconstrained reaching movements in space are strongly curved, in opposition to the widely accepted view of quasi-straightness. We argue that the curvature of the movement is due to environmental constraints that affect directly the planning of the movement.

We propose a mathematical model whereby movements are planned through the combination of two concurrent controllers for the wrist and elbow in space. Coherence constraints are enforced between the two systems to simulate biomechanical constraints at the wrist, elbow and shoulder levels. External constraints, such as the presence of obstacles, are encapsulated in a virtual force which affects the planning of the movement.

The predictions of the model are validated against kinematic data from human reaching motions. Four types were contrasted: intransitive versus transitive reaching motions and natural versus un-natural motions. In the un-natural case, subjects were requested to exaggeratedly elevate the elbow during the movement. In all four movements types, the movements are highly curved. The model renders with high accuracy the kinematics of the movements and accounts for the curvature as an effect of the virtual force.

Keywords gesture modeling, VITE model, optimization with Lagrange, unconstrained and voluntary motion, multi-joint arm movement

A. Just · B. Petreska · A. Billard
Learning Algorithms and Systems Laboratory, Ecole Polytechnique Fédérale de Lausanne, 1015 Lausanne. Switzerland

L. Craighero · A. D'Ausilio · A. Oleynik · L. Fadiga
Section of Human Physiology, University of Ferrara, 44100 Ferrara. Italy

L. Fadiga
The Italian Institute of Technology, 16163 Genova. Italy.

1 Introduction

Much attention has been devoted to the study of point-to-point reaching movements, most of which focused on movements restricted to a plane. These studies highlighted several invariant features (Gibet et al 2004), such as quasi-straightness of the hand path from initial and target positions and the so-called bell-shaped velocity profile (Morasso 1981). Soon, such simple rules were questioned when considering unconstrained motions instead of the usual paradigm of constrained motions, or so-called compliant motions (Desmurget et al 1997). Indeed, the majority of the studies of point-to-point movements were highly constrained and required subjects to hold a hand-held cursor. Unconstrained motions, in contrast, refer to free motions of the hand. Results from unconstrained studies show that the spatio-temporal characteristics of compliant and unconstrained movements are fundamentally different. (Desmurget et al 1997) showed that movement duration was higher in the compliant condition than for unconstrained movements. Furthermore, path curvature was significantly higher for unconstrained motions. Hence, compliant and unconstrained motions involve different control strategies. Evidence supports the hypothesis that unconstrained motions are not following a straight line but are slightly curved. This hypothesis is further supported by (Boessenkool et al 1998) who states that trajectory curvature is an inherent property of unconstrained arm movements.

Another largely unresolved issue of motor control relates to the redundancy of the arm joints. A simple way to illustrate this is to consider the various postures that the arm can adopt to touch the same target. Several mathematical models have tried to answer this delicate question. Choosing between describing the kinematics of the arm in Cartesian coordinates or in joint angle space is a thorny problem and evidence comes in support of either of the two representations depending on the task (Flash and Hogan 1985; Rosenbaum et al 1995; Torres and Zipser 2002). To overcome this problem, the

movements are often described more abstractly in terms of a global measure. This measure encodes the cost of each movement and the optimal movement is the one that minimizes this cost function. Cost functions may be defined using either kinematics or dynamic information on the movement.

Cost functions based on kinematic information deal with geometrical and temporal information: position, velocity, acceleration, etc. In (Flash and Hogan 1985), the cost function is defined as the square of the magnitude of the jerk (rate of change of acceleration) integrated over the entire movement. The minimum jerk model generates smooth hand trajectories which are straight and follow a bell-shaped velocity profile.

Cost functions based on dynamic information depend on the forces acting on the hand and arm. The minimum torque change model (Uno et al 1989) proposes as measure of performance the square of the first derivative of the torque integrated over the entire movement. In (Uno et al 1989) the model was compared to the minimum jerk model for unconstrained horizontal movements between two targets located in the sagittal plane. It was shown that the minimum torque change model and minimum jerk model were both predicting straight hand paths. However, for trajectories starting with the arm stretched sideways, the two models gave very different predictions. The minimum jerk model still predicted a straight-line hand paths whereas the trajectories predicted by the minimum torque model were gently curved, and thus more similar to observed human motion.

Other methods have been proposed to model the arm trajectories. Harris and Wolpert proposed the minimum variance theory (Harris and Wolpert 1998). Their model is based on the physiological assumption that the control signal is corrupted by noise. In the presence of this noise, the shape of the hand trajectory is selected so as to minimize the variance of the final arm position. In (Ogihara and Yamazaki 1999), the authors take a very different approach. They modeled the nervous system as a recurrent neural network. Given a goal position, the modeled nervous system was able to generate muscular activation signals used to move the hand to the target position. An interesting feature of this model is its ability to model the position of the whole arm. Most of the models presented previously were dealing mainly with the hand trajectory. A method has been proposed in (Kang et al 2003) to model the arm with its 4 DOFs. The arm trajectory is decomposed into intermediate positions. The model solves the joint angles for these positions by minimizing the sum of absolute value of all joints' torque work in each sub-path (trajectory between two via-positions). Their model unfortunately showed poor results for the adduction/abduction angle of the shoulder. Following this same idea, Gu et al. proposed the equilibrium point based model (Gu and Ballard 2006). The human arm motion can be seen as a sequence of short motion segments. Movements are generated by gradually shifting from one segment position to the next.

The models we have reviewed in the previous paragraphs are mostly dealing with compliant gestures or are modeling solely the hand path. Few of those have been designed to predict the evolution of movement of the entire arm, from start to target. In the present paper, we propose a method for generating the position of the entire arm for point-to-point motions. Further, since the elbow and hand locations are known, the whole arm configuration is determined, we model the control of the arm trajectory with two concurrent dynamical systems driving the hand and elbow separately, but coupled through kinematics constraints. We extend the biologically plausible VITE model (Bullock and Grossberg 1988), that describes a dynamical system to generate straight point-to-point trajectories in the Cartesian space. The extended VITE model we propose accounts for the observed curvature of the movement. Note that an extension of the VITE model that generate curved writing movements has already been proposed (Bullock et al 1993). The extension consisted in running three coupled VITE controllers to control the x-, y- displacements and wrist rotation of the hand, respectively. The curvature was the result of initiating each model at different starting times. An important disadvantage of this approach to model point-to-point movement is that it required a series of multiple arbitrary targets for each curvature change, which is not the case with the EFF-VITE model.

In order to validate the model, we conduct motion studies, in which unconstrained reaching motions are generated. Most of the literature has focused on the study of reaching movements directed at a target (Atkeson and Hollerbach 1985; Desmurget et al 1997; Magescas and Prablanc 2006). To determine if the curvature of the movement results from generating transitive (i.e. directed to a target) versus intransitive movements, we contrast two conditions in which subjects either reach for an object or do a reaching motion directed to no particular location on a table. We hypothesized that in both conditions the trajectories would be curved and argue that this curvature is necessary and fulfills two main goals: to avoid uncomfortable arm postures (for example, it is more natural to extend the elbow to the right during the motion than keeping a purely straight trajectory) and to encapsulate environmental constraints such as the presence of the table.

Furthermore, in order to better understand how the central nervous system manages to decouple the control of the upper and lower arms, when forced to do so, we investigated the kinematics of motion in which the elbow was forced to follow a trajectory more elevated than that found during natural reaching movements. (Koshland et al 2000) showed that, reaching during movements, the wrist exhibited similar characteristics as the proximal joints, demonstrating a coupling among the joints. We thus expected the curvature of the trajectories of

the wrist also to increase as an effect of the exaggerated elevation of the elbow.

In Section 2 we describe the dynamical systems driving the elbow and wrist motions and explain how coherence constraints between the wrist and elbow are enforced in the model. Section 2.2 describes the experimental set-up and procedure followed during the motion studies. A comparative analysis of the model's predictions and human data is done in Section 3, followed by a discussion of the model's biological plausibility.

2 Materials and Methods

2.1 Description of the model

Our proposed approach is based on an extension of Bullock and Grossberg's Vector Integration To Endpoint (VITE) model (Bullock and Grossberg 1988). The VITE model is a biologically inspired model that can only generate straight point-to-point trajectories. Contrary to the VITE model, the extended force-field version of the VITE model (EFF-VITE) can account for curved reaching movements, and can be used to model both the trajectories of the hand and elbow. Compared to the VITE model, the EFF-VITE model is time-independent and thus stable in case of long lasting perturbations. Furthermore, it represents a proper force governed system. In the EFF-VITE system, the trajectory of the hand or elbow is governed by the following dynamical system:

$$\ddot{x}(t) = \alpha(-\dot{x}(t) + \beta g(t)^{\delta}(h(t)+\gamma)(\frac{x^*(t)-x(t)}{\|x^*(t)-x(t)\|} + g(t)\mathbf{F}(t))) \quad (1)$$

and

$$\mathbf{F}(t) = g(t)\mathbf{u} + h(t)\mathbf{v} \quad (2)$$

where

$$g(t) = \frac{\|x^*(t)-x(t)\|}{\|x(t)-x(0)\| + \|x^*(t)-x(t)\|}$$

$$h(t) = \frac{\|x(t)-x(0)\|}{\|x(t)-x(0)\| + \|x^*(t)-x(t)\|}$$

are respectively the ratios between the distance separating the hand from the final target position x^* and the distance separating the hand from the initial position $x(0)$ over their total. The force $\mathbf{F}$ helps to comply with environmental constraints due to the volume and geometry of the body. $\mathbf{F}$ is the weighted sum of two constant force vectors that push the trajectory away from the straight line. $\mathbf{u}$ is the modulated force that perturbs the beginning of the movement, whereas $\mathbf{v}$ perturbs the end of the movement (Figure 1). The parameter $\alpha \in \mathbb{R}^+$ was fixed to a constant value. Parameters β, γ and δ control the general form of the velocity profile. β controls the asymmetry and peak value of the velocity profile. γ enables the initiation of the movement, and δ controls the final approaching phase of the movement and parameterizes the trade-off between precision and execution time. For example, lowering the value of δ shortens the movement deceleration phase but also increases the risk of overshooting the target position (Figure 2). The role of the parameters will be further discussed in Sections 3.2.2 and 3.2.3.

An arm configuration corresponds to a particular position in space of both the wrist and elbow. In the duo-EFF-VITE model, two concurrent EFF-VITE models are modeling the hand and elbow paths. As the hand and elbow are linked, these two systems are not independent. Hence, coherence constraints must be enforced in order to have a meaningful representation of the movement. Figure 3 presents the overall structure of the duo-EFF-VITE model. The outcome of the model is the position of the hand and elbow in the Cartesian space at each time step.

Let $\mathbf{x_w}$ and $\mathbf{x_e}$ be the position of the wrist and elbow in the 3D space where the origin is centered on the shoulder. The position of the arm is such that:

$$||\mathbf{x_e}|| = L_1 \quad (3)$$

and

$$||\mathbf{x_e} - \mathbf{x_w}|| = L_2 \quad (4)$$

where L_1 and L_2 are respectively the length of the upper-arm and forearm , and $||.||$ defines the vector norm.

Let ${\mathbf{x_w}}^d(t)$ and ${\mathbf{x_e}}^d(t)$ be the desired position of the wrist and elbow given by the EFF-VITE models at each time step t. In general, the variables ${\mathbf{x_w}}^d$ and ${\mathbf{x_e}}^d$ will not be consistent with kinematic constraints. In order to have consistent values, we find the values ${\mathbf{x_w}}^*$ and ${\mathbf{x_e}}^*$ that minimize the similarity measure H:

$$H({\mathbf{x_w}}^*, {\mathbf{x_e}}^*) = ||{\mathbf{x_w}}^* - {\mathbf{x_w}}^d|| + ||{\mathbf{x_e}}^* - {\mathbf{x_e}}^d|| \quad (5)$$

under constraints given by equations (3) and (4).

The problem is solved analytically by using Lagrange optimization. We define the Lagrangian as:

$$L({\mathbf{x_w}}^*, {\mathbf{x_e}}^*, \lambda_1, \lambda_2) = H + \lambda_1^T(||{\mathbf{x_e}}^*|| - L_1) + \lambda_2^T(||{\mathbf{x_e}}^* - {\mathbf{x_w}}^*|| - L_2) \quad (6)$$

To solve $\nabla L = 0$, we derive respectively $\frac{\partial L}{\partial {\mathbf{x_w}}^*}$, $\frac{\partial L}{\partial {\mathbf{x_e}}^*}$:

$$2({\mathbf{x_w}}^* - {\mathbf{x_w}}^d) + \lambda_2||{\mathbf{x_e}}^* - {\mathbf{x_w}}^*||^{-1}({\mathbf{x_w}}^* - {\mathbf{x_e}}^*) = 0 \quad (7)$$

$$2({\mathbf{x_e}}^* - {\mathbf{x_e}}^d) + \lambda_1||{\mathbf{x_e}}^*||^{-1}{\mathbf{x_e}}^* + \lambda_2||{\mathbf{x_e}}^* - {\mathbf{x_w}}^*||^{-1}({\mathbf{x_e}}^* - {\mathbf{x_w}}^*) = 0 \quad (8)$$

We thus need to solve the following system:

$$\begin{cases} 2({\mathbf{x_w}}^* - {\mathbf{x_w}}^d) + \lambda_2||{\mathbf{x_e}}^* - {\mathbf{x_w}}^*||^{-1}({\mathbf{x_w}}^* - {\mathbf{x_e}}^*) = 0 \\ 2({\mathbf{x_e}}^* - {\mathbf{x_e}}^d) + \lambda_1||{\mathbf{x_e}}^*||^{-1}{\mathbf{x_e}}^* \\ +\lambda_2||{\mathbf{x_e}}^* - {\mathbf{x_w}}^*||^{-1}({\mathbf{x_e}}^* - {\mathbf{x_w}}^*) = 0 \\ ||{\mathbf{x_e}}^*|| - L_1 = 0 \\ ||{\mathbf{x_e}}^* - {\mathbf{x_w}}^*|| - L_2 = 0 \end{cases}$$

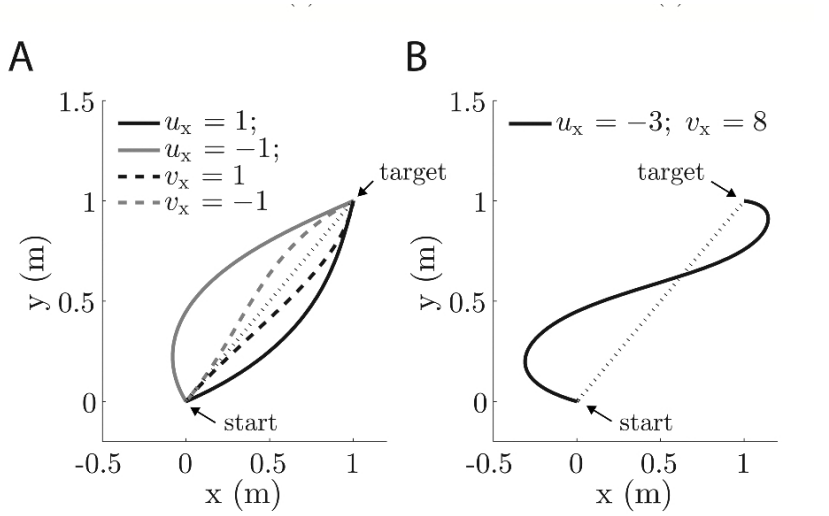

Fig. 1 Dynamics of the movement as a function of the force parameters. A: Forces are modulated such that u affects mostly the beginning of the movement and v mostly the end of the movement. The direction of the deviation from the straight trajectory is determined by the sign of the force. B: By combining the two forces u and v, trajectories that change direction can be obtained. Pararameter values: $\alpha = 50$, $\beta = 10$, $\gamma = 0.01$ and $\delta = 1$.

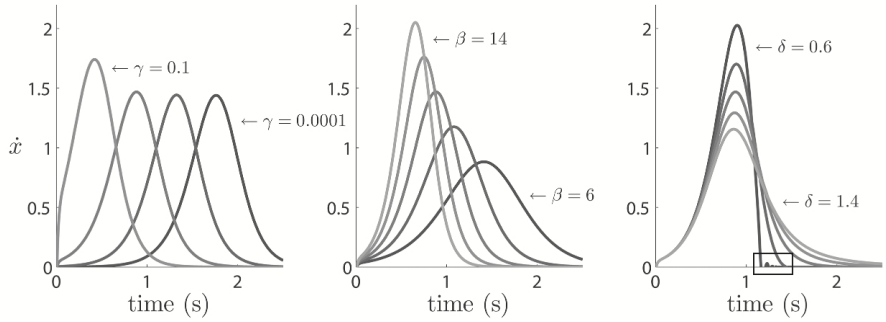

Fig. 2 Effect of the parameters γ, β and δ on the speed profile of the movements. The parameters γ (left) affects the beginning of the movement. The lower its value, the more time it takes the subject to start a movement. β (middle) controls the asymmetry and peak value of the velocity profile (α in our model is constant). δ (right) defined the approaching speed and thus parameterizes the trade-off between precision and execution time. In the rectangle, one can see the arm reaching the target too quickly and overshooting it at $\delta = 0.6$. Parameter values: $\alpha = 50$, $\beta = 10$, $\nu = 1.5$, $\gamma = 0.01$ and $\delta = 1$.

(9)

As the system has several solutions, we choose the solutions $\mathbf{x_w}^*, \mathbf{x_e}^* \in \mathbb{R}$ that minimize H. As the system is non-linear due to the presence of the norm, solutions are found numerically.

2.2 Experiments

Subjects Eight healthy subjects (4 females, 4 males, mean age 26 ±4) volunteered to perform a one-handed task consisting of point-to-point motions. All subjects were right-handed (Edinburgh Handedness Test, Oldfield (1971)) They were all naive regarding the purpose of the experiment. They reported no history of neurological or musculo-skeletal disorder. All had normal or corrected to normal vision.

Procedure Subjects sat comfortably on a chair in front of a table. They were asked to maintain a steady trunk position all along the recording session. Each hand movement started in the same rest position, with the forearm lying on the table and perpendicular to the trunk (Figure 4, left). Subjects were shown the movements by a demonstrator. There were two conditions. In the first condition, movements were directed towards an object placed 30 cm away from the subject in the sagittal plane (Figure 4, right). In the second condition, subjects had to reach in front of them and land their hand palm-down on the table. No location on the table was specified in this second condition. We refer to these two conditions

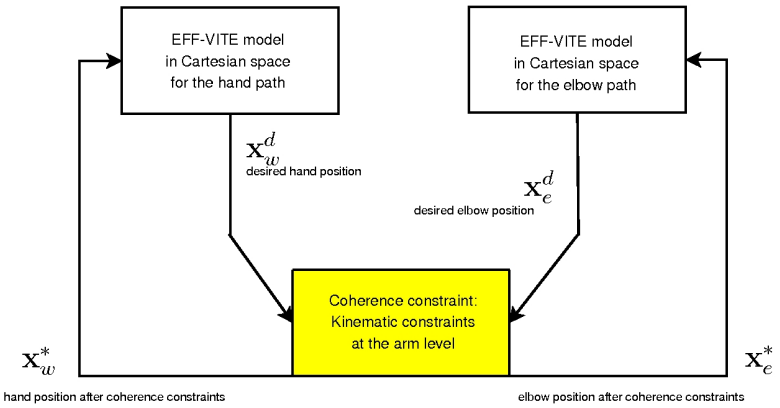

Fig. 3 The wrist-and-elbow path controller: The first EFF-VITE model (on the left) models the trajectory of the wrist in cartesian coordinates, whereas the second EFF-VITE model is used to model the elbow path in cartesian space. The coherence constraints ensure the desired positions $\mathbf{x}_w^d$ and $\mathbf{x}_e^d$ given by the EFF-VITE models are consistent relative to kinematic constraints. The modified values after coherence constraint for both the wrist and elbow positions, $\mathbf{x}_w^*$ and $\mathbf{x}_e^*$, are fed back to the EFF-VITE models.

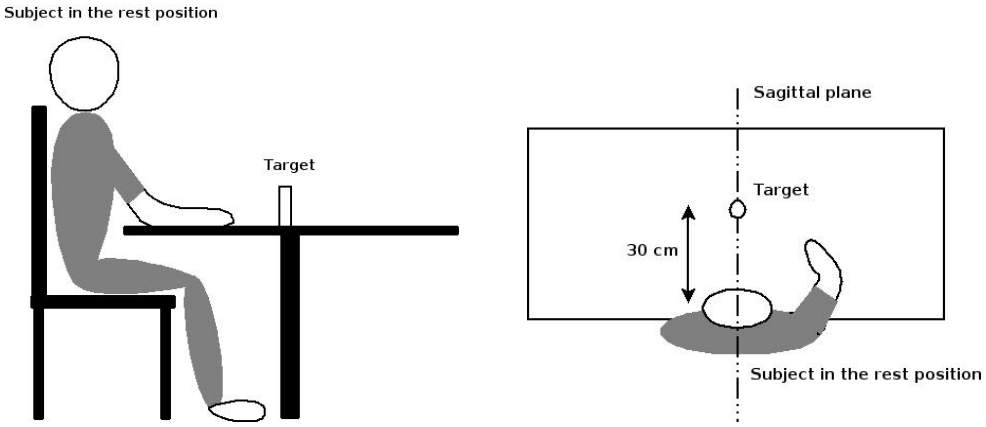

Fig. 4 Left: Experimental set-up seen from the right side with the subject in the rest position. Right: upper view of the set-up showing the position of the target when subjects performed transitive motions.

respectively as transitive (Trans) and intransitive (Intrans) movements in the rest of the paper.

For each condition, the subjects were instructed to perform two variants of the movements. In the first variant (so-called "Elb"), the subjects were asked to exaggeratedly elevate the elbow throughout the motion. In the second variant (so-called "Norm"), subjects were asked to perform motion in the way that seemed most natural to them. Movements were thus of four types: intransitive with normal kinematics (**Intrans Norm**), intransitive with an exaggerated elevation of the elbow (**Intrans Elb**), transitive with normal kinematics (**Trans Norm**) and transitive with an exaggerated elevation of the elbow (**Trans Elb**). Figure 5 presents snapshots of the four types of reaching movements.

Subjects were shown several times each movement types. Additional explanation was given when necessary. The subjects were instructed to replicate as precisely as possible these movements. A series of five movements for each condition and variant was recorded for each subject (Table 1).

Data acquisition The trajectory in space of the shoulder, elbow and wrist were recorded by using a kinematics recording system formed by three ProReflex MCU1000 cameras (QUALISYS AB, Sweden) detecting the 3D position of infrared reflecting markers (n=4) positioned on the left and right shoulders, right elbow and right wrist. The position of the markers was recorded at a frequency of 200 Hz during the execution of the movements. Figure 6 presents one subject wearing the markers as well as the shoulder-centered frame of reference used in the following of the paper to calculate wrist and and elbow trajectories.

Fig. 5 Snapshots of the four gesture types. From left to right: Intransitive action with normal kinematics and with an exaggerated elevation of the elbow. Transitive movement with normal kinematics and with an exaggerated elevation of the elbow. One can see that for the "Elb" variant the elbow position is always higher than for movements performed with normal kinematics for both the "Intrans" and "Trans" conditions.

Subjects	Repetitions	Recording sessions
8	5×4 gesture types	1

Table 1 Statistics of the database.

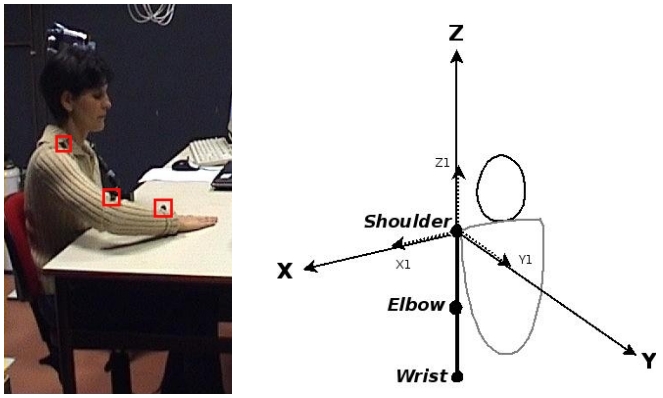

Fig. 6 Left: subject wearing markers on the right arm (markers are surrounded by red squares). Right: shoulder-centered frame of reference.

Data analysis All analyzes were performed using the Qualisys Track Manager (QUALISYS AB, Sweden) software, plus some custom programs written in Matlab (Mathworks, Natick, MA). Analysis was done solely on the reaching phase of each movement (from the rest position to the target location in the case of transitive movements, and from the rest position to the hand placement on the table in front of the subject for intransitive movements). Data were first segmented manually to remove any irrelevant movement prior to the onset of the reaching motion. We used only unfiltered raw values. The curvature index is computed as the ratio between the total arc length of the path and the Euclidian distance between the initial and final positions. A curvature index of 1 indicates a perfectly straight trajectory whereas a semi-circular path would have a curvature index of $CI = \pi/2$. The values of the model's parameters were optimized for each trial using 5^3 factorial experimental designs coupled with a local search procedure (Neter et al 1996; Hoos and Stützle 2004).

3 Results

3.1 Movement statistics

We first assessed the general characteristics of the recorded movements. For each movement type (Intrans Norm, Intrans Elb, Trans Norm, and Trans Elb), we computed the duration of the movement, path length and curvature index of the wrist and elbow on average across the 8 subjects and 20 trials (Table2).

Consistent with (Bernstein 1967)'s observations of substantial trial-to-trial variations, a three-way ANOVA analysis across subjects (eight levels), conditions (intransitive, transitive) and variants (elbow normal, elbow elevated) revealed a high *inter-subject* variability for both the duration of the movements, the length of the wrist path and the curvature index ($p < 0.001$), with a significant interaction effect for the subject/condition and subject/variant factors ($p < 0.01$ in each case, see Table 2). This high across subjects variability in performing the same motion is illustrated in Figures 7 and 8. Subject 9 tended to be very consistent across trials and

	Duration (s)	Path length (cm)		Curvature index		Elbow elevation (cm)
		Wrist	Elbow	Wrist	Elbow	
Intrans Norm	0.89 ± 0.28	25.3 ± 3.3	26.7 ± 3.5	1.16 ± 0.10	1.19 ± 0.06	-15.0 ± 2.3
Intrans Elb	1.11 ± 0.28	31.8 ± 5.7	37.2 ± 9.6	1.54 ± 0.28	1.52 ± 0.26	-7.0 ± 2.8
Trans Norm	0.84 ± 0.19	22.5 ± 3.0	23.0 ± 3.1	1.16 ± 0.09	1.16 ± 0.05	-15.9 ± 2.0
Trans Elb	1.14 ± 0.22	31.8 ± 6.2	34.9 ± 8.1	1.61 ± 0.45	1.47 ± 0.26	-6.4 ± 2.4
p-value (sub.)	< 0.001	< 0.001	< 0.001	< 0.001	< 0.001	< 0.001
p-value (cond.)	n.s.	< 0.003	< 0.001	n.s.	< 0.02	n.s.
p-value (var.)	< 0.001	< 0.001	< 0.001	< 0.001	< 0.001	< 0.001
p-value (sub*cond)	< 0.001	< 0.001	< 0.001	< 0.001	< 0.002	< 0.001
p-value (sub*var)	< 0.001	< 0.001	< 0.001	< 0.001	< 0.001	< 0.001
p-value (cond*var)	< 0.006	< 0.002	n.s.	n.s.	n.s.	< 0.001

Table 2 Duration, path length, curvature index and elbow elevation across trials and subjects. Three-way ANOVA showed that the movements performed with an exaggerated elevation of the elbow lasted longer, had a longer path for both the wrist and elbow and were significantly more curved than movements with normal kinematics. Furthermore, the recorded movements differed significantly accross subjects in their duration, path length, curvature index, and elbow elevation. The maximal height of the elbow during the movement was also significantly different accross the two motion variants.

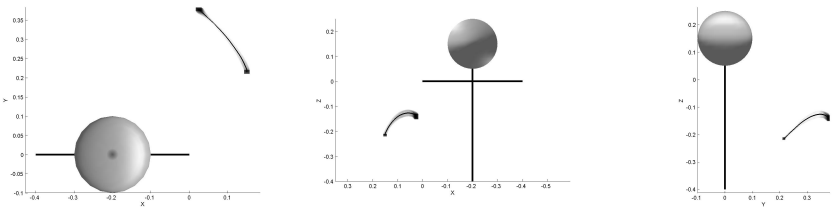

Fig. 7 Mean wrist trajectory (in black) and standard deviation envelope (in grey) for a transitive movement with an abnormal elevation of the elbow (Trans Norm) showing a small intra-variability for Subject 9.

displayed a low across trials variability of the wrist's motion (Figure 7), whereas Subject 5 displayed an overall much higher variability for the same motion (Figure 8). Given that the subjects had different arm lengths, the length of the wrist path varied importantly across subjects, especially in the intransitive case (see table 2).

All movements were curved ($CI > 1$). Most importantly for the argument of this paper, both the trajectory of the wrist and of the elbow were curved. The curvature is even more important for movements performed with an exaggerated elevation of the elbow ($CI > 1.6$). As a result, movements performed with an abnormal elevation of the elbow in both conditions (Intrans versus Trans) take significantly more time and are longer than movements performed with normal kinematics. Moreover, intransitive motions were significantly longer than transitive motions. This is likely due to the rotation of the wrist that occurs during intransitive motions (to place the palm down on the table), particularly when the movement is performed with an exaggerated elevation of the elbow (first two images in Figure 5).

3.2 Accuracy of the model

We measured the accuracy of the model to reproduce each instance of each motion type. We computed the mean deviation (MD) of the predicted wrist and elbow trajectories compared to the wrist/elbow trajectories at each time step, as well as the mean squared error (MSE) for each condition and variant of the movements. Table 3 provides these values for each gesture type. We also performed a three-way ANOVA analysis on these results for the subject, condition and variant factors. These results show no significant influence of either factor on the MSE for the wrist. For the elbow, the ANOVA analysis reveals a significant difference between the two motion variants (F=4.52, $p < 0.04$). However, the error is small and can be explained by the high variability of movements performed with an exaggerated elevation of the elbow (Elb variant).

Thus, overall, the model reproduces motions with high accuracy. It encapsulates the generic shape of both the trajectory in space and the speed profile of the wrist and elbow (Figure 9). 81% of the data for the wrist and 79% of the observed data for the elbow are reproduced by the model with a MSE inferior to the mean MSE. 3 to 4% of the errors are due to outlier data whereas another 53% are due to a poor reproduction of the start and/or end of the trajectory (Figure 10).

This is due to the fact that, like the original VITE model, the duo-EFF-VITE model, pre-supposes a smooth and gradually increasing and decreasing speed profile at the start and end of the movement, respectively. Because

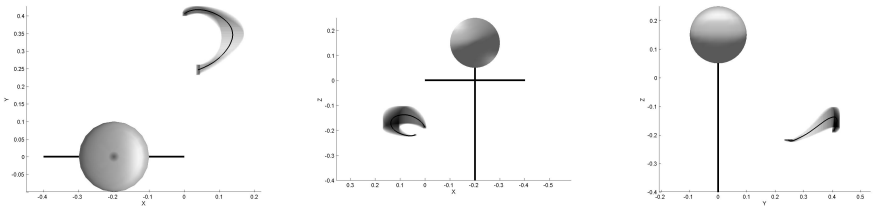

Fig. 8 Mean wrist trajectory (in black) and standard deviation envelope (in grey) for a transitive movement with an abnormal elevation of the elbow (Trans Norm) showing a high intra-variability for Subject 5.

	MD (cm)		MSE (cm^2)	
Movement	Wrist	Elbow	Wrist	Elbow
All motions	1.1 ± 0.7	1.1 ± 0.7	1.26 ± 5.16	1.09 ± 3.23
Intrans Norm	0.9 ± 0.5	0.9 ± 0.4	0.76 ± 1.32	0.65 ± 1.21
Intrans Elb	1.3 ± 0.4	1.3 ± 0.5	1.22 ± 0.86	1.15 ± 1.04
Trans Norm	0.8 ± 0.4	0.7 ± 0.4	0.48 ± 0.86	0.46 ± 1.05
Trans Elb	1.3 ± 1.1	1.4 ± 1.0	2.58 ± 10.10	2.09 ± 6.08
p-value (sub.)	< 0.02	< 0.002	n.s.	n.s.
p-value (cond.)	n.s.	n.s.	n.s.	n.s.
p-value (var.)	< 0.001	< 0.001	n.s.	< 0.04
p-value (sub*cond)	n.s.	n.s.	n.s.	n.s.
p-value (sub*var)	n.s.	n.s.	n.s.	n.s.
p-value (cond*var)	n.s.	n.s.	n.s.	n.s.

Table 3 Mean Deviation (MD) and Mean Squared Error (MSE) for the duo-EFF-VITE models on the trajectories of the wrist and elbow for each gesture type. We also provide three-way ANOVA results across subjects, movement conditions, variants, and interaction of these factors for each error type.

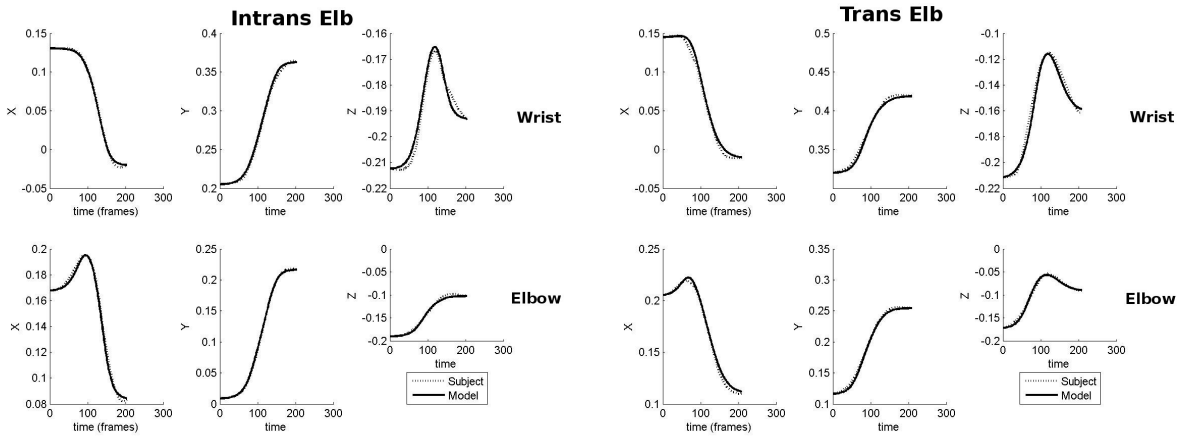

Fig. 9 Examples of movements well reproduced by the duo-EFF-VITE model.The trajectory of the subject's wrist (dotted line) and the modeled trajectory (black) are presented on top.

data were segmented manually, the speed profile was sometimes truncated and hence did not follow the typical pattern. Furthermore, some data present an atypical curvature at the start or end of the movement, due to hesitations on the subjects' parts. Because these imprecisions were minor and did not affect the generic characteristics of each motion (curvature and overall 3D spatial displacement), which we wanted the model to encapsulate, we did not eliminate the data.

3.2.1 Statistics of the model's parameters

A three-way ANOVA across subjects, conditions and variants, on the values taken by the force parameters of the model reveals that, while for the same subject the parameters for the wrist and elbow motions are consistent across conditions and variants, they vary importantly across subjects (see Tables 5 and 6). An effect of the variant (Norm versus Elb) is observed for the parameters

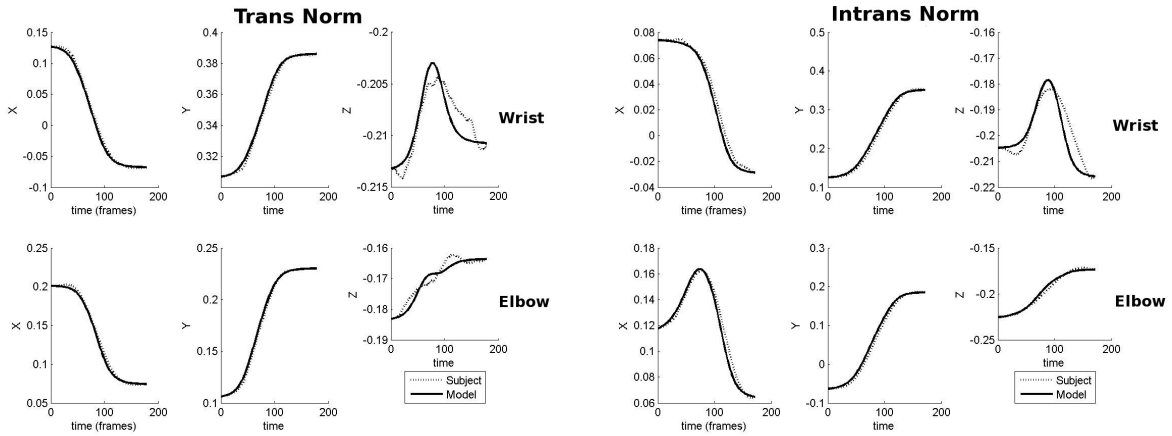

Fig. 10 Examples of movements poorly reproduced by the duo-EFF-VITE model. The trajectory of the subject's wrist (dotted line) and the modeled trajectory (black) are presented on top.

driving the elbow and this accounts for the variability with which subjects produced the required exaggerated elevation of the elbow (variability is expected given that the arm moved in an unconstrained manner).

We also computed the intra-subject variability of the wrist controller for movements with normal kinematics (Tables 8 and 9). We see that some subjects are more consistent in their movements than others, for both the force applied on the wrist and the parameters modulating the speed profile. This is particularly true for Subjects 6 and 8. This confirms the information contained in Figures 7 and 8, and is consistent with the general observation of a high inter-subject and inter-trial variability when performing the same motion, as discussed above and revealed in Table 2.

3.2.2 Meaning of the model's parameters

The parameters β, γ and δ in Equation 1 control the velocity profile of the movement. A two-way ANOVA shows that β and γ are similar across conditions and subjects (Table 4 in Annex) for the wrist controller. β controls the asymmetry and peak value of the velocity profile and γ determines the onset of the movements (Figure 2). As any irrelevant movement prior to the onset of the reaching motion has been manually removed, it is expected that γ takes a similar value across subjects and conditions. β is not significantly different across subjects, conditions and variants. Trajectories of the wrist thus follow the same velocity profile for both conditions (Intrans versus Trans) and variants (Norm versus Elb). δ controls the approaching speed of the movement. Together with β, δ determines a trade-off between overshooting the target and minimizing the execution time. Figure 11 presents the distribution of the values for β and δ for all movements. We see that the values are comprised within a region that minimizes execution time while ensuring a good precision of the movement.

3.2.3 Effect of the forces

We have already seen in Table 2 that the trajectories of both the wrist and elbow are curved. This curvature is accounted for by the values taken by the force parameters of the model (Tables 5 and 7). For each condition and variant of the movement, a non-null force is applied on the wrist and elbow. While one could have performed a straight-line motion in the normal condition, it is obvious that a straight path controller could not be envisioned for movements performed with an exaggerated elevation of the elbow. And, as expected, we observed larger values for the force parameters in the Elb variant of the movement.

The force applied along the x and y axes can also be related to the environmental and geometric constraints implied by the task. In our experiments, subjects sat on a chair with the body close to the table, the forearm resting on the table (Figure 6). To perform the movement, subjects needed to avoid the table ("table avoidance" constraint). To satisfy this constraint, the arm had to be placed above the table. Since the elbow is linked to the trunk by the upper-arm, all the possible positions of the elbow are located on a sphere centered on the shoulder and of radius the length of the upper-arm. Thus when the elbow tries to avoid the table, the elbow is also pulled away from the body along the x- and y-directions. Forces applied on the x- and y-axes are thus explained by the geometry of the body as well as the environmental constraints ("table avoidance").

The force along the z-axis (u_z and v_z) is close to zero in the "Norm" variant.However, in the "Elb" variant, the force along the z-axis at the end of the movement (v_z) (Table 7) is significantly higher (F=254.3, $p < 0.001$), with a mean value close to 1, so as to pull the elbow up during the motion. This effect is illustrated in Figures 13 and 12.

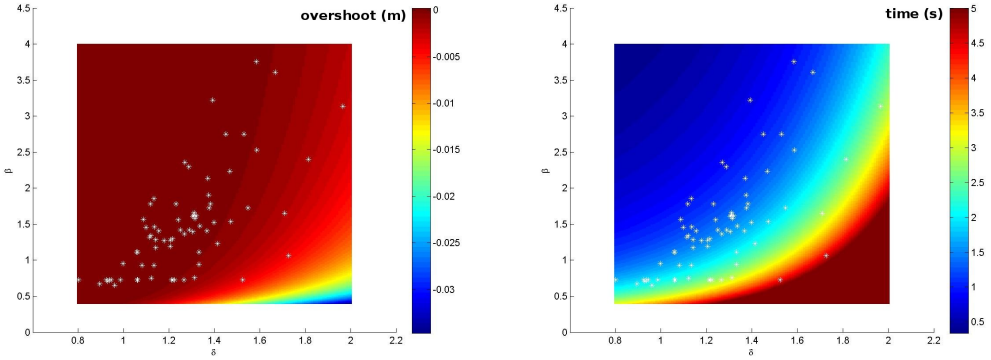

Fig. 11 Distribution of the parameters β and δ of the wrist controller, with respect to the overshoot distance (left) and execution time (right) for a 0.2 m movement. $\alpha = 50$, $\gamma = 0.02$

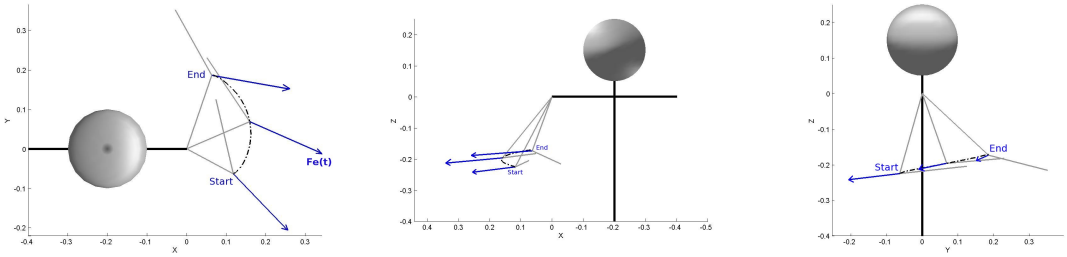

Fig. 12 Example of the force $\mathbf{F}_e$ applied on the elbow for an intransitive movement with normal kinematics. From left to right: projection in the xy-, xz- and yz-planes

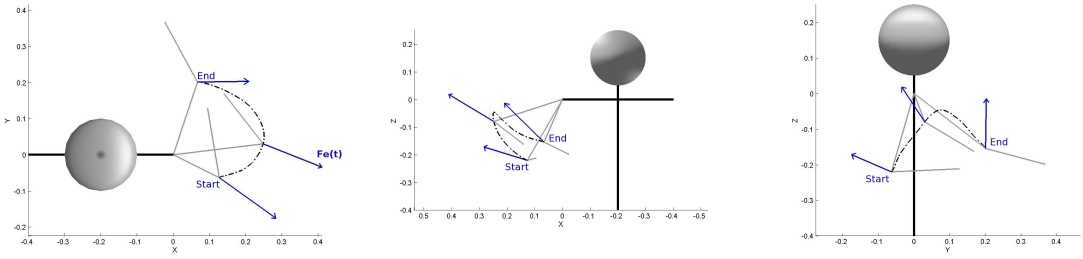

Fig. 13 Example of the force $\mathbf{F}_e$ applied on the elbow for an intransitive movement with an abnormal elevation of the elbow. From left to right: projection in the xy-, xz- and yz-planes

3.2.4 Separate controllers for wrist and elbow

As the elbow and wrist are linked by the forearm, the curvature of the hand path for movements performed with normal or exaggerated elevation of the elbow can be seen as a side effect of the elbow itself. Such correlation is revealed by looking at the Pearson coefficient between the forces [1] $\mathbf{F}_w$ and $\mathbf{F}_e$ (Equation (2)) applied on the wrist and elbow. These coefficients are respectively: $\rho(x) = 0.70$, $\rho(y) = 0.74$, and $\rho(z) = 0.18$, where $\rho(x)$, $\rho(y)$, and $\rho(z)$ are the Pearson coefficients along the x-, y- and z-axis, respectively. These results show that there exists a strong correlation between the force applied on the wrist and elbow along the x- and y-axis. The curvature of the wrist trajectories along the x- and y-axis is thus a side-effect of the elbow motion, and would contribute to confirm a view in which elbow and wrist are controlled by a single controller. In contrast, the wrist and elbow seem to be quasi-independent along the z-axis. This indicates that for the Elb variant of the movements, an exaggerated elevation of the elbow results in an increase in the amplitude of the virtual force $\mathbf{F}_e$ along the z-axis of the elbow controller only, and thus speaks in favor of

[1] The Pearson coefficient is the sum of the products of the normalized values of the two measures divided by the degree of freedom. The Pearson coefficient ranges from +1 to -1. If $\rho = 0$, then there is no linear relationship between the two variables. On the contrary, if $|\rho| = 1$, then there is a perfect linear relationship between the two variables.

having two separate controllers for the wrist and elbow, albeit correlated by geometrical constraints.

4 Discussion

4.1 Accuracy of the model

In this paper, we presented a model of reaching movements, which we validated against kinematic data of known motions in two conditions (intransitive versus transitive motions) and for two variants (movements performed with "naturally" versus movements performed with an exaggerated elevation of the elbow). We proposed an extension of the VITE model to account for both the curvature of naturally reaching movements and for the dual control of the wrist and elbow during unnatural reaching movements. The model gave an accurate account of the kinematics of the data for all the four movement types (Intrans Norm, Intrans Elb, Trans Norm and Trans Elb). Discrepancies between the model's prediction and the data for the velocity profiles at the start and end of the movement were observed in about 10% of the data. Closer analysis revealed that these errors were due to the fact that manual segmentation led to abrupt speed profiles, but also to the fact that in some cases, especially in transitive motions, the speed at the end of the reaching motion was not null (as subjects were transiting directly to a motion in which they grasped and lifted up the object). By construction, the duo-EFF-VITE model, like the VITE model, predicts a zero velocity at target. In effect, when transiting across two motions, subjects tend to displace the target of the reaching motion. One way to simulate this would be to introduce a new target position (corresponding to the final location of the subject's arm one the object had been lifted) slightly before the hand reached the original target point.

As expected, we observed significant inter-subjects and inter-trials variability across motions. To avoid these, we considered computing and modeling the mean trajectories of the wrist and elbow to capture the nature intrinsic to each movement independently from the subject and trial. This was ruled out as the mean movements of the wrist and elbow could no longer be correlated (since the correlations are not linear). Given that one of the hypotheses of the duo-EFF-VITE model is that the position of the wrist and elbow are controlled via two separate controllers acting in parallel but linked through biomechanical constraints, the effect of these biomechanical constraints would have been lost if we had worked with the mean trajectories. Besides, modeling each motion's instance allowed us to demonstrate that the curvature at the wrist level cannot be explained without taking into account the movement of the elbow.

4.2 Interpretation of the Model's Parameters

Parameters of the model are of two types. Three parameters β, γ, and δ are used to modulate the speed profile of the movement. They respectively control the general form of the velocity profile (asymmetry and peak value), enable the initiation of the movement and control the final approaching phase of the movement. Although the model's parameters were optimized to model each instance of the movements, we observed a consistency across the values of the parameters and showed that the parameter controlling the shape of the speed profile at the end of the movement takes values that optimize a trade-off between the precision and execution time of the whole movement. This is in agreement with the observation of a correlation across speed and accuracy of goal-directed movements (Plamondon and Alimi 1997; Meyer et al 1988). (Meyer et al 1988) hypothesized that this trade-off permits to cope optimally with noise in the human system.

Most importantly, the model hypothesized the existence of virtual forces that encapsulate tasks constraints to modulate a basic controller for reaching movements. We showed that these forces could explain the curvature of the movements of the wrist and elbow and could be interpreted in relation to environmental and biomechanical constraints. Further experiments should be conducted to validate this hypothesis by varying the task constraints, e.g. asking subjects to perform reaching motions by exaggeratedly lowering the elbow, and showing how the forces change as an effect of the context.

4.3 Separate Control of Wrist and Elbow

A second hypothesis inherent to the model is that elbow and wrist are driven by separate controllers, albeit correlated through imagined biomechanical constraints. Such a hypothesis corresponds to assuming that the nervous system is able to plan the mechanical effects that could arise from the motion of the arm segments (Galloway and Koshland 2001). An analysis of the relationship across the forces applied on the wrist and elbow at each time step revealed a strong correlation along the x- and y-axes. The forces along the z-axis were however quasi-independent of the elbow's elevation. The absence of correlation along the z-direction suggests that the motions of the wrist and elbow are computed separately by the brain. These conclusions are consistent with findings on multi-joint arm movements and with the Leading Joint Hypothesis (LJH) (Dounskaia et al 1998; Dounskaia 2005). The LJH states that there is one leading joint that guides the motion of the entire limb. Muscles of the secondary joints thus just play a regulatory role to ensure that the end-effector performs the required task. Interestingly, the LJH is applicable to our results if we consider the elbow as the leading joint and the wrist as the secondary joint.

4.4 Neural Correlated to the Model's Parameters

Similarly to the VITE model, the duo-EFF-VITE model depends on knowing at all time the wrist and elbow positions and velocities. Evidence that the velocity and position of the wrist may be explicitly computed and used for motor control by the nervous system exists. For instance, cells in the primary motor cortex (M1) of the monkey showed a high correlation between their discharge and the velocity profile of reaching movements (Moran and Schwartz 1999). Moreover (Wang et al 2006) confirmed the existence of a neural representation of the hand location in the motor cortex during reaching. They showed that position and velocity of the hand are simultaneously encoded by cortical motor neurons. Existence that the position and velocity of the elbow are explicitly computed is still questioned (Murphy et al 1982; Scott et al 1997; Reina et al 2001). While the duo-EFF-VITE model proposes a solution to encapsulate environmental and biomechanical constraints, it does not explain how the brain computes such constraints. As they contribute in several ways to the virtual forces, several brain areas may be involved.

Finally, the duo-EFF-VITE model is based on the idea that motions are not planned but unfold through time as the result of the inherent dynamics of the controllers. Such an approach is in line with the force-field approach (Graziano et al 2005), where the target of the motion acts as an attractor for the end-effector. Moreover, the model assumes that control is done in close-loop, taking into account the current position of the arm to correct the motion. This is supported by evidence that the nervous system is able to estimate and anticipate the state of the limb by integrating delayed sensory input and motor output, through afferent and efferent internal feedback loops (Desmurget et al 1997).

While the model exploits a representation of biomechanical constraints in the coupling of the elbow and wrist controllers, it does not account for the way the command are translated into muscle activation of the upper and lower arm limbs. While a complete understanding of the neural control of movements would require a realistic musculoskeletal model[2], we omitted such complexity in order to focus on explaining the gross dynamics of motor control. In particular, we aimed at explaining how volitional control of one specific limb (upper arm) could be done separately from that of the lower arm, as in the exaggerated elbow elevation condition considered here.

Movements presented in this paper were unconstrained. While this resulted in a high variability across trials and subjects' motions, it offered the opportunity to observe features of motion that are inherent to natural reaching motions. The duo-EFF-VITE model is however generic and could also model constrained movements. To confirm the LJH hypothesis and the use of the duo-EFF-VITE model in support of the latter, it would thus be interesting to replicate the present study with movements of the wrist constrained in the plane. The wrist would then become the leading joint and the elbow the follower. Results of such a comparative study would contribute to explaining the difference in the curvature of the hand path found for constrained and unconstrained movements (Desmurget et al 1997).

[2] Such model is very complex and difficult to obtain due to the numerous muscles and tendons present in the human arm (Cheng and Loeb 2008).

Acknowledgements This work was supported by the Sport and Rehabilitation Engineering Program at EPFL, CE Grants Robotcub, CONTACT and Poeticon, and Italian Ministry of University PRIN.

References

Atkeson C, Hollerbach J (1985) Kinematic features of unrestrained vertical arm movements. Journal of Neuroscience

Bernstein N (1967) The coordination and regulation of movements. Pergamon

Boessenkool J, Nijhof EJ, Erkelens C (1998) A comparison of curvatures of left and right hand movements in a simple pointing task. Experimental Brain Research

Bullock D, Grossberg S (1988) Neural dynamics of planned arm movements: emergent invariants and speed-accuracy properties during trajectory formation. Psychological Review

Bullock D, Grossberg S, Mannes C (1993) A neural network model for cursive script production. Biological Cybernetics

Cheng E, Loeb G (2008) On the use of musculoskeletal models to interpret motor control strategies from performance data. Journal of Neural Engineering

Desmurget M, Jordan M, Prablanc C, Jeannerod M (1997) Constrained and unconstrained movements involve different control strategies. The American Physiological Society

Dounskaia N (2005) The internal model and the leading joint hypothesis: implications for control of multi-joint movements. Experimental Brain Research

Dounskaia N, Swinnen S, Walter C, Spaepen A, Verschueren S (1998) Hierarchical control of different elbow-wrist coordination patterns. Experimental Brain Research

Flash T, Hogan N (1985) The coordination of arm movements: An experimentally confirmed mathematical model. The Journal of Neuroscience

Galloway J, Koshland G (2001) General coordination of shoulder, elbow and wrist dynamics during multijoint arm movements. Experimental Brain Research

Gibet S, kamp JF, Poirier F (2004) Gesture analysis: Invariant laws in movement. In: Gesture-based Communication in Human-Computer Interaction

Graziano M, Aflalo T, Cooke D (2005) Arm movements evoked by electrical stimulation in the motor cortex of monkey. Journal of Neurophysiology

Gu X, Ballard D (2006) An equilibrium point based model unifying movement control in humanoids. In: Robotics: Science and Systems

Harris C, Wolpert D (1998) Signal-dependent noise determines motor planning. Nature

Hoos H, Stützle T (2004) Stochastic local search: Foundations and applications. Morgan Kaufmann

Kang T, Tillery S, He J (2003) Determining natural arm configuration along reaching trajectory. In: Proc. of the Inter-

	β	γ	δ
Intrans Norm	2.04 ± 1.94	0.010 ± 0.005	1.31 ± 0.22
Intrans Elb	1.76 ± 1.53	0.006 ± 0.005	1.30 ± 0.37
Trans Norm	2.33 ± 1.75	0.011 ± 0.007	1.43 ± 0.30
Trans Elb	1.61 ± 1.36	0.007 ± 0.004	1.21 ± 0.39
p-value (sub.)	n.s.	n.s.	< 0.001
p-value (cond.)	n.s.	n.s.	n.s.
p-value (var.)	n.s.	< 0.001	< 0.009
p-value (sub*cond)	n.s.	< 0.001	n.s.
p-value (sub*var)	n.s.	n.s.	< 0.008
p-value (cond*var)	n.s.	n.s.	< 0.03

Table 4 Mean and standard deviation for the parameters modulating the speed profile for the movements of the wrist. Three-way ANOVA results for each movement type across subjects, condition and variant have been provided for each of these parameters, as well as interaction effects of the factors.

	u_x	u_y	u_z	v_x	v_y	v_z
Intrans Norm	0.36 ± 0.23	-0.36 ± 0.24	0.18 ± 0.19	0.87 ± 0.71	-0.92 ± 0.65	0.96 ± 0.47
Intrans Elb	0.68 ± 0.30	-0.54 ± 0.34	0.35 ± 0.59	0.32 ± 0.96	-0.24 ± 0.87	1.78 ± 0.60
Trans Norm	0.41 ± 0.26	-0.39 ± 0.26	0.10 ± 0.18	1.28 ± 0.56	-0.88 ± 0.72	0.77 ± 0.51
Trans Elb	0.73 ± 0.60	-0.73 ± 0.45	0.02 ± 0.50	0.71 ± 0.78	-0.14 ± 1.13	1.76 ± 1.00
p-value (sub.)	< 0.001	< 0.001	< 0.001	< 0.001	< 0.001	< 0.001
p-value (cond.)	n.s.	< 0.001	< 0.001	< 0.001	n.s.	n.s.
p-value (var.)	< 0.001	< 0.001	n.s.	< 0.001	< 0.001	< 0.001
p-value (sub*cond)	< 0.001	< 0.005	< 0.03	n.s.	n.s.	< 0.001
p-value (sub*var)	< 0.001	< 0.001	< 0.001	< 0.001	< 0.001	< 0.001
p-value (cond*var)	n.s.	< 0.02	< 0.001	n.s.	n.s.	n.s.

Table 5 Mean and standard deviation for each parameter u and v of the model describing the force at the start and end of the movements of the wrist. Three-way ANOVA results for each movement type across subjects, condition and variant have been provided for each of these parameters, as well as interaction effects of the factors.

	β	γ	δ
Intrans Norm	1.73 ± 0.66	0.011 ± 0.005	1.34 ± 0.14
Intrans Elb	1.55 ± 0.85	0.009 ± 0.004	1.22 ± 0.34
Trans Norm	1.64 ± 0.60	0.011 ± 0.005	1.33 ± 0.18
Trans Elb	1.40 ± 0.79	0.010 ± 0.005	1.27 ± 0.28
p-value (sub.)	< 0.001	< 0.001	< 0.001
p-value (cond.)	n.s.	n.s.	n.s.
p-value (var.)	< 0.03	n.s.	< 0.004
p-value (sub*cond)	n.s.	n.s.	n.s.
p-value (sub*var)	n.s.	< 0.002	< 0.001
p-value (cond*var)	n.s.	n.s.	n.s.

Table 6 Mean and standard deviation for the parameters modulating the speed profile for the movements of the elbow. Three-way ANOVA results for each movement type across subjects, condition and variant have been provided for each of these parameters, as well as interaction effects of the factors.

	u_x	u_y	u_z	v_x	v_y	v_z
Intrans Norm	0.61 ± 0.17	-0.34 ± 0.22	-0.08 ± 0.14	1.50 ± 0.033	-0.59 ± 0.39	-0.09 ± 0.58
Intrans Elb	0.85 ± 0.36	-0.63 ± 0.22	-0.06 ± 0.38	1.48 ± 0.43	-0.25 ± 0.64	1.09 ± 0.93
Trans Norm	0.50 ± 0.11	-0.38 ± 0.23	-0.03 ± 0.17	1.57 ± 0.38	-0.82 ± 0.55	-0.16 ± 0.35
Trans Elb	0.73 ± 0.36	-0.67 ± 0.27	-0.21 ± 0.29	1.44 ± 0.44	-0.56 ± 0.70	1.21 ± 1.05
p-value (sub.)	< 0.001	< 0.001	< 0.001	< 0.001	< 0.001	< 0.001
p-value (cond.)	< 0.001	n.s.	< 0.03	n.s.	< 0.001	n.s.
p-value (var.)	< 0.001	< 0.001	< 0.001	n.s.	< 0.001	< 0.001
p-value (sub*cond)	n.s.	n.s.	n.s.	n.s.	n.s.	n.s.
p-value (sub*var)	< 0.001	< 0.001	< 0.001	< 0.002	< 0.0001	< 0.001
p-value (cond*var)	n.s.	n.s.	< 0.001	n.s.	n.s.	n.s.

Table 7 Mean and standard deviation for each parameter u and v of the model describing the force at the start and end of the movements of the elbow. Three-way ANOVA results for each movement type across subjects, condition and variant have been provided for each of these parameters, as well as interaction effects of the factors.

		u_x	u_y	u_z	v_x	v_y	v_z
Sub. 1	Intrans Norm	-0.07 ± 0.20	0.03 ± 0.13	0.14 ± 0.39	-0.14 ± 0.41	0.11 ± 0.30	0.17 ± 0.45
	Trans Norm	-0.05 ± 0.15	0.02 ± 0.05	0.14 ± 0.39	-0.13 ± 0.40	0.15 ± 0.42	0.16 ± 0.44
Sub. 2	Intrans Norm	-0.05 ± 0.13	0.04 ± 0.13	0.10 ± 0.31	-0.14 ± 0.38	0.15 ± 0.43	0.17 ± 0.44
	Trans Norm	-0.06 ± 0.19	0.04 ± 0.13	0.17 ± 0.46	-0.15 ± 0.44	0.09 ± 0.25	0.16 ± 0.44
Sub. 3	Intrans Norm	-0.07 ± 0.20	0.04 ± 0.11	-0.03 ± 0.11	-0.14 ± 0.45	0.13 ± 0.35	0.17 ± 0.44
	Trans Norm	-0.09 ± 0.25	0.01 ± 0.03	0.05 ± 0.17	-0.11 ± 0.38	0.13 ± 0.35	0.21 ± 0.59
Sub. 4	Intrans Norm	-0.07 ± 0.20	0.03 ± 0.10	0.04 ± 0.17	-0.15 ± 0.42	0.20 ± 0.55	0.16 ± 0.44
	Trans Norm	-0.07 ± 0.20	0.03 ± 0.12	0.10 ± 0.30	-0.13 ± 0.40	0.18 ± 0.50	0.16 ± 0.45
Sub. 5	Intrans Norm	-0.05 ± 0.13	0.01 ± 0.04	0.21 ± 0.55	-0.13 ± 0.35	0.12 ± 0.33	0.17 ± 0.44
	Trans Norm	-0.05 ± 0.14	-0.01 ± 0.04	0.23 ± 0.61	-0.14 ± 0.39	0.04 ± 0.17	0.20 ± 0.54
Sub. 6	Intrans Norm	-0.03 ± 0.09	0.00 ± 0.01	0.14 ± 0.43	-0.12 ± 0.35	0.04 ± 0.13	0.14 ± 0.41
	Trans Norm	-0.02 ± 0.05	0.01 ± 0.03	0.23 ± 0.62	-0.10 ± 0.28	0.05 ± 0.16	0.17 ± 0.45
Sub. 7	Intrans Norm	-0.01 ± 0.08	0.01 ± 0.05	0.12 ± 0.45	0.03 ± 0.26	0.16 ± 0.44	0.20 ± 0.55
	Trans Norm	-0.03 ± 0.11	0.00 ± 0.01	0.18 ± 0.52	0.07 ± 0.21	0.06 ± 0.23	0.20 ± 0.55
Sub. 8	Intrans Norm	-0.01 ± 0.04	0.01 ± 0.04	0.15 ± 0.41	-0.15 ± 0.41	0.04 ± 0.12	0.14 ± 0.38
	Trans Norm	-0.03 ± 0.09	0.01 ± 0.03	0.18 ± 0.49	-0.18 ± 0.48	0.08 ± 0.24	0.16 ± 0.43

Table 8 Mean and standard deviation for each parameter of the model describing the force for Intrans Norm and Trans Norm movements of the wrist for each subject respectively.

		β	γ	δ
Sub. 1	Intrans Norm	0.43 ± 1.60	0.001 ± 0.002	0.04 ± 0.12
	Trans Norm	0.21 ± 0.57	0.002 ± 0.005	0.04 ± 0.12
Sub. 2	Intrans Norm	0.22 ± 0.58	0.002 ± 0.005	0.06 ± 0.17
	Trans Norm	0.36 ± 1.24	0.001 ± 0.003	0.05 ± 0.15
Sub. 3	Intrans Norm	0.25 ± 0.68	0.001 ± 0.004	0.03 ± 0.08
	Trans Norm	0.42 ± 1.46	0.002 ± 0.006	0.03 ± 0.08
Sub. 4	Intrans Norm	0.36 ± 1.57	0.001 ± 0.003	0.03 ± 0.09
	Trans Norm	0.29 ± 1.13	0.001 ± 0.004	0.02 ± 0.08
Sub. 5	Intrans Norm	0.22 ± 0.59	0.001 ± 0.003	0.04 ± 0.12
	Trans Norm	0.32 ± 1.01	0.001 ± 0.002	0.07 ± 0.20
Sub. 6	Intrans Norm	0.15 ± 0.46	0.001 ± 0.004	0.03 ± 0.08
	Trans Norm	0.23 ± 0.64	0.001 ± 0.002	0.04 ± 0.11
Sub. 7	Intrans Norm	0.24 ± 0.94	0.001 ± 0.004	0.10 ± 0.29
	Trans Norm	0.29 ± 0.94	0.002 ± 0.006	0.12 ± 0.31
Sub. 8	Intrans Norm	0.17 ± 0.45	0.001 ± 0.003	0.03 ± 0.09
	Trans Norm	0.21 ± 0.57	0.001 ± 0.003	0.04 ± 0.11

Table 9 Mean and standard deviation for each parameter of the model describing the force for Intrans Norm and Trans Norm movements of the wrist and for each subject respectively.

national Conference of the IEEE Engineering in Medicine and Biology Society

Koshland G, Galloway J, Nevoret-Bell C (2000) Control of the wrist in three-joint arm movements to multiple directions in the horizontal plane. Journal of Neurophysiology

Magescas F, Prablanc C (2006) A joint-centered model accounts for movement curvature and spatial variability. Neuroscience Letters

Meyer D, Abrams R, Kornblum S, Wright C, Smith J (1988) Optimality in human motor performance: Ideal control of rapid aimed movements. Psychological Review

Moran D, Schwartz A (1999) Motor cortical representation of speed and direction during reaching. Journal of Neurophysiology

Morasso P (1981) Spatial control of arm movements. Experimental Brain Research

Murphy J, Kwan H, MacKay W, Wong Y (1982) Precentral unit activity correlated with angular components of a compound arm movement. Brain Research

Neter J, Kutner M, Nachtsheim C, Wasserman W (1996) Applied linear statistical models. Irwin

Ogihara N, Yamazaki N (1999) Generation of human reaching movement using a recurrent neural network model. In: Proc. of the International Conference on Systems, Man, and Cybernetics

Oldfield R (1971) The assessment and analysis of handedness: the edinburgh inventory. Neuropsychologia

Plamondon R, Alimi A (1997) Speed/accuracy trade-offs in target-directed movements. Behavioral and Brain Sciences

Reina G, Moran D, Schwartz A (2001) On the relationship between joint angular velocity and motor cortical discharge during reaching. Journal of Neurophysiology

Rosenbaum D, Loukopoulos L, Meulenboek R, Vaughan J, Engelbrecht S (1995) Planning reaches by evaluating stored postures. Psychological Review

Scott S, Sergio L, Kalaskan J (1997) Reaching movements with similar hand paths but different arm orientations. ii. activity of individual cells in dorsal premotor cortex and parietal area 5. Journal of Neurophysiology

Torres E, Zipser D (2002) Reaching to grasp with a multijointed arm. i. computational model. The American Physiological Society

Uno Y, Kawato M, Suzuki R (1989) Formation and control of optimal trajectory in human multijoint arm movement. Biological Cybernetics

Wang W, Chan S, Heldman D, Moran D (2006) Motor cortical representation of position and velocity during reaching. Journal of Neurophysiology

Visual Feedback from the Own Acting Hand Modulates the Activity of Grasping Neurons in Monkey Premotor Area F5

Caselli L[1], Oliynyk A[1], Gesierich B[1,2], Craighero L[1], Fadiga L[1,3]

(1) University of Ferrara, Dept. Biomedical Sciences, Ferrara (IT)
(2) University of Trento, Center for Mind/Brain Sciences, Rovereto (IT);
(3) The Italian Institute of Technology, Genova (IT)

ABSTRACT

Visual responses in the monkey ventral premotor cortex have been explored since long time. Area F5 has been shown to contain grasping neurons that visually discharge either to 3D-object presentation (canonical neurons) or to the observation of actions performed by other individuals (mirror neurons). It has been suggested that the mirror response results from the progressive generalization to others' actions of a visuomotor link which, during action execution , associates the vision of the own acting effector with the motor program selected for the ongoing action. To start tackling this hypothesis, we specifically asked whether area F5 contains neurons responding to the observation of one's own grasping movement. A specially-designed experimental apparatus was used to test F5 neuronal discharge while monkeys were engaged in a reach-to-grasp task and either continuous or transient visual information on the ongoing movement was made available. Single-unit activity was additionally recorded from the hand region of the primary motor cortex (area F1). Neuronal responses evoked by the vision of the own entire grasping action or of brief meaningful phases of it were detected in both areas. However, F5 modulation was overall more strong and specific. The finding that neurons in area F5 exhibit discharge properties that are common to both purely motor and mirror neurons allows the formulation of important assumptions about the critical role of online visual information during grasping and the nature of the mirror discharge.

INTRODUCTION

Visual responses in the premotor cortex have been extensively studied in the last two decades. Thereby, ventral premotor area F5, residing in the posterior bank and convexity of the inferior arcuate sulcus (iAS), has turned out to be particularly important for the visuomotor transformations it carries out in the domain of visually-guided grasping movements (Rizzolatti et al. 1988; Murata et al. 1997; Raos et al. 2006). Grasping is one of the most evolved types of primate behavior, resulting from a complex visuomotor process that transforms the object's three-dimensional structure into specific motor commands to select the optimal finger configuration for grasping. During pre-shaping, fingers progressively open and straighten up to reach a point of maximum grip aperture, which is followed by closure of the grip with gradual finger flexion as the hand approaches the object (Jeannerod et al. 1995).

Intracortical microstimulation and single-unit recordings in the macaque monkey have demonstrated that grasping relies on a fronto-parietal visuomotor circuit including, besides area F5, the inferior intraparietal area AIP (Murata et al. 1996; Murata et al. 2000), the ventro-rostral part of area F2 in the dorsal premotor cortex (Raos et al. 2004) and the primary motor cortex F1 (Dum and Strick 2005; Umilta et al. 2007). Successful execution of grasping much depends on the integrity of area F1, which directly controls finger muscles and is known to be crucial for skilled hand function. Lesions or inactivation of this area produce a severe deficit of individual finger movements and, consequently, of normal grasping (Liu and Rouiller 1999; Fogassi et al. 2001). F5, which represents, through cortico-cortical connections, one of the major inputs to the hand field of area F1 (Matelli et al. 1986), is the motor region most critically involved in pre-configuring the hand according to the visual properties of the object. After inactivation of area F5, hand shaping is markedly impaired, with fingers position not properly matching the size and shape of the object, thus causing grasping failure (Fogassi et al. 2001).

In addition to purely motor grasping neurons, specifying types of hand shaping (e.g., precision or whole-hand grip), or timing the action discharging during different grasping phases, two main categories of F5 visuomotor neurons have been described so far. On the basis of their visual properties they have been named *canonical* and *mirror* visuomotor neurons.

Canonical neurons, mainly located on the posterior bank of the iAS (F5ab sector), display a 3D object-related visual selectivity that is almost congruent with the grip-specificity of their motor discharge. Area F5ab represents the main target of projections originating from area AIP, which, in turn, has been shown to contain three main classes of neurons (Taira et al. 1990; Murata et al. 2000;

Sakata et al. 1995), all of them contributing to the visuomotor transformation from object description to hand shaping selection. AIP *visual-dominant* neurons respond during object presentation and grasping only when full visual information on the movement is available (they do not discharge when grasping is performed in dark); *motor-dominant* neurons are active during grasping, independently of whether the movement is visible or not, and do not fire during object observation; *visual-motor* neurons are similar to the visual-dominant ones but they also respond during grasping in dark, though the discharge is much weaker than that displayed in full light. This latter neuronal class resembles that represented by F5 canonical neurons, suggesting that the motor activity observed in AIP may reflect a corollary discharge initiating in F5ab and maintained through a F5-AIP reverberating circuit, active during the whole grasping period (Taira et al. 1990).

It is worth mentioning that in the study by Murata et al. (2000) a particular class of AIP visuomotor neurons, devoid of any object-related visual selectivity but exhibiting a grasping motor response that was stronger in light than in dark, was additionally described. These *nonobject-type* neurons, whose discharge properties can be considered as intermediate between the motor-dominant and the visual-motor classes, have been thought to respond to handgrip selectivity or, more importantly for the purposes of the present work, to a combined view of handgrip and object. Indeed, although contradictory arm/hand kinematics results have been reported about the effects of removing online vision on the control of reach-to-grasp movements (Winges et al. 2003; Rand et al. 2007), visual feedback signals are of unquestionable importance in goal-directed hand movements, especially for the formation of finger grip during prehension (Jeannerod et al. 1995; Jeannerod 1986). An alternative account for the functional properties of these *nonobject-type* AIP neurons is that they might reflect mirror-neuron-like characteristics (see below).

Mirror neurons, mainly sited on the F5 cortical convexity (F5c), are visually triggered by the observation of a biological agent performing a given goal-directed action (e.g. grasping), typically *mirroring* the motor response normally recorded from the same neurons during the actual execution of a similar action (di Pellegrino et al. 1992; Rizzolatti et al. 1996; Gallese et al. 1996). The matching between the observed and the executed action encoded by a single mirror neuron response has been shown to encompass different levels of congruence, ranging from a very strict to a broader visuomotor correspondence. For example, neurons whose motor discharge is selective for a precision grip can either only respond to the observation of actions involving the same precision grip or can be visually triggered by any type of hand grasping. Broadly congruent mirror neurons are of particular interest since they generalize the goal of the observed action over many instances of it. A recent fMRI study performed on monkeys (Nelissen et al. 2005) demonstrated that the

ventral premotor cortex hosts at least two main distinct representations of others' actions. Besides area F5c, which was found to be active only when the observed acting person was in full view, hence displaying a highly specific context-related action representation, the anterior sector of area F5 (area F5a), located in the depth of the iAS, appeared to encode actions in a more abstract way: visual stimuli such as mimicked actions, the view of the only grasping hand or actions performed by a robotic arm were all as effective as an acting human being in triggering F5a activation.

The existence of mirror neurons in area F5 that generalize the goal of a specific observed action to many other examples of it, thus suggesting the association of different visual information to a common goal-related motor-invariant signal, and the fact that these cells are part of a neuronal circuit, additionally including the PF/PFG complex in the inferior parietal lobule (Petrides and Pandya 1984; Matelli et al. 1986; Fogassi et al. 2005; Fogassi and Luppino 2005) and the superior temporal sulcus (STS) (Perrett et al. 1989), which describes actions also in purely visual terms, have led to the formulation of a sensory feedback-based theory accounting for the generation of mirror neurons (Rizzolatti and Fadiga 1998). According to this theory, the mirror discharge develops from the observation of one's own acting effector, seen from slightly different perspectives, performing repetitively the same action. Through the visual feedback system normally guiding action execution, motor invariance is extracted from the different visual perspectives, thus initially creating a matching between the action and the vision, by the agent performing the action, of his/her own ongoing movement. Once this visuomotor link is established, it will then be progressively generalized to the observation of actions executed by other individuals. Very recent results, achieved by applying this model to an acting artificial system, showed that this could be the case (Metta et al. 2006; Craighero et al. 2007).

At present, there is no evidence in favour of the existence, in area F5, of neurons showing visuomotor responses that couple the execution with the observation of one's own actions. The presence of such neurons is a necessary prerequisite to demonstrate the validity of the sensory feedback-based theory mentioned above.

The aim of the present study was to start clarifying this issue. As a first step along this direction, we specifically investigated the presence, in area F5, of neurons similar to the non-object visually-responsive neurons previously described in area AIP (Murata et al. 2000), whose grasping-related activity is significantly strengthened when the monkey observes its own hand action (i.e., under full light conditions), with respect to a condition during which it cannot (i.e., in darkness). These discharge properties, which could be considered as transitional to those of purely motor and mirror neurons, would represent a conceivable neuronal indicator of the visuomotor matching

proposed by the aforementioned theory. However, such a modulation could also be the neuronal counterpart of the efficacy of the online visual information in properly guiding the hand during object grasping. Therefore, to better identify neurons showing activity specifically evoked by the observation of the own grasping action, we explored the influence on the F5 single-neuron responses of very brief motor-relevant visual feedbacks (i.e., light flashes delivered at precise instants during critical grasping phases) that do not modify arm/hand kinematics, though providing the system with strategically useful visual information. As a control, the activity of neurons in the hand representation of area F1 was recorded as well.

METHODS

Surgery

Single-unit activity was recorded from both ventral premotor area F5 and primary motor cortex F1 in three hemispheres (contralateral to the moving forelimb) of two awake behaving monkeys (*Macaca fascicularis*). The monkeys (one female and one male, respectively weighing 5.7 kg 4.9 kg and referred as to MK1 and MK2) were specifically trained to perform a behavioral task (see following text), while seating on a primate chair. After training, a recording chamber and head-restraint device were surgically implanted. All experimental protocols were approved by the Veterinarian Animal Care and Use Committee of the University of Ferrara, by the Italian Ministry of Health and complied with the European laws on the use of laboratory animals.

Structural CT and MRI images were respectively used in MK1 and MK2 to stereotactically place the recording chamber over the cortical region including the posterior bank of the inferior arcuate sulcus and central sulcus, where areas F5 and F1 are located. In MK1, the cortical surface was indirectly rendered after Computer Assisted Tomography (CAT) acquisition, through reversal of inner skull surface, and 3D-recontructed by using ETDIPS (NIH, NUS, http://www.cc.nih.gov/cip/software/etdips/) and Rhinoceros® 2.0 (Robert McNeel & Associates, USA) softwares. The coordinate system of the obtained 3D-images of the brain was then adjusted to the standard stereotaxic coordinates system based on the orbitomeatal plane and with a custom-designed software (Virtax, http://web.unife.it/progetti/neurolab/, Gesierich et al., in preparation) we determined the position of the target cortices by using as references both the sulcal pattern impressed on the internal surface of the skull and the stereotaxic atlas by Szabo and Cowan (Szabo and Cowan 1984). The inferior surface of the titanium recording chamber cylinders (height 20 mm, inner ∅ 24 mm, out ∅ 30 mm) was virtually modeled through Rhinoceros® 2.0 software, so to perfectly fit the skull curvature of the monkeys, maximizing adhesion between the implant and the bone. The chamber models were then manufactured by a MAXNC 15 computer-driven 3D milling machine (MAXNC inc., Arizona, U.S.A.) by using the MillWizard software (Delcam Artcam, U.K.).

All surgical implantations were carried out under aseptic procedures and general anesthesia. Monkeys were pre-medicated with atropine sulfate (0.1 mg/Kg, IM, MONICO S.p.A., Italy) and tiletamine-zolazepam (20 mg/Kg, IM, Zoletil, VIRBAC, S.A., France), and anesthetized by isoflurane (Abbott S.p.A., Illinois, U.S.A.) for the whole duration of surgery. Antibiotics and analgesics were administered postoperatively and experiments were started at least two weeks after the surgery.

Electrophysiology

Single-unit recordings were performed by using varnish-insulated tungsten microelectrodes with impedance 0.15–1.5MΩ (measured at 1 kHz). Electrodes were obtained repetitively passing the tip of tungsten rods (∅ 250 μm, A-M Systems, inc. WA, U.S.A.) through a KOH (10% in distilled water) etching solution by means of a metal electrode etcher (BAK Electronics, inc., MD, U.S.A.), and covering them with multiple layers of varnish (SIVAMID 595/38M, ELANTAS Electrical Insulation, Germany) that were oven-dried at high temperature (400°C). This procedure has the advantage of providing microelectrodes with the desired tip and highly resistant insulation.

During each experimental session, the microelectrode was inserted perpendicular to the cortical surface (i.e., with an angle of 32-40° with respect to sagittal plane) and was slowly advanced through the cortex by means of a hydraulic microdrive (Kopf Instruments, CA, U.S.A.; step resolution, 10 μm).The recorded signal was amplified ×10000 (BAK Electronics, Germantown MD, USA), filtered by a dual variable filter (VBF-8, KEMO Ltd., Backenham, UK) (300-5000 Hz bandwidth), digitized (PCI-6071E, National Instruments, USA) at a sampling rate of 10 kHz and stored for further off-line analysis. Action potentials were on-line discriminated by a dual voltage-time window discriminator (BAK Electronics, Germantown MD, USA) and fed to an Audio monitor (Grass Instruments, USA) to give the experimenter an auditory feedback on the neuron discharge during testing. Data analysis was performed after off-line discrimination of single-units from multi-spike recordings carried out by means of a custom-made LabView-based software (Olyinik et al., in preparation).

The recording microelectrodes were also used for intracortical microstimulation (ICMS, train duration, 50-100 ms; pulse duration, 0.2 ms; frequency, 330 Hz; current intensity, 3–40 μA). The current strength was controlled on an oscilloscope by measuring the voltage drop across a 10kΩ resistor in series with the stimulating electrode.

Recording sites

The chamber rostro-caudal and medio-lateral axis dimension was such as to allow to record from a brain region spanning area F1, the whole ventral premotor cortex and the caudal part of the Frontal Eye Fields (FEF). The ventral part of the agranular frontal cortex was functionally explored through single unit recordings and ICMS to assess the location of areas F1, F4 and F5. Criteria and functional characteristics described by Umiltà et al. (2001) were used to distinguish motor and premotor areas as well as regions within area F5 characterized by a high density of neurons exhibiting hand-related activity during goal-directed actions.

Naturalistic testing

Naturalistic testing was used to select neurons to be then thoroughly examined through the experimental paradigm. Single-neuron activity was studied with reference to the execution of different hand/arm movements, selected to elicit different grip types or to the application of different sensory stimuli, according to procedures described in other previous studies (Rizzolatti et al. 1990; Rizzolatti et al. 1988; Gallese et al. 1996). For example, the presentation of a small piece of food placed inside a slot required the monkey to perform a precision grip, by opposing the first phalanx of the thumb to the first phalanx of the index finger, while a syringe filled with juice evoked a power grip, with the fingers wrapped around the object and the palm in contact with it. Visual canonical properties were tested by presenting the monkey with 3D objects of different size, shape and orientation. Visual mirror properties were tested by performing a series of hand actions (grasping holding, manipulating) in front of the monkey. This functional characterization, together with the ICMS data, allowed us to select hand-related neurons predominantly selective for precision grasping. Particular attention was paid so to discard cells showing canonical or mirror visual properties and include just those showing motor discharge only.

Behavioral apparatus and paradigm

The pre-selected grasping neurons were studied by means of a behavioral apparatus specifically designed to make the animals perform a reach-to-grasp task, which naturally implied the execution of a precision grip to open the door of a container and get a piece of food which was hidden inside (Fig. 1A). The container was mounted on a vertical rack at reaching distance (approximately 30 cm) in front of the primate chair, so that, in case, the monkeys were forced to watch their own grasping trajectory. The precision grip had to be performed on a small plastic cube (0.8 x 0.8 x 0.8 mm) embedded in a groove, serving as the door handle (Fig. 1B). To ensure that the movement was accurately executed even under dark conditions, the cube was translucent and dimly back-illuminated by a red LED. The LED intensity was kept very low and did not allow the vision of the approaching hand. Each trial started with the monkey's right (or left) hand positioned close to the body, on the hip board of the primate chair. An external sliding door, overlying the target door for the animal, was opened at distance by the experimenter, giving the monkey a go-signal to start the reach-to-grasp movement (Fig. 1C). As the monkey touched the handle correctly, with both the thumb and index fingers, a TTL signal was sent via an electronic circuit to the acquisition PC to synchronize the neuronal data. Data included one second before and two seconds after handle grasping were stored for each trial.

The task was performed under four different conditions:

1) *Light* (*L*) condition: grasping was executed with continuous vision of the own hand movement (i.e., in full light).

2) *Dark* (*D*) condition: grasping was executed in absence of any visual information on the own movement (i.e., in darkness).

3) *Pre-touch (PT) flash* condition: grasping was executed in dark with instantaneous visual feedback before touching, during the handgrip shaping phase. The scene was briefly illuminated by a 20 μs xenon light flash triggered by the signal of the hand crossing an infrared barrier built by a pyroelectric sensor located 10 cm in front of the food container.

4) *Touch (T) flash* condition: grasping was executed in dark with instantaneous visual feedback at hand-object contact. The scene was briefly illuminated by a 20 μs xenon light flash delivered as both the thumb and index finger touched the target handle.

Experimental conditions were presented in blocks of twelve trials and administered with the above temporal order in all sessions. The *Light* condition was repeated at the end of each recording session just to confirm the stability of neuronal activity (*Light 2* condition).

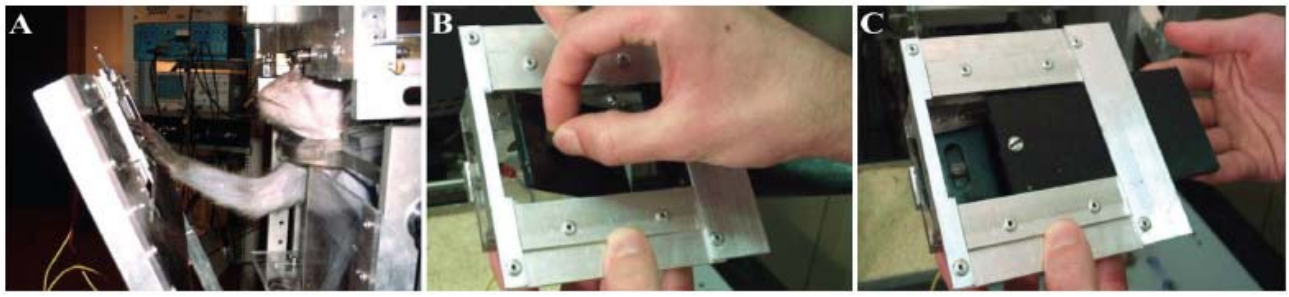

Figure 1. Experimental setup. A: Lateral view of the behavioral apparatus, requiring the monkey to perform a reach-to-grasp task. B: Demonstration of the precision grip the monkey had to execute in order to open the door of the food container. C: The target door was covered by an outer sliding door that the experimenter opened at each trial onset, giving the monkey a go-signal to start moving the hand from the resting position.

Hand kinematics acquisition

In a preliminary session, the behavioral task was administered to MK1 and kinematics of the arm/hand was recorded to ensure that it was comparable in the different grasping conditions, including *Light 2* condition. Markers were placed on the wrist of the monkey's hand to evaluate the transport component of the movement and on the last phalanx of the thumb and index finger to measure grip aperture during hand shaping. The markers were fixated on plastic strings, adjustable in length, that were tightened around the wrist and relevant fingers. After a first brief period of familiarization with the markers, the monkey was able to execute the experimental task naturally.

Twelve kinematics recordings were collected for each experimental condition. The three-dimensional trajectories of each marker were acquired (240 frames/sec) by an infrared-sensitive motion tracking system (ProReflex/Qualisys Track Manager, Qualisys AB, Sweden). The same signal used for triggering the neuronal data acquisition (hand-handle contact) was also acquired to temporally align kinematics recordings.

Spike sorting

The isolation of single neurons from multispike recordings was performed off-line by using Singular Value Decomposition of the data matrix containing the different spike waveforms, followed by Fuzzy C-mean clustering analysis of Principal Components in the multi-dimensional space (Oliynyk et al., in preparation). The good quality of the discrimination was confirmed by evaluating the single-unit interspike interval histograms and the main quantitative parameters of cluster quality, including L_{ratio} measures (Lewicki 1998; Schmitzer-Torbert et al. 2005; Bezdek et al. 1984). A custom-made software was created for this purpose and all implemented algorithms were entirely realized by LabVIEW 7.0 software (National Instruments, U.S.A.). A part of the DataEngine V.i library (MIT GmbH, Germany) for LabVIEW was used for the programming and implementation of the spike sorting algorithm.

Analysis

Kinematics analysis

The 3D position over time of the wrist, thumb and index finger markers was off-line reconstructed by using a position prediction algorithm provided by Qualisys Track Manager software (Qualisys AB, Sweden) and the following kinematic parameters of interest were extracted for each condition: maximal wrist velocity, maximal grip aperture, deceleration time, defined as the interval between the time of wrist peak velocity and handle touch instant, and aperture-closure time, defined as the interval between the time of maximal grip aperture and handle touch instant.A non-parametric one-way ANOVA (*Kruskal-Wallis test*, 5% alpha level) was performed to compare *Light*, *Dark*, *PT flash*, *T flash* and *Light 2* conditions for each of these parameters.

Single-neuron analyses

To ensure that the motor response of the selected neurons was related to hand grasping and thus was modulated by the task, the difference in activity between a baseline epoch (*epoch 1*) and a movement-related epoch (*epoch 2*) was statistically assessed in all conditions for each neuron by means of a two-way repeated-measure analysis of variance (ANOVA, 5% alpha level) with *epoch*

(*epoch 1* and *epoch 2*) and *condition* (*D*, *L*, *PT flash* and *T flash*) as factors. *Epoch 1* corresponded to a pre-movement period, during which the hand was about to initiate the movement from the starting position (first 500 ms in the trial); e*poch 2* corresponded to a 500-ms grasping-related period including both the hand shaping and finger closure phases, going from 250 ms before the instant at which the hand touched the target handle (*pre-touch* sub-epoch) to 250 ms after it (*post-touch* sub-epoch).

Neurons which did not show any significant difference in firing rates between *epoch 1* and *epoch 2* in any condition (i.e., conjunct lack of *epoch* main effect and of significant differences between epochs for one particular condition, as resulting from the *Tukey's Least Significant Difference* (LSD) post-hoc tests performed on significant *epoch x condition* interactions) were discarded from further analyses. To assess whether the activity of the neurons was modulated by the vision of the acting hand, data analyses were first focused on detecting differences in activity between *D* and *L* conditions in *epoch 2* (significant *epoch x condition* interactions, with *D* different from *L* condition in *epoch 2* at the LSD post-hoc tests). In order to better appreciate even subtle effects on the single-neuron activity, a two-tail paired *Student's t-test* (5% alpha level) comparing *D* vs. *L* mean firing rates was additionally performed on a 100-ms bin, which was stepped through the trial by 20-ms increments. Figure 5D shows the output of this analysis performed on the *D* and *L*-related activity of two single cells taken from the F5 and F1 recorded samples (Fig. 5C). A neuron was considered as significantly modulated if it displayed a statistically significant difference in activity between the two conditions in at least two consecutive time bins. According to the direction of the effect shown in the *pre-* and *post-touch* sub-epochs of *epoch 2*, each neuron was then classified as positively or negatively modulated by light in both or either of the two sub-epochs.

To investigate the effect of the light flashes on grasping-related neuronal activity, a similar approach was employed. In view of the fact that *PT flash* and *T flash* were transient visual manipulations and represented hybrid situations with respect to the *D* and *L* conditions as for both physical and functional aspects, direct comparisons between activity during flashes and *D* (or *L*) were avoided at the first-level analysis. This choice was also driven by the purpose of getting rid of any unspecific arousal-related flash effect. Thus, as a first step, the above described running *t-test* analysis was used to contrast single-neuron discharge in *PT flash* and *T flash* conditions, with the aim to primarily identify neurons firing preferentially when a light flash was delivered at a specific relevant instant in the trial. In particular, we were interested in any firing difference observed between the two flash conditions within *epoch 2*, with the idea that, even a very short-lived visual information, if relevant for the ongoing hand movement, should modulate the grasping-related activity of the neuron. Once flash-selective neurons, if any, were detected, their flash-related

activity was then compared with the activity they exhibited in the *D* and *L* condition and thoroughly studied at the population level.

Estimation of neuronal response latency and peak. Response latency was calculated using a version of the time to half-height of the peak nonparametric technique (Gawne et al. 1996), which detects the midpoint between the minimum and maximum values of the single-neuron firing rate histogram, smoothed with the optimal bandwidth. We chose to implement this technique because it gives a latency measure which is less susceptible to noise than the one obtained through other methods computing latency at the onset of the neuronal response, when the rate of change in activity is quite low and therefore characterized by an unfavorable signal-to-noise ratio. By definition, the maximum firing value in the histogram is the peak of neuronal discharge. The single-neuron spike train, averaged and aligned with respect to the handle touch instant (time 0) for each condition, was convolved with a smooth Gaussian kernel function with window width set to 20 ms, to obtain a spike density function (SDF) providing a continuous and fine (1-ms binned) time-dependent measure of the firing pattern. The first time this SDF exceeded the average of the minimum and peak values in the period including the grasping movement (first 1250 ms in the trial) was regarded as the estimated response latency of the neuron in one given experimental condition.

Population analyses

Normalization was achieved for each neuron composing a population through ms-by-ms dividing the smoothed SDF relative to one given experimental condition by the highest discharge value (peak of activity) observed across all four conditions. Population plots were obtained by simply averaging the normalized smoothed SDF of the included neurons.

Statistical analyses on latency or peak firing rates were performed assigning to each entry in a given pre-selected population, the normalized activity values respectively corresponding to the time of half-maximum or maximum activity (see above) for each single unit.

Weighted average (*WA*) latency and peak firing rates of one single neuron in a group were computed according to the following formula:

$WA_n = (\Sigma_i x_i * f_i)/\Sigma_i f_i$

where x_i is the discharge of the neuron n at the latency (or peak) time of each neuron i in the group and f_i is the latency (or peak) time of each neuron i in the group.

Analyses on the activity recorded within a specific trial period (e.g., *epoch 2*) during one particular condition were carried out on the single-neuron mean raw firing rates in the target period, normalized to the maximum activity across all four conditions, as just described.

Estimation of neuronal latency of light- and flash-selectivity. The same method used for computing single-neuron motor response latency was employed to calculate the neuronal latency of light and flash selectivity expressed at the population level. In this case, latency was defined as the time at which firing in *L* vs. *D* (or in *PT flash* vs. *T flash*) trials differed from one another in a relevant way. Therefore, we compared the time at which the difference in the population activity between the two conditions under investigation reached half of the maximum value, considering the normalized mean firing rate differences computed on a sliding 100-ms bin (sliding step, 20 ms). This method was used to have an additional measure for expressing the latency of neuronal selectivity, besides the one given by the running *t-test* analysis (see above), returning the time course of the selectivity of the neuronal population.

Estimation of magnitude of light- and flash-selectivity. The strength of light- and flash-selectivity was evaluated by using a Receiver Operating Characteristic (ROC) analysis (Metz 1978), which measures the degree of overlap between two response distributions. Hence, given for instance the two distributions of neuronal activity *L* (i.e., Light-related) and *D* (i.e., Dark-related), for each observed single-neuron firing rate, the proportion of *L* against the proportion of *D* response distribution exceeding that firing rate was plotted and the area under the plotted curve (ROC area) was computed, yielding a single value for that comparison. This method has several advantages. First, it provides an assumption-free estimate of the degree of overlap between *L* and *D* distributions: values near 0.5 indicate large overlap between the distributions, whereas values close to 0 or 1 indicate small or no overlap, with every value drawn from one distribution exceeded by the other entire distribution and vice versa. Second, it can be conveniently interpreted as the performance of an ideal observer in a two-way forced choice task. Third, it is independent of the firing rate of the neuron and can thus be used to compare the activity of neurons with widely different baseline and dynamic firing rates.

Population ROC area values, comparing *L* vs. *D* (or *PT flash* vs. *T flash*) distributions, were either computed every 20-ms step in a 100-ms bin covering all the trial period, or averaged within selected grasping epochs.

RESULTS

Kinematics results

Arm/hand kinematics parameters acquired from MK1 were analyzed. Figure 2B shows the temporal trajectories of wrist velocity and grip size for each of the five conditions considered: *L*, *D*, *PT flash*, *T flash* and *L2*.

Statistical analysis (*Kruskal-Wallis test*, 5% alpha level) on the transport component of the movement revealed that the maximal wrist velocity was significantly higher during the *Light* conditions (*L* and *L2*) than during *PT flash* ($P < 0.02$) and *T flash* ($t = 12.7$, $P < 0.05$) conditions (Fig. 2A, *Maximal velocity* plot). Accordingly, a significant faster deceleration time was observed in full light (*L* and *L2*) with respect to all dark conditions, including *D*, *PT flash* and *T flash* ($P < 0.0001$) (Fig. 2A, *Deceleration time* plot). Importantly, maximal wrist velocity and arm deceleration phase were not different in the two flash conditions and in the dark.

As far as the grip parameters are concerned, maximal grip aperture was considerably greater in the dark and flash conditions than in the light, especially if considering differences with the *L2* condition ($P < 0.03$) (Fig. 2A, *Maximal grip aperture* plot). This specific result may be explained in terms of a rebound effect: after repetitively grasping in the dark over the previous three consecutive blocks of trials (in which *D*, *PT flash* and *T flash* conditions were administered), in the *L2* condition the monkey assumed a peak grip size even less large than the one adopted in the first *L* condition. Conversely, the wider finger aperture observed under dark conditions suggests that, in absence of any visual information, the monkey was enlarging the grip size safety margin to increase the chances of successfully grasping the door handle. To this purpose, after maximal aperture was reached, fingers also closed more slowly in the dark and flash conditions than in the light ($P < 0.02$) (Fig. 2A, *Aperture-closure time* plot). Again, there was no significant difference among the dark and flash conditions, in neither grasping parameter.

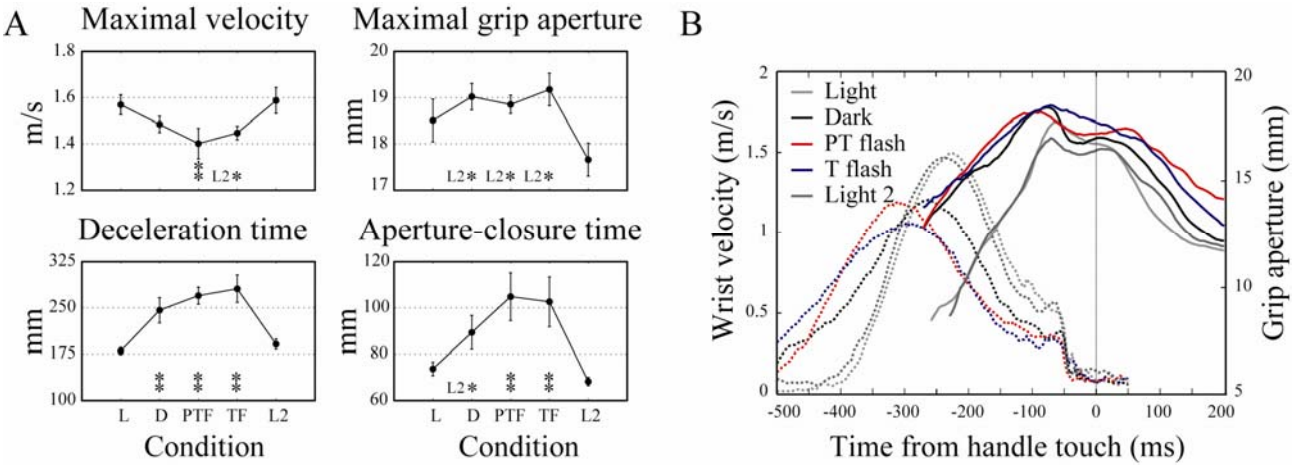

Figure 2. A: Average kinematic parameters (maximal velocity, maximal grip aperture, deceleration time, aperture-closure time) recorded for each condition during the behavioral experiment conducted with MK1. Deceleration and aperture closure times are respectively measured as the intervals from the time of maximal velocity and from the time of maximal grip aperture to handle touch instant. B: Wrist velocity (dashed lines) and grip aperture (solid lines) recorded over time for each condition(*Light 2* condition is also included). Asterisks within each plot represent significant differences (*Kruskal-Wallis test*, 5% alpha level) of D, PT flash or T flash condition with respect to either or both light conditions.

Overall, these findings confirm the results of previous kinematics studies on humans, reporting an increase in the duration of wrist deceleration and fingers closure phases when visual feedback was entirely or partially blocked during movement (Jackson et al. 1995; Schettino et al. 2003; Winges et al. 2003) or when vision of the own hand was prevented (Gentilucci et al. 1994; Churchill et al. 2000; Schettino et al. 2003; Rand et al. 2007). Also the adoption of a wider maximal grip aperture in absence of any visual feedback (Jakobson and Goodale 1991; Jackson et al. 1995) or without vision of the hand (Churchill et al. 2000) has been already previously observed.

Notably, the fact that no substantial kinematics dissimilarity was found between the two flash conditions (both resembling the dark condition) suggests that the present behavioral task represented a valuable tool to explore the effect of the vision of the own acting hand on the response of grasping neurons in cortical motor areas, without necessarily invoking kinematics variables.

Microstimulation data

We performed 149 penetrations in the three hemispheres of the two monkeys (see Table 1). The respective functional maps are illustrated in Figure 3 (A, B, C). Figure 3D displays the three-

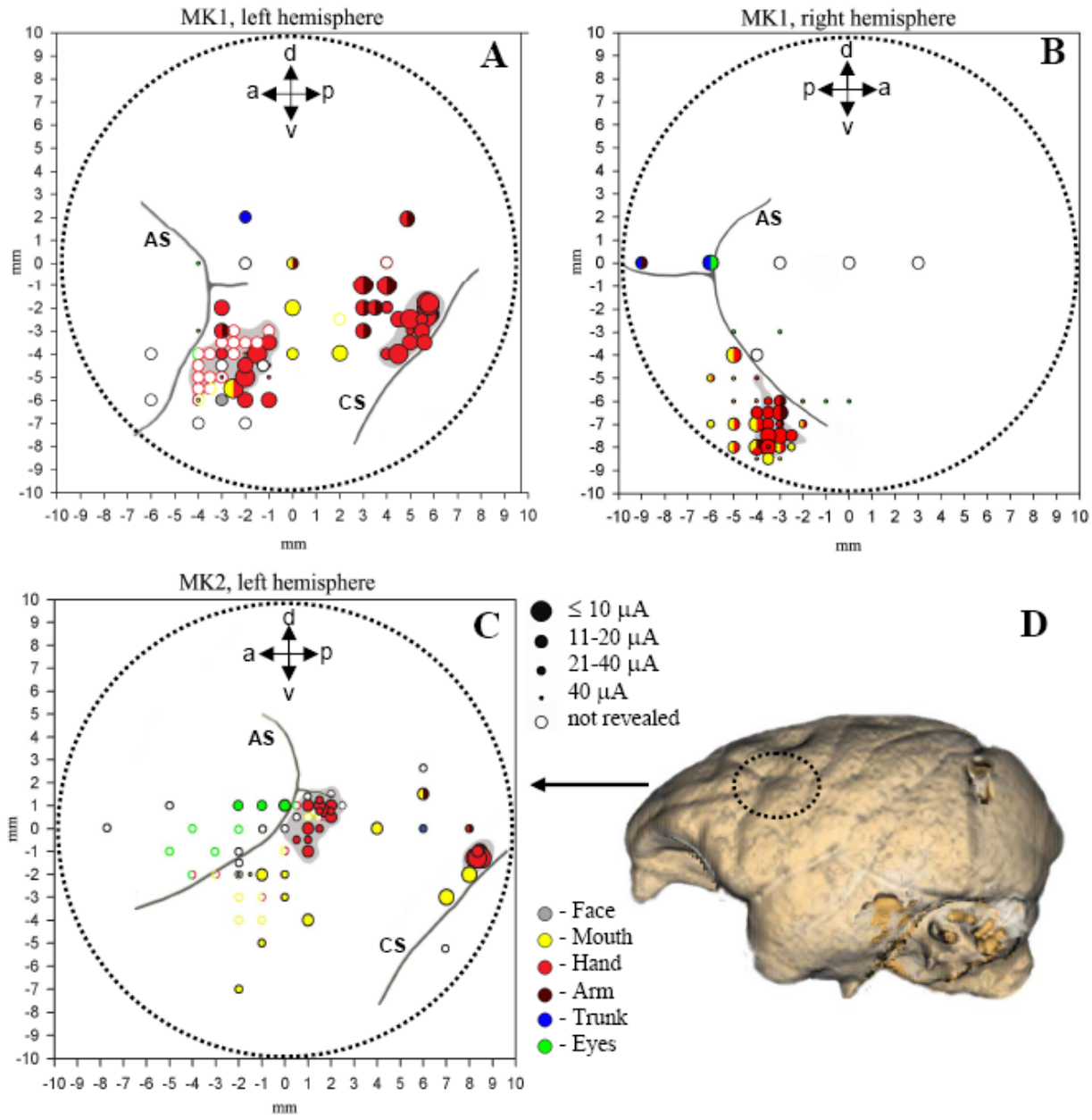

Figure 3. Penetration sites. A, B: Surface location of the electrode penetrations in both hemispheres of MK1. C: Penetrations in the left hemisphere of MK2. (D) Lateral view of the brain surface reconstruction of MK2. Encircled region shows the position of the recording chamber. Filled symbols indicate sites where intracortical microstimulation (ICMS) elicited hand movements at different current intensity thresholds. The size of the circles is correlated with the value of the lowest threshold found in each penetration, as indicated in the key of the figure. Unfilled symbols indicate sites not tested with ICMS. Each color refers to the specific body part controlled by the neurons encountered in each penetration. AS, arcuate sulcus; CS, central sulcus. Grey regions highlight penetrations where neurons were recorded while the monkeys were performing the reach-to-grasp task.

dimensional reconstruction of the brain surface of MK2 that was used to position the recording chamber on the skull. Penetrations are marked according to the specific body-part movements associated with the neuronal responses and the current intensity threshold at which those

movements were evoked through ICMS. As threshold, we defined the minimal current intensity at which visually detectable movements were evoked in 50% of stimulation trials.

All sites in the rostral bank of the central sulcus (area F1) were excitable with low-threshold currents (MK1, 9.8 ± 0.8 μA; MK2, 11.4 ± 2.2 μA, mean ± S.E.M.) evoking hand or finger movements. Microstimulation of the penetration sites rostral to F1 hand representation (estimated to be located in area F4) evoked face and axial movements at higher thresholds (MK1, 21.1 ± 5.9 μA; MK2, 27.9 ± 3.2 μA). Neurons in this region appeared to show large somatosensory receptive fields on the face and body and visual receptive fields in register with the somatosensory ones. The hand representation in area F5 was identified further rostrally, in the posterior bank of the iAS, on the basis of distal movements evoked by stimulation at the following thresholds: MK1, 24.2 ± 2.8 μA; MK2, 28.2 ± 2.3 μA. The discharge of the neurons in this region was often related to goal-directed actions, mainly including grasping. The presence of microstimulation-induced eye movements (current intensity thresholds: MK1, 25.9 ± 4.6; MK2, 24.2 ± 5.7) and the recording of saccade-related activity in a region anterior to area F5 and to the iAS, were considered as functional markers of the FEF.

Grey regions highlight penetrations where grasping motor neurons were recorded while the monkeys were engaged in performing the behavioral task. Overall, the grasping-related activity of the neuronal samples recorded from the three monkey hemispheres during the task was congruent with the functional characterization obtained through ICMS and naturalistic testing.

Neurons database

A total number of 295 and 236 grasping motor neurons were respectively isolated from F5 and F1 areas of MK1 and MK2 during 271 recording sessions. Of these neurons, 169 of area F5 and 129 of area F1 survived the selection criteria (stability of the recording throughout the duration of the task and sufficient number of trials recorded per each condition). One F1 neuron was subsequently discarded since, as revealed by the two-way *epoch x condition* ANOVA, its activity during grasping was not significantly different from that displayed during the pre-movement period. Therefore, the database for the present study consisted of 169 F5 neurons (102 recorded from the two hemispheres of MK1 and 67 recorded from the left hemisphere of MK2) and 128 F1 neurons (106 and 22 recorded from the left hemispheres of MK1 and MK2, respectively). Details concerning all recording sessions are reported in Table 1.

Table 1. Summary of the database.

	Monkey 1				***Monkey 2***			
	F5		F1		F5		F1	
	LH	RH	LH	RH	LH	RH	LH	RH
	Right hand	Left hand	Right hand		Right hand		Right hand	
Penetrations	41	32	21	--	45	--	10	--
Recording sessions	52	62	67	--	67	--	23	--
Isolated units	67	116	204	--	112	--	32	--
Analyzed database								
S: session	S = 23	S = 32	S = 67	--	S = 49	--	S = 17	--
N: neurons	N = 38	N = 64	N = 106		N = 67		N = 22	
PT flash delivery	-169 ms	-200 ms	-126 ms	--	-215 ms	--	-190 ms	--
*(median (IQR))**	(-225/-107)	(-242/-133)	(-178/-93)		(-252/-167)		(-251/-135)	

* Median and inter-quartile range (IQR) of times of *PT flash* delivery, according to the instant when the hand (right or left, depending on the recorded hemisphere) crossed the IR barrier before touching the door handle (temporal values are aligned to handle touch).

Dark vs. light conditions: types of neuronal modulations

By looking at the results of the 2-way ANOVA, post-hoc tests performed on significant *epoch x condition* interactions revealed that *within epoch 2* 14% of F5 neurons and 9% of F1 neurons showed higher activity during *L* than *D* condition, while 19% (F5) and 23% (F1) of neurons exhibited the opposite modulation. The amount of F5 and F1 neurons which did not fire differently in the two conditions (non-modulated neurons) was comparable (67% and 68%, respectively).

The running *t-test* comparing *D* vs. *L* activity throughout *epoch 2* confirmed this pattern of results, though revealing a larger amount of effects due to the less restricted significance criteria of the analysis (see *Methods*). According to the period in which the neuronal modulation was observed, neurons were classified as showing one particular effect (*L*>*D* or *D*>*L*) in the *pre-touch* sub-epoch, in the *post-touch* sub-epoch, at the instant when the hand touched the handle, or through whole *epoch 2* (Tab. 2; Fig. 4). The number of modulated neurons was comparable in the two areas (61% in F5 and 54% in F1); more precisely, the portions of F5 neurons strengthening (22%) or diminishing (39%) their activity due to full vision of the ongoing movement, mostly reflected those of F1 (22% and 32%, respectively). However, and more interestingly, in both areas, the majority of *L*-sensitive effects were clustered in the *pre-touch* sub-epoch (14% in F5 and 13% in F1), while the opposite modulations principally emerged in the *post-touch* sub-epoch (22% in F5 and 20% in F1).

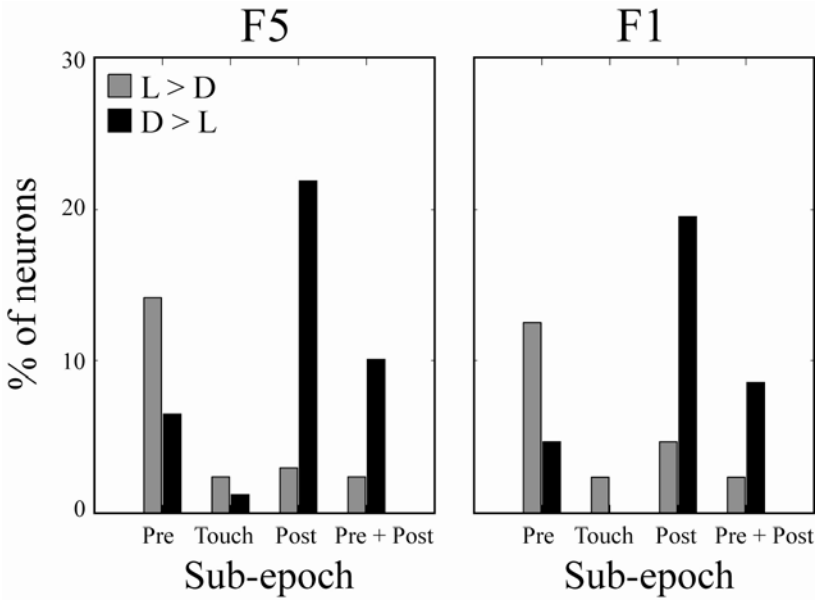

Figure 4. Distribution of F5 and F1 neurons with *L/D* modulation across the different grasping-related sub-epochs, as summarized in table 1.

Table 2. Summary of results from the running paired *t-test* analysis comparing single-neuron activity in *L* vs. *D* condition in a 100-ms bin shifted through the trial by 20 ms steps.

	Pre-touch *(-250 ms – 0 ms)*		***Touch*** *(around 0 ms)*		***Post-touch*** *(0 ms - 250 ms)*		***Pre- + Post-touch***		***Sub-total***	
	MK1	MK2	MK1	MK2	MK1	MK2	MK1	MK2	MK1	MK2
F5										
L > D	13	11	3	1	5	--	4	--	25	13
	24 (14%)		4 (2%)		5 (3%)		4 (2%)		37 (22%)	
D > L	4	7	1	1	23	14	10	7	35	32
	11 (7%)		2 (1%)		37 (22%)		17 (10%)		67 (39%)	
Modulated	*35*		*6*		*42*		*21*		104 (61%)	
Spurious									20	10
									30 (18%)	
L = D									22	13
									35 (21%)	
Total									**169** (100%)	
F1										
L > D	13	3	3	--	6	--	3	--	25	3
	16 (13%)		3 (2%)		6 (5%)		3 (2%)		28 (22%)	
D > L	4	2	--	--	21	4	10	1	35	7
	6 (5%)		--		25 (20%)		11 (9%)		42 (32%)	
Modulated	*22*		*3*		*31*		*14*		70 (54%)	
Spurious									28	6
									34 (27%)	
L = D									18	6
									24 (19%)	
Total									**128** (100%)	

Neurons are divided according to the monkey from which they were recorded (MK1 or MK2) and the specific sub-epoch within *epoch 2* (going from 250 ms before to 250 ms after handle touch) in which they showed the *D/L* modulation. The entry "*Spurious"* indicates neurons showing opposite *D/L* modulations within *epoch 2.* The percentage values always refer to the entire sample of recorded neurons.

Figures 5 and 6 show single-neuron examples of the most significant neuronal categories just described. Spike density plots and respective rasters are aligned to the instant at which the hand touched the door handle and describe the single-unit activity during the whole grasping period (first 1500 ms in the trial). For descriptive purposes, plots in Figure 6C also include the subsequent food-grasping neuronal response, not examined in the current work. The most relevant effects of light on

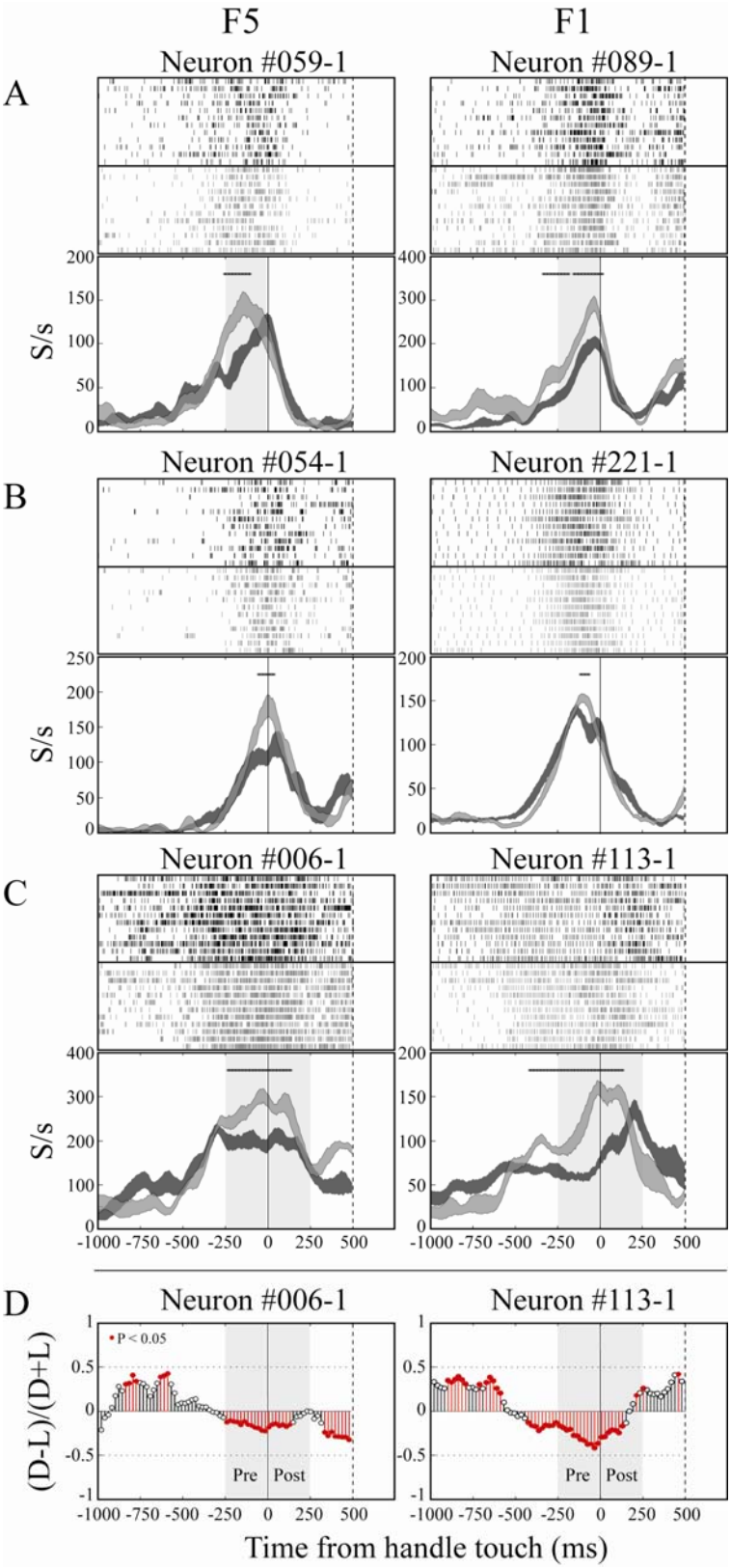

Figure 5. Single units exemplifying the most significant F5 and F1 neuronal categories determined by the running *t-test* analysis. The first 1500 ms of activity aligned to time of handle touch (solid line) are shown. Spike density plots are obtained by first smoothing each trial firing rate (spikes/sec, 5-ms bin width) by a Gaussian kernel function (20-ms window width) and then averaging across trials within each condition. Ribbons represent mean single-neuron response ± 1 S.E.M. in the *L* (grey) and *D* (black) condition. Symbols on top indicate trial bins where *t-test* result was significant

(5% alpha level). Top raster plots represent the respective spike trains recorded from the neuron in the 12 trials of the *L* and *D* conditions. A: Neurons showing *L*>*D* modulation in the *pre-touch* sub-epoch (shaded area). B: *L*-modulated neurons around the instant at which the hand touched the handle. C: Neurons expressing *L*-selectivity in both *pre-* and *post-touch* sub-epochs (shaded areas). D: Stem plots exemplifying the running *t-test* analysis performed on the *L*- and *D*-related activity of the neurons shown in (C). The activity of the neurons in the two conditions is represented by the index (D-L)/(D+L); lines extending from the baseline (index = 0) upward and downward respectively represent *D*>*L* and *L*>*D* modulations computed at each 100-ms bin. Red and black lines indicate significant and non-significant modulations, respectively. A given neuron was considered as *L*- or *D*-selective if it displayed the same significant modulation in at least two consecutive bins. The same analysis was performed also to detect *PT flash/T flash*-selective neurons.

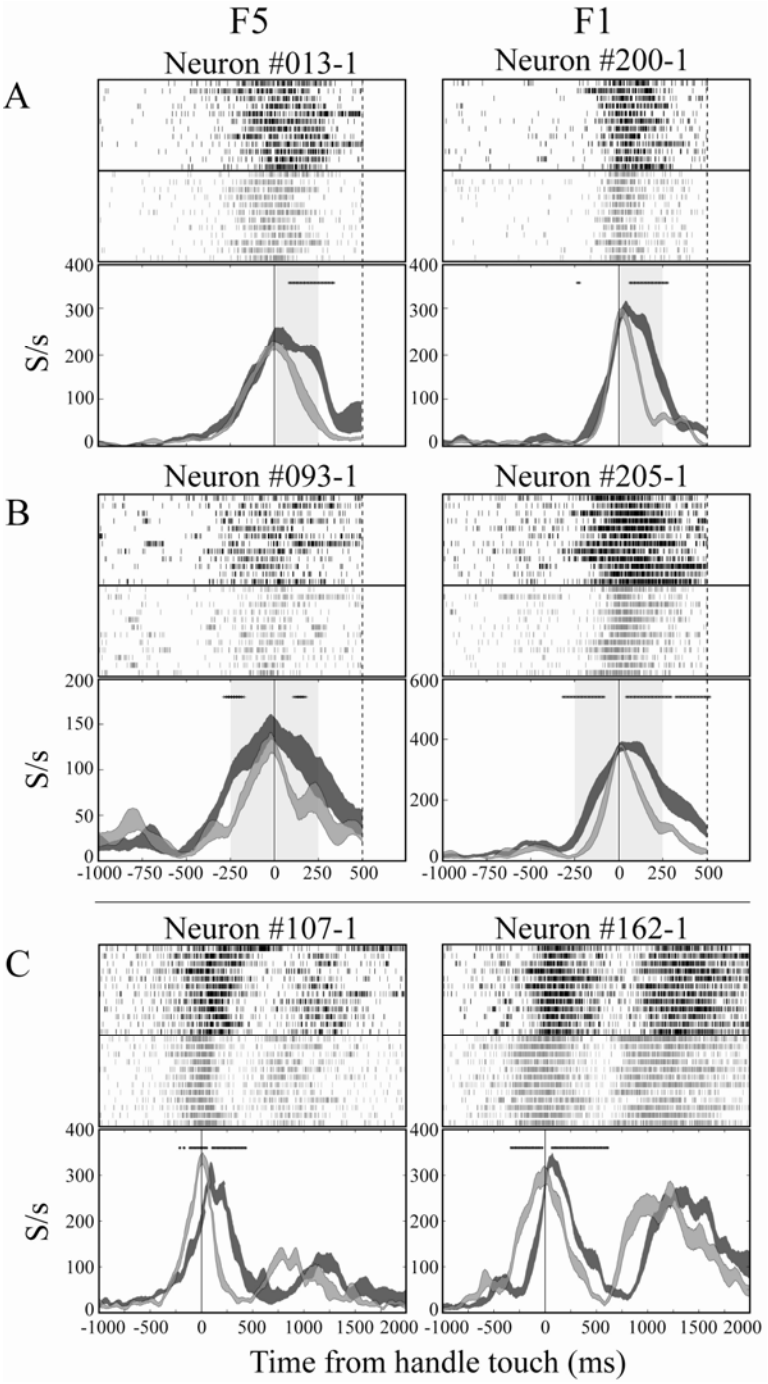

Figure 6. Single units exemplifying other significant F5 and F1 neuronal categories determined by the running *t-test* analysis. A: Neurons showing a *D>L* modulation in the *post-touch* sub-epoch (shaded area). B: Neurons with higher firing rates in the *D* condition throughout *epoch* 2 (shaded areas). C: Neurons with *spurious* effect, exhibiting opposite modulations within *epoch* 2, as a result of a shift in activity between *L* and *D* conditions. Conventions as in Fig. 5.

the grasping activity of three different units of F5 and of F1 are illustrated in Figure 5. Full vision of the ongoing action made these neurons discharge more, compared to the full dark condition, either during the hand shaping phase of grasping (Fig. 5A), or at the contact time between the hand and

the door handle (Fig. 5B) or throughout all *epoch 2*, including the very final phase of grasping (Fig. 5C). It is worth noting that these light-induced modulations were mainly expressed as additive effects to the basic motor activity of the neurons recorded in the dark; indeed, the decaying part of the discharge profile of both F5 and F1 units in Figure 5A overlapped in the two conditions and so did the ascending and descending phases of the grasping activity of the other single-neuron examples in Figure 5.

In contrast, the modulated activity of neurons in Figure 6A was of a rather different kind; these units exemplify the firing behavior of a large fraction of neurons showing a significant *D>L* effect which was actually the result of a more prolonged *post-touch D*-related response, likely associated with hand tactile/proprioceptive adjustments after the monkey's hand reached the handle under full dark conditions. In contrast, the response recorded in the *L* condition rapidly decayed after touch. The same observation holds for neurons in Figure 6B, displaying an overall more spread-out grasping activity in the *D* than in the *L* condition (with no difference at the peak activity). Single neurons in Figure 6C were largely represented both in F5 (16%) and F1 (23%) and showed a clear rightward temporal shift in the grasping response recorded in the dark, compared to that observed in the light. This was particularly evident at the discharge peak and resembled that often recorded during the following grasping of the food (see last 1500 ms of plots in Fig. 6C), when no experimental control was imposed to ensure that the movement in the dark could be performed by the monkey as accurately as the movement in the light. Statistical analysis run on these neurons returned a *L>D* (or, to a lesser extent, *D>L*) effect in the *pre-touch* sub-epoch followed by the reverse modulation in the *post-touch* sub-epoch (see *"Spurious"* entry in Table 1). Since we were mainly interested in identifying neurons showing a true *L*-related potentiation (amplitude increase) of motor activity and one can hypothesize that the timing difference just described might be strictly related to a difference in *D/L* hand kinematics, neurons of this kind were considered as a separate class, thus not influencing neither the number of cells showing a *pre-touch L>D* modulation, nor the group displaying higher activity in the dark during the *post-touch* sub-epoch.

Pre-touch light-responsive neurons in areas F5 and F1

Of all the cells which were light-responsive in the different temporal phases of grasping, the neuronal subset discharging more in *L* than *D* condition during the *pre-touch* sub-epoch was the largest one (see Fig. 4). This result is of remarkable interest for the purpose of the current work, since it suggests that, although visual information on the ongoing movement was continuously

available in the *L* condition, the activity of both F5 and F1 grasping neurons was particularly modulated just in the period when the shaping of the hand preceding grasping was taking place.

In the following paragraphs this particular class of cells will be analyzed in detail.

F5 and F1 pre-touch light-modulations had similar time course and strength

Figure 7A shows the time course of normalized *L* and *D* average activity of *pre-touch* light-responsive cells in areas F5 and F1. If one considers the temporal build-up of the light-effect, these two populations did not show any substantial difference. In both cases, the curves depicting *L*- and *D*-related grasping activity started separating in a statistically significant way (two-tail paired *Student's t-test*, 5% alpha level) at the 100-ms bin centered at 270 ms before handle touch. This similarity in the latency of light-selectivity was also confirmed by the time to half-maximum divergence in activity computed on the normalized mean firing rate differences in the sliding 100-ms window. This method returned a peak of *L* vs. *D* discharge difference in the bin centered at 80 ms prior to touch in both areas, with the half-value of this peak achieved by F5 and F1 neurons at 210 and 190 ms before touch, respectively (Fig. 7B).

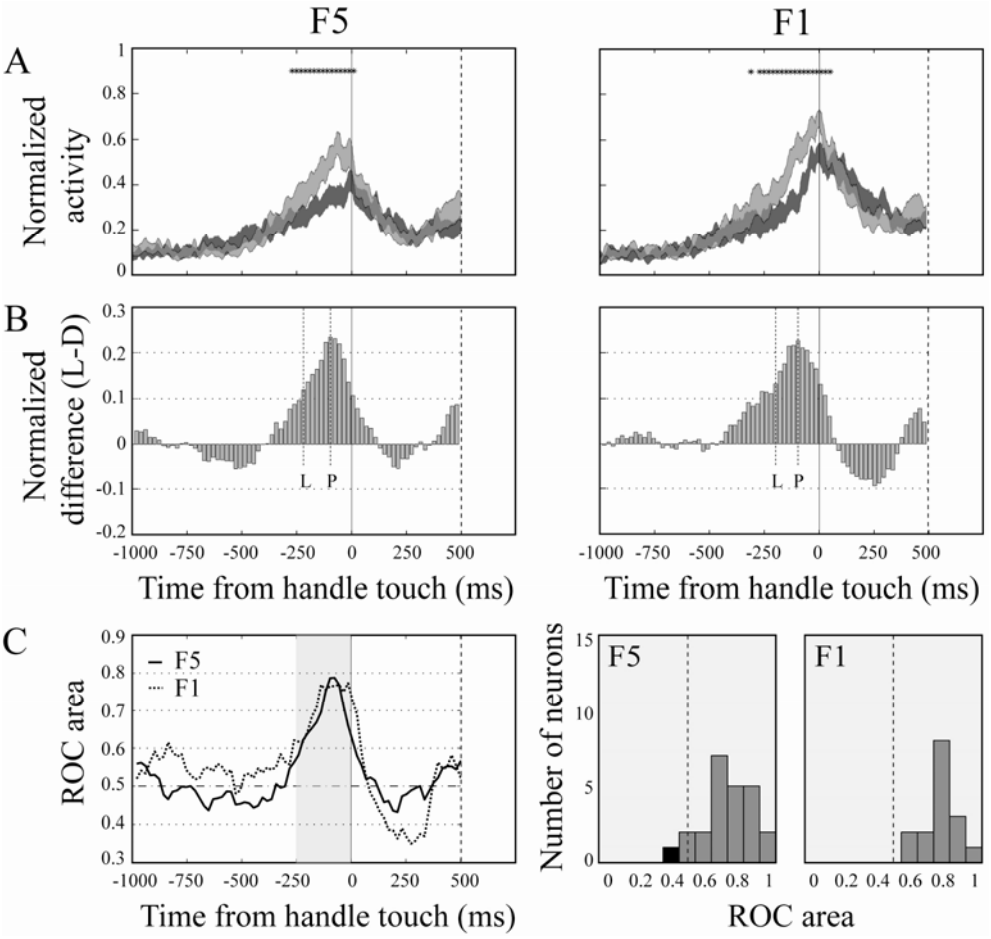

Figure 7. A: Average activity of *pre-touch* light-responsive neurons in area F5 and F1. The first 1500 ms of activity aligned to time of handle touch (solid line) are shown. Population spike density plots are obtained by first normalizing the single-neuron smoothed data (Gaussian kernel function with window width set to 30 ms) to the absolute maximum level of activity observed across all 4 different conditions and then averaging the result across all units in the populations. Traces represent the population *L*- (grey) and *D*- (black) related average response ± 1 S.E.M.. Symbols on top indicate trial bins where the running *t-test* result was significant (5% alpha level). B: Time course of the respective F5 and F1 population normalized *L-D* discharge differences, computed on a sliding 100-ms bin, shifted by 20-ms steps. Temporal peak and latency of light-selectivity (calculated as the times to maximum and to half-maximum difference in activity) are respectively represented by the P- and L-labeled dashed lines within each plot. F5 and F1 populations reached the latency (bin centered at 210 and 190 ms before touch, respectively) and peak (bin centered at 80 ms before touch, in both plots) of selectivity almost at the same time. C (left): Time course of ROC values for the *pre-touch* light-selective neurons in area F5 and in area F1. The first 1500 ms of activity aligned to time of handle touch (solid line) are shown. Traces are obtained averaging across neurons the area under the ROC curve, computed every 20-ms step and comparing *L* and *D* firing rates in a sliding 100-ms bin. C (right): Histograms showing the distribution of F5 and F1 single-neuron ROC area values in the *pre-touch* sub-epoch (corresponding shaded area in the upper plot A). ROC areas greater than 0.5 (grey) indicate neurons conveying more light- than dark-related information; ROC values less than 0.5 (black) represent neurons expressing higher activation in the *D* than in the *L* condition. Note that the presence of black bars is due to the criterion used for selecting light-responsive neurons, requiring selectivity in at least 2 consecutive 100-ms bins of *pre-touch* sub-epoch.

In addition, the strength of light-responsiveness displayed by the two neuronal subgroups, aside from some minor differences, was almost comparable. The magnitude of the *L*-effect over time was measured by computing the population mean ROC area for the two conditions on each 100-ms bin stepped on the trial. Figure 7C (left) shows that F5 and F1 light-responsiveness developed in a similar way around the handle grasping period, though F1 selectivity was overall stronger. However, F5 light-modulation was slightly higher at the peak. The distribution of *pre-touch* ROC area values across neurons in the F5 and F1 subgroups (Fig. 7C, right) confirmed that, even though statistically similar (*Student's t-test,* n.s.), the light-sensitivity level during the hand shaping phase of grasping was on average higher in F1 (0.799 ± 0.023) than in F5 (0.746 ± 0.032).

Unlike F1 neurons, F5 neurons showed significantly different response profiles under light and dark conditions

Although numerically equivalent and showing a *L*-modulation with comparable time course and magnitude, F5 and F1 populations differed substantially one from the other in regard to the discharge profile displayed during the *L* and *D* conditions. In particular, despite the fact that the *L*- and *D*-related activity profiles started diverging at the same time in the two areas, in the F1 recorded

population *L* and *D* profiles grew up and reached the peak almost in parallel, while in area F5 they developed with clearly different slopes.

Figure 8A shows the average temporal peak and latency of the F5 and F1 motor response (detailed values are reported in Table 3). It is important to point out that latency, since computed as the time to half the discharge peak, is more associated to the rise time to the peak of activity, rather than just to the onset of the grasping response. In contrast to the F1 population, showing no timing difference in the grasping activity between the two conditions (two-tail paired *Student's t-tests*, not significant at 5% alpha level), the mean peak and latency times of the F5 neuronal response in the *L* condition were significantly shorter than those observed in the *D* condition. Overall, F5 *pre-touch L*-sensitive neurons peaked much earlier in full light (-94 ± 25 ms, mean ± S.E.M.), than in full dark (-47 ± 29 ms) ($t = 2.3$, P = 0.03). They also displayed a much faster ramping activity to the peak in full light (-135 ± 27 ms) than in full dark (-81 ± 30 ms) ($t = 2.7$, P = 0.01), as revealed by the time-to-half-the-maximum parameter.

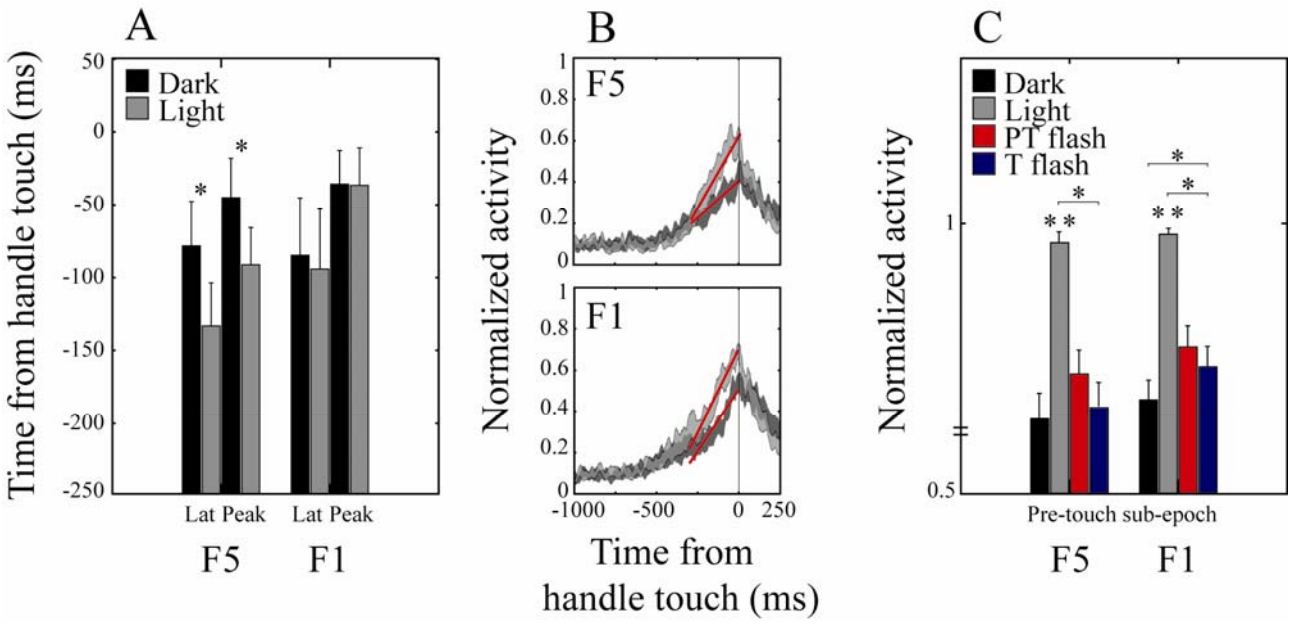

Figure 8. A: Mean latency and peak times for the *L*- (grey) and *D*- (black) related responses of F5 and F1 *pre-touch L*-selective populations. Note that latency is computed as the time to half the peak of discharge, meaning that it is more related to the rise time of activity to the peak, rather than to the actual onset of the neuronal response. Asterisks on top indicate statistically significant differences (*Student's t*-test, 5% alpha level). B: Line fitting of the *L*- and *D*-related response of F5 and F1 *pre-touch L*-selective neurons in the 300-ms window prior to touch. The regression analysis returned similar slope-intercept *L* and *D* functions for the F1 population, while F5 population displayed very different ramping activities: the median slope of the *L* and *D* response profiles was respectively 57.1° and 40° for F5 neurons and 63.7° and 49.4° for F1 neurons. C: Average activity of F5 and F1 *pre-touch L*-responsive neurons during *pre-touch* sub-epoch in the four experimental conditions. Asterisks on top of bar plots indicate main significant differences among conditions (P < 0.05, LSD post-hoc tests, subsequent to significant one-way ANOVA *condition* main effect).

Table 3. Average timing parameters of the *D*- and *L*-related response profiles of F5 and F1 *pre-touch L*-selective populations.

	Latency (ms)	*Peak (ms)*
F5		
Light	-135 ± 27	-94 ± 25
Dark	-81 ± 30	-47 ± 29
F1		
Light	-96 ± 23	-39 ± 26
Dark	-87 ± 39	-38 ± 41

Values are mean times from handle touch (ms) ± 1 S.E.M.

The half-peak timing difference could not be explained by the amount of *L*-selectivity of the F5 neurons: in addition to the fact that F5 neurons were as *L*-selective as F1 neurons (see above), the discharging difference between the two conditions in the *pre-touch* sub-epoch did not significantly correlate with the difference in latency ($r = 0.2$; P = 0.2). The difference found in the peaking times between the two conditions well supports this observation, since it could not be at all related to the significant *pre-touch* divergence between the *L* and *D* discharge profiles.

To better describe this temporal profile difference, a linear regression function interpolating the activity of each cell of the F5 and F1 *pre-touch L*-selective populations in a 300-ms window prior to touch (i.e., going from -300 to 0 ms and representing the most significant portion of the *pre-touch* neuronal response) was computed for each of the *L* and *D* condition. Neurons showing a negative slope regression parameter *m* (i.e., the first derivative) in both conditions, thus characterized by a substantially different response profile, were discarded from average. Whereas in the F1 population (n = 13) the slope regression parameter of the *L* (median $m = 63.7°$, Inter-Quartile Range, IQR = 11.4°) and *D* ($m = 49.4°$, IQR = 16.4°) ramping activities was approximately comparable (*Wilcoxon signed ranks test*, $W^+ = 1.6$, n.s.), in the F5 population (n = 20) it substantially changed (*L,* $m = 57.1°$, IQR = 33.8°; *D*, $m = 40°$, IQR = 31.7°; $W^+ = 2.8$, P = 0.003). Figure 8B shows population fitting line plots for the average *D* and *L* response profiles of F5 and F1 *pre-touch L*-selective neurons.

Importantly, none of the F5 and F1 neurons which were *L*-responsive in either of the other considered sub-epochs displayed such a significant timing difference between the *L* and *D* response profiles, indicating that this result was highly specific for the *pre-touch L*-selective neuronal population recorded from area F5. In addition, the motor discharge of the F1 *pre-touch* neurons in the *L* condition was consistently, though not significantly (*Student's t*-test, 5% alpha level), delayed (39 and 55 ms at the latency and peak, respectively; see Table 3) with respect to that of the F5 population, suggesting a functional interplay between the two areas.

Taken together, these results strongly indicate that the *L*-modulation of the *pre-touch L*-responsive F5 neurons, in contrast to that of F1 neurons, mainly consisted in a temporal gain of the *L*-related response over the D-related response. This was achieved through a faster increase of the *pre-touch* activity when the monkeys could observe their own hand during the shaping phase of grasping compared to when they could not.

F5 and F1 pre-touch light-responsive neurons were overall not modulated by flash conditions

Multiple LSD post-hoc comparisons performed on the significant main effect ($P < 0.05$) of a one-way (*condition*) ANOVA computed on the *pre-touch* sub-epoch activity of each neuron were used to test whether F5 and F1 *pre-touch L*-responsive neurons were also modulated by the transient visual feedback of the *flash* conditions. Only 2 out of the 24 F5 *pre-touch L*-selective neurons (1% of the total number of F5 neurons) displayed a significantly different response in the two *flash* conditions and the activity recorded in the *flash* condition for which they expressed selectivity was higher than that observed in full dark. None of the F1 *pre-touch L*-selective neurons showed such a combined effect. Instead, the firing rate displayed by the majority of F5 (79%) and F1 (63%) *pre-touch L*-responsive neurons in the *flash* conditions was as high as that recorded in the *D* condition, and for all neurons the activity exhibited during the *L* condition was significantly higher than that measured during *flash* and *D* conditions. Figure 8C shows the average discharge of the F5 and F1 *pre-touch L*-responsive populations in the *pre-touch* sub-epoch during the four different conditions: for both populations, the activity in the *L* condition was significantly higher than that observed in *D, PT flash* and *T flash* conditions ($P < 0.01$) and no difference was detected between flashes.

These last results suggest that in both areas, the transient visual information available at flash presentation was not as effective as the continuous vision of the own ongoing grasping movement in enhancing the activity of the *pre-touch L*-responsive neurons.

PT flash vs. T flash conditions: selectivity for specific transient visual feedbacks

To identify neurons showing selectivity for either of the two transient visual feedback conditions, the activity recorded during the *PT flash* condition was directly contrasted with that observed during the *T flash* condition. The running *t-test* analysis (see *Methods*) revealed a large portion of both F5 (48%) and F1 (43%) neurons selectively modulated by the transitory vision of the own ongoing action during specific grasping phases, namely hand shaping (F5: 19%; F1: 22%) or hand-object contact (F5: 29%; F1: 21%) (Table 4). Neurons significantly increasing their activity in response to both *PT flash* and *T flash* presentation within *epoch 2* were very few (4% in area F5 and 1% in area F1) and were not taken into consideration for the analyses. Figure 9 shows examples

of single flash-responsive neurons drawn from the F5 and F1 populations. These neurons specifically increased their activity during the grasping period of *PT flash* (Fig. 9A) or *T flash* (Fig. 9B) condition, respectively.

Table 4. Summary of results from the running paired *t-test* analysis comparing single-neuron activity in *PT flash* vs. *T flash* condition in a 100-ms bin shifted through the trial by 20 ms steps.

	Epoch 2 *(-250 ms – 250 ms)*	*Pre-touch*	*Touch*	*Post-touch*	*Pre- + Post-touch*	*Sub-total*
		Intersection with *L*-selective neurons				
	MK1 MK2					
F5						
PT flash-selective	23 9					
	32 (19%)	*4*	--	--	--	*4 (2%)*
T flash-selective	29 20					
	49 (29%)	*5*	--	*4*	*1*	*10 (6%)*
Modulated	*81 (48%)*					
Non-selective	*50 38*					
	88 (52%)					
Total	**169** (100%)					
F1						
PT flash-selective	24 5					
	29 (22%)	*1*	--	*1*	*1*	*3 (2%)*
T flash-selective	23 4					
	27 (21%)	*6*	--	*1*	--	*7 (5%)*
Modulated	*56 (43%)*					
Non-selective	*72 (57%)*					
Total	**128** (100%)					

Neurons are divided according to the monkey from which they were recorded (MK1 or MK2) and the specific flash-selectivity they showed in *epoch 2*. Intersection of each flash-selective neuronal group with *L*-selective neurons in the different time epochs (see table 1) is also shown. The percentage values always refer to the entire sample of recorded neurons.

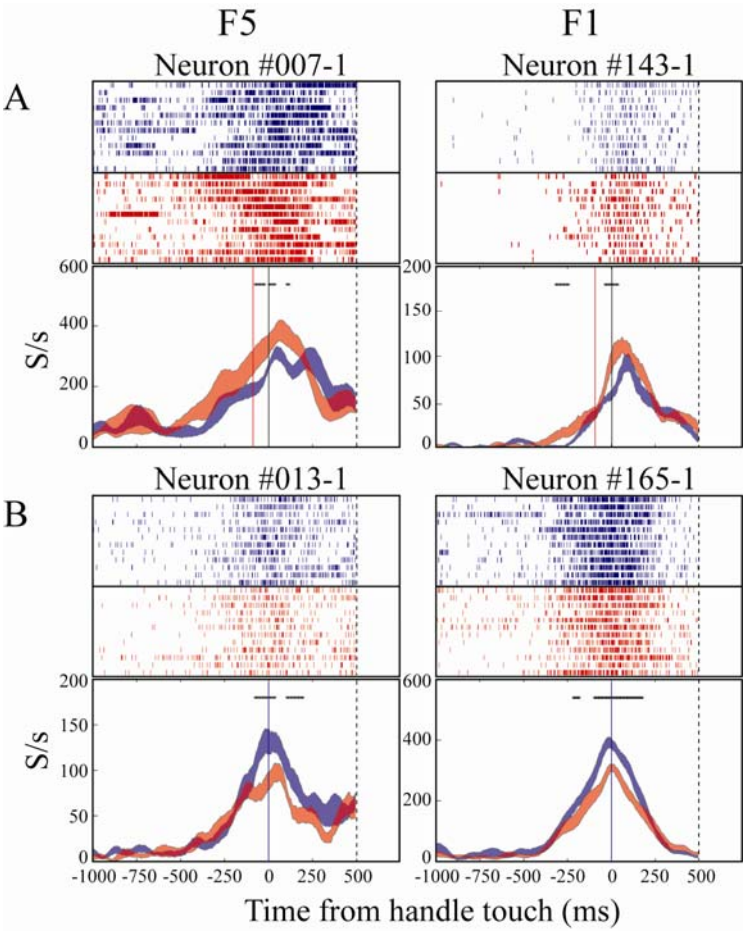

Figure 9. Examples of F5 and F1 flash-responsive single neurons, as returned by the running *t-test* analysis. A: Neurons showing significantly higher firing rates during *epoch 2* of the *PT flash* condition (red) than during *epoch 2* of the *T flash* condition (blue). B: neurons specifically responding to *T flash*. Red and blue dashed lines represent the time of *PT flash* (-91 ms in the F5 neuron and -96 ms in the F1 neuron) and *T flash* (always at 0 ms) occurrence. Other conventions as in Fig. 5.

F5 and F1 flash-modulations were displayed according to the grasping phase at which the transient visual information was delivered

Figure 10 shows the time course of *PT flash* and *T flash* average activity of the specific flash-responsive F5 and F1 populations. For both areas, the temporal build-up of the flash effect varied consistently between the *PT* and *T flash*-responsive groups, in accordance with the different grasping time at which the flash was delivered. Specifically, the two flash-related activity curves began diverging much earlier in the *PT* than in the *T flash*-selective neuronal groups: F5 and F1 *PT flash*-responsive neurons started firing significantly higher (two-tail paired *Student's t-tests*, 5% alpha level) in the *PT flash* condition at the 100-ms bin centered respectively at -430 and -410 ms

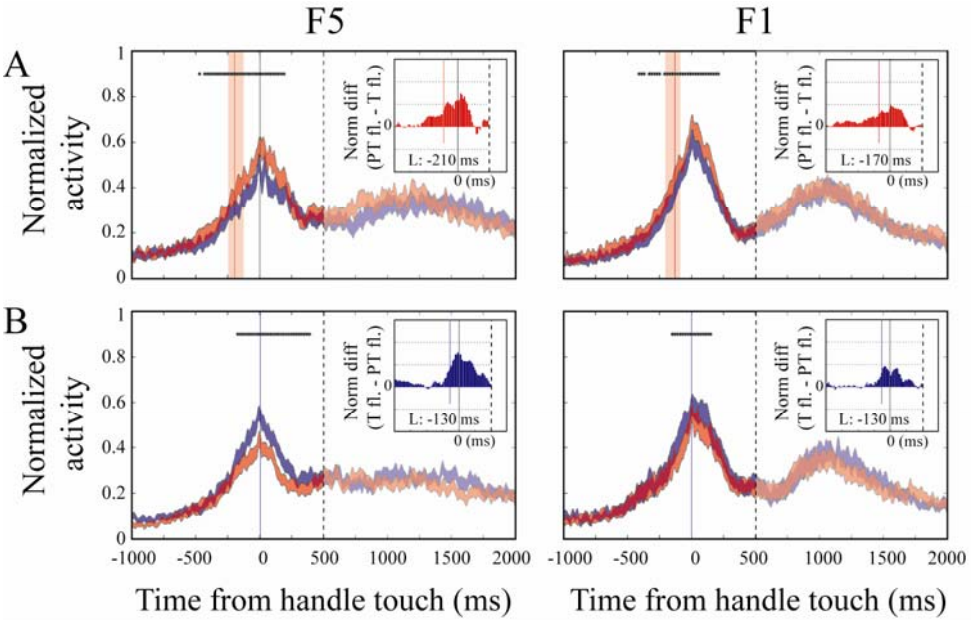

Figure 10. Average activity of flash-responsive neurons in area F5 and F1. Activity in *PT flash* (red) is plotted vs. activity in *T flash* (blue) condition. A: *PT flash*-selective populations. Red dashed lines and red shaded areas respectively represent the median time of *PT flash* occurrence and respective interquartile range (-201 m, IQR = 115 ms in the F5 population; -133 ms, IQR = 113 ms in the F1 population). B: *T flash*-selective populations. Blue dashed lines represent the time of T flash occurrence (always at 0 ms). Other conventions as in Fig. 7A.

Inset plots show time course of population normalized *flash*-related discharge differences, computed on a sliding 100-ms bin, shifted through the first 1500 ms in the trial by 20-ms steps. Latency of flash-selectivity (calculated as the time to half-maximum difference in activity) is represented by the L-labeled dashed line within each plot. Flash-selectivity latency of both F5 and F1 *PT flash*-responsive populations (bin centered at 210 and 170 ms before touch, respectively) was shorter than that of F5 and F1 *T flash*-responsive populations (bin centered at 130 ms before touch, in both plots). X- and y-axis scales as in Fig. 7B.

before handle touch, even well in advance of flash delivery, respectively occurring at around -201 ms and -133 ms. This latter difference in flash presentation was related to the fact that F5 neurons were recorded from both hemispheres of the same monkey, forced to reach and grasp first with the right and then with the left hand, and that left-hand movements were much slower than the right-hand ones (details concerning the time of *PT flash* presentation are reported in Table 1). In contrast, the first time window in which both the F5 and F1 *T flash*-responsive groups showed significantly enhanced *T flash* activity was respectively centered at -170 and -150 ms. In this case, flash selectivity was observed much later than in the *PT flash*-selective populations, though again clearly before the hand-handle contact, triggering *T flash* presentation (occurring at 0 ms). This anticipatory flash-related response of the neurons was likely dependent on the experimental design, implying a blocked presentation of conditions, so that the time of flash presentation within one specific flash trial block could be expected, and thus predicted. The difference in latency of the two specific flash-

related modulations was confirmed by computing the time to half-maximum divergence in activity between the two flash conditions, which was shorter for the *PT flash*-responsive neurons (F5: -210 ms; F1: -170 ms, see inset plots in Figure 10A) than for those specifically sensitive to *T flash* (F5: -130 ms; F1: -130 ms, see inset plots in Figure 10B).

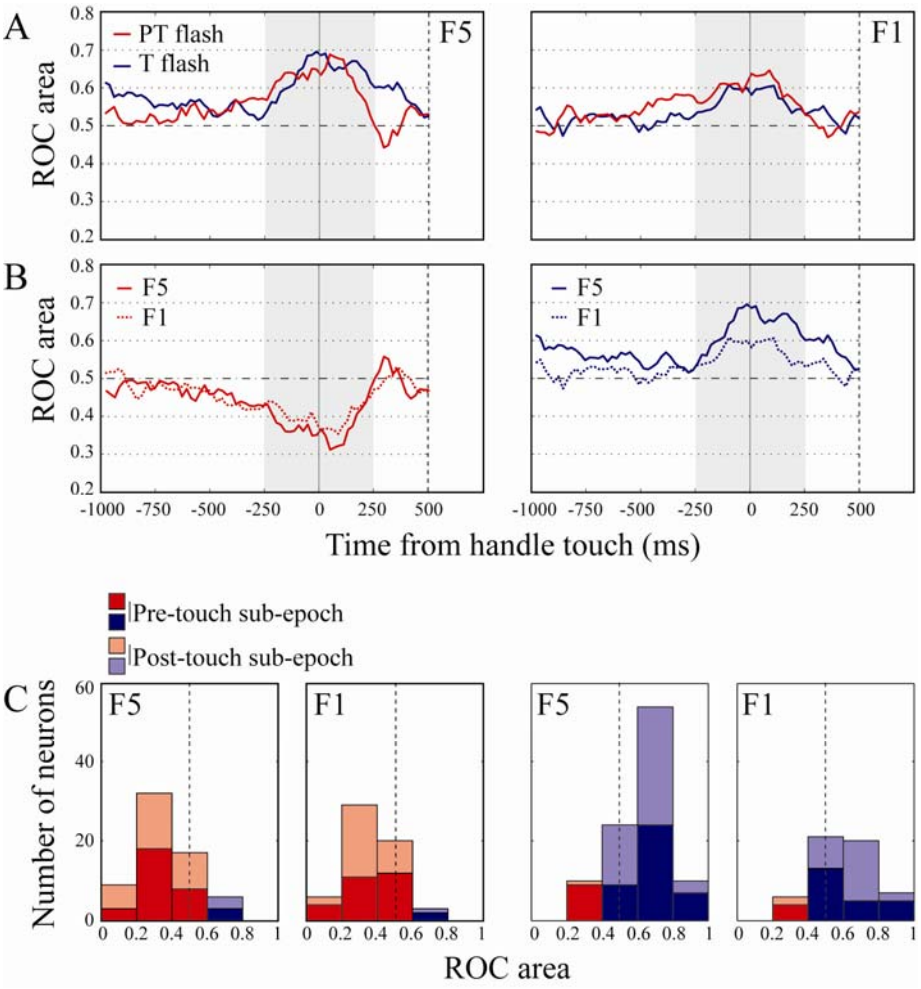

Figure 11. A: Time course of ROC values for *PT* (red) and *T* (blue) *flash*-selective neuronal groups in area F5 and F1. The first 1500 ms of activity aligned to time of handle touch (solid line) are shown. Traces are obtained averaging across neurons the area under the ROC curve, computed every 20-ms step and comparing *PT flash* and *T flash* firing rates in a 100-ms bin covering all the trial. Both traces are represented with positive ROC values to better contrast them. B: Same traces as in (A) but grouped according to type of flash selectivity (left plot: *PT flash*-responsive neurons; right plot: *T flash*-responsive neurons), to emphasize differences between areas. C: Histograms showing the distribution of single-neuron ROC area values in both *pre-touch* (dark blue and dark red) and *post-touch* (pale blue and pale red) sub-epochs within *PT flash*- and *T flash*-responsive groups recorded from the two brain regions. ROC areas greater than 0.5 (blue) indicate neurons conveying more *T flash*- than *PT flash*-related information; ROC values less than 0.5 (red) represent neurons expressing the opposite effect. Note that the presence of bars of the opposite color within each plot is due to the criterion used for selecting flash-responsive neurons, not requiring selectivity through all *epoch 2* but at least in 2 consecutive 100-ms bins of it.

Close examination of the time course of the modulations, as processed by the ROC analysis (Fig. 11A), revealed a clear-cut temporal shift of the flash effects in area F5, specifically depending on the time of flash presentation (Fig. 11A: compare ROC for F5 *PT flash*-selective neurons, in red, and ROC for F5 *T flash*-selective neurons, in blue). The time course of *PT flash*-related selectivity was characterized by a gradual increase during the pre-shaping phase of grasping, followed by a fast decay immediately after touch. Conversely, *T flash*-related selectivity increased rapidly before touch, reached the highest value at the hand-handle contact and declined slowly in the *post-touch* sub-epoch, persisting throughout the final phase of grasping. According to the running *t-test* analysis, the *PT flash* effect became manifest 260 ms earlier than the *T flash* effect; likewise, it also disappeared 200 ms earlier (the *PT* and *T flash* last significant bins were respectively centered at 190 ms and 390 ms after touch, see Fig. 10A).

The latencies of *PT* and *T flash* signals in area F1 showed a time lag (200 ms) comparable to that observed in the activity of F5 flash-responsive neurons. However, in contrast to F5, F1 *T flash* effect was more temporally locked to the handle touch instant, decaying 60 ms earlier than the *PT flash* effect (see Fig. 10B and Fig. 11A).

Flash-related signals were stronger in area F5 than in area F1

Flash-related information conveyed by F5 neurons within *epoch 2* was overall higher than that of F1 neurons, especially considering *T flash* selectivity. This was visible when comparing the time course of ROC values of the flash-responsive groups recorded from the two brain regions (Fig. 11B).

PT flash-selectivity in F5 was overlapping in strength that of F1 during the pre-movement period (*epoch 1*); then, around 250 ms before handle touch, it reached a higher level which was maintained for all the *pre-touch* sub-epoch and till about 100 ms after touch. Even more evidently, *T flash*-selectivity in F5 started increasing approximately at the same time (-250 ms) as the one observed in F1, nevertheless diverging considerably from it around 100 ms prior to hand-object contact. This ROC area difference then remained through all *touch* and *post-touch* sub-epochs, only decaying after the grasping movement was concluded (at around 450 ms after touch). Accordingly, although overall not statistically different (*Student's t-test*, 5% alpha level), the ROC area values expressed by F5 *T flash*-selective single neurons were higher than those measured in the *T flash*-responsive population of F1, both during the *pre-touch* (F5, 0.623 ± 0.028; F1, 0.594 ± 0.034) and the *post-touch* (F5, 0.644 ± 0.019; F1, 0.616 ± 0.03) sub-epochs (Fig. 11C). Seemingly, average ROC area measured in *PT flash* neurons was higher in area F5 (*pre-touch* sub-epoch: 0.364 ± 0.025;

post-touch sub-epoch: 0.354 ± 0.032) than in area F1 (*pre-touch* sub-epoch: 0.376 ± 0.029; *post-touch* sub-epoch: 0.36 ± 0.027).

F5 and F1 flash-selective neurons were overall not light-responsive

The majority of both F5 and F1 flash-selective neurons did not show any significant light responsiveness. Only a small fraction of *PT flash*-responsive neurons (2% in both F5 and F1 area) and *T flash*-responsive neurons (5% in F5 and 6% in F1) displayed significantly higher firing rates in full light than in full dark and mainly during the *pre-touch* sub-epoch (see Table 4). Therefore, flash-selective neurons formed relatively mixed populations with regard to the behavior they expressed in *L* and *D* conditions, with a relevant portion of them pertaining to non-selective or *D>L* populations (overall, 21% and 11% in F5 and F1, respectively). Figure 12 shows the average activity of each flash-selective population in all four experimental conditions along the trial.

To better weight the flash selectivity of these populations against the activity shown in *D* and *L* conditions, a one-way ANOVA with *condition* (*D*, *L*, *PT flash* and *T flash*) as factor was performed on the response of each flash-responsive neuron acquired during the epoch *(epoch 2*), in relation to which flash-selectivity was determined. A large amount of both F5 (37/81: 46%) and F1 (31/56: 55%) *flash*-selective neurons showed significantly higher firing rates in the *flash* condition for which they were selective than in both *D* and *L* condition, as well as than in the other flash condition.

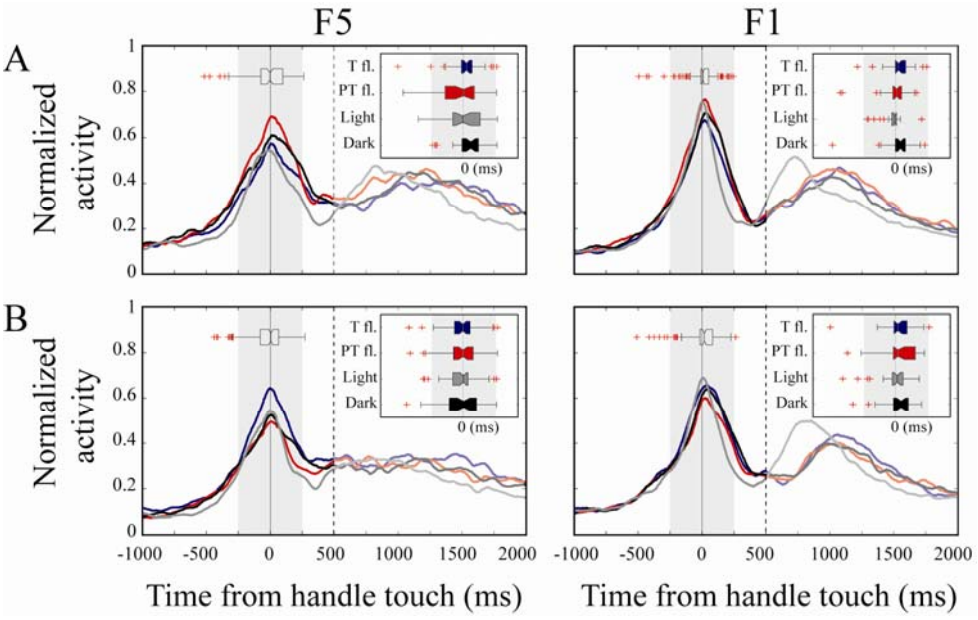

Figure 12. Average activity of flash-responsive neurons in area F5 and in area F1. Activity is aligned to time of handle touch (solid line). Population spike density plots are obtained by first normalizing the single-neuron smoothed data (Gaussian kernel function with window width set to 100 ms, to better emphasize the neuronal response profile) to the absolute maximum level of activity observed across all 4 different conditions and then averaging the result across all

units in the populations. Average activity in *PT flash* (red), *T flash* (blue), *L* (grey) and *D* (black) conditions is plotted for each group. A: *PT flash*-selective populations. Box plots on top indicate the temporal distribution of the discharge peaks of the neurons within a population. The distance between left and right limits of the box define inter-quartile range (IQR) of the sample, which is a robust estimate of the dispersion of the data. The line in the middle is the sample median, whiskers represent the extent of the rest of the data and red crosses are outliers. Inset plots show the temporal spread of the discharge peaks of each flash-selective group in the four conditions. IQR details are given in table 5. Grey-shaded areas represent *epoch 2* on which the one-way ANOVA (see main results in Fig. 13A) has been performed.

The same analysis was performed also at the population level. Figure 13A illustrates the main statistical results: *PT flash*-responsive neurons of both areas F5 and F1 (left bar groups in the respective plots) showed the strongest grasping response during the *PT flash* condition (firing rates recorded during the other experimental conditions were significantly lower; $P < 0.05$, ANOVA LSD post-hoc tests). In addition, F5 *PT flash*-selective neurons fired significantly more in full dark than in full light ($t = 3.4$, $P = 0.002$) or when a light flash was delivered at the handle touch ($t = 2.6$, $P = 0.01$). F1 *PT flash*-selective neurons showed a significant *D>L* effect ($t = 2.1$, $P = 0.04$) as well. Similarly, *T flash*-related discharge of the F5 *T flash*-responsive population (Fig. 13A, F5 right bar group) was much higher compared to the activity displayed by the same neurons in *L*, *D* and *PT flash* conditions ($P < 0.0001$). Conversely, F1 *T flash*-selective neurons (Fig. 13A, F1 right bar group) only showed a significant difference between the two flash conditions ($t = 5.5$, $P < 0.0001$).

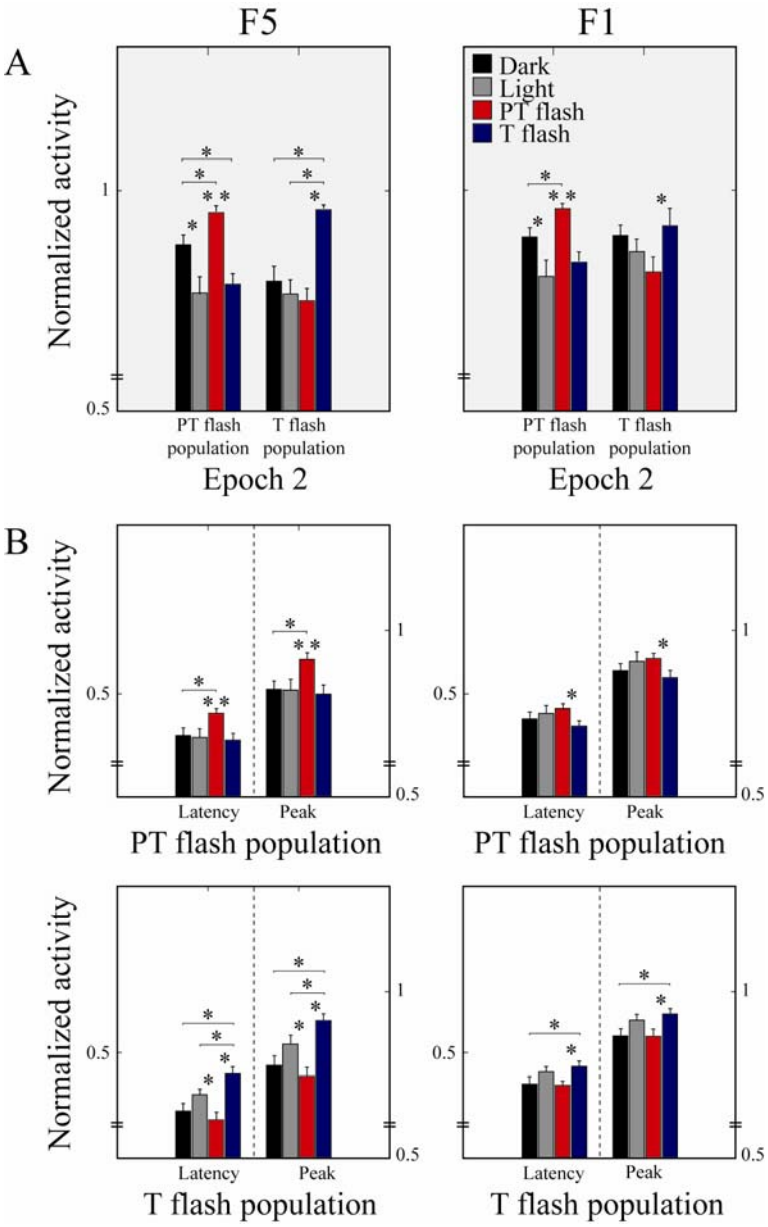

Figure 13. Average activity of *PT* and *T flash*-responsive neurons in area F5 and F1, both during *epoch 2* (A) and at the time of maximum (*Peak*) and half-maximum (*Latency*) discharge (B) in the four experimental conditions. Asterisks on top of bar plots indicate main significant differences among conditions ($P < 0.05$, LSD post-hoc tests, subsequent to significant one-way ANOVA *condition* main effect).

Flash-related signals were more specific in area F5 than in area F1

When looking at the population plots of the flash-selective neurons in the two recorded areas (Fig. 12), the following interrelated considerations can be drawn: first, the ANOVA results just described do not exactly reflect the level of neuronal activation expressed by the different populations in the grasping period of the four conditions, as it appears in the plots (see activity within shaded areas in Fig. 12). More precisely, the mean neuronal discharge in *epoch 2* (Fig. 13A)

does not seem to be the appropriate measure to explain the differences among conditions in the neurons' grasping-related response profiles, particularly in the case of area F1.

Second, the average response profile of the neurons assigned to the different flash-responsive groups varied a lot across areas and conditions. In particular, if considering the temporal distribution of the neurons' discharge peaks as an index of the population response profile variability (see Table 5 and inset box plots in Fig. 12), flash-selective cells of area F5 exhibited, on average, a rather spread-out grasping-related response (IQR = 144 ms), as opposed to the more compact one of the F1 flash-selective neurons (IQR = 71.5 ms). A dispersion test (*Ansari-Bradley test*, 5% alpha level) applied to F5 and F1 peak distributions revealed that the peaks dispersion was significantly different in the two areas ($W^* = 5.8$, $P < 0.0001$), particularly when contrasting the F5 and F1 *PT flash*-selective populations (IQR = 161 ms and 56 ms, respectively; $W^* = 7.3$, $P < 0.0001$). In contrast, the temporal dispersion in the activity peaks of the non-flash-responsive neurons was comparable in the two areas (F5 IQR = 125 ms; F1 IQR = 122.5 ms; $W^* = 1.1$, n.s.). Most importantly, the average response profile displayed by F5 flash-selective neurons across conditions specifically varied according to the flash condition for which they expressed selectivity (see inset box plots relative to area F5 in Fig. 12A and 12B). In particular, the firing dispersion shown by the F5 *PT flash*-responsive neurons in the *PT flash* condition (IQR = 214 ms) was significantly greater than that calculated in the same neurons during the *D* (IQR = 120 ms; $W^* = 2.1$, $P = 0.04$) and *T flash* (IQR = 78 ms; $W^* = 2.9$, $P = 0.003$) conditions. Conversely, the discharge peaks of the F5 *T flash*-selective neurons were consistently less dispersed in the *T flash* condition (IQR = 114 ms) than in the *D* (IQR = 199 ms; $W^* = 1.9$, $P = 0.05$) and *PT flash* conditions (IQR = 144 ms; $W^* = 1.1$, n.s.). Importantly, in both *PT* and *T flash*-responsive populations, the discharge peaks distribution observed during the flash condition for which the neurons were selective approached that assumed in the *L* condition (IQR = 199 ms and IQR = 112

Table 5. Temporal distribution of the discharge peaks of *PT* and *T flash*-selective populations in area F5 and F1. Median and inter-quartile range (IQR) are reported for each condition.

		Peak IQR (ms)	
		F5	**F1**
Flash-selective neurons		144*	72
PT flash-selective		161	56
	Dark	120**	73****
	Light	199	34
	PT flash	214	65****
	T flash	78**	75****
T flash-selective		134	93

	Dark	199	108
	Light	112***	79
	PT flash	144	160****
	T flash	114***	96
Non-selective neurons		125	123

* Significant difference (*Ansari-Bradley test* for samples with different dispersions, 5% alpha level) between F5 and F1 flash-selective neurons.

** Significant differences with respect to *PT flash* condition within the same neuronal population.

*** Significant differences with respect to *Dark* condition within the same neuronal population.

**** Significant differences with respect to *Light* condition within the same neuronal population.

ms, respectively), which, in turn, differed substantially from that measured in the *D* condition (for details, see Tab. 5).

Opposite to what observed in area F5, the average response distribution of F1 flash-selective neurons in the flash condition on which they conveyed information was not significantly different from that of the *D* condition. Independently of the specific F1 flash-responsive population they were assigned to, these neurons showed firing peaks with similar temporal dispersion in the *PT flash*, *T flash* and *D* conditions. In all three conditions, a more spread-out neuronal response profile was observed, compared to that measured under full light conditions (see inset box plots relative to area F1 in Fig. 12A and 12B and Table 5).

Given these remarks, in order to have a more detailed picture of the grasping-related behavior of each specific neuronal population during the different experimental conditions, the following additional analyses were carried out: first, a one-way repeated-measure ANOVA was used to reveal differences in the absolute peak discharge values reached by the neurons within each condition. Main results are summarized in Figure 13B. For completion, firing rate differences among conditions assessed at the time to half-maximum activity (referred to as the latency) of the neurons are also reported for each population. As far as the *F5* flash-selective populations are concerned, this analysis confirmed the ANOVA results obtained considering all *epoch 2* (Fig. 13A). In addition, it revealed a significant *L>PT flash* effect in the mean latency ($t = 2.4$, P = 0.02) and peak ($t = 2.4$, P = 0.02) activity of the *T flash*-selective neurons, emphasizing the strong *T flash* information carried by this population, also due to the suppression of the *PT flash*-related signal. On the contrary, the F1 flash-responsive groups did not show any distinct peak predominance of the specific flash condition for which they showed selectivity over all the other conditions, especially in the case of *PT flash*-selective neurons. *Touch flash* maximum activity of F1 *T flash*-responsive neurons was higher than that of *PT flash* and *D* conditions (P < 0.01), but not significantly different from that measured in the *L* condition ($t = 1.4$, P = 0.2).

Second, to evaluate the average peak response in each condition also taking into account the corresponding population temporal peak distribution, the peak discharge of each neuron was weighed to the peak times of all the other neurons belonging to the same population (see *Methods*). A further one-way ANOVA was then used to test the differences among the new peak-related weighed values calculated for each condition. Main results are illustrated by bar plots in Figure 14. This analysis returned an important result regarding the *PT flash*-responsive neurons in F5. Contrary to what was obtained in the previous statistical analyses, the average weighted maximum response computed in the *PT flash* condition was not significantly higher than that measured in the *D* condition (see Fig. 14, *Latency* and *Peak* of the F5 *PT flash* population). However, as reported above, this neuronal group was the only one to show an increase, rather than a decrease, in the temporal dispersion of the firing peaks during the flash condition for which selectivity was conveyed. This evidence, besides suggesting that the appearance of a light flash during the hand

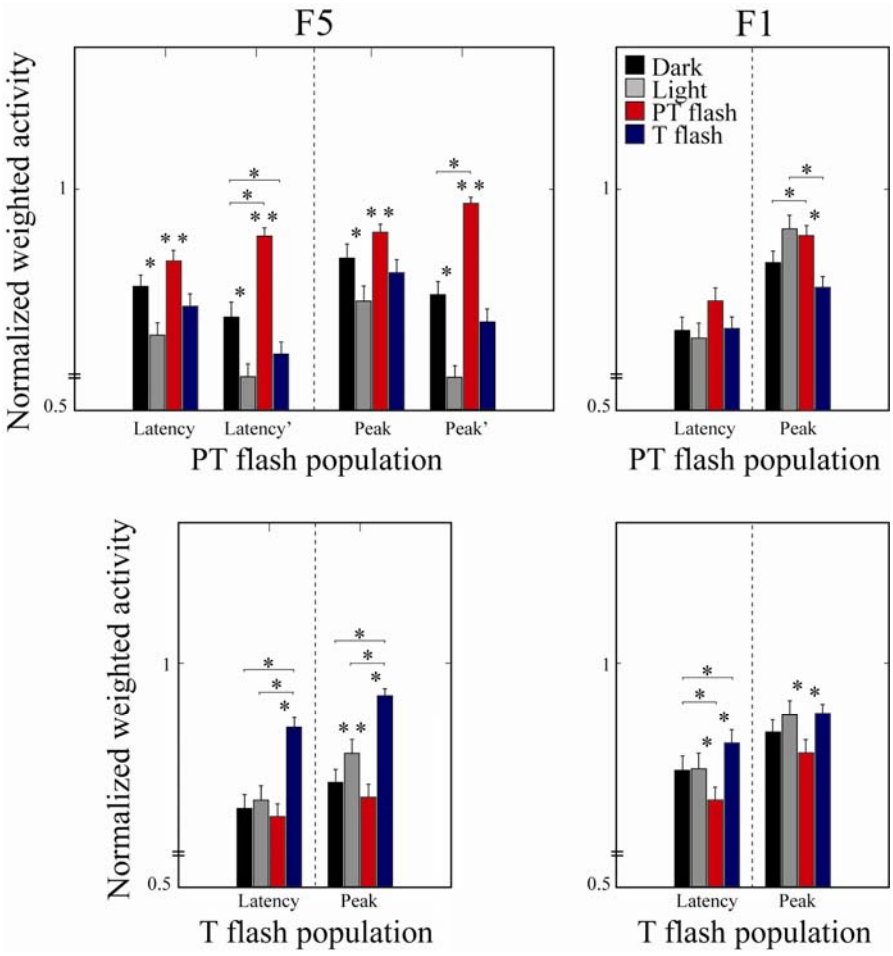

Figure 14. Average normalized activity of *PT* and *T flash*-responsive neurons of area F5 and F1, weighted to the time of maximum (*Peak*) and half-maximum (*Latency*) discharge displayed by all the neurons in the population in the four experimental conditions. Asterisks on top of bar plots indicate main significant differences among conditions ($P < 0.05$, LSD post-hoc tests, subsequent to significant one-way ANOVA *condition* main effect). *Latency'* and *Peak'*: average

discharge latency and peak of F5 *PT flash*-selective population, after that the firing temporal distribution within each condition has been leveled to that of *PT flash* condition, i.e., the most dispersed one.

shaping phase of grasping principally affected F5 recorded cells inducing a larger discharge timing variability (that can thus be considered a hallmark of the response of area F5 to *PT flash*), implied that the average peak discharge of the F5 *PT flash*-selective neurons was particularly lowered in the *PT flash* condition, where the highest data dispersion was detected. Indeed, by making the population homogeneous from the aspect of the firing temporal dispersion (i.e., by leveling the peaks distribution exhibited in each condition to the largest observed, that of *PT flash* condition), a strong *PT flash*-selectivity came out (see Fig. 14, *Latency'* and *Peak'* of the F5 *PT flash* population).

To summarize the results obtained with the last described analyses, the presence of a transient visual feedback on the own ongoing action strongly influenced the response of F5 neurons (and much more than that of F1 neurons) in the following ways: (1) the activity recorded during the delivery of the relevant light flash for a given flash-selective population was consistently higher compared to that expressed in all the other experimental conditions, including full light (on the whole, F1 flash-related firing rates did not rise above *L*-related discharge in neither population).(2) This strong flash-selectivity was evident both when comparing the absolute peak discharge reached by the neurons in each condition and the single-unit maximum activity counted against the time of peak discharge of all the neurons in a given population. (3) On average, F5 neurons, as opposed to F1 neurons, maintained their flash-selectivity well before and after arriving at the peak activity, as shown by the analysis carried out contrasting the mean firing rates during all the 500-ms grasping window of each condition. (4) F5 *PT flash*-selective neuronal group reacted to *PT flash* presentation rearranging their grasping-related response in a more distributed way (see difference between temporal peak IQR of these neurons and that measured for all the other F5 and F1 flash- and non-flash-selective populations in Tab. 5).

DISCUSSION

The present study investigates whether ventral premotor area F5 contains visuomotor neurons which do not show any visual response associated to the observation of 3D objects (canonical neurons) or to actions performed by other individuals (mirror neurons), but rather, are sensitive to the observation of the monkey's own hand during an ongoing grasping movement. These neurons, which we proved to be present, exhibit visuomotor properties that are common to both purely motor and mirror neurons, hence allowing new speculations on the critical role of online visual information during grasping execution and on the nature/genesis of the mirror neuron visual response. Indeed, both in area F5 and in primary motor cortex (area F1) a significant percentage of neurons modulate their grasping-related activity as a function of the duration (continuous or transient) and of the instant (hand preshaping- or hand-object contact) of the hand-related visual feedback. The effects observed in these two motor areas present some important differences, suggesting a distinct functional contribution of the ventral premotor and primary motor cortices to the analysis of motor-relevant visual feedback.

Both F5 and F1 neurons potentiate their motor activity during hand shaping in light, but F5 neurons show a faster increase of light-related responses

By comparing the grasping-related activity of the neurons during light and dark conditions, a variety of neuronal categories could be distinguished, both in area F5 and in area F1, depending on the time course of their modulation. The main modulation was mostly due to a more prolonged activity when the monkey was grasping in dark, with respect to full vision condition. For example, while a large amount of neurons in both areas displayed overlapping pre-touch responses both in light and dark, they differentiated their response in the post-touch phase, mainly because of the contrast between the rapid firing decay observed in light and the more long-lasting activity characterizing the post-touch phase in dark. This neuronal behavior, that statistically produced a post-touch *D>L* effect, was rather likely related to finger posture corrections ensuing proprioceptive feedbacks from the hand-object contact in the dark, as we observed in some pilot kinematics experiments. However, being the aim of our study the detection of neurons sensitive to the vision of the own grasping hand, we concentrated on neurons that, in full light, potentiated their discharge within the period preceding the contact with the to-be-grasped object. This neuronal class was the most represented one, both in area F5 (14%) and in area F1 (13%). This result is particularly relevant since, although visual information on the own ongoing action was continuously achievable in the light condition, the activity of the majority of light-responsive recorded neurons was mainly

affected by it during hand pre-shaping and landing onto the object. We will therefore comment now in detail some properties of these pre-touch light-responsive neurons.

While the percentage of these neurons was similar in the two motor areas, both in terms of time course and in terms of light-responsiveness, an important timing difference characterized the grasping-related response of the F5 sub-population in the light condition. When the reach-to-grasp task was performed under constant online visual feedback, the latency and peak times of the discharge were significantly shorter than those observed during the execution of the same task in absence of any visual information. Conversely, F1 neurons did not show any anticipation of the grasping response recorded in light with respect to that recorded in the dark. These visuomotor neurons resemble those previously described in area AIP (Murata et al. 2000; Sakata et al. 1995) which have been suggested to play some role in encoding the pattern of hand movements during handgrip formation. The light-sensitive neurons reported in the present work, as well as the AIP "nonobject-type" neurons, did not respond to object presentation, as shown by the naturalistic testing and by the absence of any response to the mere observation of the to-be-grasped object during the formal testing.

The present findings concerning pre-touch light-dependent neuronal effects can be actually subjected to more than one specific interpretation, including, first of all, the critical influence that the online visual feedback may exert on grasping kinematics. Indeed, although the experimental apparatus was designed so as to minimize at best hand movement variations between light and dark conditions (the to-be-grasped object was made visible also in the dark), analyses carried out on the kinematic trajectories recorded during the behavioral experiment revealed some crucial, though subtle, differences between the two conditions. As reported in literature (Churchill et al. 2000; Schettino et al. 2003; Winges et al. 2003), an increase in the duration of the deceleration phase and of finger closing was found when grasping was performed in the dark. Moreover, maximum grip aperture became wider, indexing that, without vision, the monkey tended to increase the grip size safety margin for grasping the door handle successfully (Rand et al. 2007).

Consistent with these findings might be the evidence that neurons of both areas enhanced their activity just in the pre-shaping phase of the light condition. Even more relevant could be the temporal gain that pre-touch light-selective F5 neurons showed in their motor response, when the sight of the ongoing movement was allowed, compared to when it was not. This facilitation was mainly expressed as a faster rate of ramping activity of these neurons in full light, as opposed to the slow, gradually increasing firing rates during the pre-touch phase in dark. Accordingly, a 50-ms anticipation of the light over dark was measured both at the latency and peak of the grasping-related neuronal response. These F5 light-dependent timing effects, which most likely finally ended with

the strengthening of the pre-touch discharge shown by F1 neurons during light, well inversely correlate with the longer grasping approach, adopted by the monkey in the final part of reaching-grasping in absence of any visual feedback. The behavior expressed by many neurons in anticipating their motor response under full light condition (16% in F5 and 23% in F1), possibly associated with modifications of movement velocity, would well support the hypothesis that these data mostly relate to hand kinematics differences, than to observation-evoked responses. Even more generally, the finding that a higher percentage of neurons were strengthening (31%, including both areas), rather than diminishing (13%), their activity in the most critical period of the grasping movement (*pre-touch/touch* period) during light, appears to favor this interpretation. It is thus arguable that, these visuomotor cells could be present in both F5 and AIP, two strongly interconnected areas, and might form a sub-circuit specifically relevant to visual feedback-based adjustments of the handgrip during movement. More direct evidence is however required to support this hypothesis, based on systematic studies of the correlation between hand kinematics and neuronal activity.

Another possible account for the light-modulated grasping response of these neurons is that it may represent one of the many instances of the observation-evoked motor activation that is typical of mirror neurons. Indeed, it has been demonstrated that the F5 mirror visual discharge can reflect the neuron's motor selectivity at several degrees of abstraction (Nelissen et al. 2005; Gallese et al. 1996; di Pellegrino et al. 1992). Recently, also single-neuron activity in area F1 has been shown to be similar during both execution and passive observation of a familiar task. Interestingly, in the observation condition, F1 neurons fired in response to the view of a reliable surrogate of the monkey's own hand (a visual cursor projected on a screen), moving in an abstract workspace (Tkach et al. 2007).

In our study, monkeys were observing their own, as opposed to others' (co-specific or human), *active* movements. In this particular case, the action which the cells contribute to generate, perfectly matches the one potentially evoking a neuronal response in the same cells through observation. Hence, because mapped on the same active movement, the discharge elicited by observation is not easily dissociable from the one related to execution. It is thus plausible that, to be appreciated, any neuronal activation potentially induced by the vision of the own grasping movement, must be almost exclusively represented by an increase (or decrease) in light, of the activity recorded during grasping execution in dark, as in the case of the light-responsive neurons described here. However, the observation-related meaning of such a modulation cannot be distinguishable from a kinematics effect

Both F5 and F1 neurons selectively respond to motor-relevant transient visual feedbacks, but area F5 shows a higher specificity for the type of grasping-related information they bring

To exclude any influence of kinematics on the observation-dependent responses of the recorded neurons, two light flash conditions were introduced in our experiment. No substantial hand kinematic difference was indeed found between the two flash and the full dark conditions. Conversely, several recorded neurons displayed specific selectivity for either of the two light flash conditions, suggesting that the behavioral paradigm succeeded in revealing neuronal effects dependent on the vision of brief fragments of the own grasping action. Specifically, a large number of both F5 (48%) and F1 (43%) cells statistically showed a difference in the grasping-related activity, dependently of whether transient visual information was fed back from the handgrip configuration period or hand-object contact instant. Importantly, the latency of flash-selectivity displayed by these neuronal populations tightly reflected the point in time of flash occurrence, that is, earlier in the trial when visual feedback was given during pre-shaping, with respect to when it was delivered at the handle touch. One possible criticism may be that the found neuronal modulations rather depended on an arousal effect, time-locked to flash presentation. Our results show that this was not the case.

First, since the analysis consisted in directly contrasting the activity displayed by the same cell in the two flash conditions, all neurons showing a significant response to both flashes (that could be indicative of an arousal reaction in the monkey) were automatically not taken into consideration. Second, the flash selectivity of the neurons did not generally emerge immediately after one given flash was delivered (that would suggest the existence of a strict temporal relationship between the arrival of a transitory visual event and the onset of the neuronal response); rather, it appeared at different times around flash presentation and, in some cases, even in advance of it, meaning that neurons were not only online signaling, but also 'expecting', the availability of the flashed motor-relevant visual information (the experiment was performed in blocks). Moreover, particularly in area F5, cells continued conveying this information well after flash offset, denoting that this was somehow a meaningful event, rather than simply a startling stimulus, for the animal engaged in performing the grasping movement.

It is also to note that the degree of overlap between any of the light-sensitive neuronal classes and flash-selective neurons was poor in both areas, supporting the assumption that the neuronal modulations due to continuous vision of the movement were, in all probability, of a different kind with respect to those observed during brief illumination of the motor action scene. In particular, since kinematics and arousal are not to be considered important confounding variables,

the hypothesis that flash-related sensitivity represented the selective response of the neurons to the observation by the monkey of its own ongoing grasping at specific time windows (when the view of the movement was briefly made accessible), can be strongly put forward.

The fact that observation-evoked responses were recorded also in the primary motor cortex is not surprising. Significant changes in M1 cortical activity during action observation have been reported by several human studies, using different techniques (Fadiga et al. 1995; Muthukumaraswamy and Johnson 2004; Caetano et al. 2007; Cheng et al. 2007). In addition, the study mentioned above (Tkach et al. 2007) has tackled the issue of observation-related M1 activation at the single-unit level, describing neuronal discharge and local field potentials associated with the passive view of own movements.

However, the detailed analysis of the visually-modulated activity of the neurons recorded in the present research revealed that F1 flash-evoked neuronal effects differed from those found in F5 as far as some critical features are concerned. First, the level of flash selectivity, defined as the relative difference in the neuron's grasping activity between the two flash conditions, was lower in area F1 than in area F5. More relevant, the signal related to transient action observation brought by F1 neurons was in general not significantly stronger than the one they showed under continuous visual feedback conditions. In contrast, F5 neurons exhibited the maximal discharge in response to the delivery of the light flash which they were sensitive for, both at the peak and during the whole grasping time, suggesting that the visual information conveyed by the brief enlightenment of the hand movement was extremely efficient in strengthening the ongoing motor activity of these neurons.

Moreover, population analyses showed that the pattern of activation of F5 neurons was highly specific for the type of visual feedback received. In particular, the transient observation by the animal of its own movement during the handgrip configuration phase of grasping, besides augmenting considerably the motor response of the neurons, specifically increased the temporal dispersion of the discharge peaks compared to the dark condition. Conversely, the F5 population selectively active in the final period of grasping, when the monkey could briefly look at its own hand contacting the door handle, displayed a more temporally compact distribution of the neurons' firing peaks. Interestingly, a comparable firing dispersion was displayed by these populations during grasping performed in full light, whereas in the flash condition for which no selectivity was shown, the behavior of the same neurons moved towards the opposite distribution trend, approaching that taken on in absence of any visual feedback. Hence, the same visual stimulus, presented at different critical stages of the grasping action, differentially affected F5 neuronal response. This suggests that the possibility of transitorily access the view of meaningful bits of the

own ongoing action, online specifically reinforced the motor program used to execute that particular action. The computational study of motor control has provided important working principles concerning the relationship between sensory signals and motor commands. It is currently thought that the motor system is governed by two main internal processing models, also called predictors, which control the causal link between actions and their consequences (Wolpert and Ghahramani 2000). Inverse models implement the transformation from the desired consequences (i.e., the goal) of an action to the motor commands necessary to execute that action. Any form of motor pre-programming, as in the case of the present reach-to-grasp task, implicitly involves this inverse relationship. Forward models, instead, monitor the state of the current motor commands by continuously predicting the consequences of them, through sensory feedback from the periphery. Thereby, forward models can support sensorimotor control by minimizing sensory and motor noise in many ways, including integrating, invalidating or anticipating the kind of sensory inflow that constantly update predictions (Miall 2003; Bays and Wolpert 2007).

In the context of the present experiment, for instance, estimation of the state of the system could have supplemented noisy or absent visual information during grasping in full dark, or generated the appropriate adjustment signals for online grip control after, or in advance of, a visual reafference from the transient observation of the action during flash delivery. Indeed, the enhancement of motor activity in the flash-selective populations in response to the brief illumination of the grasping hand might be the result of forward predictions, intervening over the ongoing inverse sensorimotor transformation for handle grasping. In addition, the increased timing variability in the firing peaks of the neurons (measured during the brief view of the own hand before the contact with the handle) might be directly reflecting the uncertainty of handgrip estimation and thus be related to the error signal produced to fast rearrange the posture of the fingers with respect to the target. Conversely, the compacted strengthened discharge of the neurons, in response to the sight of the handle touch instant (a grasping event that is perceptually and temporally more defined than pre-shaping and hence, more easily predictable) might be indicative of a reinforcement signal, confirming the correct forward estimation of the state of the system at that point of grasping.

Taken together, these results confirm that area F5 contains visuomotor neurons which are specifically activated by the transitory observation of meaningful phases of the own grasping movement. Moreover, to a minor extent, similar effects are shown to be present also in area F1.

Turning to the issue, initially addressed, of the nature of the visuomotor coupling at the basis of the mirror response, what then might be the role of these F5 neurons, showing these peculiar visuomotor properties? How can these findings be interpreted in the framework of a theory

supposed to explain the development of mirror neurons? Finally, what might be the functional interplay between F5 and F1 neurons displaying observation-evoked motor responses of the kind described by our work?

Interpretational issues

It has been suggested that mirror cells, originally described in area F5, lie at a crucial interface between inverse and forward models (Iacoboni et al. 2005; Carr et al. 2003). Connections from STS to PF, and frontward to mirror neurons in F5, would represent an inverse model mapping the visual description of actions onto the motor commands that are needed to execute them. The reverse projections from F5 to PF and backward to STS would instead correspond to a forward model translating the actual motor plan into a predicted sensory representation of it. This two-way model could be responsible for the activation of mirror neurons during both action execution and observation. However, though very elegant, this scheme presents some contradictory points.

First, the predictions made by forward models are, by definition, very specific, as they are to provide the motor system with helpful information to constantly control movement outcome. On the other hand, F5 observation-related mirror responses are characterized by different levels of generality. Second, forward models originally imply that estimations about the current state of the motor system mainly involve our own actions, whereas the mirror visual discharge has never been described as concerning first-person motor action observation. The hyper-MOSAIC computational model developed by Wolpert et al. (2003) takes into account the former argument, proposing that multiple paired forward/inverse models act in parallel to estimate and control motor states at different hierarchical levels of abstraction (Wolpert et al. 2003). Whereas lowest levels would imply an extremely congruent matching between executed and observed actions, the highest layers would represent the behavioral goal of actions, unbounded from the specific motor effector or kinematic details of the action. Intermediate stages would progressively receive from previous layers, coding actions at increasingly more abstract levels. How the lowest layers of this architecture can be neuronally generated is not yet well understood. The visuomotor neurons described in the present study, for the fact that they receive facilitatory inputs activated by the sight of specific phases of the own action, thus showing perfectly matched execution- and observation-related activity, could be the most appropriate elements to underpin the lowest-level forward/inverse models. In addition, given that superior layers develop from these basic models, the discharge properties of these neurons might play a critical role in the generation of the mirror visual response. This gives support to the theory which asserts that the observation of the agent's own acting effector is a fundamental step in the biological process leading to neuronal activation associated to the observation of actions performed by others (Rizzolatti and Fadiga, 1998).

The hypothesis hereby proposed is that, through the forward models normally guiding action execution, the motor system progressively extracts motor-invariant (goal-related) visual signals from the repetitive experience of performing one given action from slightly different perspectives or under conditions implying variability in the availability of the visual information relevant to the action. These visual signals that continuously change, for instance, depending on the relative position of the head and the eye with respect to the acting hand or the target object, would be generalized by virtue of the fact that they are generated by very similar motor programs, all issued to achieved the same goal. Once this generalization process, that is supposed to play a relevant part not only during development but also during learning of new motor acts in adults, is sufficiently established, it would be then gradually transferred also to actions performed by others. In so doing, the visual representation of a given observed action would gain access to the corresponding motor representation due to the coherent action description that the observer has previously acquired through the visuomotor link concerning his/her own movements. In computational terms, the more similar the observer's hyper-MOSAIC is to the actor's hyper-MOSAIC, the easier it will be to make associations between them. These associations would be at the basis of the *recognition* operations played by F5 mirror neurons and the flash-related effects found in this study, confirming that in area F5 there exist neurons that specifically respond when the agent observes his/her own movement, would represent the mechanismthrough which visual signals mapped on the own motor programs are progressively acquired.

Additional experiments are required to more deeply explore this complex topic, such as studying the response of these neurons when visual information about the ongoing movement is disrupted and extending the testing to F5 mirror neurons. It is interesting to note that experiments performed in artificial robotic systems aiming at simulating the development of mirror neurons through the observation of one's own hand during execution of grasping (Metta et al. 2006; Craighero et al. 2007) seem to confirm this hypothesis.

Despite that many studies, principally conducted on humans, have reported observation-evoked responses also in primary motor cortex, there is to date no evidence about the existence of mirror neurons in this area. These F1 modulations have been proposed to be not functional but simply a reflection of the strong cortico-cortical interconnections with area F5 (Fadiga et al. 1995, Kilner and Frith 2007). It is well known that F5 can influence hand muscles via its dense projections to F1 (Dum and Strick 2005). Conditioning F5 stimulation results in significant facilitation of F1 corticospinal activity and, consequently, of responses in hand motoneurons (Cerri et al. 2003; Shimazu et al. 2004; Schmidlin et al. 2008). Hence, according to this interpretation, F1

modulation during action observation could be considered as an effect of the simultaneous strong activation of area F5. An alternative hypothesis is that F1 neurons might play a specific functional role, by representing the observed actions in a different coordinate system with respect to that used by F5. In particular, it might be that whereas F5 decodes the extrinsic features of the observed action (i.e., the relative positions of the hand and of the target in space), F1 describes the intrinsic pattern of muscle activation involved in the action, similarly to what is coded by the two areas during the actual action execution (Kakei et al. 2001). Specific experiments should be carried out to test both hypotheses. However, the poor action observation-related activation of F1 found in the present study, strongly suggests that it may be rather the reflective result of the highly significant modulation characterizing neuronal responses in F5.

Conclusions

By this work we demonstrate that ventral premotor area F5 contains visuomotor neurons selectively strengthening their motor response during continuous or transient vision of the monkey's own grasping movement. These findings confirm that F5, as well as area AIP in the parietal lobe, is crucial for the visual control of handgrip formation during grasping. Furthermore, our results lay the ground for a visuomotor theory about the generation of mirror neurons. The specific observation-evoked motor responses described here can be thought of as the key step for transferring the meaning attributed to our own movements to actions performed by other individuals, both during development and learning of new actions.

ACKNOWLEDGEMENTS

This work has been supported by EU Grants Mirror and RobotCub to LF

REFERENCES

1. **Bays PM and Wolpert DM**. Computational principles of sensorimotor control that minimize uncertainty and variability. *J Physiol* 578: 387-96, 2007.

2. **Bezdek JC, Ehrlich R and Full W**. FCM: Fuzzy C-Means Algorithm. *Computers and Geoscience* 10: 191–203, 1984.

3. **Caetano G, Jousmaki V and Hari R**. Actor's and observer's primary motor cortices stabilize similarly after seen or heard motor actions. *Proc Natl Acad Sci U S A* 104: 9058-62, 2007.

4. **Carr L, Iacoboni M, Dubeau MC, Mazziotta JC and Lenzi GL**. Neural mechanisms of empathy in humans: a relay from neural systems for imitation to limbic areas. *Proc Natl Acad Sci U S A* 100: 5497-502, 2003.

5. **Cerri G, Shimazu H, Maier MA and Lemon RN**. Facilitation from ventral premotor cortex of primary motor cortex outputs to macaque hand muscles. *J Neurophysiol* 90(2): 832-842, 2003.

6. **Cheng Y, Meltzoff AN and Decety J**. Motivation modulates the activity of the human mirror-neuron system. *Cereb Cortex* 17: 1979-86, 2007.

7. **Churchill A, Hopkins B, Ronnqvist L and Vogt S**. Vision of the hand and environmental context in human prehension. *Exp Brain Res* 134: 81-9, 2000.

8. **Craighero L, Metta G, Sandini G and Fadiga L**. The mirror-neurons system: data and models. *Prog Brain Res* 164: 39-59, 2007.

9. **di Pellegrino G, Fadiga L, Fogassi L, Gallese V and Rizzolatti G**. Understanding motor events: a neurophysiological study. *Exp Brain Res* 91: 176-80, 1992.

10. **Dum RP and Strick PL**. Frontal lobe inputs to the digit representations of the motor areas on the lateral surface of the hemisphere. *J Neurosci* 25: 1375-86, 2005.

11. **Fadiga L, Fogassi L, Pavesi G and Rizzolatti G**. Motor facilitation during action observation: a magnetic stimulation study. *J Neurophysiol* 73: 2608-11, 1995.

12. **Fogassi L, Ferrari PF, Gesierich B, Rozzi S, Chersi F and Rizzolatti G**. Parietal lobe: from

action organization to intention understanding. *Science* 308: 662-7, 2005.

13. **Fogassi L, Gallese V, Buccino G, Craighero L, Fadiga L and Rizzolatti G**. Cortical mechanism for the visual guidance of hand grasping movements in the monkey: A reversible inactivation study. *Brain* 124: 571-86, 2001.

14. **Fogassi L and Luppino G**. Motor functions of the parietal lobe. *Curr Opin Neurobiol* 15: 626-31, 2005.

15. **Gallese V, Fadiga L, Fogassi L and Rizzolatti G**. Action recognition in the premotor cortex. *Brain* 119 (Pt 2): 593-609, 1996.

16. **Gawne TJ, Kjaer TW and Richmond BJ**. Latency: another potential code for feature binding in striate cortex. *J Neurophysiol* 76: 1356-60, 1996.

17. **Gentilucci M, Toni I, Chieffi S and Pavesi G**. The role of proprioception in the control of prehension movements: a kinematic study in a peripherally deafferented patient and in normal subjects. *Exp Brain Res* 99: 483-500, 1994.

18. **Iacoboni M, Molnar-Szakacs I, Gallese V, Buccino G, Mazziotta JC and Rizzolatti G**. Grasping the intentions of others with one's own mirror neuron system. *PLoS Biol* 3: e79, 2005.

19. **Jackson SR, Jackson GM and Rosicky J**. Are non-relevant objects represented in working memory? The effect of non-target objects on reach and grasp kinematics. *Exp Brain Res* 102: 519-30, 1995.

20. **Jakobson LS and Goodale MA**. Factors affecting higher-order movement planning: a kinematic analysis of human prehension. *Exp Brain Res* 86: 199-208, 1991.

21. **Jeannerod M**. The formation of finger grip during prehension. A cortically mediated visuomotor pattern. *Behav Brain Res* 19: 99-116, 1986.

22. **Jeannerod M, Arbib MA, Rizzolatti G and Sakata H**. Grasping objects: the cortical mechanisms of visuomotor transformation. *Trends Neurosci* 18: 314-20, 1995.

23. **Kakei S, Hoffman DS and Strick PL**. Direction of action is represented in the ventral premotor cortex. *Nat Neurosci* 4: 1020-5, 2001.

24. **Kilner JM and Frith CD**. A possible role for primary motor cortex during action observation. *Proc Natl Acad Sci U S A* 104: 8683-4, 2007.

25. **Lewicki MS**. A review of methods for spike sorting: the detection and classification of neural action potentials. *Network* 9: R53-78, 1998.

26. **Liu Y and Rouiller EM**. Mechanisms of recovery of dexterity following unilateral lesion of the sensorimotor cortex in adult monkeys. *Exp Brain Res* 128: 149-59, 1999.

27. **Matelli M, Camarda R, Glickstein M and Rizzolatti G**. Afferent and efferent projections of the inferior area 6 in the macaque monkey. *J Comp Neurol* 251: 281-98, 1986.

28. **Metz CE**. Basic principles of ROC analysis. *Semin Nucl Med* 8: 283-98, 1978.

29. **Metta G, Sandini G, Natale L, Craighero L and Fadiga L**. Understanding mirror neurons: a bio-robotic approach. *Interaction Studies* 7(2): 197-232, 2006.

30. **Miall RC**. Connecting mirror neurons and forward models. *Neuroreport* 14: 2135-7, 2003.

31. **Murata A, Fadiga L, Fogassi L, Gallese V, Raos V and Rizzolatti G**. Object representation in the ventral premotor cortex (area F5) of the monkey. *J Neurophysiol* 78: 2226-30, 1997.

32. **Murata A, Gallese V, Kaseda M and Sakata H**. Parietal neurons related to memory-guided hand manipulation. *J Neurophysiol* 75: 2180-6, 1996.

33. **Murata A, Gallese V, Luppino G, Kaseda M and Sakata H**. Selectivity for the shape, size, and orientation of objects for grasping in neurons of monkey parietal area AIP. *J Neurophysiol* 83: 2580-601, 2000.

34. **Muthukumaraswamy SD and Johnson BW**. Primary motor cortex activation during action observation revealed by wavelet analysis of the EEG. *Clin Neurophysiol* 115: 1760-6, 2004.

35. **Nelissen K, Luppino G, Vanduffel W, Rizzolatti G and Orban GA**. Observing others: multiple action representation in the frontal lobe. *Science* 310: 332-6, 2005.

36. **Perrett DI, Harries MH, Bevan R, Thomas S, Benson PJ, Mistlin AJ, Chitty AJ, Hietanen JK and Ortega JE**. Frameworks of analysis for the neural representation of animate objects and actions. *J Exp Biol* 146: 87-113, 1989.

37. **Petrides M and Pandya DN**. Projections to the frontal cortex from the posterior parietal

region in the rhesus monkey. *J Comp Neurol* 228: 105-16, 1984.

38. **Rand MK, Lemay M, Squire LM, Shimansky YP and Stelmach GE**. Role of vision in aperture closure control during reach-to-grasp movements. *Exp Brain Res* 181: 447-60, 2007.

39. **Raos V, Umilta MA, Gallese V and Fogassi L**. Functional properties of grasping-related neurons in the dorsal premotor area F2 of the macaque monkey. *J Neurophysiol* 92: 1990-2002, 2004.

40. **Raos V, Umilta MA, Murata A, Fogassi L and Gallese V**. Functional properties of grasping-related neurons in the ventral premotor area F5 of the macaque monkey. *J Neurophysiol* 95: 709-29, 2006.

41. **Rizzolatti G, Camarda R, Fogassi L, Gentilucci M, Luppino G and Matelli M**. Functional organization of inferior area 6 in the macaque monkey. II. Area F5 and the control of distal movements. *Exp Brain Res* 71: 491-507, 1988.

42. **Rizzolatti G and Fadiga L**. Grasping objects and grasping action meanings: the dual role of monkey rostroventral premotor cortex (area F5). *Novartis Found Symp* 218: 81-95; discussion 95-103, 1998.

43. **Rizzolatti G, Fadiga L, Gallese V and Fogassi L**. Premotor cortex and the recognition of motor actions. *Brain Res Cogn Brain Res* 3: 131-41, 1996.

44. **Rizzolatti G, Gentilucci M, Camarda RM, Gallese V, Luppino G, Matelli M and Fogassi L**. Neurons related to reaching-grasping arm movements in the rostral part of area 6 (area 6a beta). *Exp Brain Res* 82: 337-50, 1990.

45. **Rizzolatti G and Luppino G**. The cortical motor system. *Neuron* 31: 889-901, 2001.

46. **Sakata H, Taira M, Murata A and Mine S**. Neural mechanisms of visual guidance of hand action in the parietal cortex of the monkey. *Cereb Cortex* 5: 429-38, 1995.

47. **Schettino LF, Adamovich SV and Poizner H**. Effects of object shape and visual feedback on hand configuration during grasping. *Exp Brain Res* 151: 158-66, 2003.

48. **Schmidlin E, Brochier T, Maier MA, Kirkwood PA and Lemon RN**. Pronounced reduction of digit motor responses evoked from macaque ventral premotor cortex after reversible inactivation of the primary motor cortex hand area. *J Neurosci* 28(22): 5772-83,

2008.

49. **Schmitzer-Torbert N, Jackson J, Henze D, Harris K and Redish AD**. Quantitative measures of cluster quality for use in extracellular recordings. *Neuroscience* 131: 1-11, 2005.

50. **Shimazu H, Maier MA, Cerri G, Kirkwood PA and Lemon RN**. Macaque ventral premotor cortex exerts powerful facilitation of motor cortex outputs to upper limb motoneurons. *J Neurosci* 24: 1200-11, 2004.

51. **Szabo J and Cowan WM**. A stereotaxic atlas of the brain of the cynomolgus monkey (Macaca fascicularis). *J Comp Neurol* 222: 265-300, 1984.

52. **Taira M, Mine S, Georgopoulos AP, Murata A and Sakata H**. Parietal cortex neurons of the monkey related to the visual guidance of hand movement. *Exp Brain Res* 83: 29-36, 1990.

53. **Tkach D, Reimer J and Hatsopoulos NG**. Congruent activity during action and action observation in motor cortex. *J Neurosci* 27: 13241-50, 2007.

54. **Umilta MA, Brochier T, Spinks RL and Lemon RN**. Simultaneous recording of macaque premotor and primary motor cortex neuronal populations reveals different functional contributions to visuomotor grasp. *J Neurophysiol* 98: 488-501, 2007.

55. **Umiltà MA, Kohler E, Gallese V, Fogassi L, Fadiga L, Keysers C and Rizzolatti G**. I know what you are doing. a neurophysiological study. *Neuron* 31: 155-65, 2001.

56. **Winges SA, Weber DJ and Santello M**. The role of vision on hand preshaping during reach to grasp. *Exp Brain Res* 152: 489-98, 2003.

57. **Wolpert DM, Doya K and Kawato M**. A unifying computational framework for motor control and social interaction. *Philos Trans R Soc Lond B Biol Sci* 358: 593-602, 2003.

58. **Wolpert DM and Ghahramani Z**. Computational principles of movement neuroscience. *Nat Neurosci* 3 Suppl: 1212-7, 2000.